Power System Restorations Assisted by Wind Power

Doctor of Philosophy

Paulo Murinelli Pesoti

Department of Electrical and Electronic Engineering

University of Strathclyde, Glasgow

22 August 2018

This thesis is the result of the author's original research. It has been composed by the author and has not been previously submitted for examination which has led to the award of a degree.

I dedicate this to my parents Isabel and
Paulo, and to my sister Isabella.

Acknowledgements

I thank...

My family for always supporting me during this journey, and my beloved Amanda for her kindness and partnership.

My supervisors Prof. Olimpo and Prof. Lo for their knowledge and patience, not to mention Prof. Zambroni for opening so many doors, so I could study in Scotland.

Jackie McNamara and Dr Jan van den Hoven for their technical support.

My colleagues Gisele, Fernando, Adriano and Marcos for their constant help throughput this process, and my colleagues from *DN*, *Marisalles* and *Cactus* for their technical support.

CAPES for the financial support.

> I learned that courage was not the absence of fear, but the triumph over it. The brave man is not he who does not feel afraid, but he who conquers that fear.
>
> Nelson Mandela

Abstract

This thesis investigates power systems restoration procedure and the possibility of using wind power to assist restorations. Three main factors motivate this approach: the sharp growth on wind power production during recent years, the absence of wind power on restoration procedures, and recent blackouts cases which stability issues delayed the restoration procedure.

Stability studies are the base of this investigation, where a series of tools are proposed and developed due to the disparate condition of a restoration procedure. The first tool is a power flow routine, where stochastic simulations address wind speed's randomness. This computational program calculates indexes of collapse for voltage stability.

This computational routine also encompasses a methodology built from an energy function tool for visualizing power systems' vulnerable and robust areas. This thesis applies the tool for restoration analysis, where its validation has been published on an academic journal. This thesis also proposes a novel methodology for visualizing the robustness areas, which uses the energy function output to form a graphical representation as the system diagram's background.

This thesis designs procedures and controllers for the dynamic simulation analysis. The first is the definition of a procedure used to simulate the synchronization of wind farms during restorations. This procedure aims to mitigate impacts caused by wind farms on power systems, where two loop controls achieve the desired response. Finally, one can find an initialization procedure for wind

turbines, regarding restoration conditions.

The robustness areas tool validation shows that one can achieve positive results on angular stability by reinforcing vulnerable areas. The guidelines proposed by the robustness areas tool test the Brazilian system operator's restoration procedure.

A number of analysis and simulations assess the proposed approach efficiency. The IEEE 30 bus system, which is a benchmark for stability studies, shows the impact of wind power on restorations. Part of the Brazilian power system addresses the proposed methodology on a real case scenario.

Finally, this thesis presents a list of recommendations, which intends to guide future works to include wind power on restorations and to extend the proposed approach to other power systems.

Keywords: Power system restoration, Voltage stability, Angular stability, Frequency stability, Energy function, Brazilian power system.

Contents

List of Figures

List of Tables

Symbols

$\|VT\|$ Tangent Vector Euclidean norm.

β Wind turbine's blade pitch angle.

C_p Wind turbine coefficient of power.

δ Synchronous machine rotor angle.

ΔQ Reactive power load margin.

$\Delta\ t_c$ Coordination time.

E'_d Transient internal voltage aligned to the direct axis.

E_{fd} Synchronous machine field voltage.

$E_p(X^s, X^u)$ Unstable part of energy function calculated for a bus or a region.

E'_q Transient internal voltage aligned to the quadrature axis.

J Power flow Jacobian matrix.

λ System load margin.

λ Tip speed ratio (see context).

$^{\mu}$ Mean value of a distribution.

P_{ac} Synchronous machine accelerating power.

Symbols

P_{ele} Synchronous machine active power dispatch.

P_{mec} Mechanical power.

P_{out} Wind farm active power output.

Q_{ele} Synchronous machine reactive power dispatch.

Q_{out} Wind farm reactive power output.

S Asynchronous machine rotor slip.

X^s System variable relating to power flow stable solution.

X^u System variable relating to power flow unstable solution type-1.

List of Acronyms

BS black-start.

CP Coordinated Phase.

DFIG Doubly Fed Induction Generator.

EF Energy Function.

FP Fluent Phase.

FSWG Fixed Speed Wind Generator.

GU Generator Unit.

ISO Independent System Operator.

LVS Low Voltage Solution.

MG Microgrid.

NERC North American Electric Reliability Council.

PMU Phasor Measurement Unit.

PSR Power System Restoration.

PSS Power System Stabilizer.

List of Acronyms

RA Robustness Area.

RL Robustness Level.

SEP Stable Equilibrium Point.

SPA Standing Phase Angle.

TV Tangent Vector.

UEP Unstable Equilibrium Point.

VSWG Variable Speed Wind Generator.

WF Wind Farm.

WG Wind Generator.

WT Wind Turbine.

Chapter 1

Introduction

Electric power is an essential element for modern society, and the demand for it has been growing on the last years. This trend shall continue on the same path, therefore, a reliable power supply is the foundation for a healthy economy growth. Despite the fact that power grids receive large amounts of money for expansion and reinforcements works, short-term outages can occur, thus power systems must be prepared to overcome them [1]. The set of actions that lead a power system from a blackout condition to its fully operational mode is the Power System Restoration (PSR). Planning PSRs requires a number of background studies and simulations, so system operators can foresee a wide range of outage scenarios and build a plan tailor-made for each system [2]. Although restoration plans are specific for each power grid, it is possible to summarize the main steps for a successful PSR [3, 4]:

1. Black-start (BS) power plants and restore local loads;
2. Restore the bulk power system, connecting power plants to each other;
3. Reconnect urban areas and major loads, regarding frequency level, voltage control and thermal limits.

In order to supply the continuously growing demand and reach carbon emis-

sion goals, many countries are changing their main energy source [5], completely changing power grids' operational approach [6]. This new paradigm on power generation encourages the usage of renewable power for restoration plans. The problem, however, is that renewables (especially wind and solar power) depend on weather conditions, which make them disadvantageous for BS. For years, the solutions was to neglect renewable sources during restoration, connecting them on later stages when the bulk power system was restored [7, 8]. As renewables technology developed and replaced high carbon emissions power plants, such approach is no longer attending restorations requirements, hence the inclusion of renewable sources during earlier restoration stages is on this thesis scope.

Aiming to highlight the renewable sources' impact on power systems, a list of United Kingdom's and Scotland's renewable capacity are presented in Table A.1 and in Table A.2 respectively (see Appendix A), where [9] contains the complete document.

Table A.1 shows that wind power has the largest penetration among the renewables representing 19835.3 MW, however, solar PV has sharply increased on the last five years (628.6%) reaching 12775.7 MW, matching with onshore wind power. Biomass has a considerable influence as well, totalling 6047.1 MW, if one considers all types.

Referencing the aforementioned data to the wind power capacity, solar PV represents 64.4%, while biomass refers to 30.5%, showing the considerable investments on wind power, however, if one compares the total energy production on the last year (2017), the numbers considerably differs, where solar PV represents 23.0%, while biomass refers to 63.7%. This is due to differences on load factors, which enables biomass production to be more constant than weather dependant renewable sources.

For Scotland's power gird, Table A.2 shows a scenario where wind power is by far the most prominent renewable source, while hydro generation comes in second.

This is positive for restoration purposes where hydro power plants presents short BSs period, and encourages this thesis to use wind power to assist the main hydro power plants restoration.

1.1 The challenge of power system restorations

The first step in a restoration is to BS power plants [1]. BS is the power plants' ability to restore its Generator Units (GUs) relying only on own resources. Power plants without BS capability have to wait for the power grid to connect their ancillary services and ultimately restore them. Consequently, the number of self restorative GUs directly impacts on the total restoration time [10]. The GU nature dictates how long it takes to BS, where one can organize in four main categories [11–13], namely:

Hydro power plants - can BS in matter of minutes;

Gas turbines - turbines based on Brayton cycle also BS in a period of minutes;

Steam turbines - steam turbines based on Rankine cycle take up to 24 hours to restore due to mechanical issues;

Nuclear power plants - take even longer than steam turbines to BS, because of safety issues.

It is worth noting that combined cycle plants can BS their gas turbines initially, working with reduced capacity while their steam turbines are cooling down.

In some cases there is the possibility to include steam based power plants during restorations as a fast option, by using an islanding technique [14, 15] that separates GUs from the rest of the power system before it is necessary to cease generation. The fast valving approach [16–18], which consists in bypassing the

steam from the boiler directly to the condenser, avoids turbine's shaft acceleration during the islanding procedure. Due to condenser limitations, this bypass can operate for small periods, however, enough to control the main steam flow and adjust it to the new load profile. The hot start approach [19–21] can also include steam turbines during the restoration procedure [22, Chapter 9] after approximately 8 hours standing still.

1.1.1 Recurrent problems during restorations

Along the years, data collected shows recurrent issues related to PSRs. A ten year data provided by the North American Electric Reliability Council (NERC) [23] shows the most common problems during PSRs, as presented in Figure 1.1.

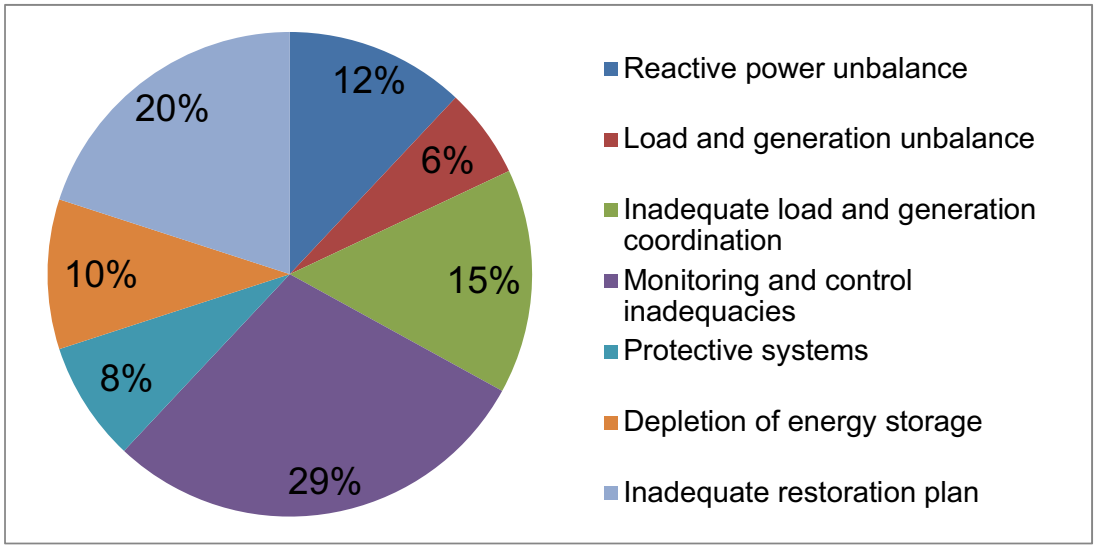

Figure 1.1: North American Electric Reliability Council (NERC) restoration issues - 10 year data. Source: [1].

From Figure 1.1:

Reactive power unbalance involving generators under-excitations, sustained overvoltage, and undue switched capacitors/reactors;

Load and generation unbalance including responses to sudden increases in load, and under-frequency load shedding;

Inadequate load and generation coordination including lack of black-start capability, problems with switching operations, line overloads, and control centre coordination;

Monitoring and control inadequacies that encompass SCADA system capabilities, communication, computer overloading, display capabilities, simulation tools, and system status determination;

Protective systems including synchronization and synchro-check, interlocking schemes, Standing Phase Angles (SPAs), and problems with other types of relays such as under-frequency, differential, distance, and excitation;

Depletion of energy storage covering low-pressure compressed air/gas and discharged batteries. This also includes substations storage systems;

Inadequate restoration plan including lack of planned procedure, outdated procedure, procedure not being followed, inadequate training, and, lack of standard communication vocabulary.

1.1.2 Power plants black-start

During PSR first stages, power plants rely on energy storage systems to restart their GUs [7,11] until they are able to power themselves. In case of backup system failure, GUs are not able to BS and will have to draw power from the grid to do so. As presented in Figure 1.1, lack of storage energy is responsible for 10% of the problems during PSR.

Another recurrent problem during PSRs is the minimum load required by steam turbines [19, Chapter 12]. In case power demand is under a certain level,

these machines have to switch off, due to fuel burner limitations, known as *minimum load* or *minimum stable load* [19, Chapter 7], that depends on the fuel used, the governor type, and the turbine's construction features.

1.1.3 Rebuilding the bulk power system

Transmission lines are physically long elements, which means that capacitance, resistance and inductance occur along the length of the line, as shown in Figure 1.2. When building the bulk power system, power grid operators restore several transmission lines, and the re-energization provokes electromagnetic transients along the equipment, manifesting in the form of voltage spikes and current surges [24]. Consequently, a number of studies [25] are carried out to ensure that these phenomena do not lead to any major problems during PSRs. Examples of issues that may occur are: arresters operation, insulation damage, and protective system tripping out.

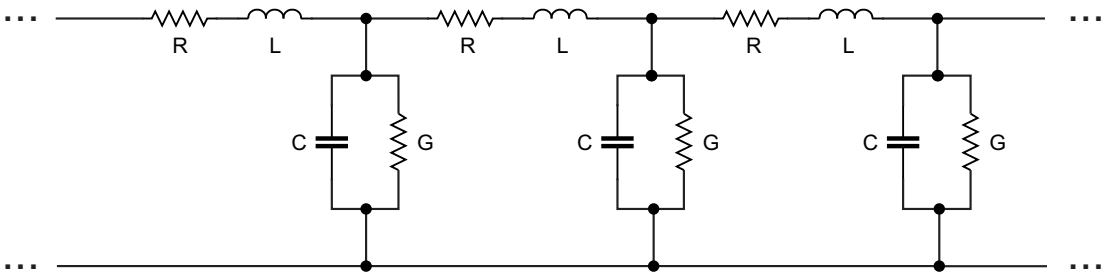

Figure 1.2: Transmission line segment showing the distributed parameter model.

Transmission lines' capacitance effect leads to intense reactive power injection, causing sustained overvoltage. This is due to Ferranti effect [26] and is more pronounced in long distance unloaded transmission lines, being the main reason for reactive power unbalance problem (12% of the total in Figure 1.1).

Loop closures are also an issue during restorations. For every closure, transmission lines face the SPA [27], which is defined by the difference of the voltage

argument between the terminals to be connected. The larger is the SPA, the higher is the power flowing through the line on the loop closure instant [28], creating a sudden power flow variation. High SPAs impact heavily on switchers, reduce generators shaft life-cycle [29], and can also lead to oscillations and dynamic instability. Consequently, several techniques [30] ensure that SPAs are under safety margins.

1.1.4 Dynamic stability issues on restorations

Angular stability is the ability of interconnected synchronous machines on a power system to remain in synchronism [31]. In power systems, uncontrolled rotor acceleration causes the instability, leading to progressive rotor angle displacement and lack of damping torque [32]. The angular stability problem involves the studies of electromechanical nature relying on simulations in a range of tenths of seconds [33]. Figure 1.3 shows the instability mechanism where two distinctive behaviours differ the stable and the unstable case.

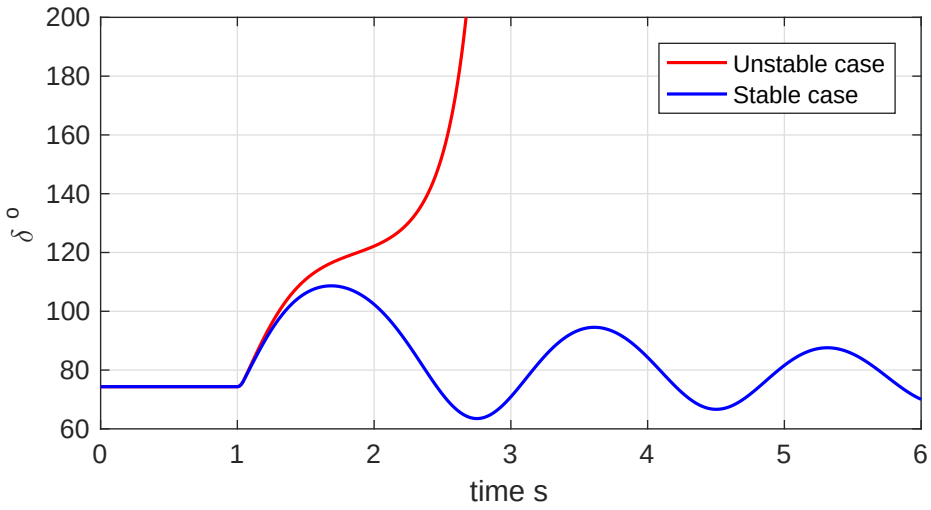

Figure 1.3: Frequency curves showing different control methods used in power systems.

On the field of PSR, angular stability can be a serious issue, due to the reduced number of branches interconnecting areas. This scenario limits the power

transmission capacity, and events such as load pick-ups can lead to large oscillations, breaking the synchronism among machines [34, 35]. Other factors can also reduce system stability condition, naming: low machines' internal voltage level, controllers out of operation range and low spinning inertia provision.

A second point of concern during restoration procedures relates to frequency control. Power plants have to respond adequately to load pick-ups and neutralize the mismatch between load and generation. At this point controlling load ramp is vital for a successful restoration, which is performed by controlling load pick-ups amount [30]. It is worth noting that active power generation control strongly relates to frequency deviations, in fact, governors' control loop work by monitoring angular speed, as main feedback variable [27].

1.2 Literature review

1.2.1 Wind power performing restorations

Considering the high wind power penetration and the short black-start period presented by Wind Farms (WFs), projects have been developing novel approaches for restoration using WFs. One can organize the usage of wind power during restorations in two main groups:

- microgrid restoration
- utility power grid restoration

This classification comes from the different strategies required to restore each type of power grid. The technology used and the scale of WFs are also different in each case, consequently authors usually direct their projects for one of the mentioned areas.

1.2.2 Wind farms performing restorations in microgrids

Microgrids (MGs) can play an important role during restoration, due to their operational flexibility and fast black-start capability [36, 37]. MGs are local area power systems, formed by low voltage branches and connected to a main grid via a step-up transformer. Despite of the connection to a main grid, MGs are able to operate autonomously because of their ability to supply its own load via micro power sources based on renewable energy [38]. It is worth noting that this thesis does not exploit the MGs' ability to help the main grid restoration.

The possibility to operate in islanding mode enables MGs to perform their own restoration prior to the main grid [39, 40]. Authors in [41] show such ability in a small system containing several small scaled renewable sources, including a wind turbine.

Authors in [42] describe a complete MG restoration, where a 1500 kW Wind Generator (WG) and a battery group working as storage system restores a 0.415 kV system. Authors propose to connect the battery bank at the back-to-back converter DC link, reducing installation costs. The rotor side converter is responsible for charging the battery in case of energy surplus, while the grid side converter is responsible for voltage reference and grid frequency control. To accomplish that, converters are oversized, and an extra control loop performs primary and secondary frequency control.

Authors in [39] point out that a major advantage for MGs during restoration is the reduced complexity, due to the lower number of controllable variables. They also rely on low voltage systems, reducing reactive power balance problems. However, it is not expected to find a large number of conventional synchronous machines that are capable of frequency and voltage control.

1.2.3 Wind farms assisting restorations in utility power grids

Utility power grid restoration has different challenges when compared to MGs, consequently, they have redeveloped PSR philosophies. The main advantage of large scale grids is the presence of traditional synchronous generators that are able to act as voltage source. On the other hand, utility power grids rely on high voltage systems and long transmission lines, leading to reactive power balance problems [1]. Another implication is the impracticability in considering storage energy units in these cases [2], thus requiring different approaches in load/generation coordination.

Authors in [43] present basic concepts for using wind power in utility power grid restoration. According to the authors, wind speed fluctuations can collapse the restoring system, due to the lack of frequency control and active power reserve from wind generators. This discussion strongly relates to load/generation coordination, which wind power can affect. Restorative power systems may not sustain large wind variations due to the reduced number of restored power plants. These large wind speed excursions could lead GUs to reach thermal limits or minimum stable load [19, Chapter 7].

Researchers in [44] address load/generation coordination during restoration, where simulations in a 22 bus system show that the load is restored faster when an offshore WF is considered to assist the restoration. The system without the WF is faster at the beginning of restoration (from 27 minutes to 35 minutes), however it takes longer to restore the total system load. Results presented encourage the wind power usage from the first PSR's stages, using it as a tool to control reactive power dispatch and improve system transmission capacity.

1.2.4 Load pick-up and frequency stability during restoration

Picking-up load during restoration is not an easy task, due to the low inertia scenario combined with the limited load ramp provision [45]. In order to avoid frequency collapse, a series of stability studies determine *when* and *how much* load to connect at time. A common approach to control load ramp [45] is to connect loads into predefined "chunks" with a certain interval among them called coordination time $\Delta\ t_c$.

As renewable sources [5] substitute high carbon emissions power plants [9, 46, 47], system inertia provision reduces, limiting load pick-up capability. Authors in [48] use the Irish system to point out this problem. Authors in the paper compared the inertia provision for different types of WGs and calculated the impact that a high wind penetration would have in power system. Attempting to increase the inertial provision on Doubly Fed Induction Generator (DFIG) based WGs the authors propose an additional control loop that uses the kinetic energy from rotors in WGs with variable speed technology.

Extending this issue to restorative systems, wind power can make vulnerable load pick-up capability. Frequency control loops can bypass such issues by de-loading turbines' dispatch to obtain a spinning reserve [49]. Onshore and offshore WFs can integrate this feature, as authors show in [50]. The major issue regarding this method is the lack of economical appeal [51, 52], as the lower power dispatch impacts on the final revenue income by the equipments' owners, which makes this frequency control controversial [53].

Finally, authors in [54] propose an approach to reduce the swing time response in distant machines by using Phasor Measurement Unit (PMU) during restoration. The IEEE 39-bus New England system tests the proposed approach, presenting satisfactory results.

1.3 Motivation and objectives

The PSRs field has a considerably reduced number of works, if compared to other electrical engineering areas, where such scenario is more evident for renewable sources performing PSRs. This is mainly due to the concept that the stochastic nature of renewables can lead power systems to collapse during restoration [53]. As renewable energy takes high emissions sources' place, the number of BS generators available reduces, making PSRs procedure increasingly challenging. This way, it is a matter of time until renewable sources take an important role on restorations [55, 56].

This thesis aims to further investigate the impact wind power would cause on PSRs when assisting a main BSs source. The base idea is that WFs power injection can improve power systems controllability [57], by assisting reactive power compensation, reducing loop closure SPA [27–30], minimizing the possibility of collapse [58], and improving angular stability indexes [31–33, 59, 60].

An important goal here envisaged is to improve the Brazilian grid restoration, which has recently undergone a series of outages, putting its PSR philosophy to the test [61]. Brazilian substantial growth in wind power motivates this thesis, with the extra challenges in which a system with long transmission distances imposes.

This investigation proposes the usage of an energy function tool to infer the voltage stability condition [62]. The final goal is to use dynamic stability analysis via time domain simulations to validate the proposed approach, leading to recommendations on the restoration field.

1.4 Original contribution

This thesis' contributions are:

- An investigation on power system restoration procedures using an energy function tool, where one can identify robust and vulnerable areas along restoration procedures;
- Validation for the energy function tool through tests in real case scenario systems, where parallels are found between a robust system and angular stability indexes;
- Wind turbines initialisation procedure for restoration purposes;
- A WF reconnection procedure for systems in restoration procedure;
- Development of a computational tool, which calculates power flow, indexes of collapse and energy function, under the stochastic point of view. Due to computational cost associated with this activity, parallel processing is employed;
- A novel visualisation method for robustness areas via heatmaps;
- Application of the proposed methodology on the Brazilian power grid restoration, where wind power usage for such procedure is a novelty.

1.5 Thesis structure

This introductory chapter, which presents key characteristics associated to the restoration challenge, compose this thesis, with seven more chapters, four appendices and one annex. Chapter 2 shows electric power system component models used for PSRs studies, aiming power flow and stability analysis.

Chapter 3 presents the proposed approach to assess the impact wind power provokes on PSRs, namely: power flow, voltage stability, energy function and dynamic stability studies.

Using the proposed studies, test system restorations are proposed and presented in Chapter 4, where the IEEE 30 Bus system show key characteristics of the proposed approach.

Chapter 5 and Chapter 6 present the proposed PSRs assessment methodology in a part of the Brazilian power system. These chapters aim to test the system restoration philosophy.

Chapter 7 presents the list of recommendations based on thesis' findings, while Chapter 8 shows this work's final considerations and a list of future work.

Appendix A presents the statistics regarding renewable power generation in the UK. Appendix B shows the machines' formulation used for stability studies. Appendix C and Appendix D show complete results for the test system and the Brazilian power grid, respectively.

Finally, the paper, which validates the proposed robustness areas tool, is located in Annex A. This paper shows the possibility of using the robustness areas technique for stability analysis on restoration procedure.

1.6 Publications

It follows the list of papers that are direct outcome of this thesis.

Published:

- P. Murinelli Pesoti, E. V. de Lorenci, A. C. Zambroni de Souza, K. L. Lo, and B. I. Lima Lopes, "Robustness area technique developing guidelines for power system restoration," *Energies*, vol. 10, no. 1, 2017, Article No 99. Accessed on: 10/04/2018. [Online]. Available: `http://www.mdpi.com/1996-1073/10/1/99`

Under development:

- P. Murinelli Pesoti, O. Anaya-Lara, and K. L. Lo "A methodology for power

systems stability assessment for restorations using wind power." Expected submission: July 2018.

- P. Murinelli Pesoti, O. Anaya-Lara, and K. L. Lo "Wind power impact on power systems dynamic stability during restoration." Expected submission: August 2018.

Chapter 2

Modelling power systems for restorations studies

2.1 Modelling electrical power systems components

Modelling power system is an important step during stability studies, where some elements require static models, while others include their dynamic response. Static models can include: loads, transmission lines, transformers, capacitors and reactors are represented by static models for power system stability studies. Elements that require dynamic models are: turbines, electric machines, static VAr compensation, excitation systems and governor controls. This section presents power grids' elements modelling, aiming for power flow studies, voltage stability studies and dynamic simulations.

2.1.1 Buses

Buses are arranged according to the information previously known or specified, which leads to the following classification [63, 64]:

PQ buses

In these buses, active and reactive power injected are specified, hence voltage magnitude and voltage argument are the variables to be calculated. They are used for load buses in general, where one can calculate or estimate the power demand.

PV buses

Active power and voltage magnitude are known, thus voltage angle and reactive power injection are calculated. These are mainly used for generation buses, since they are able to control voltage level of their terminals.

Swing buses

They are also known as slack or Vθ buses. For this type of bus, voltage magnitude and voltage angle are known beforehand, thus active power and reactive power dispatch are variables. At least one Vθ bus must be present in load flow analysis, because they are the system's angular reference.

2.1.2 Generators

Regarding power flow studies, the amount of power injection defines generators. Figure 2.1 presents the symbolic representation of a generator [31]. According to Figure 2.1: P_g^i is the active power injected in bus (i); and Q_g^i is the reactive power injected in bus (i)

Usually, these equipments are represented as voltage controlled buses (PV buses) or reference buses in load flow studies. It is worth noting that power plants can reach their maximum/minimum reactive power limit, where they lose the ability to control voltage level, hence they change their representation to PQ buses. This is a result of machines components limitation, or stability thresholds, creating an operational zone called capability chart.

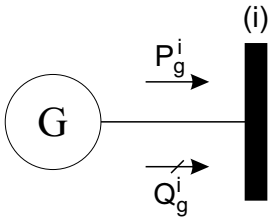

Figure 2.1: Generator symbolic representation.

2.1.3 Synchronous machine dynamic model

The synchronous machine probably is the electrical device with most literature on it, where one can find a vast amount of material in almost every stability book. This thesis uses the nonlinear magnetic circuit model present in [33, Chapter 3]. This model encompasses the two swing machine rotor equation, two transient voltage equation, two subtransient flux equation and two for describing the field flux. This model also represents the magnetic core saturation effect, because of its considerable influence on angular stability. The set of equations describing the synchronous machine for stability purposes is located in Appendix B.

2.1.4 Loads

Power systems stability is directly related to their loads characteristics [65]. Therefore, models have to be flexible enough to represent several load types and their behaviour. This thesis uses the polynomial model that describes active power and reactive power demand as a polynomial function of terminal voltage level. The most commonly used polynomial form considers loads to be a composition of constant impedance Z_{cst}, constant current I_{cst}, and constant power P_{cst}. It is named as ZIP model [66–69], and is expressed by:

$$P = P_0 \left(aV_r^2 + bV_r + c \right) \tag{2.1}$$

$$Q = Q_0 \left(dV_r^2 + eV_r + f \right) \tag{2.2}$$

$$V_r = \frac{V}{V_0} \tag{2.3}$$

where: V_0 is the voltage level where P_0 and Q_0 occurs; V is the voltage level correspondent to P and Q; a is the active power constant impedance factor, b is the active power constant current factor; c is the active power constant power factor; d is the reactive power constant impedance factor; e is the reactive power constant current factor; f is the reactive power constant power factor; $a+b+c = 1$; and $d + e + f = 1$.

2.2 Modelling wind power

One fundamental contribution of this project is to investigate the impact of wind power on power systems restoration, hence this section details wind turbines' and generators' models.

2.2.1 Wind statistical model

Proposed by W. Weibull in 1951 [70], the Weibull distribution is the most commonly used model to describe wind stochastic behaviour in power systems studies [71]. The Weibull distribution is described by:

$$f(v_w|a,b) = \begin{cases} 0, & v_w < 0 \\ \dfrac{b}{a}\left(\dfrac{v_w}{a}\right)^{b-1} e^{-(v_w/a)^b}, & v_w \geq 0 \end{cases} \tag{2.4}$$

where: $f(v_w|a,b)$ is the probability density function; v_w is the wind speed; a is the scale parameter (same unit as v_w); and the shape parameter b is dimensionless.

A probability density function when integrated over a region gives the probability of a random variable to fall within this region [71]. This statement leads to the cumulative density function of $f(v_w|a,b)$, which is given by:

$$F(v_w|a,b) = \int_0^{v_w} f(t|a,b)\,\mathrm{d}t = 1 - e^{-(v_w/\lambda)^k} \tag{2.5}$$

2.2.2 Wind turbines

A wind turbine is a mechanical device that converts kinetic energy from wind to rotational power, which drives an electrical generator [72]. One can organize into two main groups, according to the axis position:

Horizontal axis wind turbines

These are the common style wind turbine. It has a design similar to windmills, with blades similar to propellers that spin on the horizontal axis. Connected to the main rotor, they have an electrical generator at the top of a tower, and they must be pointed into the wind direction [73].

Vertical axis wind turbines

This group of turbines main feature is that the turbine does not need to be pointed into the wind direction. This is an advantage where wind direction is highly variable or turbulent. With a vertical axis, the generator and other primary components can be placed near the ground, so there is no need for tower does to support it. The main disadvantage is the drag created by the blades and the reduced wind speeds near the ground [74, 75].

This project considers only horizontal axis wind turbines for analysis, since these are the most common application for Wind Farms (WFs) in power systems, and present elevated energy efficiency.

There are several approaches to model turbines' aerodynamic response. The most commonly used are [76]:

Blade element momentum

This is one of the most detailed methods, reproducing wind turbines with

extremely accuracy. In this model, it is necessary to represent how wind behaves along turbine's swiped area and how it interacts with the blades. It requires great computational effort when applied in simulations.

Approximation via coefficient of performance

In this case, turbine's mechanical torque is assumed to follow an algebraic equation function of wind speed, angular speed and blade pitch angle. This relation is called coefficient of performance and is represented by $C_p(\lambda, \beta)$. It is indicated for power system dynamic simulations, with enough accuracy for transient and long-term electromechanical stability studies. The disadvantage is the algebraic considers a fast torque response for wind speed variations, while these are smoother in reality.

Approximation via power curve

In this approach, dynamics are neglected and the coefficient of performance is assumed to be constant. This model is used for power flow studies where the steady state is assumed and turbine controllers have enough time to adjust $C_p(\lambda, \beta)$ to its maximum.

This thesis uses the approximation via power curve model for power flow and voltage stability studies, while it uses the approximation via coefficient of performance model for dynamic stability studies.

2.2.3 Wind turbine model for stability studies

The power provided by the wind in a swiped area is given by [74, 75]:

$$P_w = \frac{1}{2}\rho A v_w^3 \tag{2.6}$$

where: P_w is the available wind power, ρ is the air density, A is the swiped area, and v_w is the wind speed.

The power captured by wind turbines is a fraction of P_w, depending on the wind turbine angular speed and blade pitch angle. The relation between wind power and turbine captured mechanical power P_t defines the coefficient of performance $C_p(\lambda, \beta)$ [77], and is given according to:

$$P_t = C_p(\lambda, \beta)P_w = \frac{1}{2}\rho A C_p(\lambda, \beta)v_w^3 \tag{2.7}$$

$$C_p(\lambda, \beta) = a_1 \left(\frac{a_2}{\lambda_i} - a_3\beta - a_4\beta^{a_5} - a_6 \right) e^{\frac{a_7}{\lambda_i}} \tag{2.8}$$

$$\lambda_i = \frac{1}{\frac{1}{\lambda + a_8\beta} - \frac{a_9}{\beta^3 + 1}} \tag{2.9}$$

$$\lambda = \frac{R\omega_t}{v_w} \tag{2.10}$$

where: λ is turbine tip speed ratio; β is blades pitch angle; R is the blades length; ω_t is turbine angular speed; and finally, a_1 to a_9 are turbines' parameters.

Typical $C_p(\lambda, \beta)$ curves are presented in Figure 2.2 in function of tip speed ratio for a 20^o interval of β. From (2.10) one can conclude that it is possible to adjust Wind Generators (WGs) rotor speed to meet the maximum $C_p(\lambda, \beta)$ for every wind profile, in generators with speed control.

Generator's capacity and safety constrains bound the power delivered by Wind Turbines (WTs). The first limit is the cut in wind speed, or v_{cut-in}, the minimum wind speed in which it is feasible to produce electrical power. It means that for $v_w < v_{cut-in}$ the power output is zero. The second limitation is the thermal machine limitation, bounding the output power to the generator rated capacity P_{rated}. The wind speed that matches to the generator P_{rated}, is called v_{rated}. Finally, the maximum wind speed limit $v_{cut-off}$ is when wind turbine must stop for safety issues. Considering all limits, WTs output power can be rewritten by [73]:

$$P_t = \begin{cases} 0, & v_w < v_{cut-in} \\ \frac{1}{2}\rho A C_p(\lambda,\beta) v_w^3, & v_{cut-in} \leq v_w < v_{rated} \\ P_{rated}, & v_{rated} \leq v_w < v_{cut-off} \\ 0, & v_w \geq v_{cut-off} \end{cases} \tag{2.11}$$

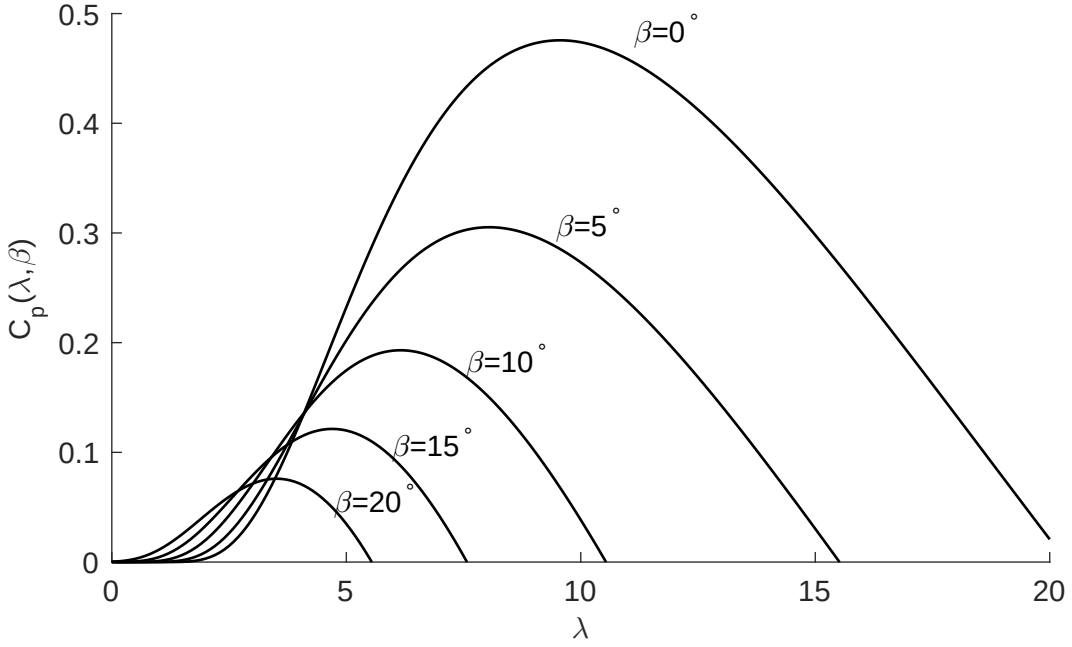

Figure 2.2: Coefficient of performance $C_p(\lambda, \beta)$ versus tip blade speed ratio λ for $0^o \leq \beta \leq 20^o$ in steps of 5^o.

It is worth noting that the tip speed ration symbol adopted in the literature is the same as the symbol adopted for the active power load margin, which is later explained. This thesis maintains the same symbol for both greatness as the literature adopts, because the context explains the case in question.

2.2.4 Variable speed wind generators

Variable Speed Wind Generators (VSWGs) are alternate current machines that can fully control their rotor speed. In this thesis, synchronous machines with field

controlled excitation are adopted as the main model for VSWGs, as Figure 2.3 depicts. The major advantages of this model are: the lower cost of the machine side converter, which is a diode rectifier and a DC link booster, and the absence of gearbox [73]. Control systems implemented by several manufacturers use the machine's side converter to provide torque/speed control [78], adjusting λ and β to obtain the maximum C_p.

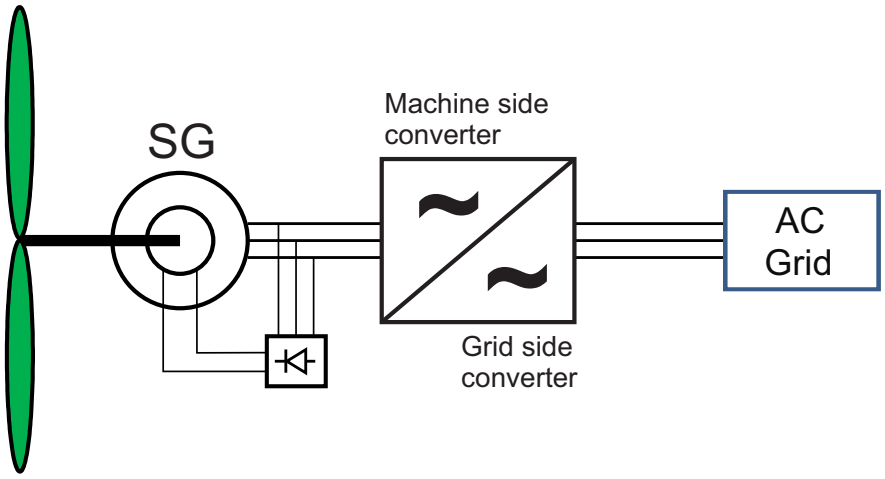

Figure 2.3: Field controlled synchronous generator arrangement.

The grid side converter is responsible for providing reactive power, though it is thermal capacity limited. Therefore, WFs that provide voltage control for all operational range have the grid side converter slightly oversized than the generator [79–82]. Figure 2.4 illustrates the reactive power control problem in VSWGs. For this thesis, generators are supposed to provide at least 50% of reactive power in relation to the maximum active power [83].

Regarding the power flow analysis, PV buses can represent VSWGs, where the active power dispatch is calculated as function of the wind speed, while the reactive power dispatch is calculated according to the desired voltage level. It is also possible to consider such buses as PQ model, where they operate either as constant reactive power dispatch or on constant power factor mode.

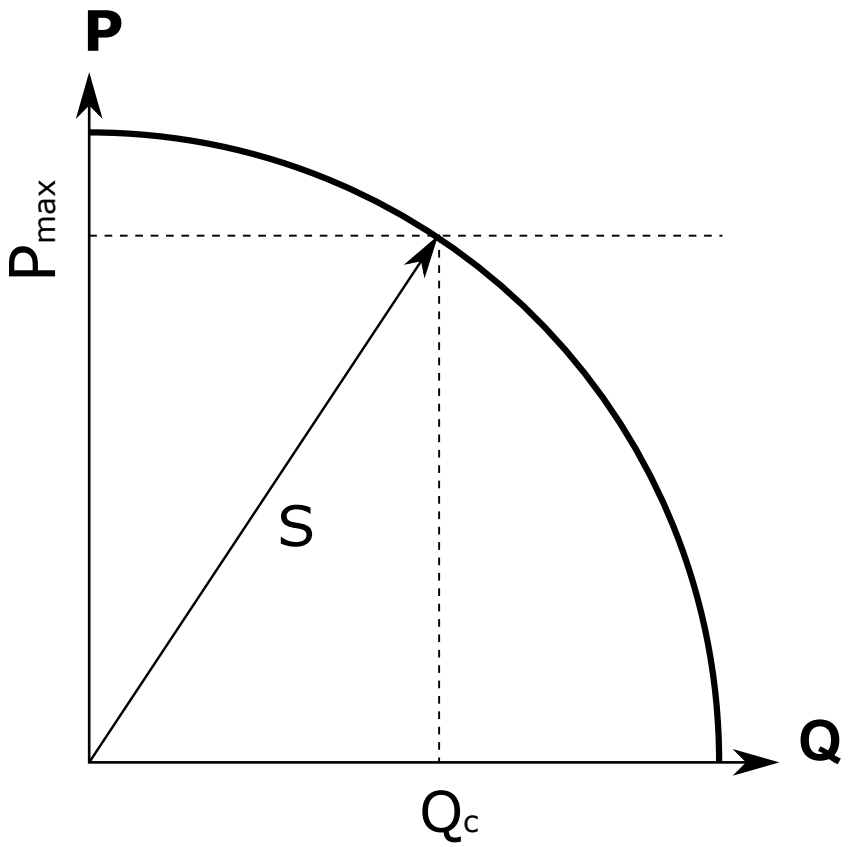

Figure 2.4: Apparent power in a VSWG showing reactive power limitation in function of active power dispatch, where: P_{max} is the generator's rated active power; Q_c is the maximum reactive power for P_{max}; and $S = \sqrt{{P_{max}}^2 + {Q_c}^2}$.

2.2.5 Fixed speed wind generators

Older wind farms rely on Fixed Speed Wind Generators (FSWGs) that are induction machines directly connected to the grid. The name comes from the idea that generators rotating field are tied to the grid [84], being calculated by:

$$n_{rpm} = \frac{60f}{p} \tag{2.12}$$

where: f, the grid frequency, is constant; n is the rotor speed in rpm; and, p is the number of pairs of poles.

The power flow representation for FSWGs is an induction generator directly

connected to the grid, as Figure 2.5 shows. The complete power flow equations deduction is located in Appendix B.

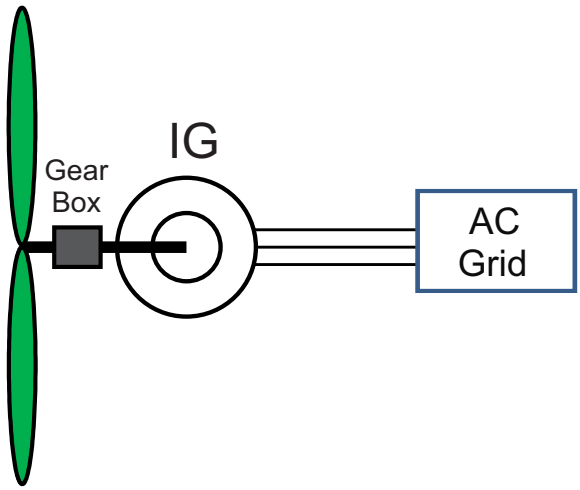

Figure 2.5: Diagram of a wind generator composed by an induction generator directly connected to the grid.

2.2.6 Induction machine dynamic model

The dynamic model for the induction generator in this thesis uses three differential equations, where one relates to the rotor dynamics (mechanical power, electrical power, and damping torque), while the other two equations are related to the voltage source behind the transient inductance X'_s [76, 84]. The set of algebraic-differential equations modelling the induction machine for dynamic stability studies is located in Appendix B.

2.3 Conclusion

Modelling power system elements is the cornerstone for power system stability studies, where a model that does not depicts components correctly leads to imprecise conclusions. During Power System Restorations (PSRs) such modelling

can be very tricky, because voltage and frequency excursions are much broader than regular operation, which can extrapolate the models boundaries.

Wind power relies on meteorological variables, hence it is important to represent it by stochastic models, while analysing and planning power system restorations. For this sake, during the planning phase, a computational routine creates random wind profiles according to (2.4), and it later uses them as the input for the load flow analysis. The next chapter elucidates the proposed methodology for PSRs analysis.

Chapter 3

Proposed methodology for restoration analysis

3.1 Introduction

This chapter shows the proposed methodologies and assumptions used in this thesis to simulate and assess power system restoration performance using wind power. The previous chapter presents the models used for analysis, while the introductory chapter shows the challenges imposed by Power System Restorations (PSRs).

Firstly, this chapter presents the proposed power flow routine regarding wind's stochastic behaviour, followed by a novel application for the energy function tool. On the dynamic field, this chapter details a sequence for restoring Wind Farms (WFs), and the control loop programmed into the turbines' controller allowing a smooth reconnection. Finally, this thesis proposes an initialization routine for wind turbines, regarding constrains related to restoration.

3.2 Proposed computational tool for restoration analysis

To overcome high cost computational calculations, a power flow routine is proposed and implemented in Fortran language, which leads to faster calculations due to its high performance when working with large matrices and linear systems. Parallel processing is also used to speed-up the stochastic process. In this approach, multiple instances of the mentioned Fortran power flow are executed simultaneously, in the several processing elements available on the machine used for simulation [85]. To achieve such goal, a Matlab manager routine is responsible for randomly select wind profiles, co-distribute along the **processing elements**, and trigger the Fortran power flow routine. Once the power flow and the collapse indexes are calculated, the data returns to the manager routine, who saves it. Figure 3.1 shows how the combined process is organized.

It is worth noting that heavy numerical calculations are entirely performed by the Fortran routine, while the MATLAB manager is responsible for low computational effort tasks, and also to create the parallel processing environment. Routines are detailed as follows.

3.2.1 The manager routine

As discussed in Chapter 2, this thesis address wind speed's intermittent behaviour stochastic approach. This methodology randomly samples wind speed profiles according to the Weibull distribution (2.4), and uses them as input for (2.11) for calculating WFs' dispatch. Hence, for every wind profile sampled, a load flow is triggered, forming the stochastic approach proposed [85].

The manager routine is responsible for creating the environment for the proposed Fortran tool. It reads the input variables, where wind parameters are located, and creates an array of samples by using a Weibull distribution random

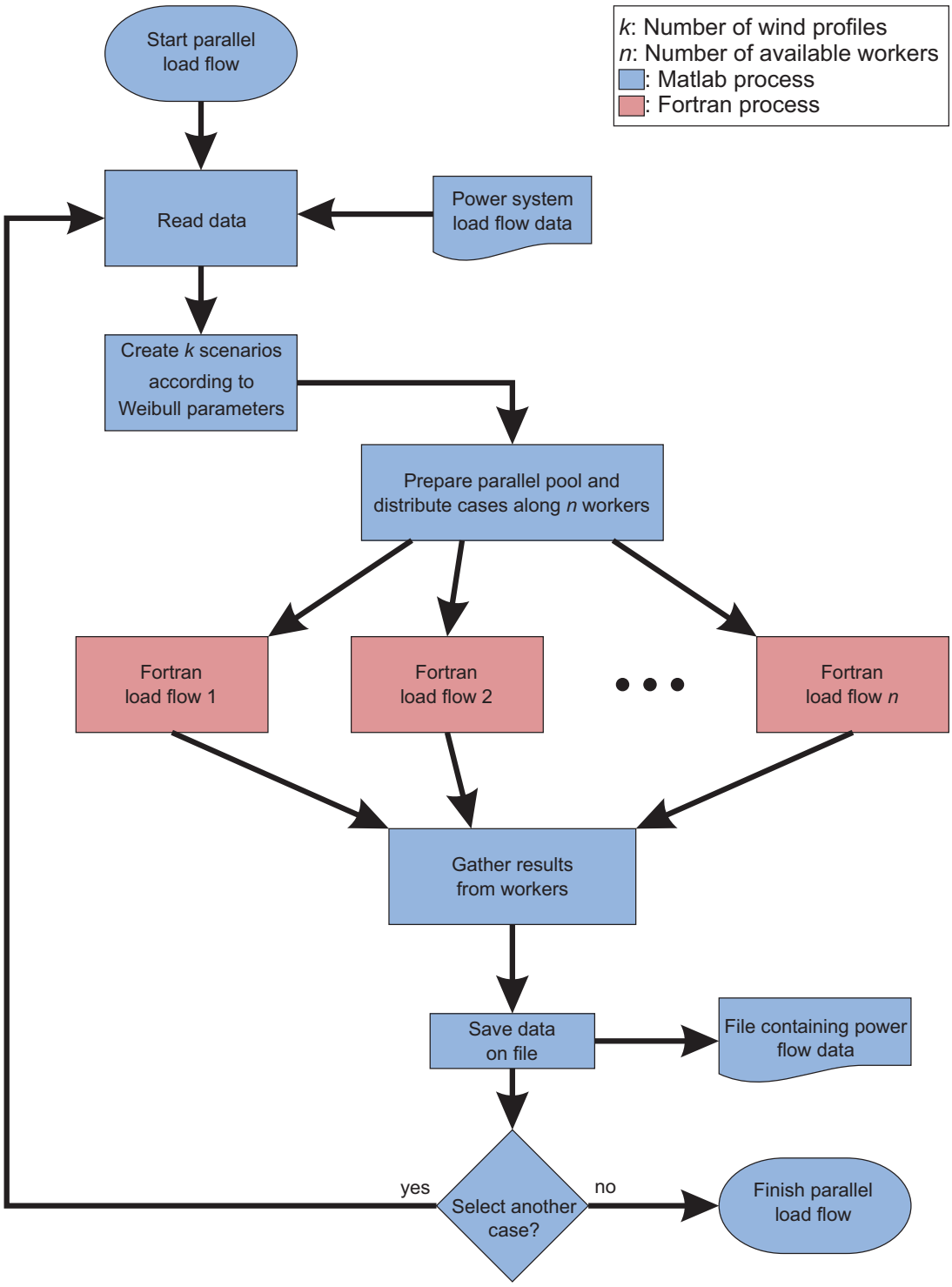

Figure 3.1: Diagram depicting the combined MATLAB-Fortran parallel processing routine for power flow calculation considering stochastic simulation.

number function *wblrnd*. Then, the routine *co-distributes* input and output data arrays along the available processing elements.

During the parallel processing, the manager is responsible for sending data to the Fortran routine, wait for its response (or kill non-responsive cases), and read back the power flow results from all available processing elements independently. Finally, the manager retrieves information from processing elements via *gather* function, compact and saves results on disk. Visit MATLAB help on [86] for more information.

3.2.2 Power flow studies

Power flow or load flow studies aim to determine power systems operative point under steady state condition. This is the base for all other analysis in this thesis, it means that results acquired here are used later for other studies. This way, power systems are studied in function of four main electrical quantities:

- **V** – voltage level or magnitude;
- θ – voltage argument or phase angle;
- **P** – active power injected to a bus;
- **Q** – reactive power injected to a bus.

To obtain the power flow solution one has to solve the following set of non-linear equations [63, 64] for all system buses, each indicated by the index i:

$$\begin{cases} P_i = \sum_{k=1}^{n} \left|\left|\bar{V}_i\right|\right| \left|\left|\bar{V}_k\right|\right| \left[G_{ik}\cos\left(\theta_i - \theta_k\right) + B_{ik}\sin\left(\theta_i - \theta_k\right)\right] \\ \\ Q_i = \sum_{k=1}^{n} \left|\left|\bar{V}_i\right|\right| \left|\left|\bar{V}_k\right|\right| \left[G_{ik}\sin\left(\theta_i - \theta_k\right) - B_{ik}\cos\left(\theta_i - \theta_k\right)\right] \end{cases} \tag{3.1}$$

where: P_i and Q_i are respectively the active power and reactive power injected in bus i; $\|\bar{V}_i\|$ is the voltage module or magnitude at bus i; G_{ik} and B_{ik} are respectively the real and imaginary parts of the element $\bar{Y}_{ik}$, as in the nodal admittance matrix $\mathbf{Y}$; θ_i is the phase angle of bus i, while θ_k is the phase angle of bus k; and n is the number of buses in the system.

3.2.3 The tangent vector

By linearising the power flow equations (3.1) it is possible to obtain the sensitivity for the operational point as follows [87]:

$$\begin{bmatrix} \Delta P \\ \Delta Q \end{bmatrix} = \begin{bmatrix} \dfrac{\partial P}{\partial \theta} & \dfrac{\partial P}{\partial V} \\ \dfrac{\partial Q}{\partial \theta} & \dfrac{\partial Q}{\partial V} \end{bmatrix} \begin{bmatrix} \Delta \boldsymbol{\theta} \\ \Delta \mathbf{V} \end{bmatrix} = J \begin{bmatrix} \Delta \boldsymbol{\theta} \\ \Delta \mathbf{V} \end{bmatrix} \tag{3.2}$$

where: ΔP and ΔQ are active power and reactive power variations respectively; ΔV and $\Delta \theta$ are voltage magnitude and phase angle variations respectively; and, the matrix containing power flow equations partial derivatives is the Jacobian matrix J.

One can calculate the Tangent Vector (TV) by multiplying both sides of (3.2) to the inverse of the Jacobian matrix J, as follows:

$$\mathbf{TV} = \begin{bmatrix} \Delta \boldsymbol{\theta} \\ \Delta \mathbf{V} \end{bmatrix} = J^{-1} \begin{bmatrix} \Delta P \\ \Delta Q \end{bmatrix} \tag{3.3}$$

Even though (3.3) suggests that calculating the tangent vector is a costly computational process, it is already done during the power flow calculation by the Newton-Raphson methodology, hence it is possible to obtain the TV with no extra computational effort.

At this point, an important definition emerges: the **critical bus**. This bus is associated with the highest absolute entrance in the tangent vector and it is

the most likely to first reach the critical point [87]. As the system moves to the critical point, the critical bus may change and the bus with the highest entrance on the maximum load point is the critical bus at the collapse point, and it is associated with the voltage collapse.

3.2.4 The continuation method

The voltage stability problem is a local problem in essence, however, it has global impacts. Several blackouts are associated to local voltage instability incidents that led power grids to a cascade of events culminating with the voltage collapse. Author in [88, pp. 59-61] presents a major review in blackouts associated with voltage stability incidents. In the voltage stability field, proximity to the collapse point is measured by the load margin λ, which is calculated using the PV curve and the reactive power load margin ΔQ calculated via the QV curve. One can refer to page 21 for disambiguation on the load margin symbol.

Tracing PV curve, QV curve and calculating load margin may present convergence problems to conventional power flow routines on the vicinity of the critical point because the Jacobian matrix becomes ill conditioned. This thesis uses the continuation method to overcome this problem. It is a two phase iterative process with predictor and corrector steps, and is obtained by the reformulated power flow equations as follows:

$$f(\mathbf{x}, \lambda) = 0 \tag{3.4}$$

where: $\mathbf{x}$ represents the system state variables and λ represents the parameter that moves the system towards the maximum load point [89, 90].

From a known operational point $(\mathbf{x}_i, \lambda_i)$ the predictor step estimates the next point solution $(\mathbf{x}_i + \Delta\mathbf{x}_i, \lambda_i + \Delta\lambda_i)$. The corrector step refines the predictor step's estimative.

Expressing $P = P_0\,(1 + \Delta\lambda)$ and $Q = Q_0\,(1 + \Delta\lambda)$, the TV is calculated by:

$$\begin{bmatrix} \dfrac{\Delta\boldsymbol{\theta}}{\Delta\lambda} \\ \dfrac{\Delta\mathbf{V}}{\Delta\lambda} \end{bmatrix} = J^{-1} \begin{bmatrix} \Delta P_0 \\ \Delta Q_0 \end{bmatrix} \tag{3.5}$$

The parameter $\Delta\lambda$ decreases along the continuation method in order to increase precision and the PV curve resolution. $\Delta\lambda$ is calculated along the procedure by:

$$\Delta\lambda = \frac{k}{\|\mathbf{TV}\|} \tag{3.6}$$

where: $\|\mathbf{TV}\|$ stands for the tangent vector Euclidean norm, and k is an accelerating constant.

The whole procedure is as follows:

1. The predictor step uses the TV from the power flow solution scaled by $\Delta\lambda$ to predict the next PV curve point;

2. The corrector step is addressed as a power flow problem using the predictor step as the initial guess.

3.2.5 The Fortran routine

Finally, the Fortran routine runs as Figure 3.2 shows.

3.3 Energy function applied on restoration analysis

One novel contribution in this thesis is the application of an energy function tool to evaluate robustness areas during restorations. This energy function tool is classified as a direct method for stability analysis, because it calculates system

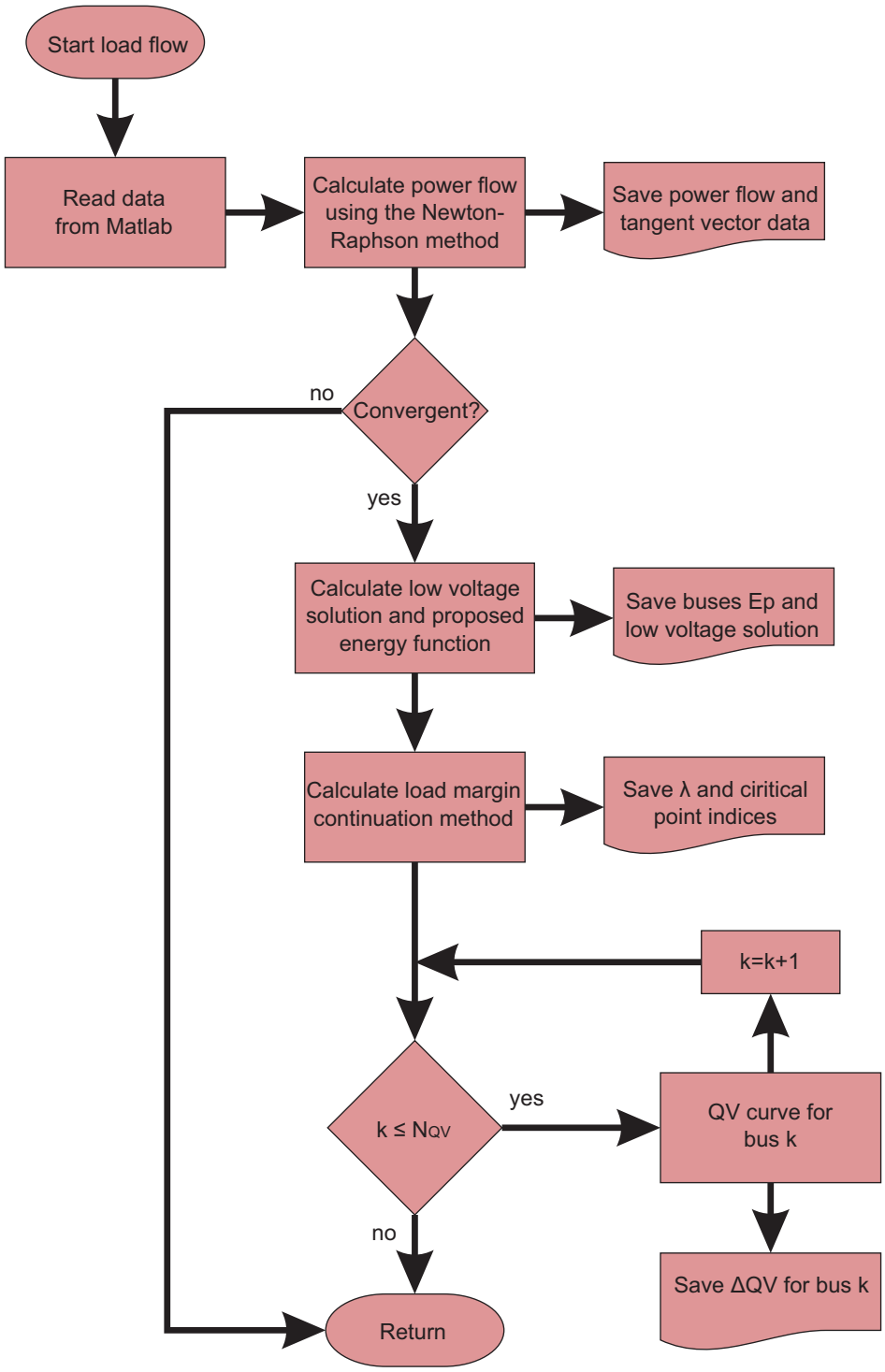

Figure 3.2: Diagram depicting the Fortran power flow routine, where the proposed energy function and the indexes of collapse are calculated. In this picture k is the bus number in which ΔQ is calculated.

stability conditions without time domain simulations. For this sake, the system is modelled according to an Energy Function (EF) that takes into consideration system parameters. Obtaining the corresponding EF is a difficult task [91, 92], especially when complex controllers are considered along power systems. The voltage stability field uses EFs to determine the proximity to the critical point [58], without the calculation of several load flows that have a high computational cost [33]. Instead, it uses the energy difference between stable and unstable solutions [93], as it can infer the critical point's proximity [94].

3.3.1 Power flow multiple solutions

Energy function analysis compares the energy level between the Stable Equilibrium Point (SEP) and a corresponding Unstable Equilibrium Point (UEP) [95,96]. This way, multiple power flow solutions satisfy a load/generation condition [97]. Figure 3.3 shows a two bus system used to exemplify the multiple power flow solutions, where applying the Kirchhoff's nodal laws at bus 2 it comes:

$$\begin{cases} 0 = P_l - V_2 V_1 B_{21} \sin(\theta_2 - \theta_1) \\ 0 = Q_l + V_2 V_1 B_{21} \cos(\theta_2 - \theta_1) \end{cases} \tag{3.7}$$

SEP and UEP are obtained by solving (3.7), where Table 3.1 presents the multiple solutions. It is noticeable that the UEP solution presents extremely low voltage at bus 2 (0.102 pu) and elevated Q_g, indicating that it is an infeasible operational point. The UEP presented has one bus working on the lower part of PV curve, therefore it is classified as UEP type-1 [97], and is the sort of solution required in this thesis.

In large power systems, obtaining a Low Voltage Solution (LVS) can be complicated, since power flow routines tend to diverge from the solution, due to reduced region of attraction for LVSs [98]. A controlled Newton-Raphson method

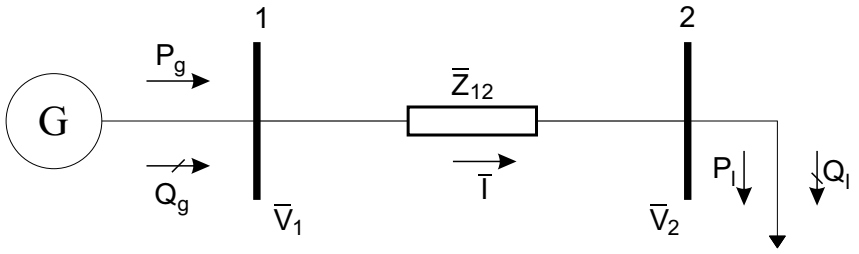

Figure 3.3: Two bus test system showing multiple power flow solutions. System data: $\bar{V}_1 = 1.0 \angle 0\,\text{pu}$, $\bar{Z}_{12} = \text{j}0.1\,\text{pu}$, $S_{BASE} = 100.0\,\text{MVA}$

addresses the convergence problem for the UEP, where a constant reduces the correction on iterations.

Table 3.1: Possible load flow solutions for system depicted in Figure 3.3.

Stable Equilibrium Point						
Bus	Voltage [pu]	Angle (°)	P_g MW	Q_g MVar	P_l MW	Q_l MVar
1	1.000	0.00	100.0	10.1	0.0	0.0
2	0.995	-5.77	0.0	0.0	100.0	0.0
Unstable Equilibrium Point						
Bus	Voltage [pu]	Angle (°)	P_g MW	Q_g MVar	P_l MW	Q_l MVar
1	1.000	0.00	100.0	989.9	0.0	0.0
2	0.102	-84.36	0.0	0.0	100.0	0.0

3.3.2 Voltage stability by the means of energy function

In power systems, energy function infers voltage stability condition by calculating the potential energy difference between the SEP and UEP of interest [93]. As the system moves towards the maximum load point, the energy difference diminishes until it reaches zero, where SEP and UEP merge into one solution [94,95]. Figure 3.4 shows the merging solutions as the system moves from P_1 towards P_{max}, where SEP and UEP coalesce at the critical point [96].

Based on the power flow equations and regarding the voltage stability issue, the potential energy difference between the SEP and UEP is calculated by [99]:

$$
\begin{aligned}
\upsilon(X^s, X^u) = &- \sum_{i=1}^{n} Q_i \ln \frac{V_i^u}{V_i^s} - \sum_{i=1}^{n} P_i \left(\theta_i^u - \theta_i^s\right) \\
&- \frac{1}{2} \sum_{i=1}^{n} \sum_{j=1}^{n} V_i^u V_j^u B_{ij} \cos\left(\theta_i^u - \theta_j^u\right) \\
&+ \frac{1}{2} \sum_{i=1}^{n} \sum_{j=1}^{n} V_i^s V_j^s B_{ij} \cos\left(\theta_i^s - \theta_j^s\right) \\
&+ \sum_{i=1}^{n} \sum_{j=1}^{n} V_i^s V_j^s G_{ij} \cos\left(\theta_i^s - \theta_j^s\right) \left(\theta_i^u - \theta_i^s\right) \\
&+ \sum_{i=1}^{n} \sum_{j=1}^{n} V_j^s G_{ij} \sin\left(\theta_i^s - \theta_j^s\right) \left(V_i^u - V_i^s\right),
\end{aligned}
\tag{3.8}
$$

where: $X^s = (\theta^s, V^s)$and $X^u = (\theta^u, V^u)$ are the system variables associated with the SEP and UEP respectively.

As the system moves toward P_{max}, $\upsilon(X^s, X^u)$ tends to zero. This way, the energy function value serves as a measure for calculating proximity to critical point. There is also the possibility of eliminating the sum along the index i and

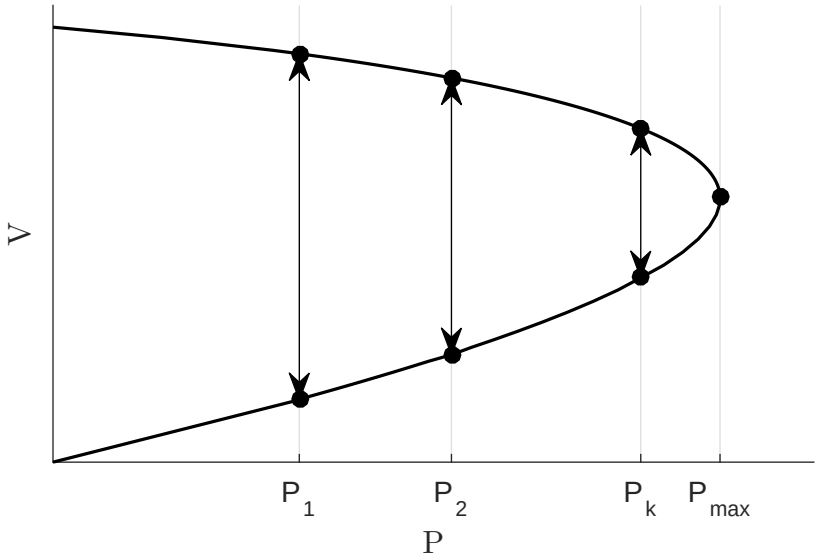

Figure 3.4: PV curve showing the merging solutions as system moves towards P_{max}, and the energy difference between SEP and UEP reduces.

extract from (3.8) the energy participation of each bus, thus identifying both vulnerable and strong areas. Equation (3.8) requires low voltage solutions for all buses and is an infeasible procedure for large scale systems [98, 100].

3.3.3 Proposed robustness areas evaluation

This research brings to the restoration field the robustness areas technique, by using an alternative EF proposed by De Lorenci et al. [62, 101, 102]. Extracting from (3.8) the contribution related to X^u for a bus i, and considering $j = 1, 2, \ldots, n, j \neq i$, one obtains:

$$\begin{aligned} E_p(X^s, X^u)_i = {} & Q_i \ln\left(V_i^u\right) + P_i\left(\theta_i^u\right) \\ & + \frac{1}{2}\sum_{\substack{j=1 \\ j\neq i}}^{n} V_i^u V_j^u B_{ij} \cos\left(\theta_i^u - \theta_j^u\right) \\ & - \sum_{\substack{j=1 \\ j\neq i}}^{n} V_i^s V_j^s G_{ij} \cos\left(\theta_i^s - \theta_j^s\right) \theta_i^u \\ & - \sum_{\substack{j=1 \\ j\neq i}}^{n} V_j^s G_{ij} \sin\left(\theta_i^s - \theta_j^s\right) V_i^u \end{aligned} \tag{3.9}$$

where: $E_p(X^s, X^s)_i$ is the Robustness Level (RL) for the i^{th} bus.

Equation (3.9) calculates RL of each bus i using the SEP state variables X^s, and a single UEP (X^u). Differently from the classical energy approach presented above, the robustness areas approach is not computational costly, because it needs only one LVS. The choice for the LVS uses the TV methodology, which indicates the critical bus [87].

3.3.4 Robustness areas visualization

This thesis proposes a visualization approach for the robustness areas by using heatmaps integrated with systems diagram. It consists in creating a background for systems diagram that shows each bus robustness level $E_p(X^s, X^u)$, according to a colour scale. This methodology has been presented on a published article [62] (see Annex A).

Creating such diagram requires mainly two sorts of data: $E_p(X^s, X^u)$ for each bus and buses coordinates on the diagram adopted. With this information, a grid is created with evenly spaced points on the x-y plane, while the z axis represents $E_p(X^s, X^u)$. Using this grid, the MATLAB function *contour* creates the heatmap. Finally, an image editing software places the diagram on the heatmap background forming the figures presented in [62] and in this thesis.

3.3.5 Using robustness areas tool for restoration planning

The proposed energy function calculates the robustness level for all system buses, regarding a specific operational point, hence it is possible to identify vulnerable areas and how wind power impact on them. The proposed methodology to assess wind power impact on PSRs using energy function can be summarized by [62,101]:

1. Calculate the operable power flow solution SEP (X^s);
2. At this operating point, determine the critical bus by using the TV;
3. Calculate the UEP (X^u) associated for the critical bus;
4. For each bus in the system, calculate its related RL using (3.9);
5. Group buses into areas, according to their robustness level, forming a heatmap diagram with $E_p(X^s, X^s)$ as the background;

6. Compare the proposed cases, and infer the wind power impact on the PSR under analysis.

3.3.6 Robustness areas validation

The validation of the robustness areas technique in restoration procedure is an important step since it assures the proposed methodology effectiveness. Because of the validation relevance, an article published in a journal [62] dedicates to it, and one can find it on Annex A.

This paper uses the robustness areas tool to investigate the current restoration procedure in Brazil, where improvements are proposed based on reinforcing vulnerable areas. The outcome is a system with higher stability indexes during restoration.

This paper also introduces the heapmap visualization approach, and applies it in part of the Brazilian power grid.

3.4 Proposed wind farm synchronization approach

Considering the angular stability and the frequency control issues surrounding the restoration field (see Chapter 1), a novel methodology is proposed for synchronizing WFs without jeopardizing system stability [103]. This project divides WFs synchronization procedure in three phases [103, 104], as follows:

Acceleration - During the acceleration phase, the turbine's controller removes the safety brakes and varies the pitch angle so **wind** accelerates generators up to their synchronization initial speed. For Fixed Speed Wind Generators (FSWGs) this is the synchronous speed, thus $s = 0$, while for Variable Speed

Wind Generators (VSWGs) this is the speed where active power dispatch is null, and it varies from one manufacturer to another.

Connection - During the connection phase, circuit breakers connect generators to the grid, hence, from this point on the WF has influence on the power system dynamics. This phase may have relevant impact on angular stability for FSWGs, due to angular variations provoked.

Power ramp - During the power generation phase, Wind Generators (WGs) increase their power dispatch, until P_{out} reaches operational level. This is the most influential phase for stability, on the account of the low spinning reserve provided by power plants and the fast power dispatch ramp wind generators provide.

3.5 Wind generator synchronization controllers

3.5.1 Active power control loop

This thesis proposes a control loop, aiming to mitigate the power ramp impact. It controls wind turbines' output power by controlling pitch angle's variation rate $\frac{\mathrm{d}\beta}{\mathrm{d}t}$, based on the turbines equations: (2.7) to (2.10). The maximum pitch angle variation rate $\Delta\beta_{max}$ is calculated by [105]:

$$\Delta\beta_{max} = \frac{\beta_0 - \beta_{ref}}{t_{rp}} \tag{3.10}$$

where: β_{ref} is the reference signal calculated by the control loop, β_0 is the initial pitch angle value calculated prior the simulation (later explained), and t_{rp} is the desired reconnection ramp time.

Figure 3.5 depicts the control loop, that limits $\frac{\mathrm{d}\beta}{\mathrm{d}t}$ by calculating dynamic limits for the pitch angle control [104]. For every simulation step, the routine

updates β_{min}^{dyn} and β_{max}^{dyn}, respecting the global minimum and maximum values. When the switcher moves from the fixed initial value β_0 to the reference angle β_{ref}, controller's action is limited, hence $\beta_{control}$ transition takes t_{rp} to shift to the reference value.

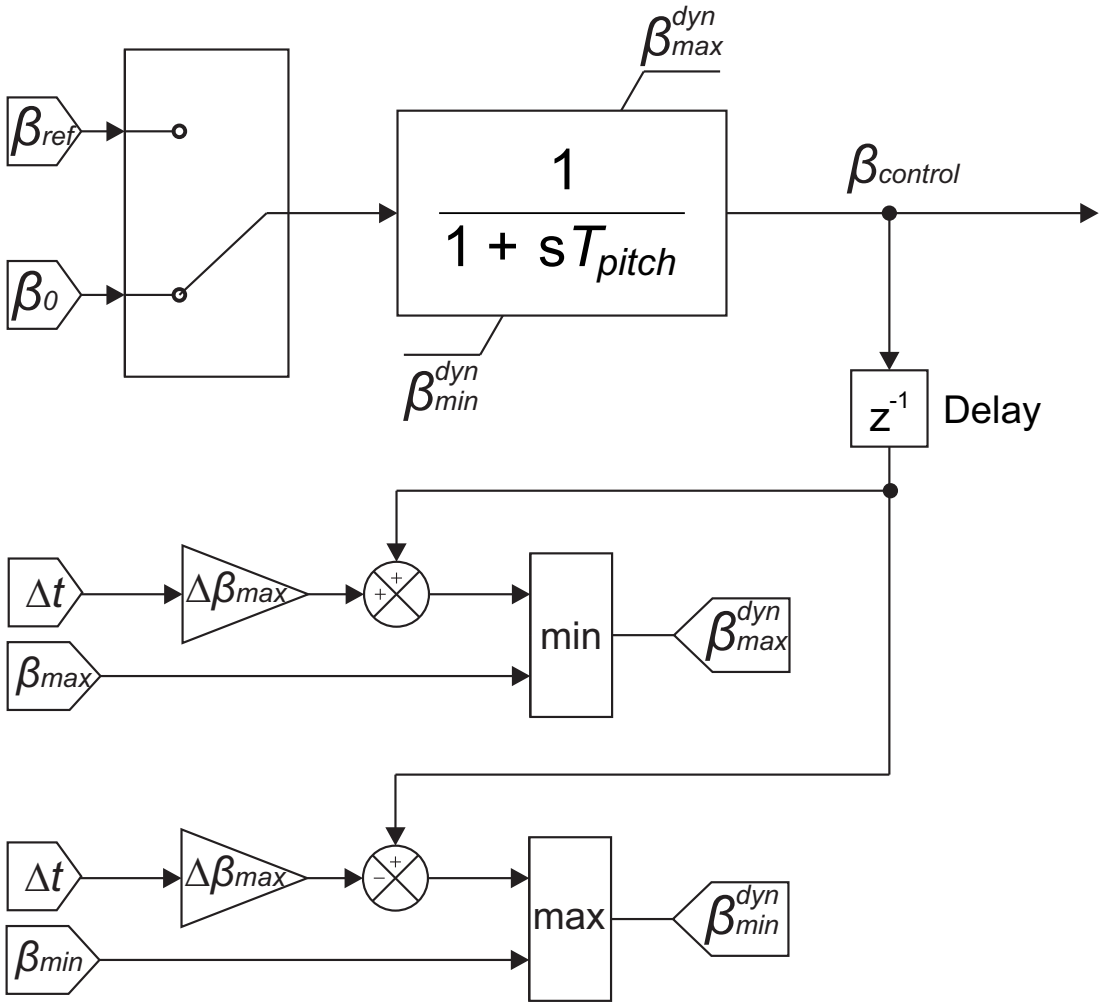

Figure 3.5: Wind turbine's blade pitch angle dynamic variation control. In this picture: β_{ref} is the reference signal calculated by the control loop, β_0 is the initial pitch angle value calculated prior the simulation, β_{min}^{dyn} and β_{max}^{dyn} are the minimum and maximum dynamic limits for the pitch angle respectively, β_{min} and β_{max} are the static limits for pitch angle, $\Delta\beta_{max}$ is the variation rate limit, Δt is the step length, T_{pitch} is the pitch control time constant, and $\beta_{control}$ is the pitch angle output signal from the proposed speed limiter.

The active power ramp time is calculated by a relation between the wind

farm's capacity and the restored power plants capacity, and is given by:

$$t_{min} = k_t \frac{P_{wf}}{P_{system}} \tag{3.11}$$

where, t_{min} is the minimum time for the ramp, k_t is the constant that dictates the ramp inclination, P_{wf} is wind farm's installed capacity, and P_{system} is the restored power plants capacity. This way:

$$t_{min} \leq t_{rp} \tag{3.12}$$

The value for constant k_t adopted in this thesis is $k_t = 0.005\,\text{s}$.

3.5.2 Reactive power control loop

This thesis proposes a reactive power control loop, which sets a voltage ramp for VSWGs. Figure 3.6 shows the loop which works by adding the ramp signal V_{rp} to the initial reference value V_0 to form the final reference voltage level V_{ref}. Two switches control the initial and final time, and a constant k_{rp} dictates signal's inclination [105]. k_{rp} is calculated by:

$$k_{rp} = \frac{V_0 - V_{final}}{t_2 - t_1} \tag{3.13}$$

where: V_{final} is the final voltage level set for the controlled bus, and V_0 is the bus voltage level prior the wind farm connection.

3.6 Proposed wind generator initialization routine

The previous section shows that the control loop requires an initial β_0. This comes from the fact that the wind turbine begins its operation on a point outside

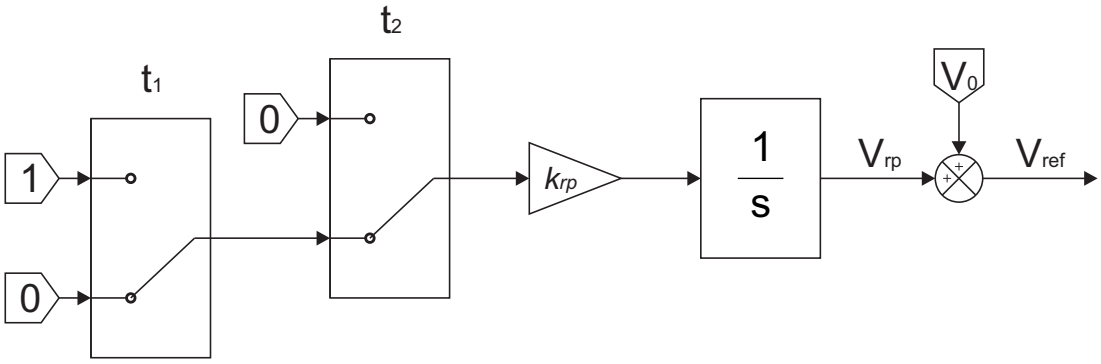

Figure 3.6: Wind generator's voltage level ramp control. In this picture: t_1 is the voltage ramp initial point, t_2 is the voltage ramp final point, k_{rp} is the slope constant, V_{rp} is the slope part of reference level, V_0 is the initial part of reference level, and V_{ref} is reference voltage level.

the optimal region, and the default initialization procedure does not work properly. Therefore, a novel initialization is presented, because wind turbines initial dispatch is very low, smoothly reaching the maximum power dispatch.

The starting line is the power flow calculation that returns the mechanical power applied to the generator's shaft. The initial electric power dispatch is null, however, due to losses there is a minimal torque required by the generator to maintain spinning during the connection phase. From the mechanical power, the coefficient of performance C_p is calculated by (see (2.7)):

$$C_p = \frac{2\ P_t}{A\ \rho\ v_w^3} \tag{3.14}$$

The second step depends on the wind generator's technology. FSWGs uses the induction machine slip s from the power flow to calculate the electrical speed by: $\omega_{el} = 1 - s$, where ω_{el} is the electrical frequency in pu. This procedure differs for VSWGs because these follow curves that relates the output power, and these curves vary from one manufacturer to another. Using ω_{el} the tip speed ratio λ is calculated according to:

$$\lambda = \frac{4\ \pi\ f_n\ \omega\ R}{N_p\ R_g\ v_w} \tag{3.15}$$

where: λ is the tip speed ratio, f_n is the rated frequency, R is the blade length, N_p is the number of poles, R_g is the gearbox relation, and v_w is the wind speed.

Having C_p and λ in hands, one can use (2.8) to calculate the initial pitch angle β_0. Due to equation's complexity, this thesis uses a numerical method to calculate the desired solution (see *fzero* function on MATLAB help [86].) The difference from this initialization method is that a pitch angle is calculated given the power dispatch and a wind speed, while default routines confider C_p as maximum as possible for the scenario, and calculate wind speed given the power dispatch.

3.7 Conclusion

This chapter details the proposed methodologies used to simulate and assess power system restorations performance using wind power. The combined MATLAB-Fortran routine overcomes the high computational costs associated to stochastic simulations by using parallel processing that allows a number of computer processors to share a long task, and especially by programming the load flow and energy function routine in a lower level language.

The robustness areas approach is presented as a powerful tool to infer stability condition during restorations, and promoting positive impacts on dynamic stability. The heatmaps visualizations for this tool is useful in identifying vulnerable areas that can jeopardize system stability condition during restorations. Such approach validation has been published on a peer-reviewed journal, as one can see in Annex A [62].

The WFs reconnection methodology refers to the angular and frequency stability problem recurrent on restorations [1], as presented in the introductory chapter. A control loop is used to limit pitch angle variation "speed" and implemented on

the models used in this thesis [33].

The conditions regarding restoration makes wind turbines' default initialization routine infeasible. Hence, a novel calculation is presented to set wind turbines out of their optimal range for the connection phase, and later smoothly seek the maximum power dispatch by using the proposed control loop.

Finally, the next chapters show the proposed assessment methodology applied to the IEEE 30 bus system and part of the Brazilian power grid, where wind power used for restorations purposes is a novelty.

Chapter 4

IEEE 30 bus system restoration

4.1 The IEEE 30 bus system restoration

The IEEE 30 bus system is a benchmark for power system stability studies, where one can find its data online on [106]. Figure 4.1 depicts the IEEE 30 bus system along with its restoration plan. This thesis presents the system with two main power plants, where the power plant at Bus 1 is modelled as a hydro power plant, while the power plant at Bus 2 is modelled as a gas turbine (Brayton cycle) power plant. This combination is recurrent on Power System Restorations (PSRs) due to the ability of both technologies to perform short term black-start [107]. This combination also aims to emphasize different time responses during restorations that compel power plants to operate out of the region for which their controllers are tuned [108].

The wind farms included in this system sum 30 MW, where 25 MW is installed at Bus 31, while 5 MW is installed at Bus 13. This distribution is based on the synchronous condensers replaced by the wind farms. Bus 31 is an extra node which enables wind farm's inclusion. Authors in [109] proposes the restoration plan, which this thesis adopts for analysis and presents on Table 4.1.

Three steps from Table 4.1 are selected for analysis: Step 15, Step 21, and Step

Table 4.1: IEEE 30 Bus system restoration. Source: [109].

Step	Description	Previous step	$\Delta\ t_c$ [s]
1	Start		
2	Energize Bus 1	1	
	→ Maintain V=1.000 pu		30
3	Energize line 1→2	2	30
4	Energize Bus 2	3	
	→ Maintain V=0.990 pu		30
	→ Restore 12 MW		60
	→ Restore 10 MW		60
5	Energize line 2→4	4	30
6	Energize Bus 4	5	
	→ Restore 4 MW		60
7	Energize line 2→5	6	30
8	Energize Bus 5	7	
	→ Restore 20 MW		60
	→ Restore 20 MW		60
9*	Energize transf. 5→31	8	
10*	Energize Bus 31	9	
	→ Restore wind farm		60
	→ Maintain V=0.980 pu		
11	Energize line 2→6	10	30
12	Energize Bus 6	11	
13	Energize line 6→7	12	
14	Energize Bus 7	13	
	→ Restore 10 MW		
15	Close loop buses 7→5	30	
16	Energize transf. 4→12	15	
17	Energize Bus 12	16	
	→ Restore 5 MW		60
18*	Energize transf. 12→13	17	
19*	Energize Bus 13	18	
	→ Restore wind farm		60
	→ Maintain V=0.985 pu		
20	Energize line 12→14	19	30
21	Energize Bus 14	20	
	→ Restore 3 MW		60
22	Energize line 6→28	21	30
23	Energize Bus 28	22	
24	Energize transf. 28→27	23	
25	Energize Bus 27	24	
26	Energize line 27→30	25	30
27	Energize Bus 30	26	
	→ Restore 5 MW		60
28	Finish	27	

* Steps included to restore wind farm

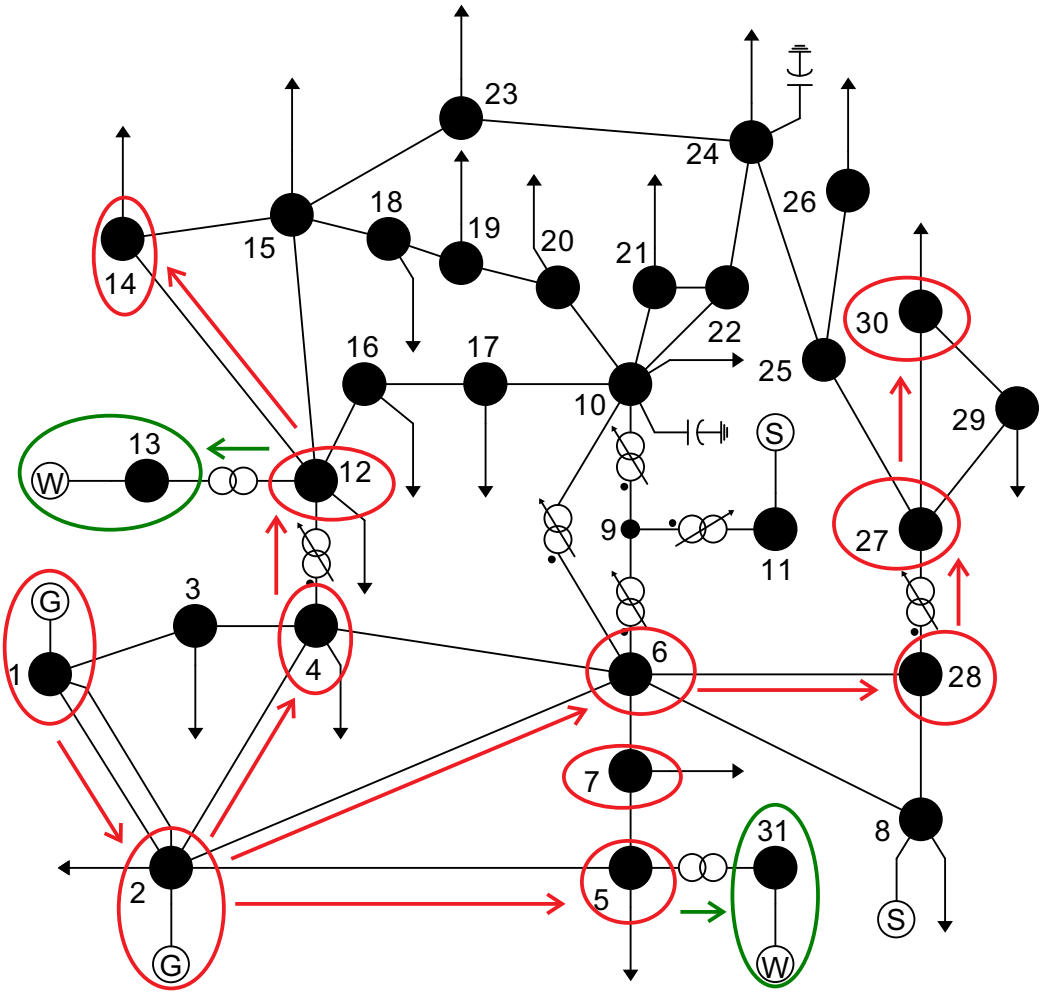

Figure 4.1: Increased IEEE 30 bus system diagram with restoration path highlighted. The green path indicates the steps for restoring wind farms.

27. Step 15 is selected because it represents the completion of the main higher voltage system restoration, including the main load buses in this area, while Step 21 and Step 27 show terminal areas restoration. Simulations are performed for the base case, Fixed Speed Wind Generator (FSWG) case and the Variable Speed Wind Generator (VSWG) case.

Table 4.2 presents the boundaries for frequency and voltage level, where it shows different limits that are set for transient and steady state period, where the transient period adopted is: $t_{trans} \leq 60\,\text{s}$. It is worth noting that these limits

are usually broader than regular operation, due to the emergency involved.

Table 4.2: Frequency and voltage level limits for IEEE 30 bus restoration.

	Frequency	Voltage
Transient	±2 Hz	±15 %
Steady State	±1 Hz	±10 %

4.2 Power flow and robustness areas analysis for the presented restoration plan

Addressing the stochastic nature of wind speed, a sample size of 5000 wind speed profiles are used as input for the proposed analysis tool. It is worth noting that Wind Farms (WFs)' wind speed are completely independent from each other, since it is assumed that they are far enough so no correlation is observed. The Weibull parameters adopted are collected from a weather station in Campbeltown - Scotland [110], where: $a = 6.4307\,\mathrm{m/s}$, and $b = 1.7643$. Power flow results are saved and indexes of collapse are presented.

The first index used to assess the proposed restoration is the reactive power load margin ΔQ. Six buses are selected for reactive power margin calculation, due to computational limitations: 4, 5, 6, 14, 28, 30.

Figure 4.2 shows ΔQ calculated for the buses on the Step 15 of restoration. It is possible to observe that all three cases (base case, FSWG, and VSWG) present small differences on ΔQ level for the tested buses. This behaviour, in fact, manifests for Step 21 and Step 27 presented in Figure 4.3 and Figure 4.4 respectively.

The load margin λ results in Figure 4.5 indicate an enlarged λ for the VSWG case and a reduced λ for the FSWG case, if compared to the base case. Take into account that both wind power cases are tested with the same wind replicates, and they only differ on the ability to control reactive power, one can conclude that this

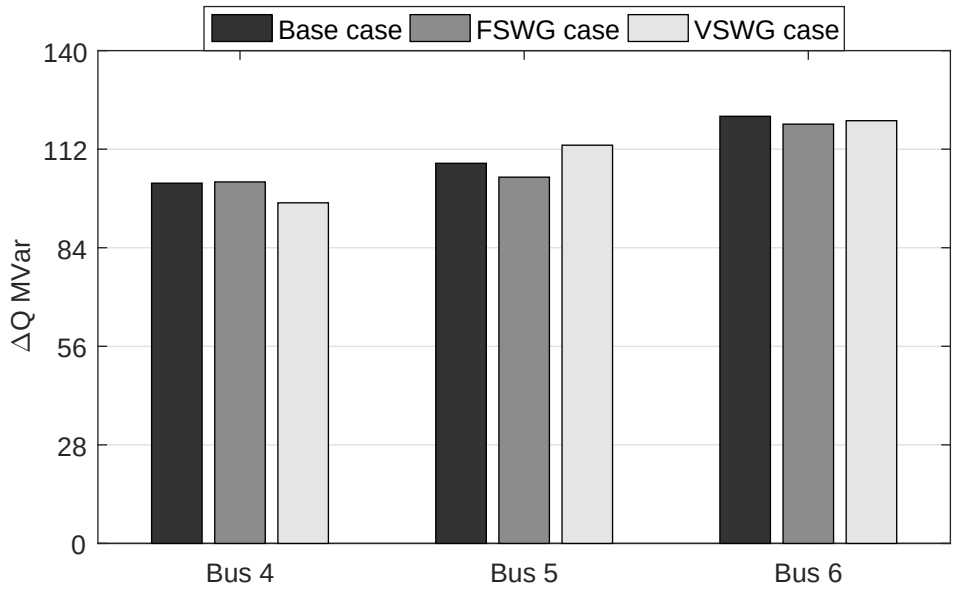

Figure 4.2: Reactive power margin for Step 15 completed according to the IEEE 30 Bus system restoration plan presented in Table 4.1.

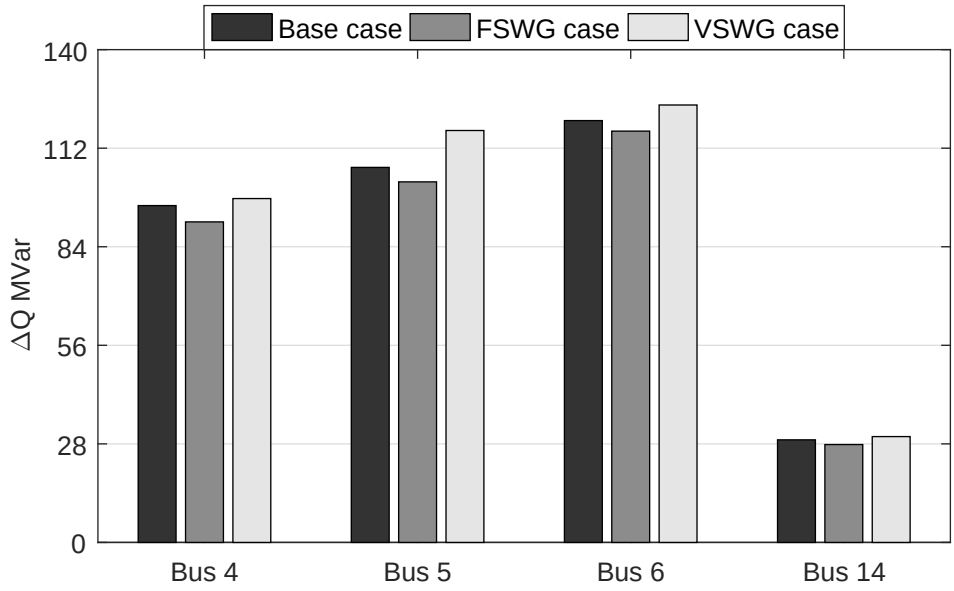

Figure 4.3: Reactive power margin for Step 21 completed according to the IEEE 30 Bus system restoration plan presented in Table 4.1.

is the VSWG's advantage. Thus, results show the importance of reactive power control and how it influences system stability. Tangent Vector (TV) norm in

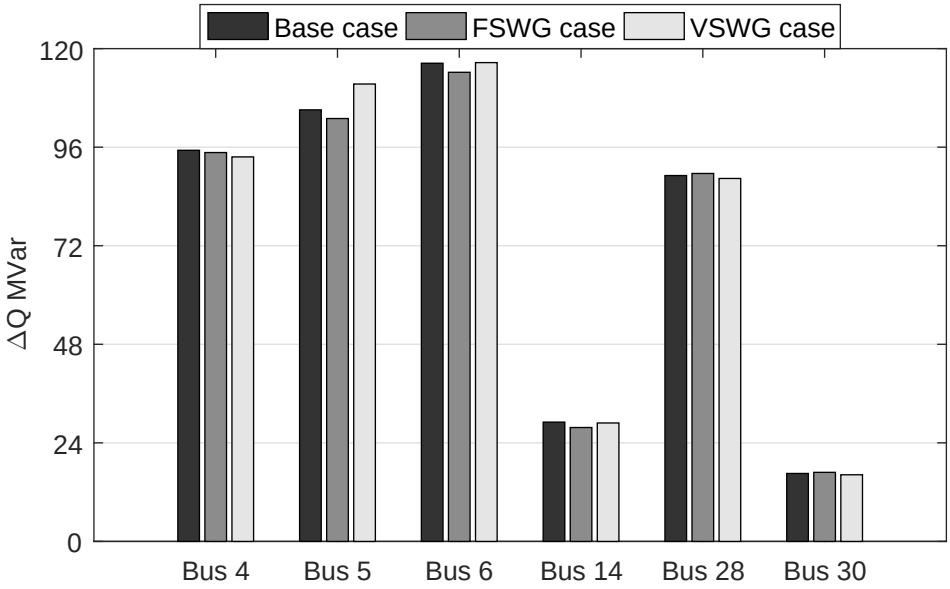

Figure 4.4: Reactive power margin for Step 27 completed according to the IEEE 30 Bus system restoration plan presented in Table 4.1.

Figure 4.6 shows similar results as the load margin simulations, in which VSWG case reduces sensitivity for load variations.

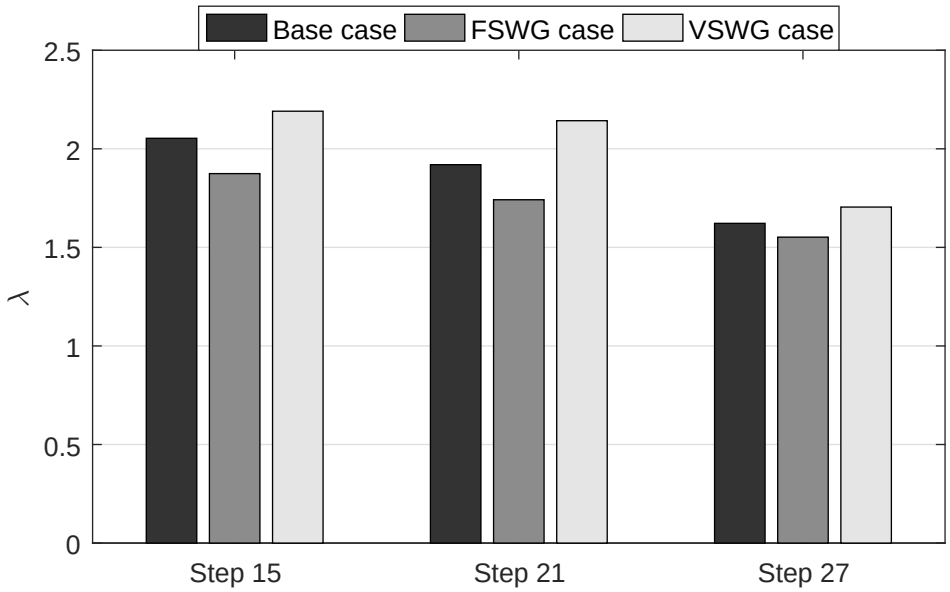

Figure 4.5: Load margin λ calculated for IEEE 30 Bus system.

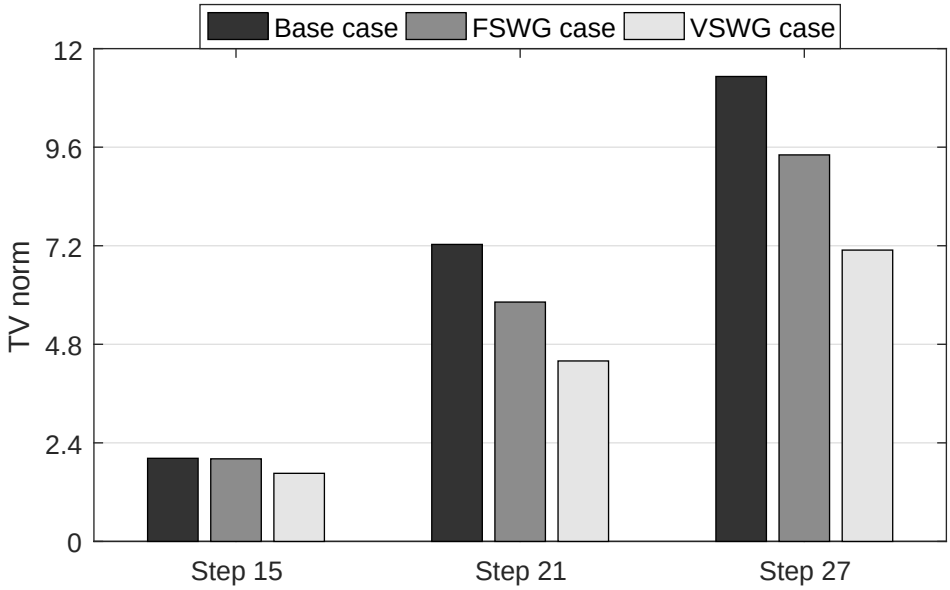

Figure 4.6: Tangent vector norm calculated for IEEE 30 Bus system.

Despite the fact that reactive power control is the most influential feature for WFs, active power also influences the system's stability. Figure 4.7 depicts λ distribution as a function of total wind power dispatch where trends emerge. The operational region corresponding to the VSWG case shows λ enlargements for positive increments in active power dispatch along the entire range of P_{wind}. FSWG case shows different response, where λ loses sensitivity to wind power variations within the region: $18\,\text{MW} < P_{wind} \leq 30\,\text{MW}$. Despite the fact that the average load margin for the FSWG case is lower than the base case, the system experiences points where $\lambda_{FSWG} > \lambda_{Base}$. Therefore, the ability to perform restoration using wind power can be associated to the weather conditions.

4.2.1 Robustness areas analysis

The investigation on IEEE 30 Bus robustness areas is performed by the proposed energy function tool [62] described by (3.9). This system analysis caries on by using the $E_p(X^s, X^u)$ levels of each bus defining the diagram background colours.

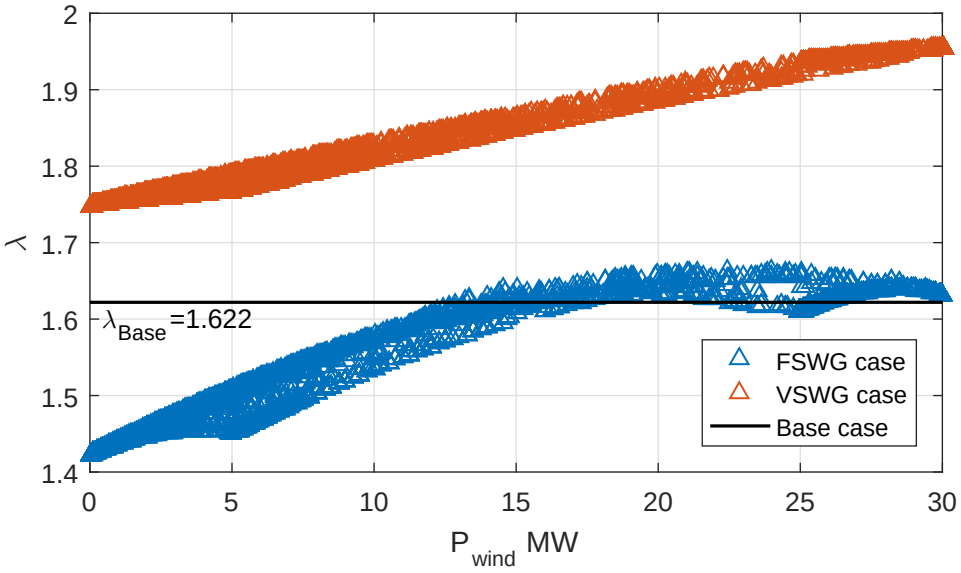

Figure 4.7: λ distribution as function of total wind power dispatch for Step 27 according to the IEEE 30 Bus system restoration plan presented in Table 4.1.

The power flow results are placed on Table C.1 to Table C.3 (Appendix C), where Stable Equilibrium Point (SEP) and Unstable Equilibrium Point (UEP) solutions are presented.

Figure 4.8 presents a graphical representation of $E_p(X^s, X^u)$, where buses are grouped within robustness level. In summary, each bus has a background colour representing its $E_p(X^s, X^u)$ value, where low $E_p(X^s, X^u)$ and high $E_p(X^s, X^u)$ indicates vulnerable and robust areas, respectively. Non-connected equipments are depicted in a light shade of gray and no $E_p(X^s, X^u)$ is associated to them, while connected equipments and buses are in black colour and the correspondent energy level associated dictates their background colour and surroundings areas.

The analysis from Appendix C and Figure 4.8 shows a vulnerable area covering Bus 14, Bus 27 and Bus 30 for all proposed cases. This result points out the difficulty this system experiences in transmitting power to its lower voltage area, especially during restoration that it operates in emergency conditions. The philosophy of restoring lower voltage level systems is used during PSRs to deal

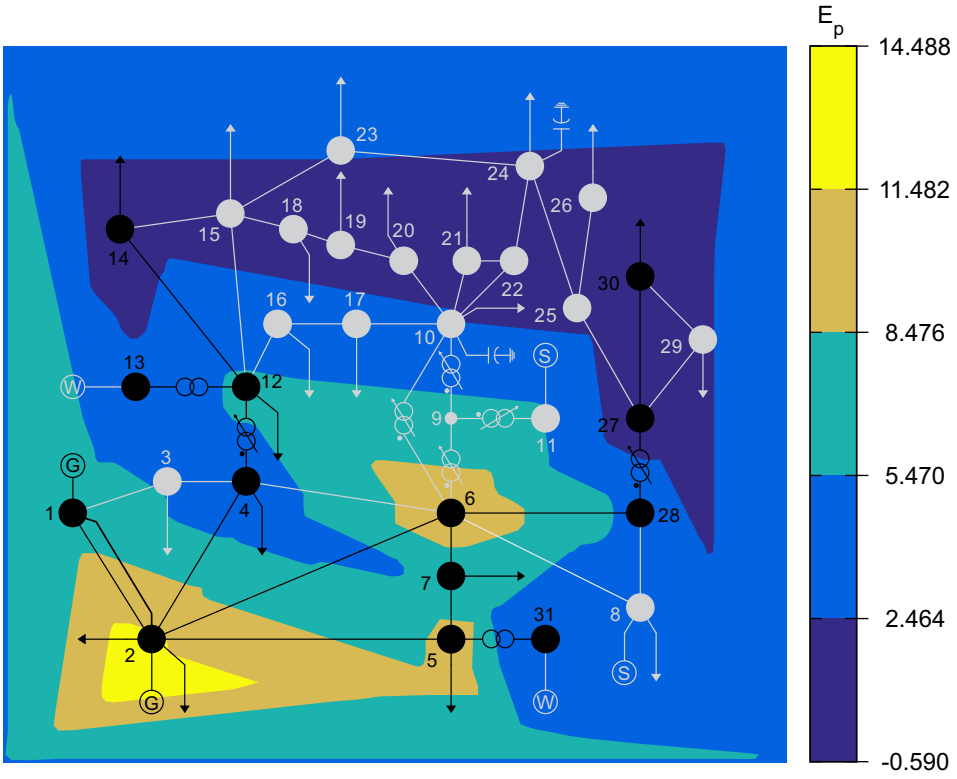

(a) Base case.

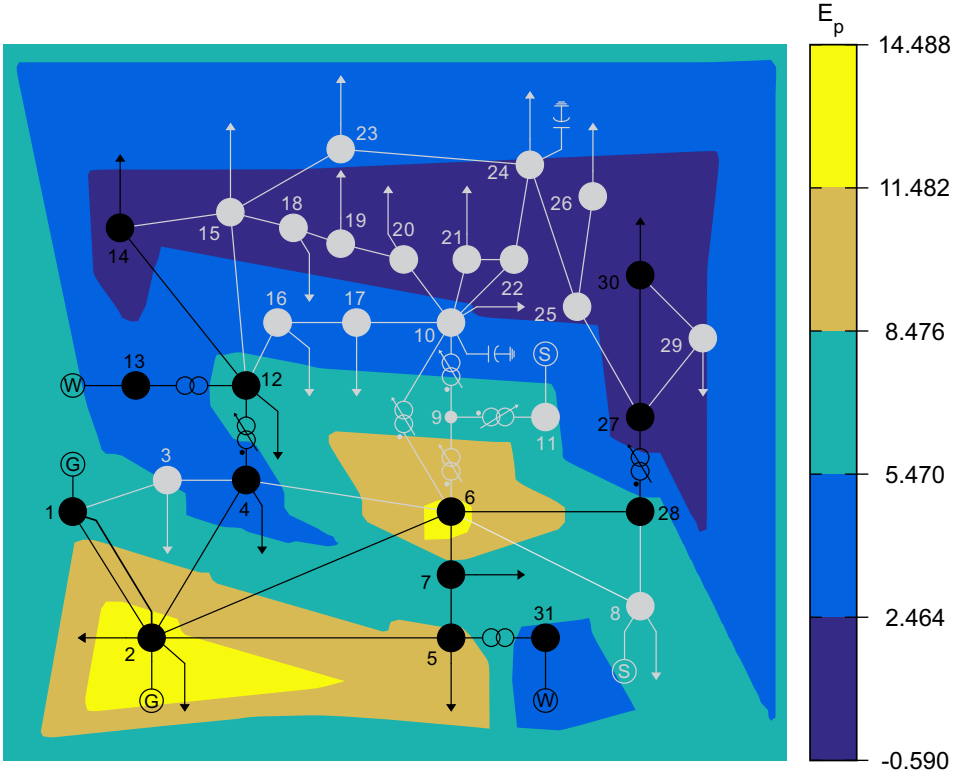

(b) FSWGs.

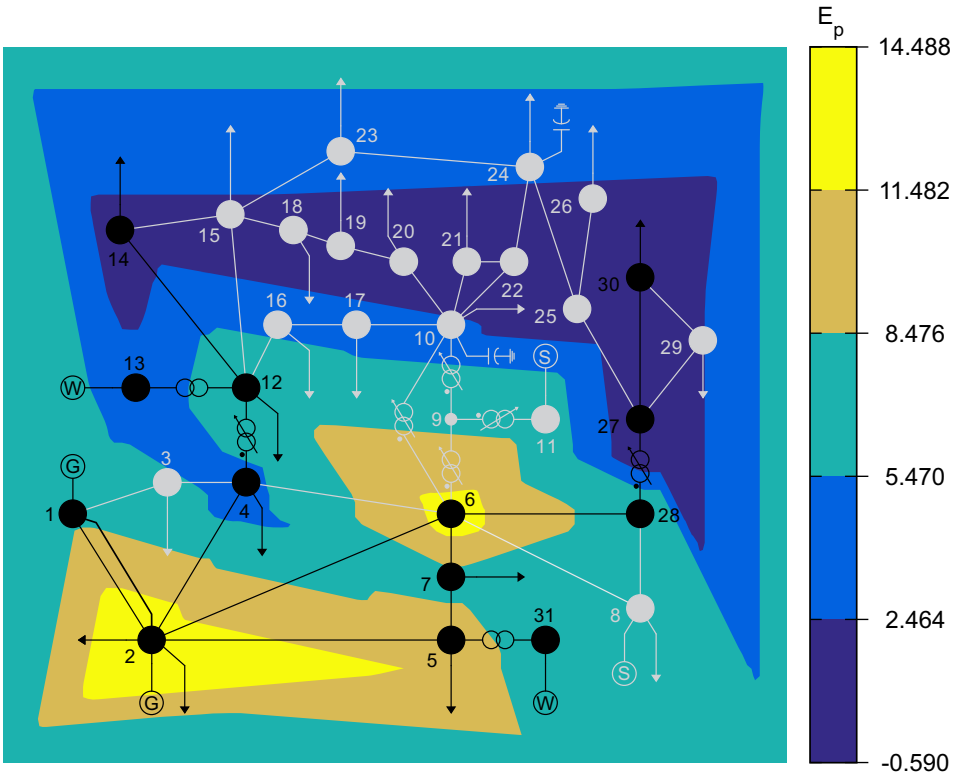

(c) VSWGs.

Figure 4.8: Robustness areas diagram for the IEEE 30 bus system. The background colour indicates $E_p(X^s, X^u)$ level of each bus, where high $E_p(X^s, X^u)$ represents robust buses and low $E_p(X^s, X^u)$ vulnerable buses.

with reactive power of unloaded transmission lines [43, 44]. However, it can lead to stability issues, as the energy function points out.

For the IEEE 30 bus system, the main obstacle in transmitting power are the system transformers. They impose a high reactance level, creating a "bottle neck" that is presented by the robustness areas tool as two distinctive areas.

The usage of wind power to assist the IEEE 30 Bus restoration leads mainly to local $E_p(X^s, X^u)$ improvements rather than to global improvements. The robustness areas tool shows similar results between the wind power cases, showing that this methodology is less sensitive to reactive power control than the indexes of collapse. This way, $E_p(X^s, X^u)$ presents a different point of view, that in fact relates to the ability in transmitting power, aggregating information for the

stability analysis.

4.3 Dynamic stability studies for the presented restoration plan

The cases proposed for dynamic stability studies are: the WF synchronization at Bus 31, and a load shedding at Bus 5. The former investigates the synchronization methodology as discussed in the previous chapter, the latter is a recurrent problem during PSRs that leads to stability issues [109]. The time domain simulations carries out by using the simulation parameters presented in Table 4.3.

Table 4.3: Time domain simulation parameters for the IEEE 30 bus system.

Parameter	Value
Integration step	1.0 ms
Output frequency	5
Simulation time	Variable
Simulation Software	ANATEM®
Loads composition	$0.5\mathrm{Z_{cst}} + 0.0\mathrm{I_{cst}} + 0.5\mathrm{P_{cst}}$

4.3.1 Wind farm at Bus 31 synchronization

The first step is to use the initialization routine to calculate initial β_0 for the given wind speed: $v_w = 10\,\mathrm{m/s}$. This way the calculated initial pitch angles are: FSWG $\beta_0 = 0.245\,\mathrm{rad}$, and VSWG $\beta_0 = 0.500\,\mathrm{rad}$.

Figure 4.9 depicts the IEEE 30 bus system wind farm synchronization procedure as presented in the previous chapter. The WF connects to the grid at $t_s = 5\,\mathrm{s}$, and it is followed by 15 s coordination time for voltage adjustments ($t_1 = 10\,\mathrm{s}$ and $t_2 = 20\,\mathrm{s}$ for the voltage control ramp). Finally, the pitch angle β control provides a smooth variation is set for 20 s range, which avoids excessive solicitations on the turbine's structure and mitigates system frequency variation.

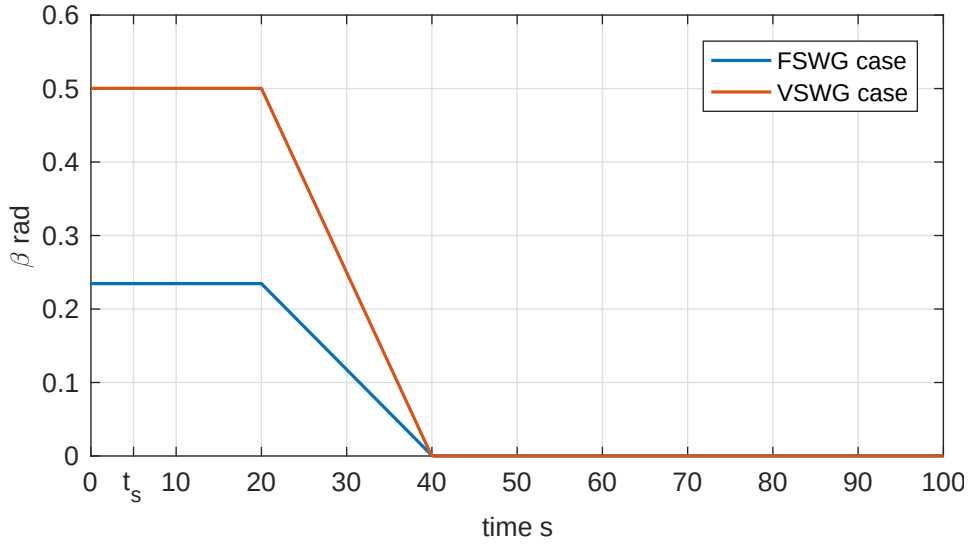

Figure 4.9: Wind turbine's blades pitch angle β demonstrating the proposed controller action for the wind farm at Bus 31 on the IEEE 30 Bus system. t_s stands for the synchronization time.

Wind farms' active power dispatch curves show the different response between the FSWG and the VSWG, as depicted in Figure 4.10. The FSWG case presents an initial transient that shortly neutralizes, and a direct correlation to β is seen, as it aims to the optimal point for the wind profile provided. The VSWG case does not present any significant initial transient, due to the inverter ability to decouple the machine from the grid. It is worth noting that any transient here mentioned is related to electromechanical time frame, hence fast transients (such as electromagnetic) can be neglected for this analysis.

Figure 4.10 shows that the FSWG case has a P_{out} that is almost a straight ramp, while the VSWG case's P_{out} has a more complex response, due to the VSWG's controller that has a dual control, simultaneously adjusting β and the rotor speed. This dual control makes the synchronization procedure slightly slower for the proposed scenario, though this control methodology is what enables VSWGs to operate with higher efficiency.

WFs reactive power export Q_{out} shows how each case behaves during

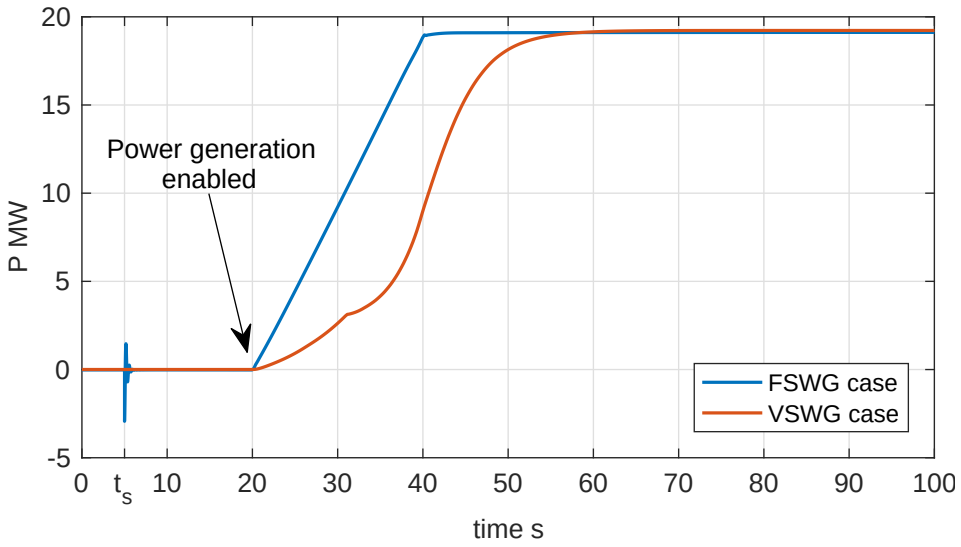

Figure 4.10: Wind farm active power output P_{out} in the event of the synchronization of the wind farm at Bus 31. The point where the power generation is enabled indicates the instant where the proposed controller is activated.

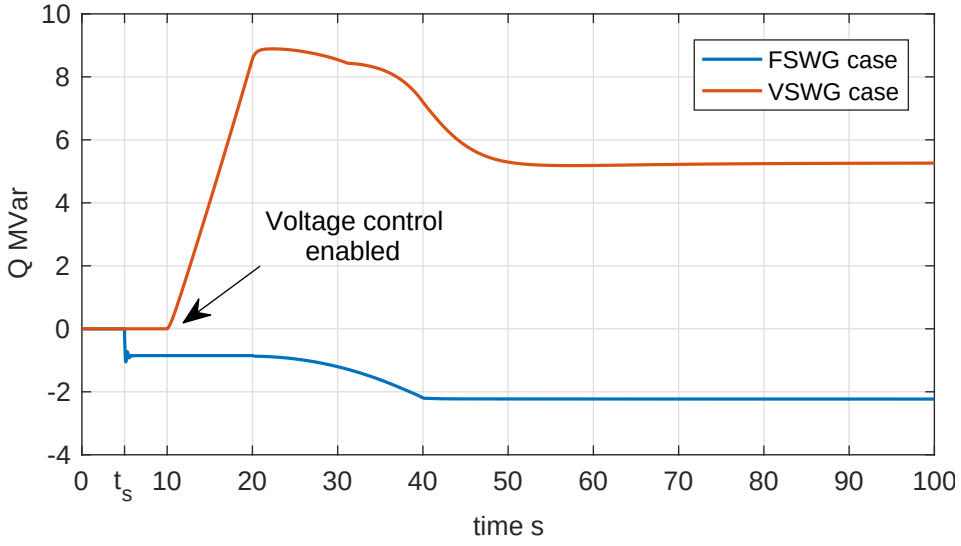

Figure 4.11: Wind farm reactive power output Q_{out} in the event of the synchronization of the wind farm at Bus 31. The point where the voltage control is enabled indicates controller's t_1.

synchronization. Figure 4.11 depicts Q_{out} that for the FSWG case, where one can see a sudden Q_{out} drop on the instant of synchronization t_s, due to the generator windings reactive power demand. The Q_{out} value for the VSWG does not present any significant response on t_s, however, it presents a controlled ramp, as the proposed voltage control takes place.

Q_{out} strongly relates to voltage level response on Bus 31 V^{31}, as Figure 4.12 depicts. One can observe the VSWG's ability in control voltage level for $t > 20\,\mathrm{s}$, where no significant voltage variation occurs. The FSWG case, however, shows that P_{out} variations influences voltage level, due to reduction on power flowing along the transmission lines. This effect can turn into a problem during PSRs that recurrently face overvoltage scenarios [4]. Despite variations, both cases maintain voltage level within acceptable range, as proposed on Table 4.2.

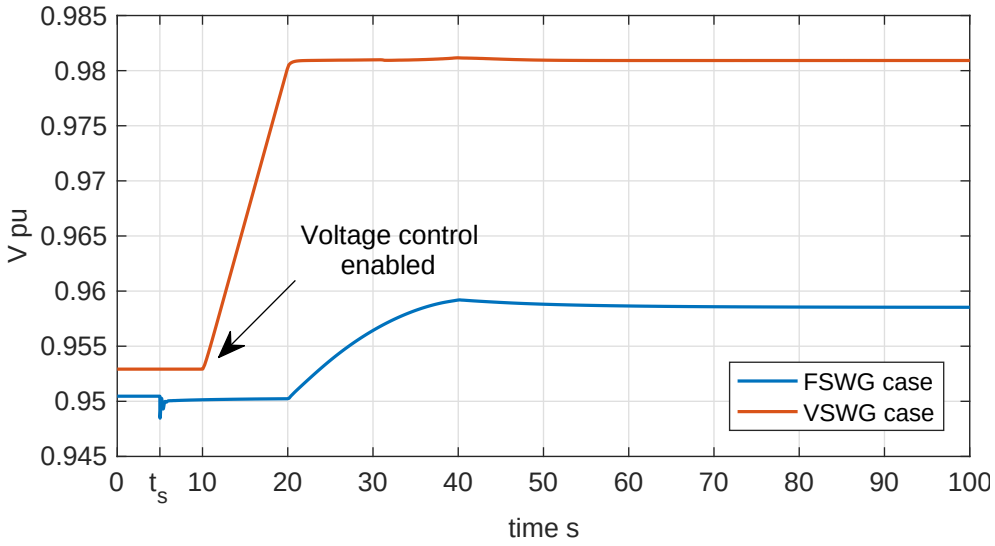

Figure 4.12: Voltage level at wind farm terminals in the event of the synchronization of the wind farm at Bus 31. The point where the voltage control is enabled indicates controller's t_1.

Three main variables investigates wind power impact on restoration: mechanical power P_{mec}, accelerating power P_{ac}, and rotor frequency f.

Figure 4.13 and Figure 4.14 show P_{mec} delivered by the Bus 1 and Bus 2 tur-

bines respectively. P_{mec} curves show the impact caused the wind power synchronization, thus demonstrating the proposed pitch angle control's relevance. Because Bus 1 is modelled as Vθ and has a secondary frequency control, for $t > 40\,\mathrm{s}$ Bus 1 slowly restore system's frequency to the rated value by controlling P_{mec}.

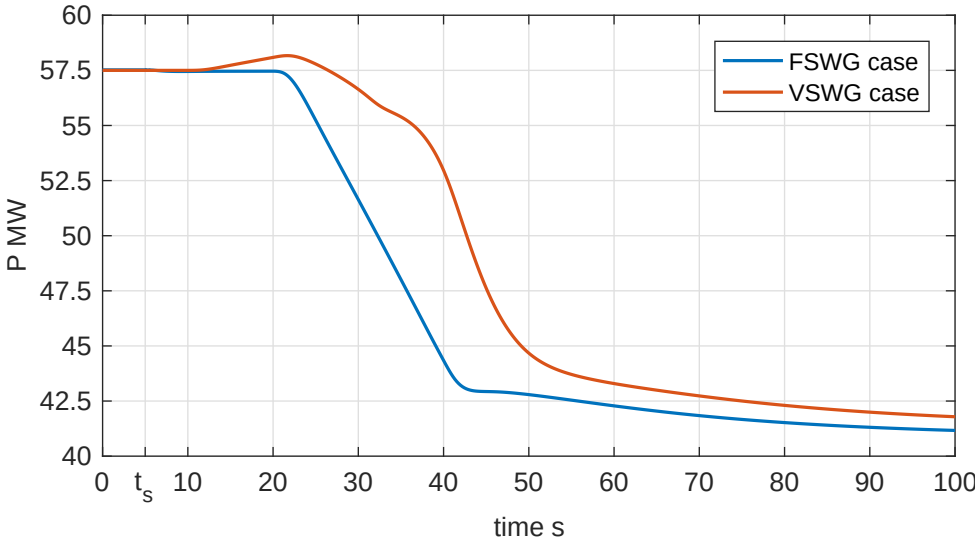

Figure 4.13: Mechanical power P^1_{mec} generated by the power plant at Bus 1 in the event of the synchronization of the wind farm at Bus 31.

Figure 4.15 and Figure 4.16 depicts accelerating power curves P_{ac} for Bus 1 and Bus 2 respectively.

On the instant of connection, one can see the transient caused by FSWGs, while the VSWG case shows no significant transient. During the power dispatch phase, where WF's P_{out} increases, machines' P_{ac} remain on the positive side, as controllers keep adjusting system's frequency. This scenario changes after power ramp has concluded and frequency control reduces machines' dispatch. The different responses between the two cases is a consequence of their power dispatch characteristics during synchronization.

Wind farms' synchronization procedure directly affects the grid's frequency f_{grid}, where Figure 4.17 shows Bus 1 rotor frequency which is used to represent f_{grid}. One can see that the synchronization procedure causes a f_{grid} overshoot,

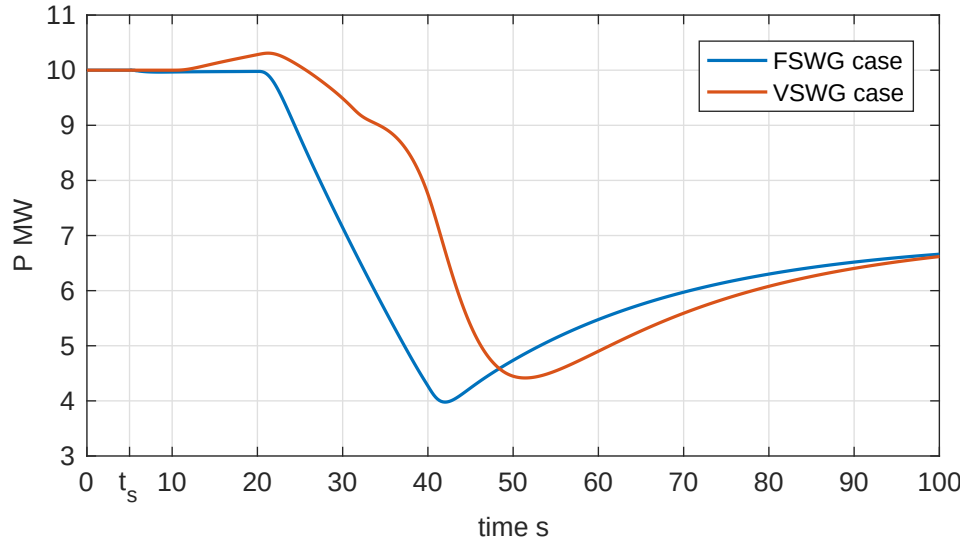

Figure 4.14: Mechanical power P^2_{mec} generated by the power plant at Bus 2 in the event of the synchronization of the wind farm at Bus 31.

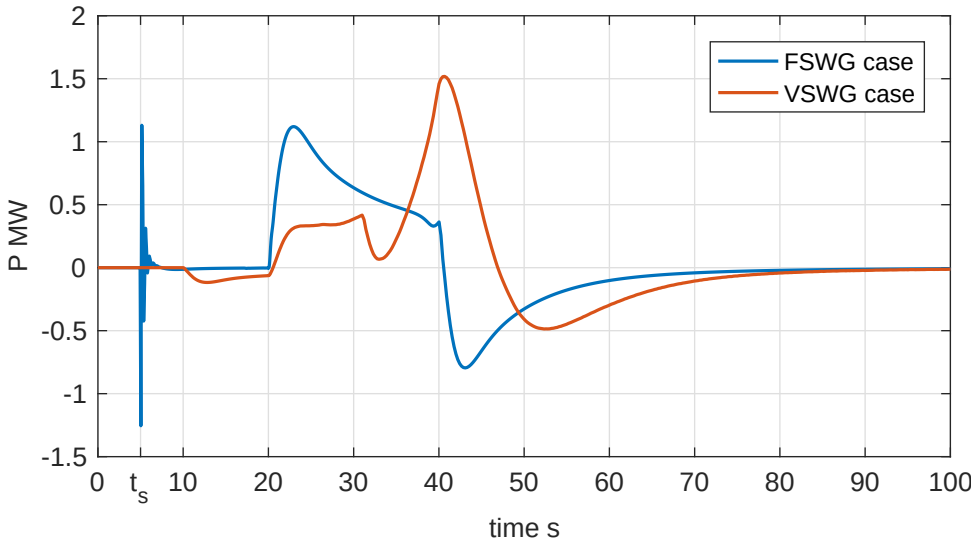

Figure 4.15: Accelerating power P^1_{ac} at Bus 1 in the event of the synchronization of the wind farm at Bus 31.

though within proposed limits, showing pitch angle's limiter influence.

As mentioned earlier, Bus 1 power plant is equipped with hydro Generator Units (GUs) while Bus 2 has gas cycle GUs. In general, water turbines are slower

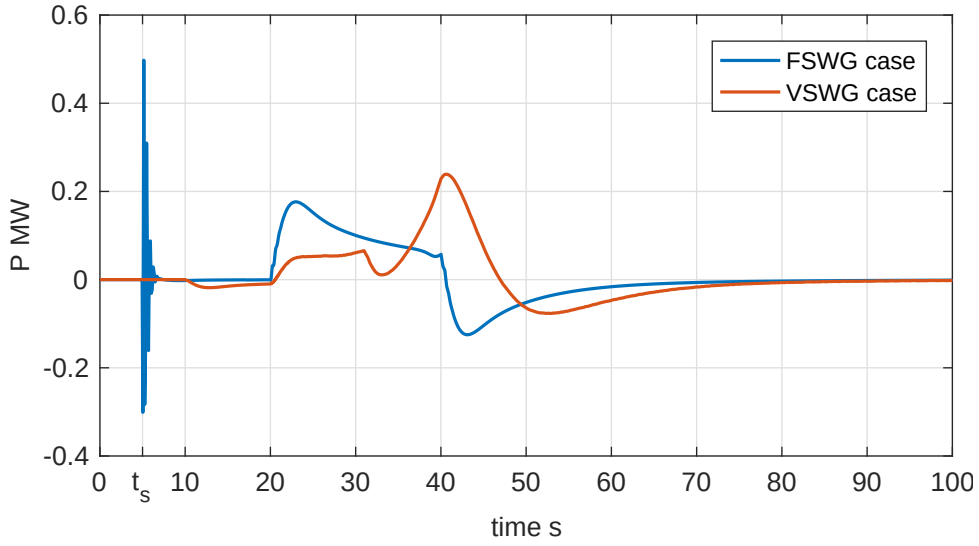

Figure 4.16: Accelerating power P_{ac}^2 at Bus 2 in the event of the synchronization of the wind farm at Bus 31.

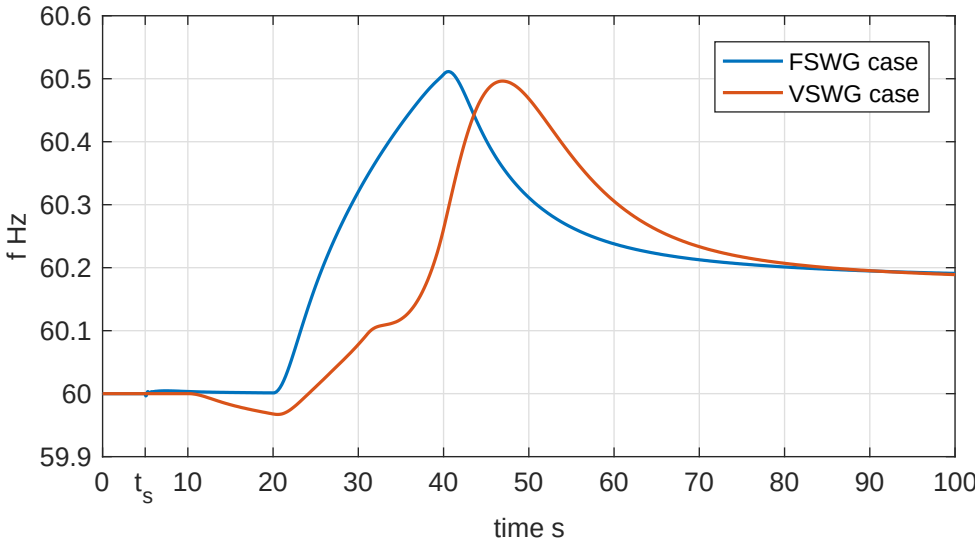

Figure 4.17: Bus 1 power plant frequency response f^1 representing grid frequency f_{grid} in the event of the synchronization of the wind farm at Bus 31.

than thermal machines in the event of dispatch variations, because of the water inertia inside the penstock [32, 33].

Figure 4.18 presents Bus 2 rotor angle, using Bus 1 and angular reference,

denoted in the form of a two-index notation $\delta_{2\text{-}1}$. From the angular stability point of view, the wind farm synchronization has low impact on machines' rotor angle, as $\delta_{2\text{-}1}$ varies in a few degrees.

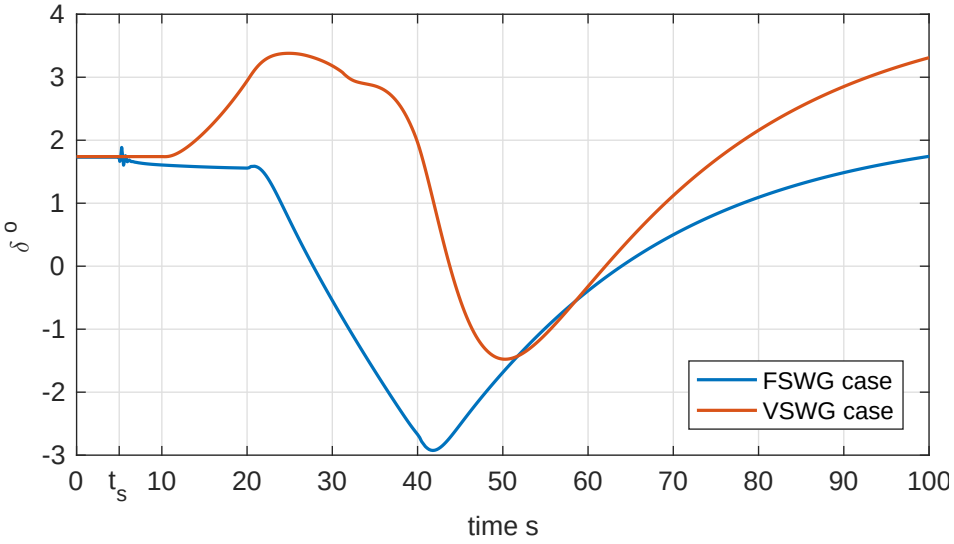

Figure 4.18: Bus 2 rotor angle in relation to Bus 1 rotor $\delta_{2\text{-}1}$ in the event of the synchronization of the wind farm at Bus 31.

4.3.2 Load shedding at Bus 5

The second scenario for analysis is a load shedding at Bus 5. Load shedding is a recurrent problem during restoration [4], usually caused by protective system (undue) action. This event leads to a series of issues that must be addressed during the background studies, such as: sustained overvoltage levels, frequency increase, minimum stable load, and angular stability issues. This way it is possible to investigate the wind power influence on a high impact event.

This scenario sheds 50% of the entire Bus 5 load, where t_s stands for the load shedding time. The analysis performs time domain simulations, in 40 s time frame. Figure 4.19 presents Bus 5 active power load, where minor emerges for the load variation, due to load voltage sensitivity. Figure 4.20 depicts Bus 5

voltage level V^5, where curves show acceptable voltage variations for transient and steady state period. The VSWG case presents reduced voltage variation, due to the reactive power control effect.

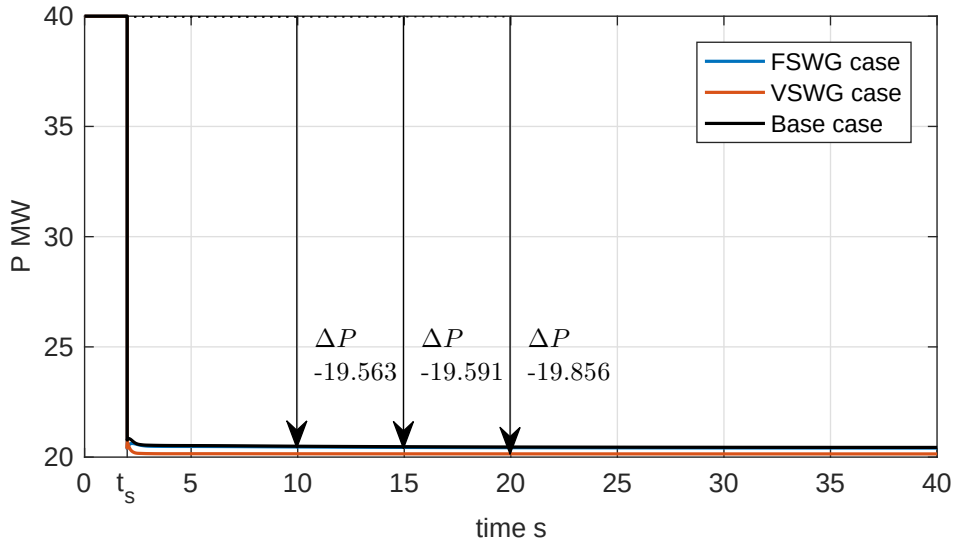

Figure 4.19: Bus 5 load demand P_l^5 in the event of the load shedding at Bus 5. t_s stands for the load shedding time.

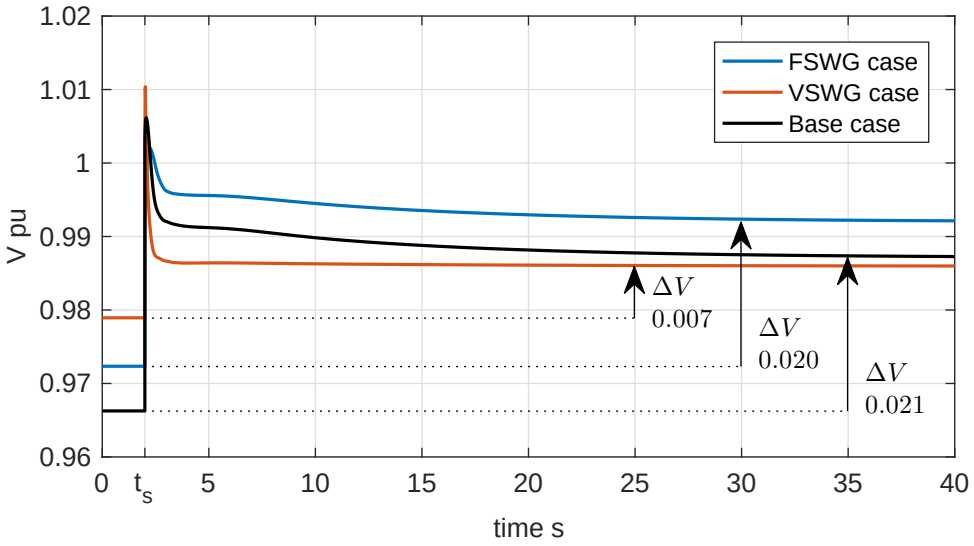

Figure 4.20: Bus 5 voltage level V^5 in the event of the load shedding at Bus 5.

Figure 4.21 to Figure 4.24 depict WFs dispatch for the event, where P_{out} and

Q_{out} for Bus 31 and Bus 13 are presented.

P_{out} curves show the inertia provided by FSWG, where P_{out} reduces while system frequency is increasing. As the load sheds in Bus 5, the transmission system is pushed to a new scenario where capacitance effect is predominant. Figure 4.22 shows this fact, where Bus 31 Q_{out}^{31} has a large excursion, in an attempt to avoid voltage variations along the system. Scenarios similar to this can make WFs to reach their thermal capacity, leading to loss of voltage control.

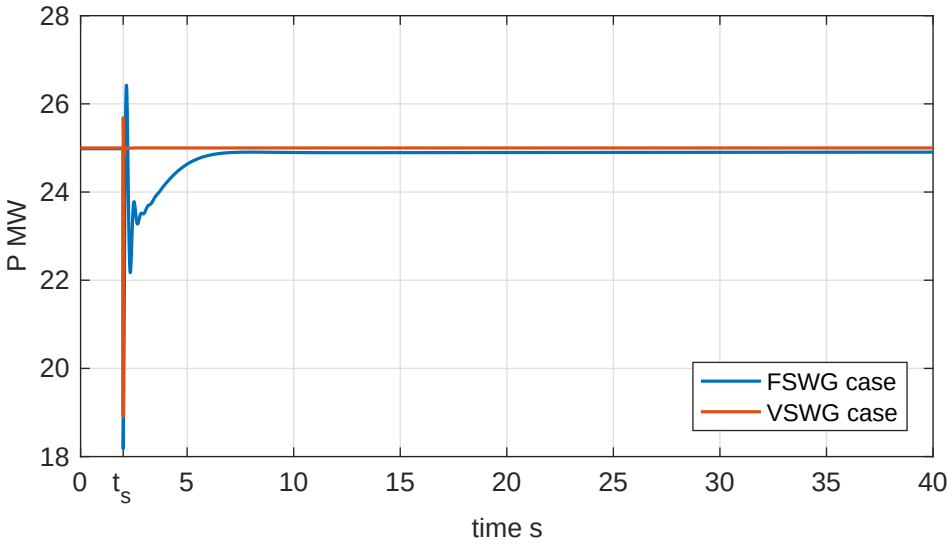

Figure 4.21: Bus 31 wind farm active power output P_{out}^{31} in the event of load shedding at Bus 5.

Figure 4.25 presents Bus 1 machine's frequency f^1 that represents the system frequency response f_{grid} for the load shedding. One can observe that the base case and the VSWGs case present similar response, within the acceptable limits for transient and steady state periods, as proposed in Table 4.2. The FSWG case presents a slightly reduction for the initial frequency peak, because of the inertia effect in their rotors provided to the system. It is worth noting that the proposed pitch angle control does not have impact during regular operation, so wind farms are constantly on the maximum dispatch for the scenario.

Figure 4.26 shows P_{ele}^1 which presents distinct active power dispatch levels

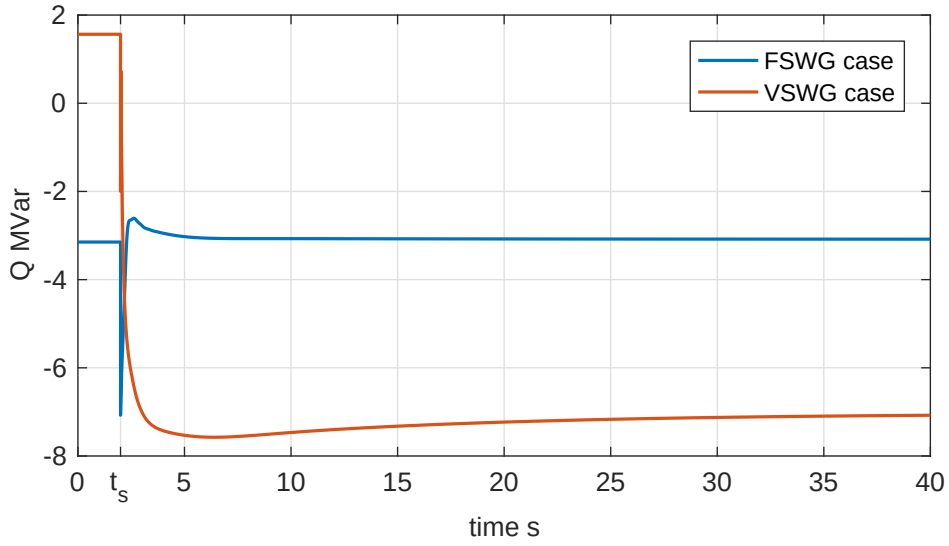

Figure 4.22: Bus 31 wind farm reactive power output Q_{out}^{31} in the event of load shedding at Bus 5.

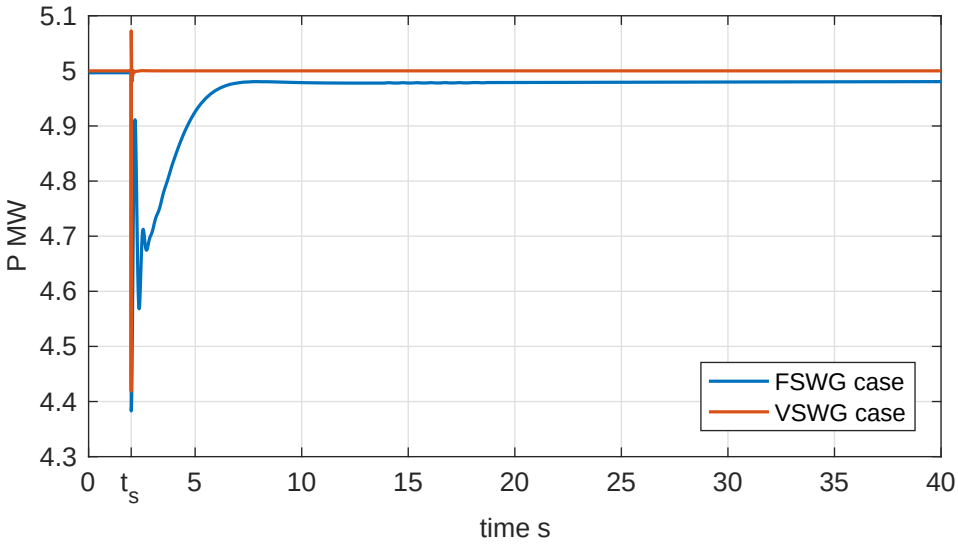

Figure 4.23: Bus 13 wind farm active power output P_{out}^{13} in the event of load shedding at Bus 5.

between the base case and the proposed wind power scenarios. This is because Bus 1 is a Vθ model (or slack) for the power flow studies, and it is responsible for balancing the power mismatch caused by the inclusion of WFs. P_{ele} curves

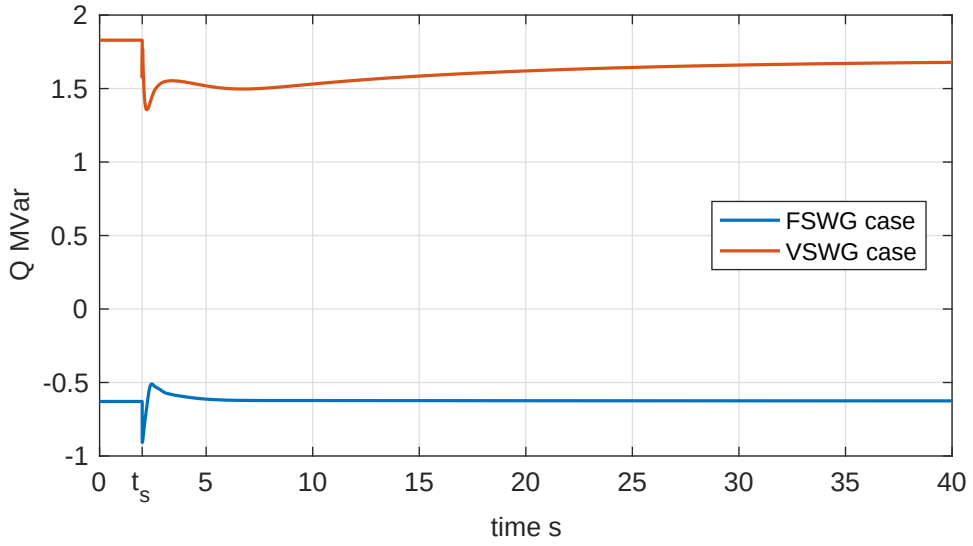

Figure 4.24: Bus 13 wind farm reactive power output Q_{out}^{13} in the event of load shedding at Bus 5.

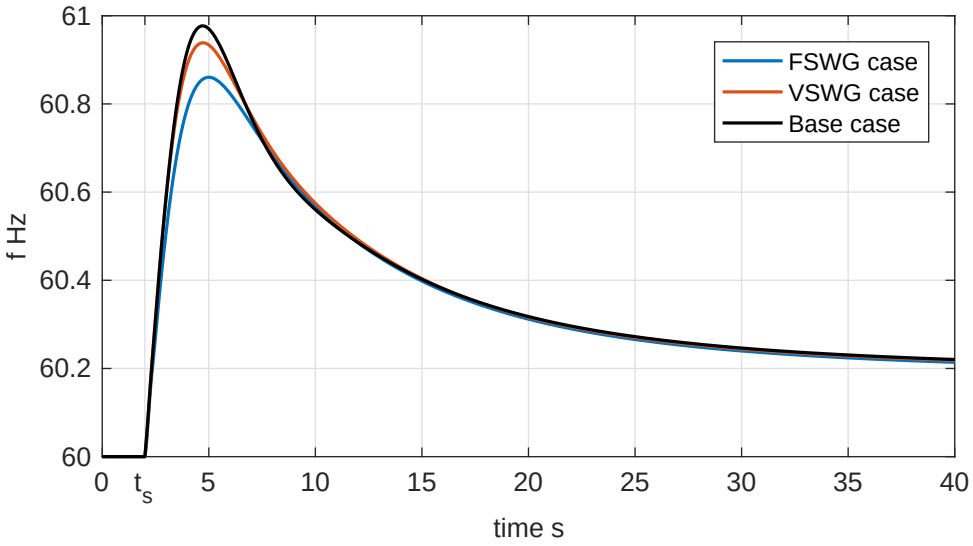

Figure 4.25: Bus 1 power plant frequency response f_1 representing grid frequency f_{grid} in the event of load shedding at Bus 5.

show similar variation for all cases, even though different initial values for the considered scenarios.

Figure 4.27 shows P_{ele}^{2}, where similar behaviour is presented by the three

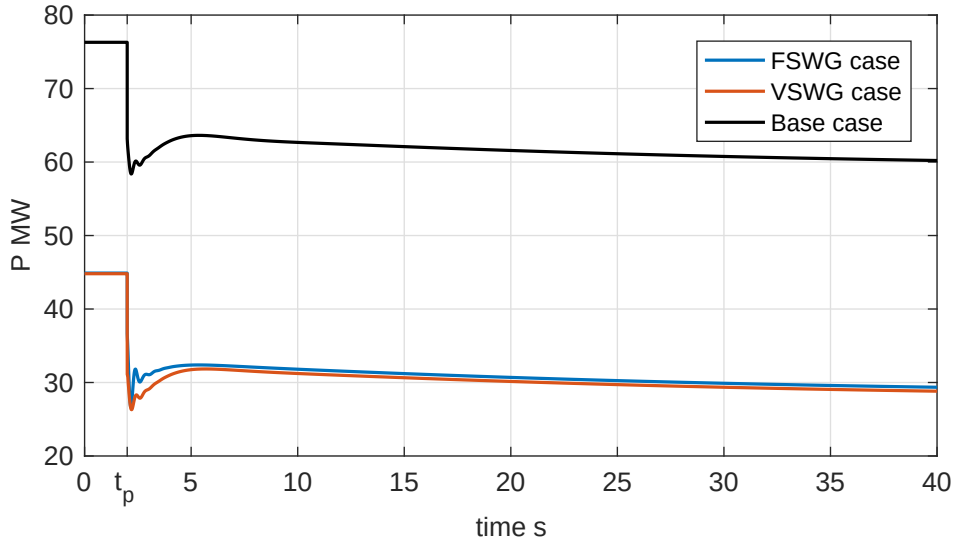

Figure 4.26: Bus 1 active power dispatch P^1_{ele} in the event of load shedding at Bus 5.

considered cases, with a slightly reduced initial sag for the FSWGs case that has extra spinning inertia in its WF. One can observe that Bus 1 and Bus 2 share the initial load variation (droop control), however Bus 1 restores system's frequency in the long term by adjusting its power dispatch, making Bus 2 P^2_{ele} move towards its initial value.

Figure 4.28 and Figure 4.29 show reactive power dispatch for Bus 1 and Bus 2, respectively. VSWG's reactive power dispatch has a great impact on power plants reactive power dispatch, assisting on system voltage control. It is worth noting that the proposed voltage control loop works during wind farms reconnection only, and not to interfere during regular operation.

Figure 4.30 presents system angular stability, where Bus 2 rotor angle in relation to Bus 1 rotor angle $\delta_{2\text{-}1}$ is presented. Bus 2 is a faster power plant for dispatch adjustments than Bus 1, therefore, $\delta_{2\text{-}1}$ experiences an initial reduction phase, and after few seconds $\delta_{2\text{-}1}$ regains and keeps increasing until the IEEE 30 Bus system reaches the steady state.

Although different initial $\delta_{2\text{-}1}$ values, the FSWG case and the base case present

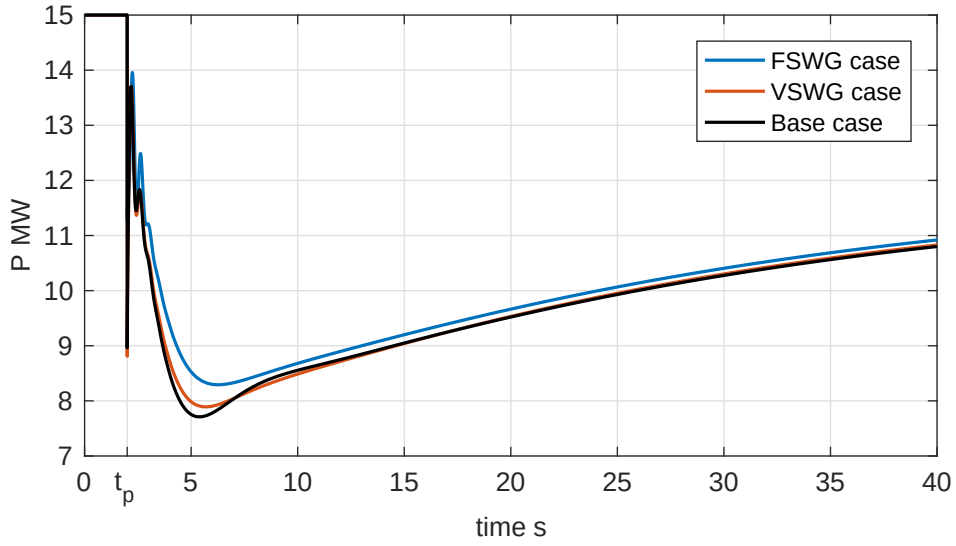

Figure 4.27: Bus 2 active power dispatch P^2_{ele} in the event of load shedding at Bus 5.

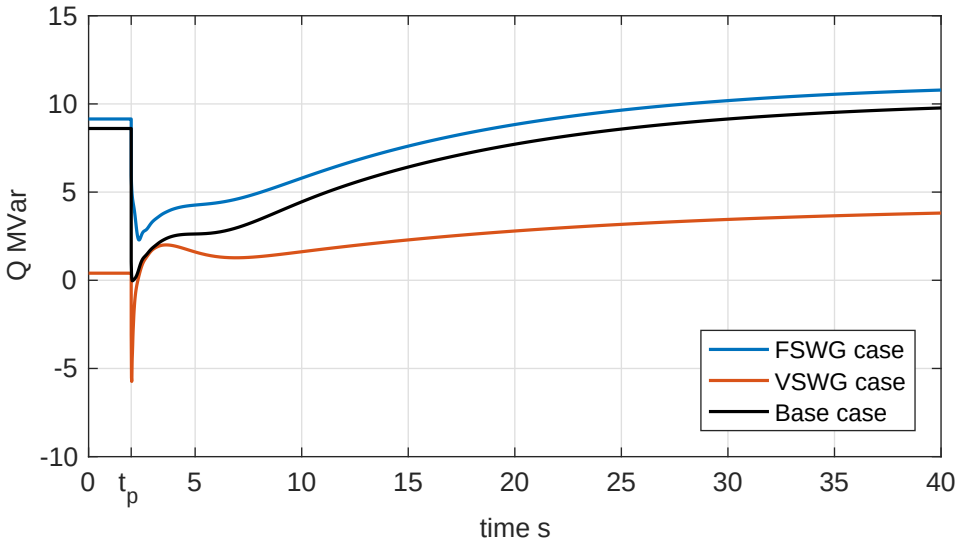

Figure 4.28: Bus 1 reactive power dispatch Q^1_{ele} in the event of load shedding at Bus 5.

similar response, while the VSWG case has reduced $\delta_{2\text{-}1}$ variation during the regain phase $t > 6\,\text{s}$. This is consequence of the wind farm's Q_{out}, which reduces power flowing along system lines.

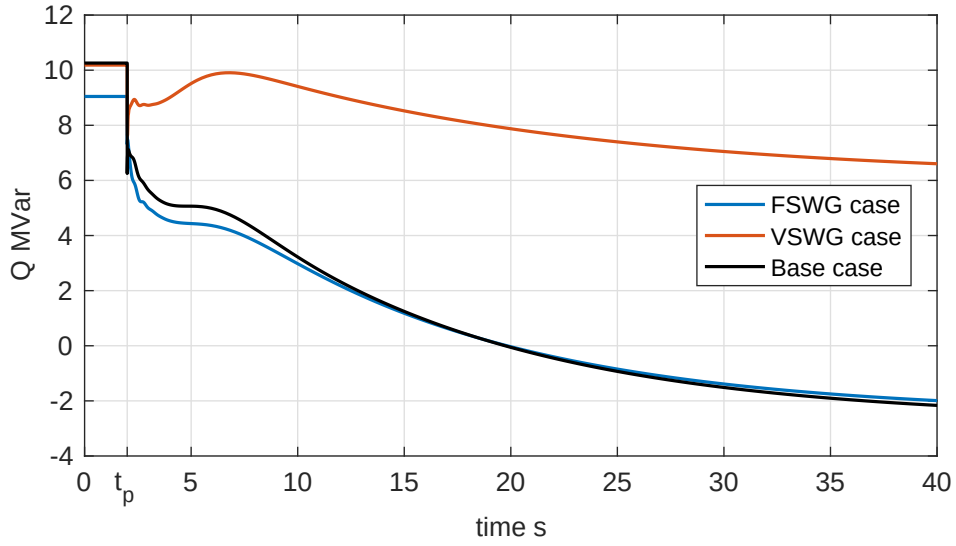

Figure 4.29: Bus 2 reactive power dispatch Q^2_{ele} in the event of load shedding at Bus 5.

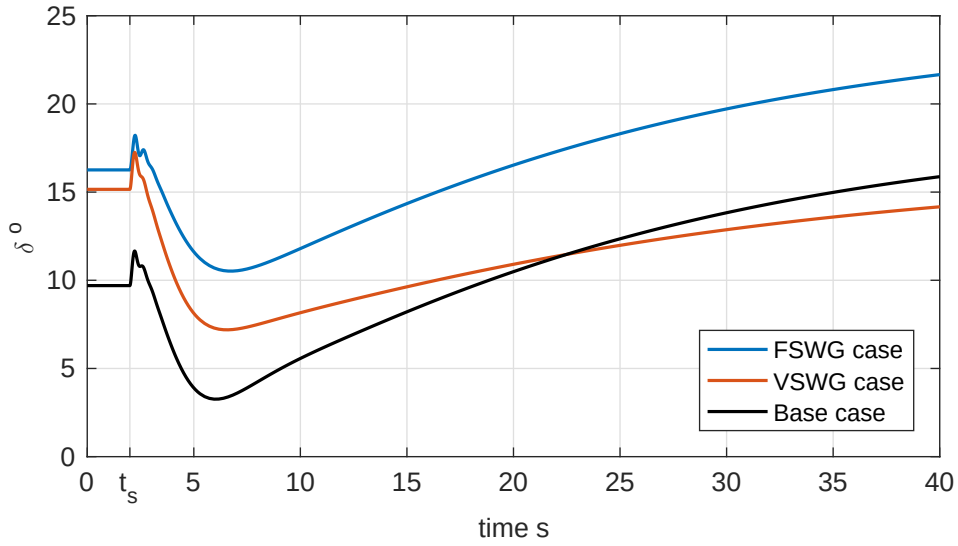

Figure 4.30: Bus 2 rotor angle in relation to Bus 1 rotor $\delta_{2\text{-}1}$ in the event of load shedding at Bus 5.

4.4 Conclusion

This chapter investigates the feasibility and the impact of using wind power during PSRs by carrying on simulations and analysis on the IEEE 30 bus system. In

general, the inclusion of wind power during PSRs imposes extra challenges by increasing the number of tasks required to complete the entire procedure. The results in this chapter show that it is possible to anticipate WFs restoration to increase system controllability during such a complex event.

The power flow and voltage stability analysis show that the wind power has potential to improve system collapse indexes, specially the VSWGs because of their ability to perform reactive power control. Improved collapse indexes indicate a system working further from the critical point, leading to a safer operation and reducing the probability of disconnections during restorations.

The energy function analysis shows improvements on system robustness areas with the inclusion of WFs for PSRs. Reduced buses vulnerabilities indicate a power system more capable in successfully transmitting power along its branches. This tool brings complementary information to the stability analysis where it is not as sensitive to reactive power dispatch as the indexes of collapse. The proposed approach for robustness areas visualization brings more details to the analysis and allows a fast identification of vulnerable areas.

Finally, dynamic simulations show the proposed synchronization approach and loop controls performance. The synchronization approach is able to reconnect wind farms without compromising frequency level and voltage control. This is only possible due to the proposed control loops that are able to provide smooth power dispatch curves, allowing system power plants to restore frequency and voltage level as the wind dispatch increases. Controllers show no interference on regular operational mode, or outside the power ramp phase.

Chapter 5

Brazilian power system restoration assisted by wind power

5.1 Introduction

This chapter and the following analyse the proposed wind power restoration approach on the Brazilian power grid. This chapter presents the restoration philosophy and the local area restoration, while Chapter 6 is dedicated to the wide area restoration phase.

5.2 Brazilian grid restoration philosophy

Restoration philosophy for the Brazilian power grid has been developing since the second half of the 1980's decade, when wide area blackouts put in check the old restoration philosophy. From April 1984 to September 1985, three wide area outages led the South/South east Brazilian system to blackout, and the former restoration philosophy has been called into question. At the time, the idea was

to centralize all operations and decisions in a head office aiming to coordinate the entire restoration. However, the result did not correspond to the plan, and the excessive need for communication congested lines. The dependence on the recently acquired SCADA system also turned into a problem when it crashed during the blackout in one of the mentioned events [61].

Based on the lessons learned from the 1980's unsuccessful restorations, the former Centre for Coordinated Operations proposed a new philosophy in 1989, which divides the restoration procedure in two phases: **Fluent Phase (FP)** and **Coordinated Phase (CP)**. This separation aimed to reduce the need for communication among system agents, and speed up the restoration procedure by allowing several areas to restore in parallel [111].

Today's Power System Restoration (PSR) philosophy follows the same guidelines proposed in 1989, with some amendments to adequate to the current reality. The two-phase procedure is described as follows [61, 111–114]:

Fluent phase

During this phase, power plants restore electrical islands without continuous communication with the head office. Each system agent receives a document containing their area restoration instructions where is clearly designated the action they are expected to perform and the conditions to be fulfilled [109]. After the entire area restoration, agents keep on stand-by for further instructions to proceed towards the CP.

The electrical island's area is determined during the background studies when electrical and geographical characteristics are considered. Even though restoration areas can restore by themselves, the Independent System Operator (ISO) supervises the entire procedure, and in case an area is unable to complete its own restoration, the ISO's head office takes control and complete the local area restoration.

Coordinated phase

This phase takes place after the FP, and it is coordinated entirely by the ISO, hence any action must be approved before execution [30]. During the CP, electrical islands connect to each other, following a predefined script provided. The first link between two areas is the parallel connection, while any following connection is called loop closure. The inter-area power transfer in this phase enables large load chunks reconnection, speeding up restorations [34].

5.3 State of São Paulo power grid

The São Paulo State is one of the 27 Brazilian states, covering an area of 248,222 km^2 (for comparison, the UK has 242,495 km^2). Historically, two main grids had formed the state's bulk power grid: one in 345 kV and the other in 440 kV. The former was commissioned during the late 1950's by the Brazilian government to deliver power from the *Furnas Power Station* to the Southeast region of Brazil where key cities such as São Paulo and Rio de Janeiro are located. The State of São Paulo built the 440 kV system, aiming to connect its hydro power plants in the west border to main cities distributed along the state area. This São Paulo State grid has its own control office ensuring a considerable degree of independence.

Today the Brazilian power grid is operated by the ISO, however, the São Paulo State restoration still follows an independent path (under the philosophy described above), due to its history and infrastructure. Figure 5.1 shows the restoration grid in a geographical map, representing the system used in this thesis.

The recent international pressure for cleaner energy sources has been forcing governments and companies to invest in renewable energy, which recently led the São Paulo State government to issue a wind atlas and a plan to install up

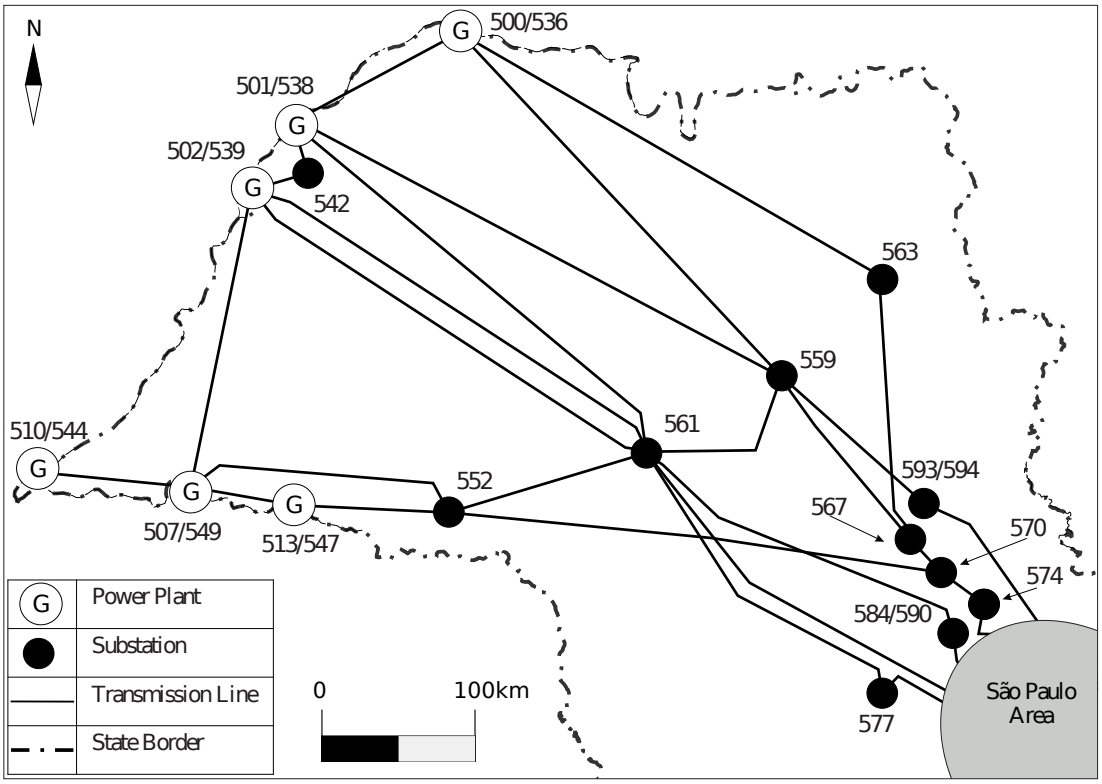

Figure 5.1: Diagram of the São Paulo State restoration grid. The highlighted São Paulo Area refers to the capital city's metropolitan region.

to 4.7 GW in Wind Farms (WFs) in a long-term horizon [115–118]. Some of the areas with high wind potential are close to the 440 kV and the 345 kV substations, which leads to great savings on transmission infrastructure. This plan to increase the amount of renewable power in the São Paulo State motivates this thesis to apply the proposed methodology to investigate the wind power impact on the state's grid restoration.

5.4 Fluent phase restoration for the Jupiá area

The Jupiá restoration area is named after the hydro power plant responsible for its black-start. It is selected for analysis because of two main reason: power plant's slow characteristics and the large wind power investments on this area.

Power plant's slow characteristics (see Chapter 6) can stress frequency control during wind farms restorations, putting the proposed control into test. The large investments in this area is due to the wind distribution as one can see in [116–119].

Restoration areas in this system receives the designation of corridors, because of their long shape that connects the power plants in the west border to loads along the state. The entire Jupiá restoration area, or simply Jupiá corridor, is depicted in Figure 5.2, where the power plant is located on Bus 502, and three WFs are connected along the system, according to the wind atlas provided [116–119].

Load ramp is a major concern during the São Paulo state grid FP due to absence of power transfer among corridors. In order to mitigate frequency variations, large load chunks are broken in smaller parts, and reconnected one after another, respecting a coordination time $\Delta\ t_c$. For this system, the ISO adopts a $\Delta\ t_c = 60\,\text{s}$.

The ISO bounds voltage level and grid frequency throughout the procedure, to avoid faults or further disconnections, where Table 5.1 shows such limits for FP and CP. For other parts of the Brazilian power grid, these limits may vary depending on the local equipments.

Table 5.1: Frequency and voltage level limits for the São Paulo grid throughout restoration.

	Frequency	Voltage
Fluent Phase	$\pm 2\,\text{Hz}$	$\pm 10\,\%$
Coordinated Phase	$\pm 1\,\text{Hz}$	$\pm 10\,\%$

Table D.1 (Appendix D) shows the systematic instruction guide for Jupiá area, where all actions from Generator Units (GUs) black-start to the end of FP are presented. This corridor restores in a range of 60 min to 120 min. Once this corridor restoration is complete, the CP takes place, where corridors connects to each other.

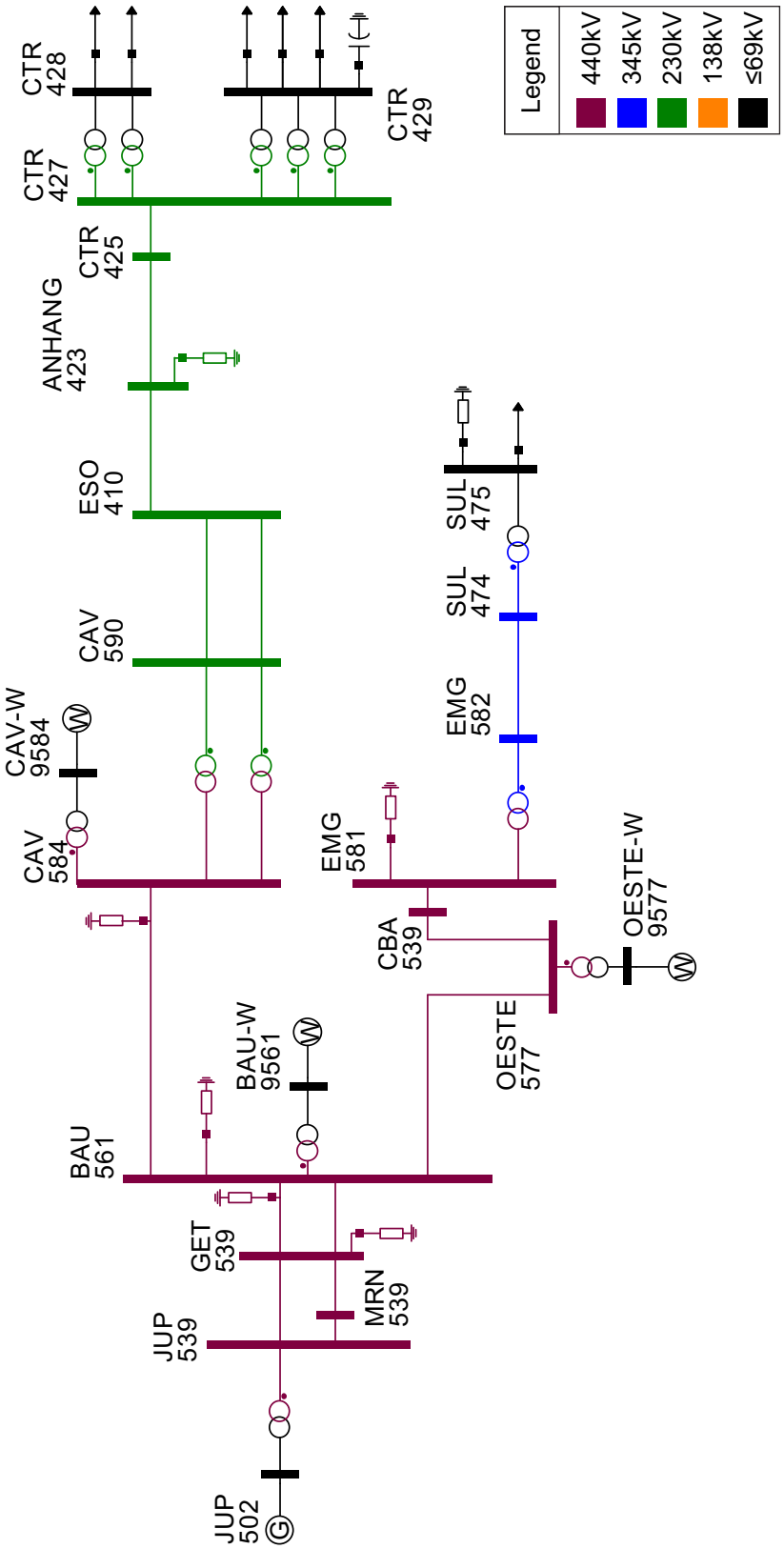

Figure 5.2: Jupiá FP restoration area.

The first issue in using wind power for the FP is the low load profile that remains until CTR substation (buses 427, 428 and 429 in Figure 5.2) restores. Restoring a WF before the load restoration would cause the power offer to overcome the load demand, which is impracticable. To overcome this problem, the WF restores at the end of this corridor FP so load is larger than wind power generation. In addition, only the wind farm at CAV substation (Bus 9584) is restored, limiting the wind power dispatch.

5.5 Power flow simulations and voltage stability analysis for the Jupiá corridor

In order to apply the proposed methodology on the local area restoration, the WF's synchronization simulation follows the parameters presented in Table 5.2.

Table 5.2: Power flow simulation parameters for the Jupiá restoration area.

Simulation parameter	Value
No. wind profiles	5000
Weibull parameter a	6.4307 m/s
Weibull parameter b	1.7643
Total wind penetration	100 MW
Power flow mismatch tolerance	1.0×10^{-6} pu

Figure 5.3 presents the reactive power load margin ΔQ results, where the Variable Speed Wind Generator (VSWG) case enlarges system ability to provide reactive power, while Fixed Speed Wind Generator (FSWG) case reduces it. The ability to control its own reactive power output is a great advantage for the VSWG case where it compensates unloaded transmission lines during the initial stages of restoration, providing voltage control throughout the restoration process. This feature is highly desirable during PSRs where voltage control is one of the most difficult challenges to overcome, especially in a long radial system as this corridor.

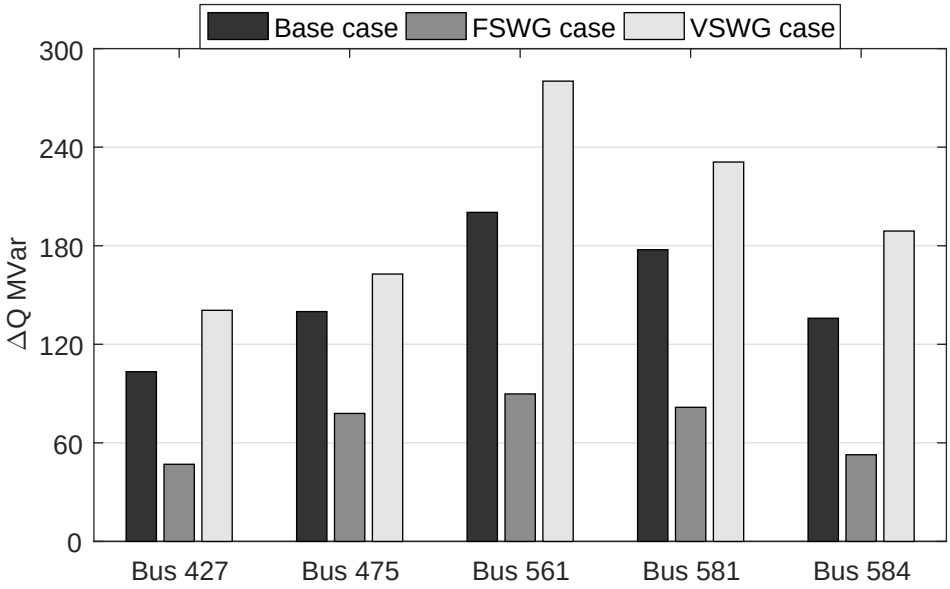

Figure 5.3: Reactive power load margin ΔQ for the completed Jupiá corridor restoration procedure, as described in Table D.1.

Figure 5.4 shows active power load margin λ in function of wind power dispatch P_{out}, where one can observe the active power influence on load margin. The VSWG case is able to enlarge its λ as P_{out} increases. The FSWG case has the same behaviour, however in a limited range.

The power flow tangent vector's Euclidean norm $\|\mathbf{TV}\|$ in function of P_{out} shows that positive increments in wind power dispatch leads to reduction on system stability to load variations. Trends show that the FSWG has a larger influence on $\|\mathbf{TV}\|$ than the VSWG.

5.6 Robustness areas analysis

The investigation on Jupiá Bus robustness areas is performed by the proposed energy function tool [62,101] described by (3.9). This system analysis is made by using the $E_p(X^s, X^u)$ levels of each bus defining the diagram background colours. The power flow solution and $E_p(X^s, X^u)$ is located on Table C.1 to Table C.3

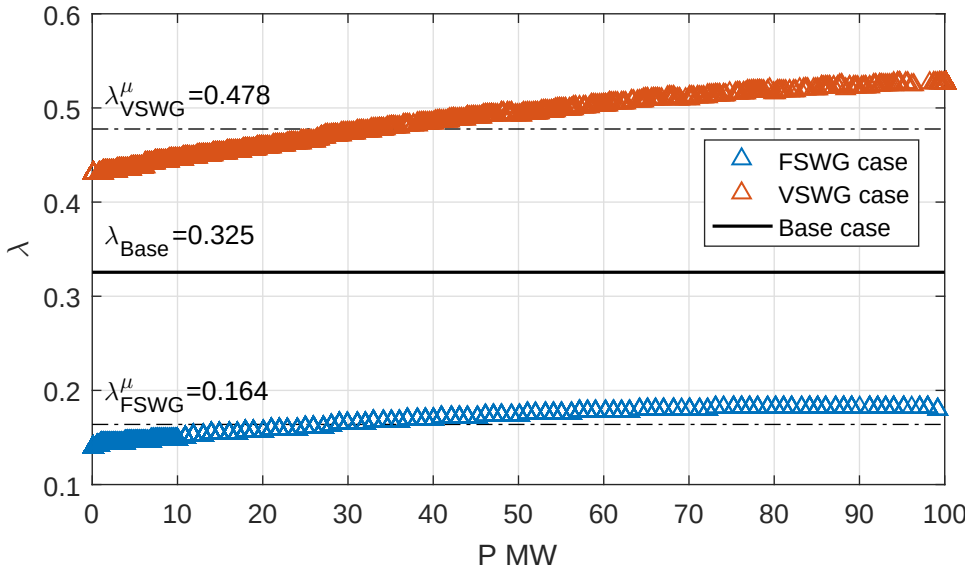

Figure 5.4: λ distribution as function of total wind power dispatch P_{out} for the Jupiá system completed restoration. λ^{μ}_{FSWG} and λ^{μ}_{VSWG} stand for the mean value for its respective distribution.

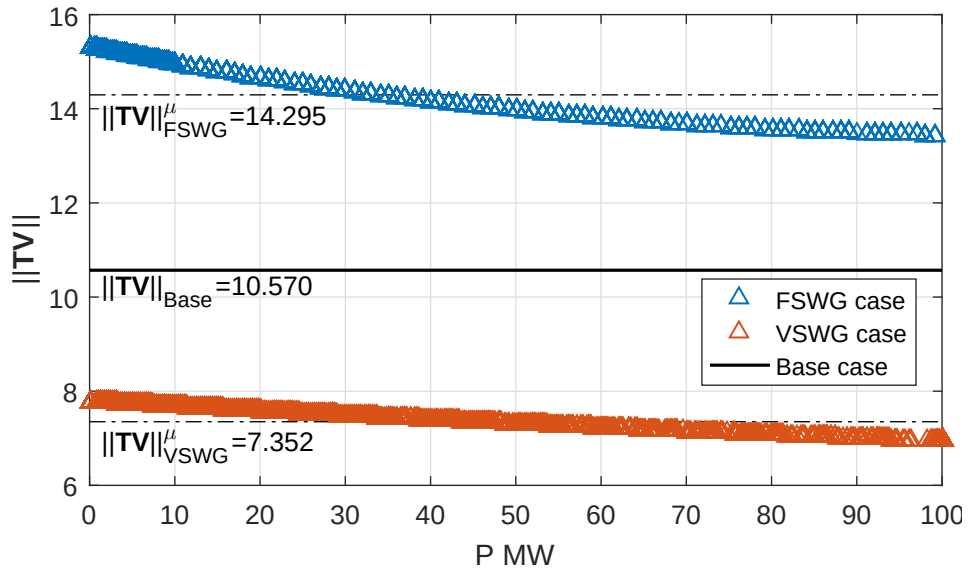

Figure 5.5: $\|\mathbf{TV}\|$ distribution as function of total wind power dispatch P_{out} for the Jupiá system completed restoration. $\|\mathbf{TV}\|^{\mu}_{FSWG}$ and $\|\mathbf{TV}\|^{\mu}_{VSWG}$ stand for the mean value for its respective distribution.

(Appendix C), where Stable Equilibrium Point (SEP) and Unstable Equilibrium Point (UEP) solutions are presented.

Figure 5.6 shows a graphical representation of system's robustness areas. In summary, each bus has a background colour representing its $E_p(X^s, X^u)$ value, where low $E_p(X^s, X^u)$ and high $E_p(X^s, X^u)$ indicates vulnerable and robust areas, respectively. For the sake of image contrast, the vulnerability level is bounded as follows: $-2.00 \leq E_p(X^s, X^u) \leq 80.00$.

Figure 5.6 analysis shows a vulnerable area covering the terminal section of both system radials, with a high influence on the CTR substation radial. One can also observe that the first three buses from the power plant are in a vulnerable/intermediate vulnerability region, especially for the Base case scenario. Both problems relate to system struggle in transmitting power, where the end part imports active and reactive power, while the generation area imports reactive

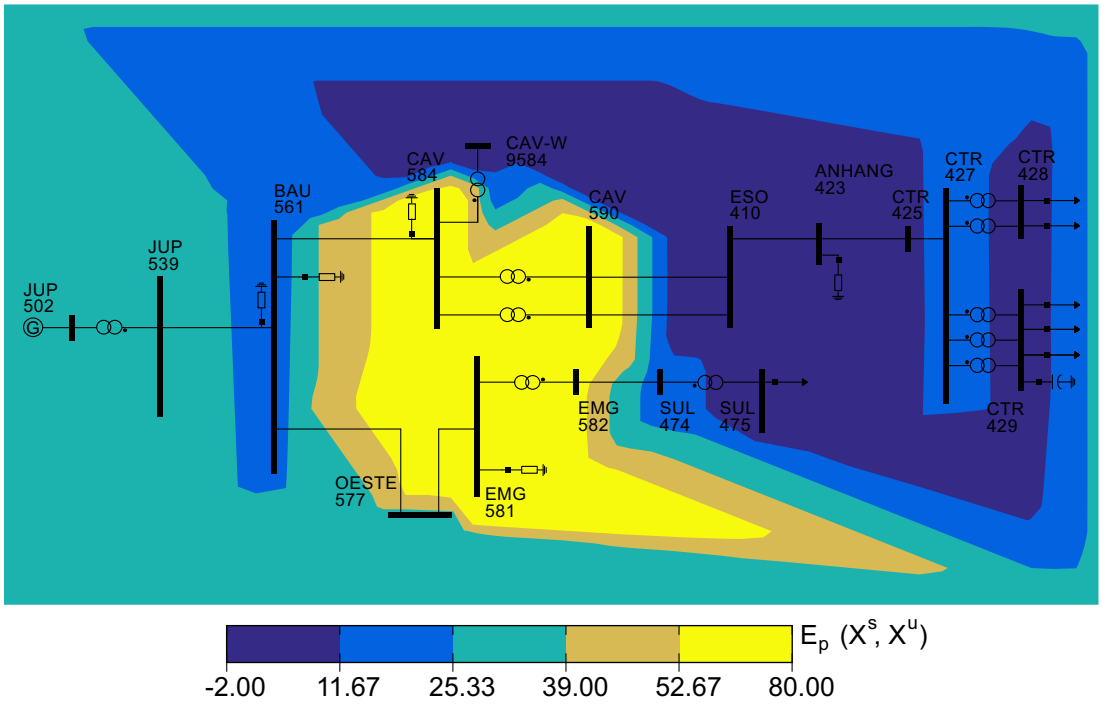

(a) Base case.

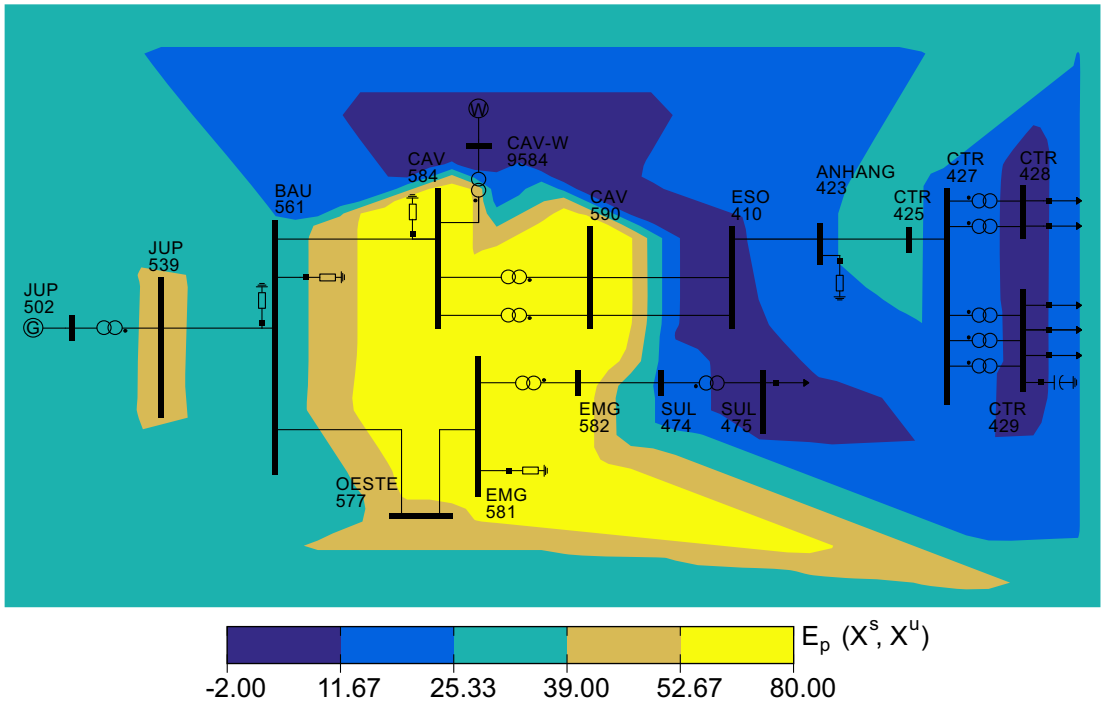

(b) FSWG case.

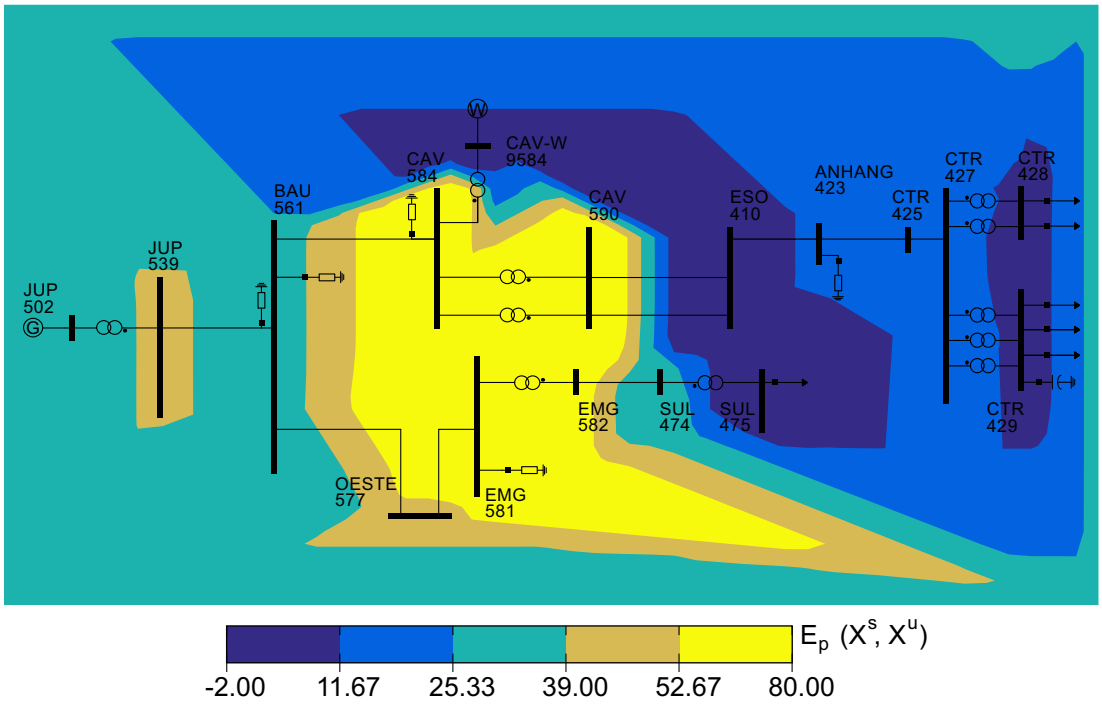

(c) VSWG case.

Figure 5.6: Robustness areas diagram for the Jupiá restoration corridor.

power and exports active power. The intermediate area, near Bus 581 and Bus 584, does not present heavy reactive power flow, which increases the area ability to supply loads, leading to a robust classification by $E_p(X^s, X^u)$ function.

Regarding the wind power usage in the Jupiá restoration corridor, the effect on the system's robustness is considerably positive, as Figure 5.6 shows. Buses robustness is considerably affected by the wind farm at Bus CAV, with a special attention to the FSWG case that shows the most $E_p(X^s, X^u)$ enlargement for this system. This shows that wind power has the ability to assist restorations by increasing system stability level.

5.7 Dynamic stability studies for the Jupiá area

The cases proposed to assess the Jupiá corridor dynamic stability are: the WF synchronization at Bus CAV 9584, and a load shedding at Bus CTR 428. Table 5.3 summarizes simulation parameters used for the Jupiá corridor.

Table 5.3: Dynamic time domain simulation parameters for the Jupiá .

Parameter	Value
Integration step	1.0 ms
Output frequency	5
Simulation time	Variable
Simulation Software	ANATEM®
Loads composition	$0.5\mathrm{Z_{cst}} + 0.0\mathrm{I_{cst}} + 0.5\mathrm{P_{cst}}$

5.7.1 Wind farm at Bus 9584 synchronization

The WFs synchronization procedure adopted for the Jupiá system follows the approach proposed in Chapter 3. This way the first step is to use the initialization routine to calculate initial β_0 for the given wind speed: $v_w = 10\,\mathrm{m/s}$. The calculated initial pitch angles are: FSWG $\beta_0 = 0.245\,\mathrm{rad}$, and VSWG $\beta_0 = 0.500\,\mathrm{rad}$.

Figure 5.7 shows controllers action on the turbine's pitch angle β, that is settled to vary in a 40 s ramp. For the sake of the model availability, Wind Generators (WGs) models used for the São Paulo restoration grid are the same as those used for the test system in the previous chapter.

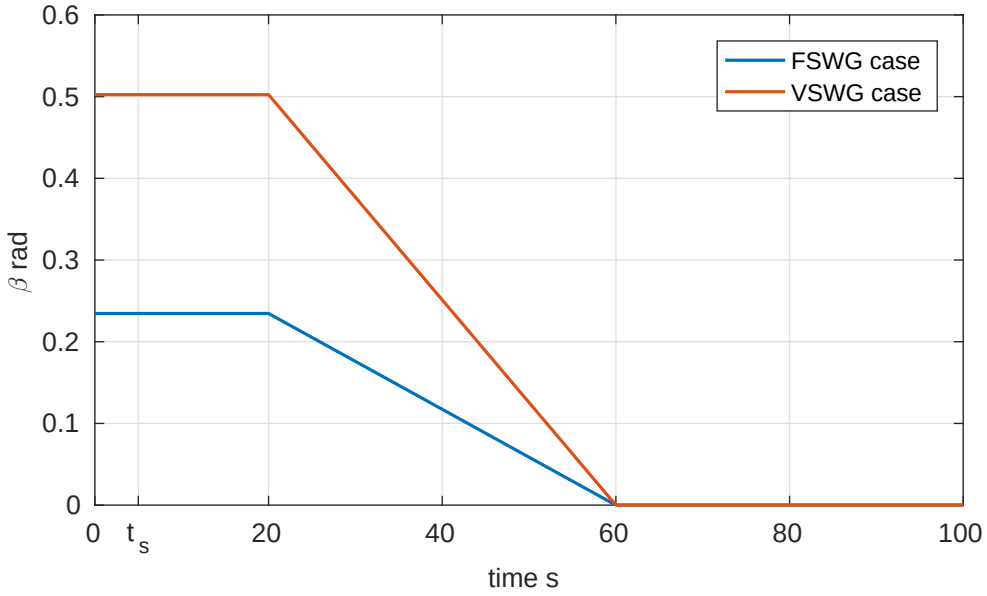

Figure 5.7: Wind turbine's blades pitch angle β demonstrating the proposed synchronization procedure for the wind farm at Bus 9584 on the Jupiá system. t_s stands for the synchronization time.

Wind farms' active power dispatch curves show the different responses between the FSWG and the VSWG, as depicted in Figure 5.8. The FSWG case presents an initial transient, and a direct correlation to β is seen, as it aims to the optimal point for the wind profile provided. The VSWG case does not present any significant initial transient, due to the inverter ability to decouple the machine from the grid. It is worth noting that any transient here mentioned is related to electromechanical time frame, hence fast transients (such as electromagnetic) can be neglected for this analysis.

Wind farm's reactive power export Q_{out} shows how each case behaves during synchronization. Figure 5.9 depicts Q_{out} for the FSWG case, a sudden Q_{out} drop

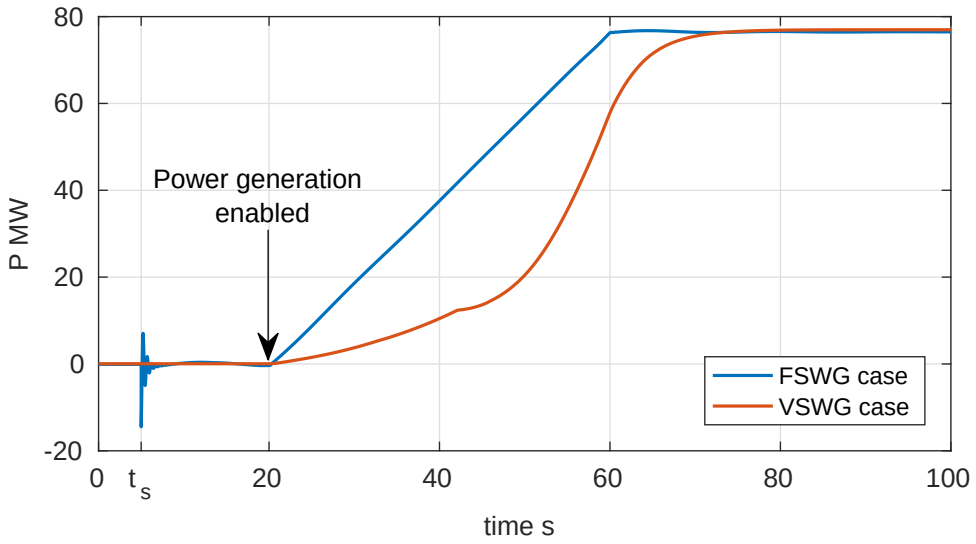

Figure 5.8: Wind farm active power output P_{out} in the event of Bus 9584 wind farm synchronization. The point where the power generation is enabled indicates the instant where the proposed controller is activated.

on the instant of synchronization t_s is seen due to the generator windings reactive power demand. Q_{out} for the VSWG does not present any significant response on t_s, however, it presents a controlled ramp, as the proposed voltage control takes place.

Figure 5.10 shows voltage level for the synchronization procedure. For both scenarios, voltage level remains within acceptable range as predefined by the ISO (see Table 5.1). This shows that the smooth control provided by proposed controllers allow enough time to adjust voltage level.

Wind power impact on Bus 502 power plant is investigated by using three key variables: mechanical power P_{mec}^{502}, accelerating power P_{ac}^{502}, and frequency rotor f^{502}.

Figure 5.11 shows P_{mec}^{502} delivered by hydro turbines to generators at Bus 502. The FSWG case presents an initial oscillation that is attributed to the voltage level reduction upon wind farm's reconnection. During P_{out} ramp, P_{mec}^{502} compensates system extra power injection by reducing its dispatch. The VSWG case

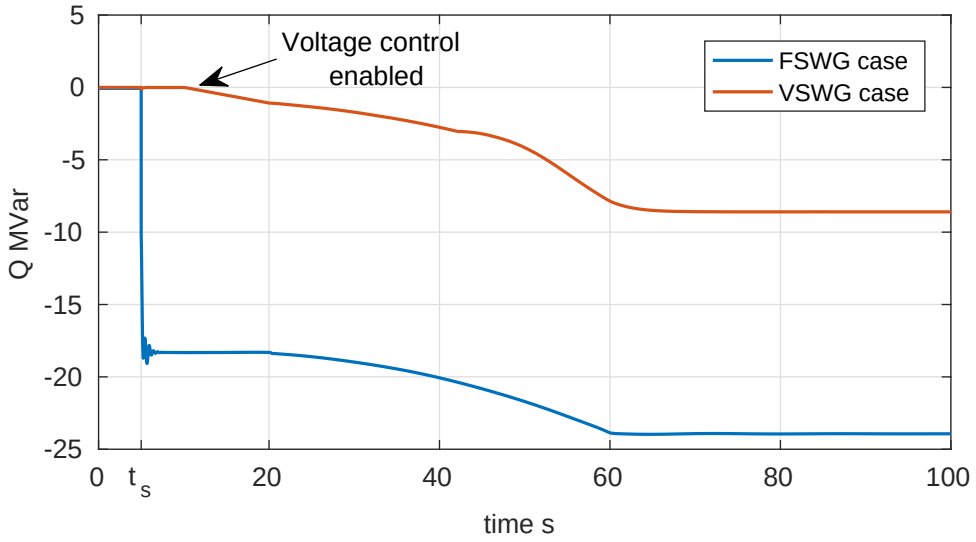

Figure 5.9: Wind farm reactive power output Q_{out} in the event of Bus 9584 wind farm synchronization. The point where the voltage control is enabled indicates controller's t_1.

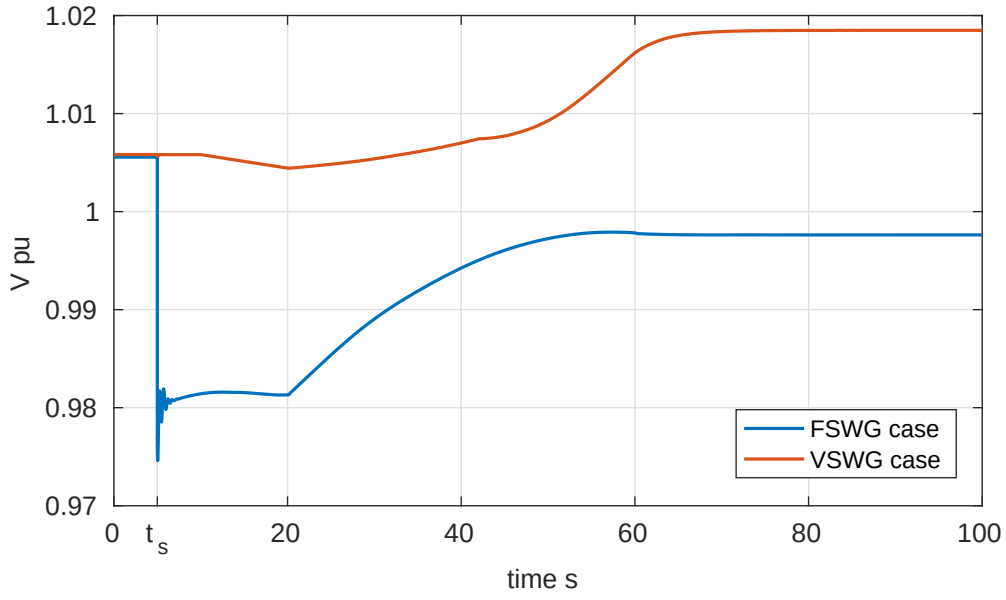

Figure 5.10: Voltage level imposed at Bus 584 in the event of Bus 9584 wind farm synchronization.

induces a different response on P_{mec}^{502} with a smooth behaviour and no initial oscillations, as this case also has the proposed reactive power ramp control.

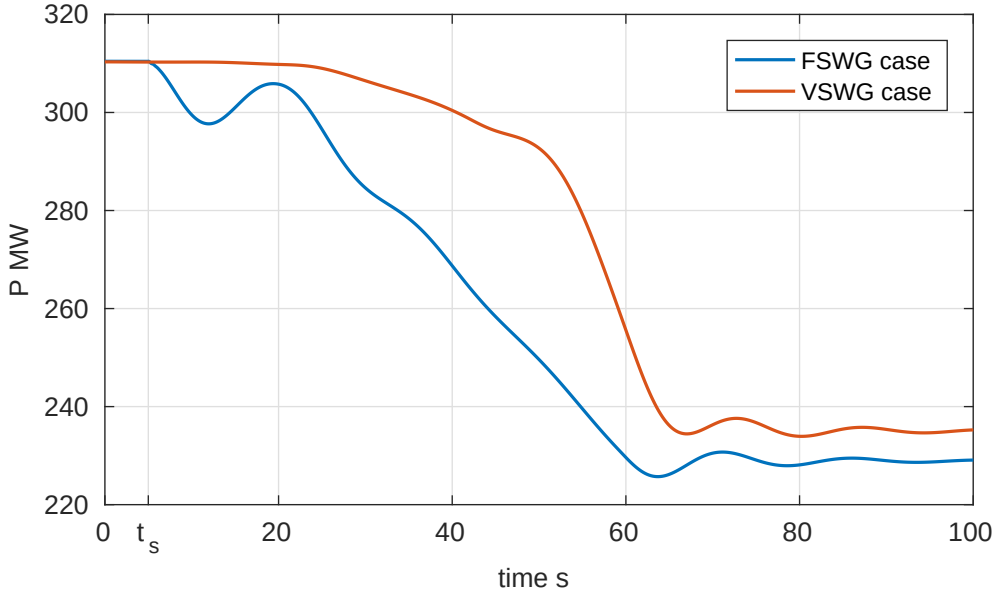

Figure 5.11: Mechanical power P_{mec}^{502} generated by the power plant at Bus 502 in the event of Bus 9584 wind farm synchronization.

The P_{ac}^{502} curves complement P_{mec}^{502} analysis, as presented in Figure 5.12. Despite the initial transient for the FSWG case, Bus 502 accelerating power remains within a 5.0 MW range $\Delta P_{ac}^{502} = \pm 5.0\,\text{MW}$, which is negligible compared to its 1,551.2 MW installed capacity, showing the proposed dynamic limiter's efficiency.

Figure 5.13 shows the synchronization impact on system's frequency control. Both cases respect the fluent phase frequency limits with a special attention to the lager VSWG case overshoot on the end part of its power dispatch ramp.

5.7.2 Load shedding at Bus 428

The second proposed scenario for analysis is a load shedding at Bus CTR 428, where $S = 30 + j9.9\,\text{MVA}$ is disconnected. Load shedding is a recurrent problem during restoration [4,30,34,113], usually caused by protective system tripping off

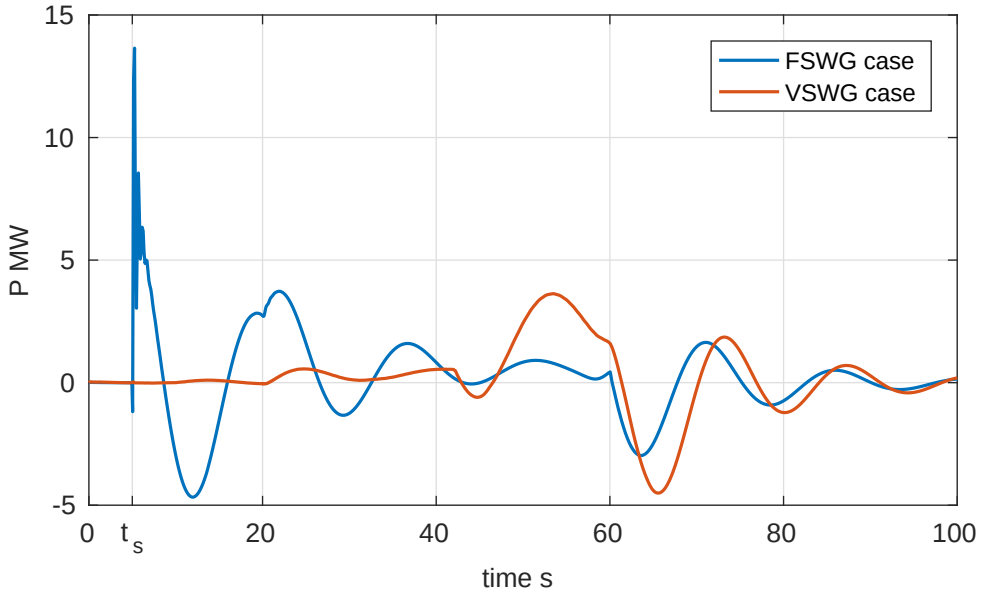

Figure 5.12: Mechanical power P_{ac}^{502} generated by the power plant at Bus 502 in the event of Bus 9584 wind farm synchronization.

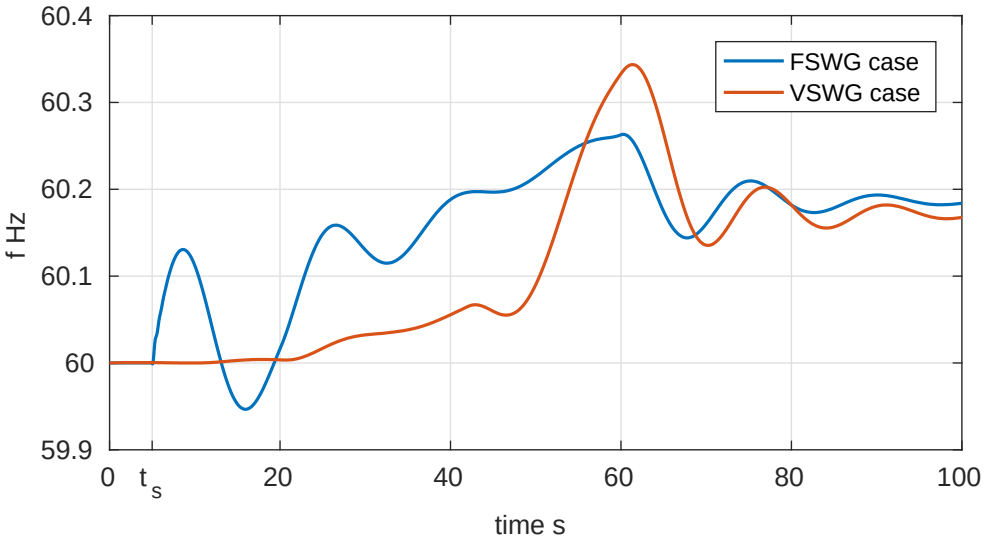

Figure 5.13: Bus 502 power plant frequency response f_{mac}^{502} representing grid frequency f_{grid} in the event of Bus 9584 wind farm synchronization.

due to branch overload or voltage level out of safe region.

Figure 5.14 shows Bus 428 load P_l^{428}, which differ among cases, due to different voltage level variation, as presented in Figure 5.15. Despite considerable variation, all three cases remain within proposed bounds as defined in Table 5.1.

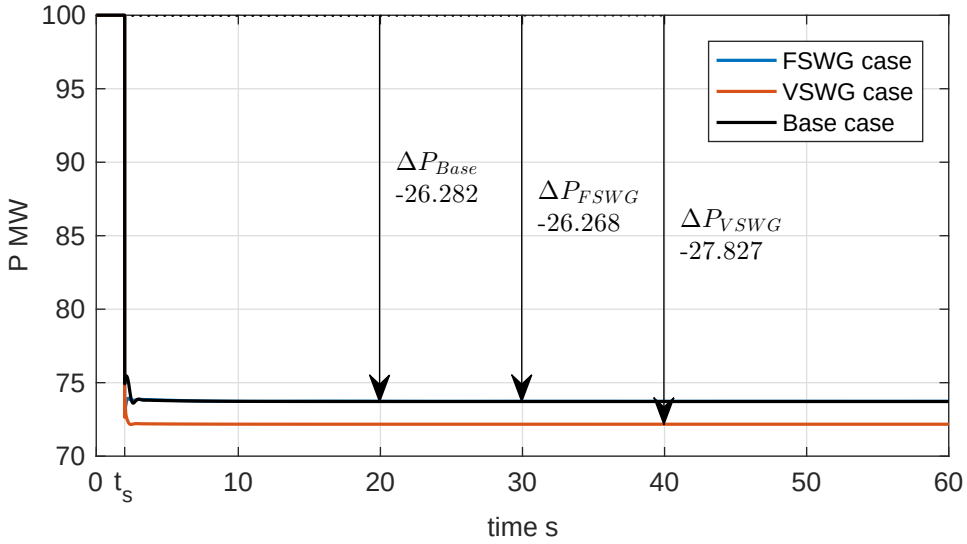

Figure 5.14: Bus 428 load demand P_l^{428} in the event of the proposed Bus 428 load shedding. t_s stands for the load shedding time.

Figure 5.16 depicts the load shedding impact on wind farm's dispatch, where P_{out} curves show the inertia provided by FSWG, while the VSWG case does not have any major impact on system stability as rotor frequency is decoupled from the grid.

As the load sheds, the capacitance effect becomes more pronounced, increasing voltage level along the restoration area. This makes VSWGs act to control voltage level by reducing their reactive power dispatch, as Figure 5.17 shows. The FSWG case has a negligible Q_{out} variation, with exception from the transient period.

Figure 5.18 presents Bus 502 machine's rotor speed f_{mac}^{502} that is used to represent the system frequency response for the load shedding. One can observe that the VSWGs case presents a higher initial frequency peak due to the larger load reduction during the event, as shown in Figure 5.14. The FSWG case presents a

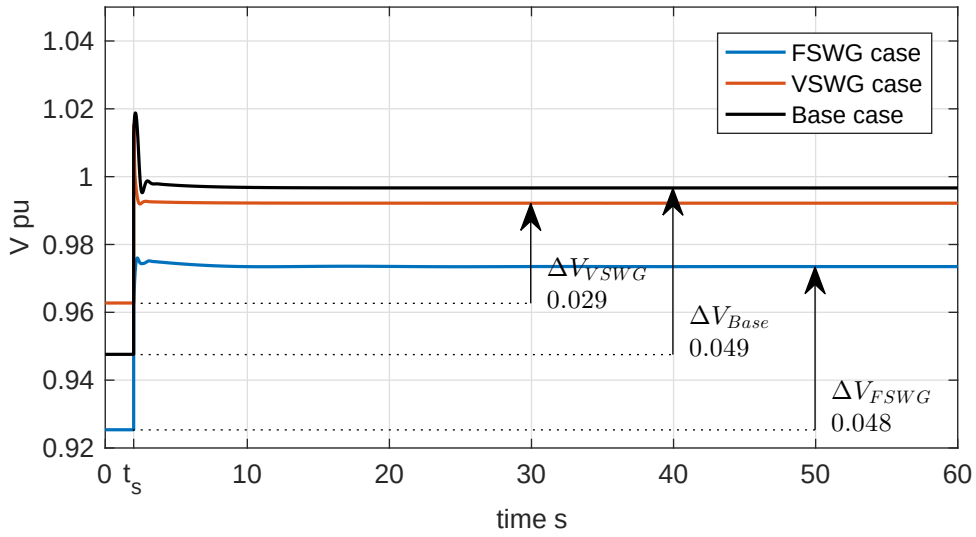

Figure 5.15: Bus 428 voltage level V^{428} in the event of the proposed Bus 428 load shedding.

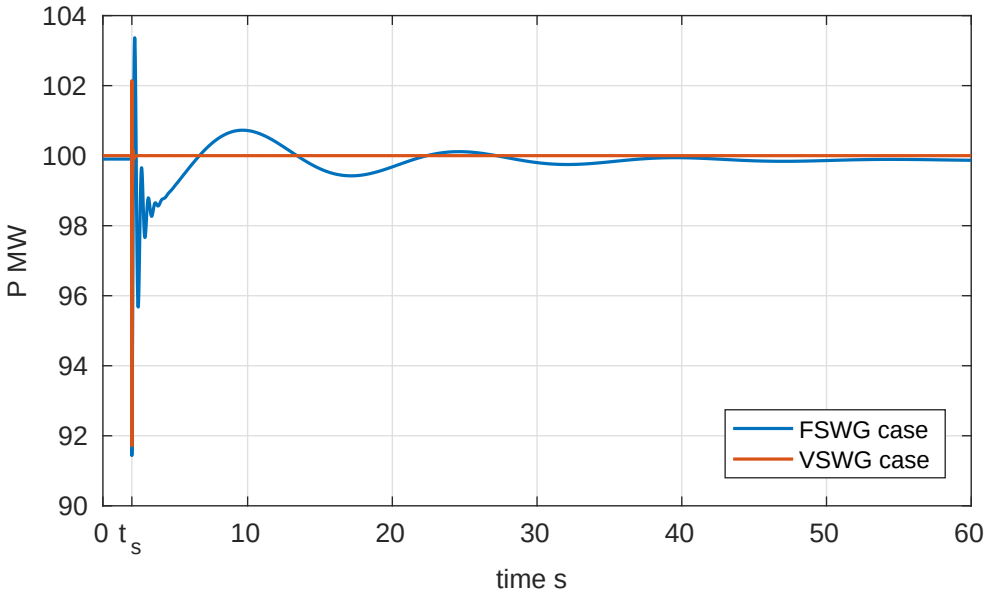

Figure 5.16: Bus 9584 wind farm active power output P_{out} in the event of the proposed Bus 428 load shedding.

slightly reduction for the initial frequency peak, and a faster damping characteristics, due to WF's rotors inertia and damping effect.

Figure 5.19 shows Bus 502 electrical power dispatch P_{ele}^{502} where the base case

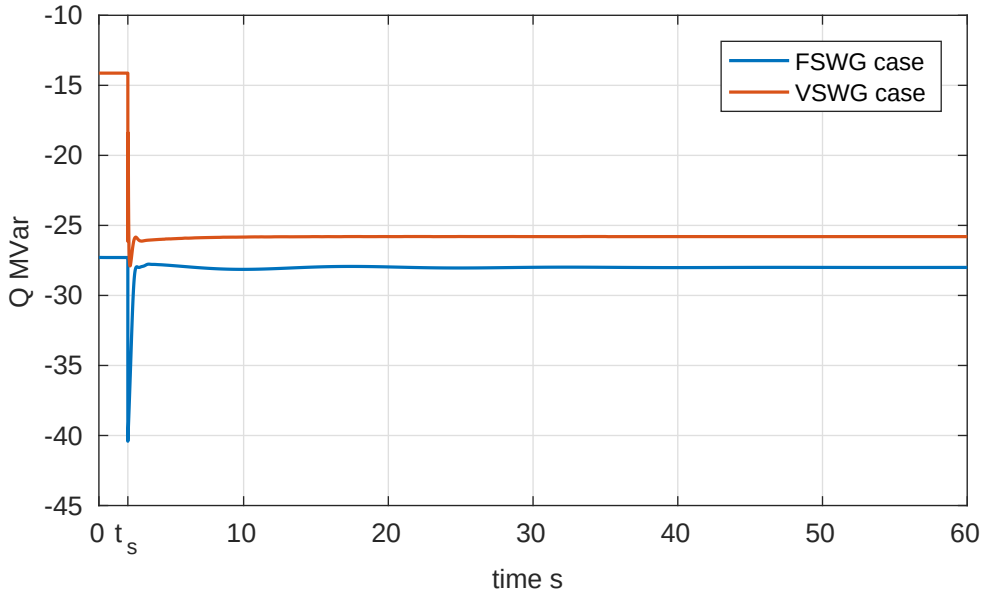

Figure 5.17: Bus 9584 wind farm reactive power output Q_{out} in the event of the proposed Bus 428 load shedding.

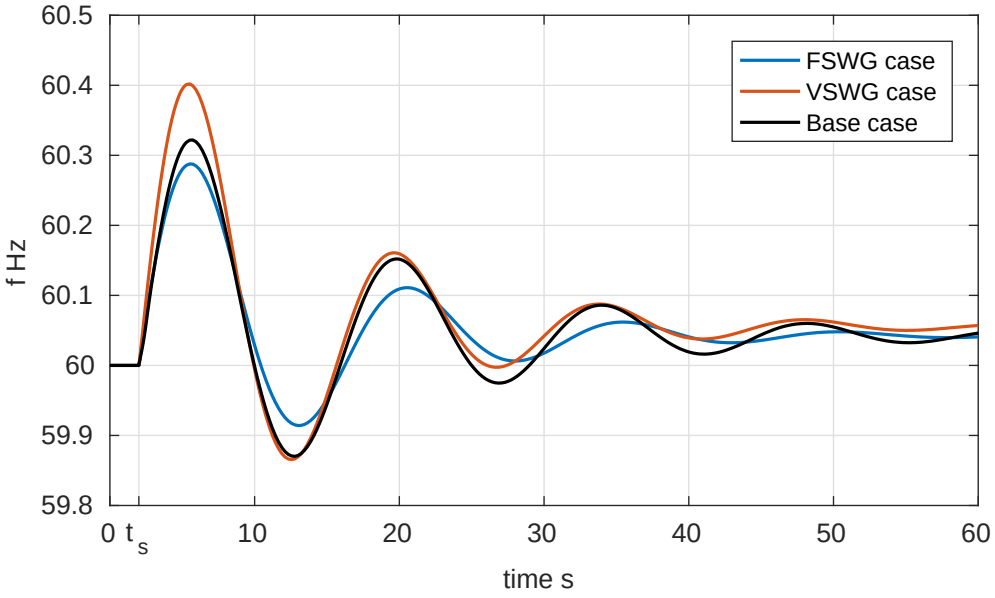

Figure 5.18: Bus 502 power plant frequency response f_{mac}^{502} representing grid frequency f_{grid} in the event of the proposed Bus 428 load shedding.

and the proposed wind power scenarios present different initial levels. This occurs because Bus 502 is the angular reference (or Vθ) for the power flow studies, and it is responsible for balancing the power mismatch caused by the WFs inclusion. P_{ele} curves show similar behaviour for all cases, even though different initial values for the considered scenarios [34].

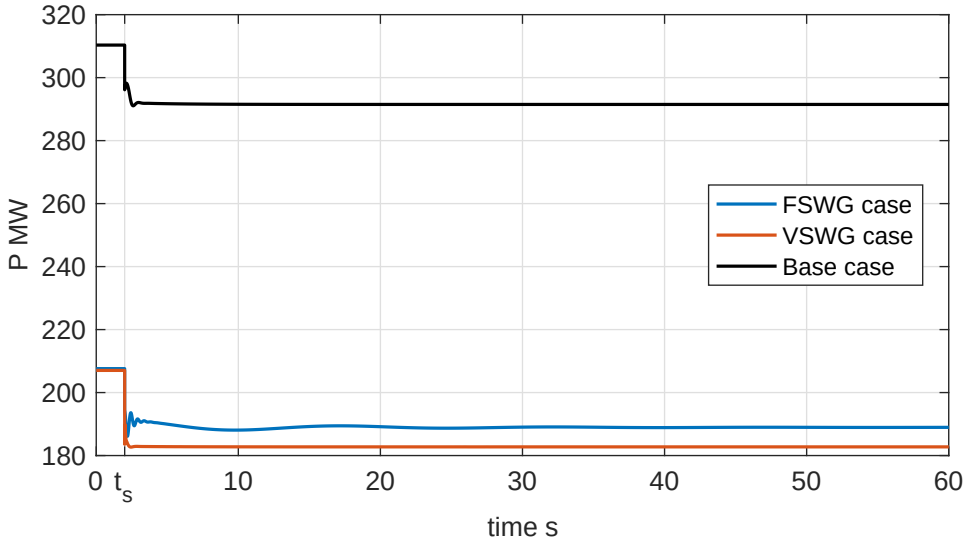

Figure 5.19: Bus 502 active power dispatch P_{ele}^{502} in the event of the proposed Bus 428 load shedding.

Figure 5.20 shows reactive power dispatch for Bus 502 Q_{ele}^{502}, where similar behaviour is seen among all three cases. A first key characteristic observed is the reduced variation that the VSWG case presents, due to WF ability to control reactive power dispatch. This can avoid Bus 502 to reach its minimum reactive power dispatch, where GUs lose voltage control.

Finally, Figure 5.21 depicts Bus 502 mechanical power deviation from the initial point ΔP_{mec}^{502}, where curves show the impact of stock pipe water time constant that makes hydro power plants frequency control slower than thermal power plants. This fact shows the importance in providing a smooth power ramp for wind farm's synchronization, allowing enough time for frequency adjustments.

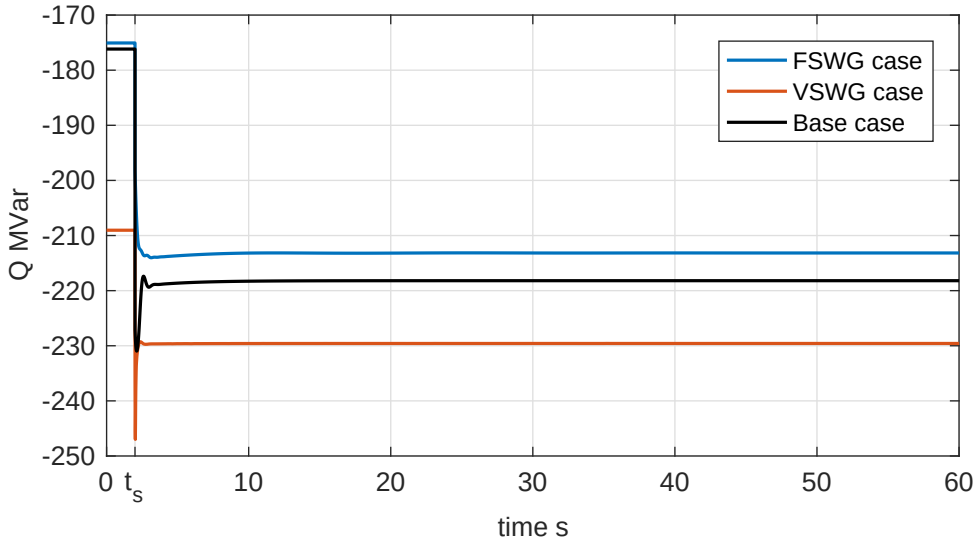

Figure 5.20: Bus 502 reactive power dispatch Q_{ele}^{502} in the event of the proposed Bus 428 load shedding.

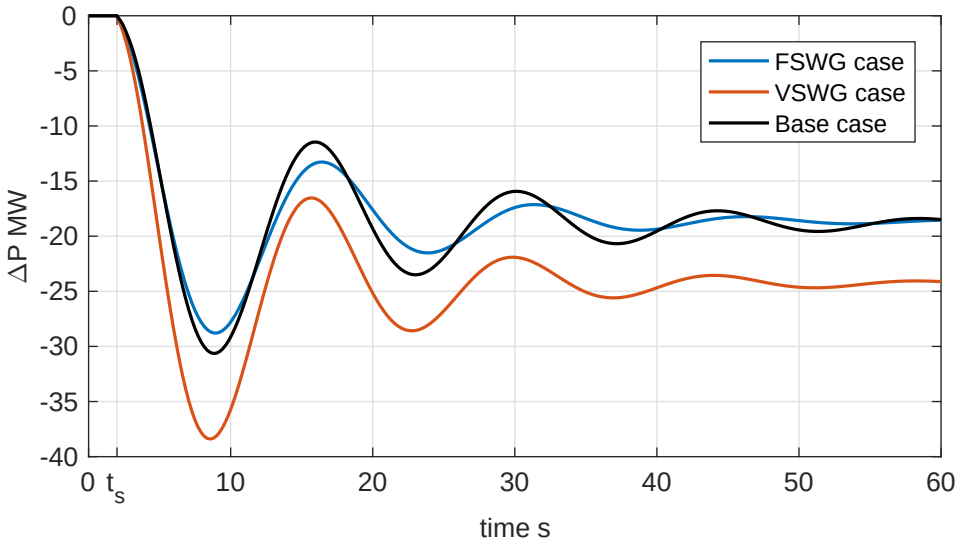

Figure 5.21: Variation on the mechanical power for Bus 502 ΔP_{mec}^{502} in the event of the proposed Bus 428 load shedding.

5.7.3 Conclusion

The power flow analysis shows the proposed routine performance in dealing with a stochastic simulation in a real case scenario. Routine's output allows the in-

vestigation on wind power impact on stability. The VSWG case shows positive impacts for the indices of collapse, by increasing load margin and system ability to supply local reactive power demand, while the FSWG case pushes the system closer to the collapse point in average, reducing system operative margin in case of load increase.

The robustness areas technique allows the visualization of the improvements wind power brings to power system stability. Wind power presents considerable increase on system robustness level, what leads to positive impacts on dynamic stability [62, 101].

Synchronizations controllers for wind farms presented acceptable performance on the real case scenario. They provided smooth power dispatch transition, avoiding large frequency and voltage level variations. This shows the methodology efficiency, encouraging the application of this approach in the next phase of restoration, as it follows in the next chapter.

Chapter 6

Coordinated phase restoration

6.1 Introduction

This chapter presents the continuation on the Brazilian power grid restoration, which shows the Coordinated Phase (CP) of restoration.

6.2 Restoration plan for the São Paulo State grid

Figure 6.1 shows the São Paulo state grid restoration system operated by the company CETEEP, which independently restores from the surrounding areas during earlier stages of CP. In this system, five corridors restore the majority of São Paulo state grid, naming:

- Água Vermelha - **AGV** - 1396 MW;
- Capivara - **CPV** - 619 MW;
- Jupiá - **JUP** - 1551 MW;
- Ilha Solteira - **ILS** - 3444 MW;

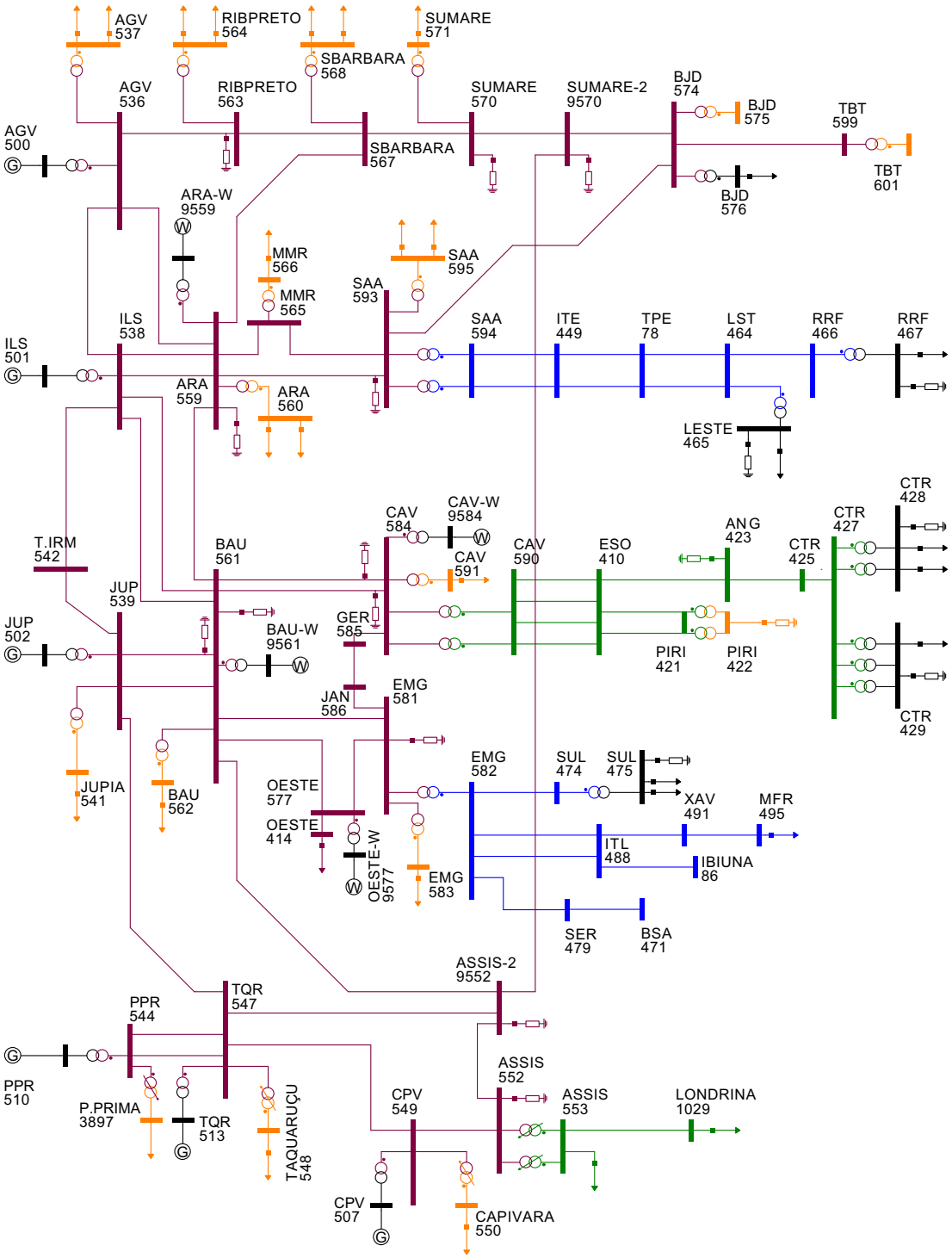

Figure 6.1: São Paulo State transmission grid during restoration CP. System data on Table D.4 and Table D.5.

- Porto Primavera - **PPV** - 1540 MW, this corridor also includes the Taquaruçu **TQR** power plant 554 MW.

The above list shows the abbreviations which this thesis uses. One can note that each corridor is named after the largest power plant connected to it. Regarding the restoration plan, this thesis divides in two tables: Table D.2 and Table D.3 (page 175 and page 176 respectively) The former contains instructions regarding corridors synchronization, and the latter is the bulk system restoration.

Synchronizing two corridors is a complex task, requiring specific equipment and trained personnel, which narrows the number of substations capable to perform it. The corridors synchronization leads to power interchange, improving frequency control for load pick-ups and reactive power control.

The investigation on the wind power impact on CP and the proposed methodology performance follows the steps on Table D.3.

6.3 Power flow simulations and voltage stability analysis for the presented restoration plan

Two steps are selected from Table D.3 for voltage stability studies in this thesis: step 5, and step 11. These steps represent cycles of branch and load restorations, recurrent on Power System Restorations (PSRs). Table 6.1 shows simulation parameters.

Table 6.1: Power flow simulation parameters for the Jupiá restoration area.

Parameter	Value	
	Step 5	Step 11
No. wind profiles	5000	5000
Weibull parameter a	6.4307 m/s	6.4307 m/s
Weibull parameter b	1.7643	1.7643
Total wind penetration	3×100 MW	4×100 MW
Power flow mismatch tolerance	1.0×10^{-6} pu	1.0×10^{-6} pu

Figure 6.2 and Figure 6.3 presents ΔQ results for step 5 and 11 respectively. One can see that the Variable Speed Wind Generator (VSWG) case enlarges system ability to provide reactive power, while Fixed Speed Wind Generator (FSWG) case reduces it for the majority of buses tested. The ability to control its own reactive power output is a great advantage for the VSWG case where it compensates unloaded transmission lines during the initial stages of restoration, providing voltage control. This feature is highly desirable during PSRs where voltage control is one of the most difficult challenges to overcome, especially in power systems with large transmission distances involved. It is worth noting that such feature provides positive results for the Fluent Phase (FP) and for the CP.

Figure 6.4 shows active power load margin λ for step 5 and step 11 of São Paulo power grid restoration. Results show that the VSWG case enlarges λ, while FSWG has slightly reduced λ, following the pattern from the test system and the Jupiá corridor. One can observe that for these cases, the wind power influence is lower than the previous cases, because of the corridor interconnections, allowing a less restricted power flow along the system. This way, as the CP develops towards its completion, the wind power impact tends to be faded under power plants control region.

Figure 6.5 shows the power flow tangent vector's Euclidean norm $\|\mathbf{TV}\|$ in function of total P_{out} where trends emerge. Figure 6.5a depicts step 5 where the wind power presence makes system more sensitive to load variations, indicating a proximity to the collapse point in comparison to the base case scenario. For step 11, Figure 6.5b shows that the VSWG case makes system less sensitive to load variation than the base case.

One can observe on the scatter plots that positive increments in P_{out} leads to reduction in $\|\mathbf{TV}\|$ for the VSWG case, while the FSWG case presents an almost constant $\|\mathbf{TV}\|$ for variations in P_{out}. This shows that the FSWG loses ability to provide positive impacts by increasing its dispatch.

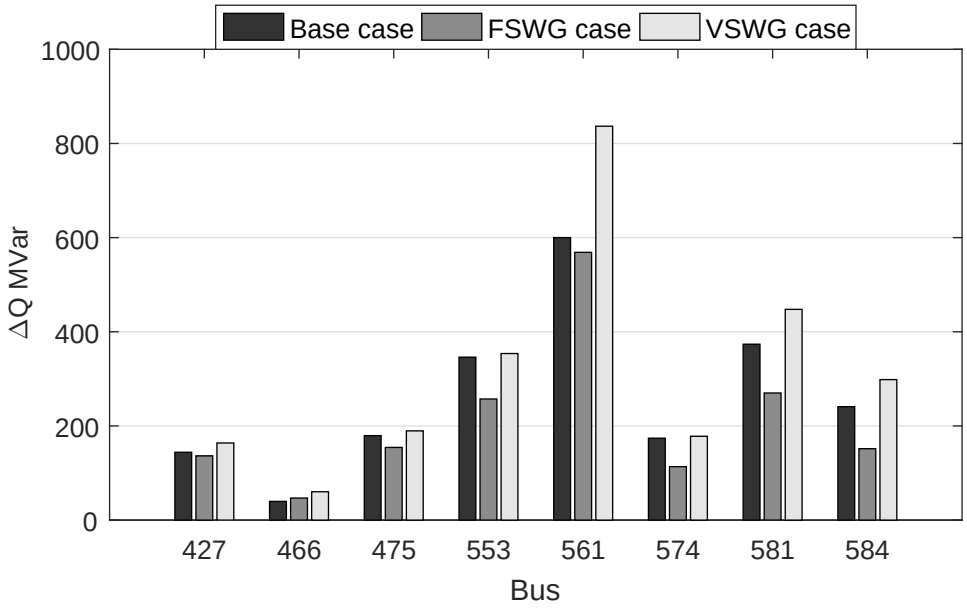

Figure 6.2: Reactive power load margin ΔQ for step 5 of Brazilian system restoration.

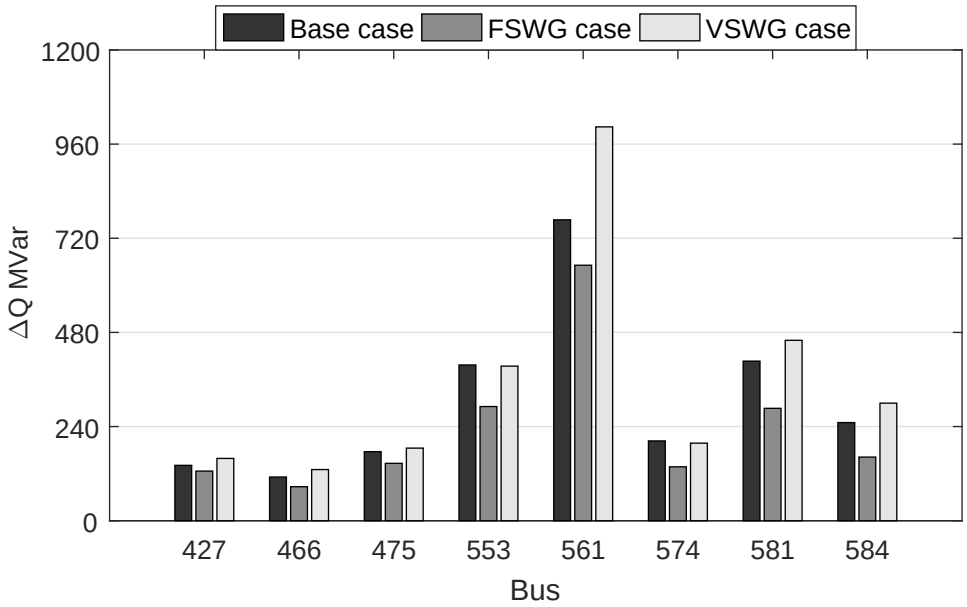

Figure 6.3: Reactive power load margin ΔQ for step 11 of Brazilian system restoration.

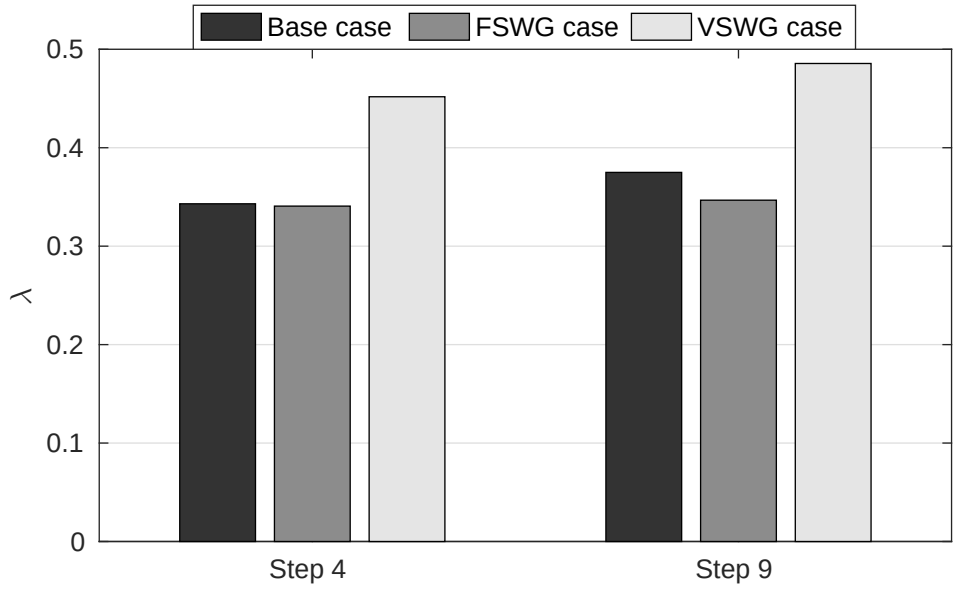

Figure 6.4: Active power load margin λ for the completed Jupiá corridor restoration procedure.

6.4 Energy function analysis

The investigation on São Paulo state Robustness Areas (RAs) uses the proposed energy function tool [62,101] described by (3.9). This system analysis is made by using the $E_p(X^s, X^u)$ levels of each bus defining their vulnerability, thus indicating the impact of wind power in this system. Table D.6 (Appendix D) presents $E_p(X^s, X^u)$ that is calculated considering the system in step 5 and in step 11 (Table D.3), that are the two points with dynamic stability studies on the following section. For this system images with $E_p(X^s, X^u)$ background are infeasible, due to the large scale in consideration.

The analysis from Table D.6 shows scattered improvements along the system, especially for the FSWG case, however such improvements are not significant as they are for the FP restoration. In fact, such improvements tend to attenuate as restoration develops. This is due to the corridors interconnections and the possibility of power interchange among them, which reduces wind power interference

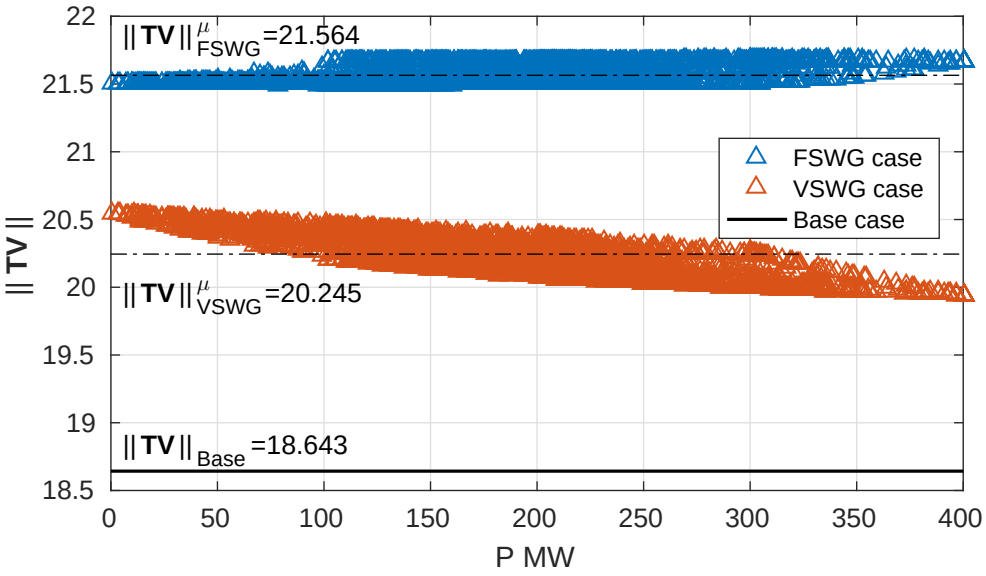

(a) Step 5.

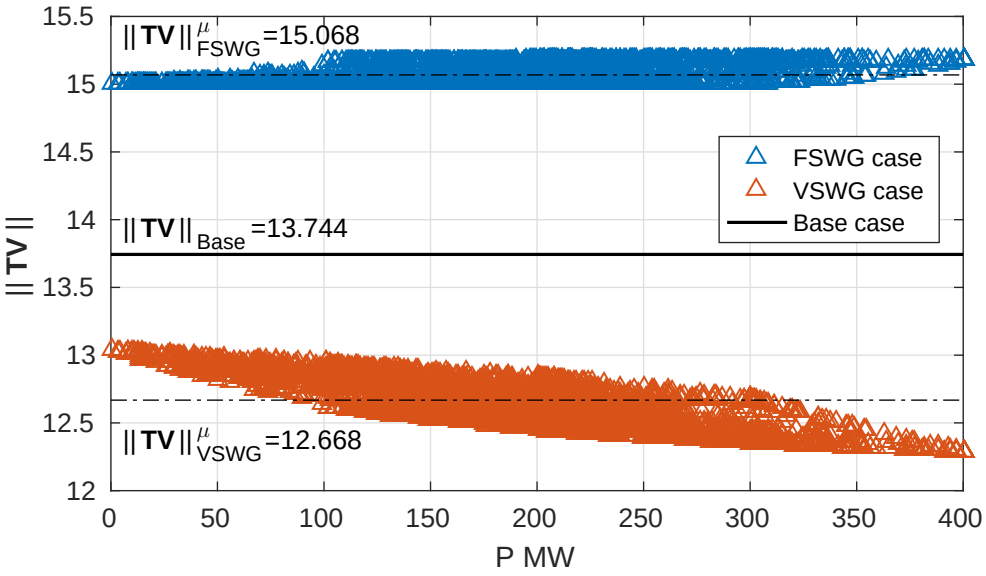

(b) Step 11.

Figure 6.5: $\|\mathbf{TV}\|$ distribution as function of total wind power dispatch P_{out} for the Jupiá system completed restoration. $\|\mathbf{TV}\|^{\mu}_{FSWG}$ and $\|\mathbf{TV}\|^{\mu}_{VSWG}$ stand for the mean value for its respective distribution.

area.

6.5 Dynamic stability studies for the presented restoration plan

The events proposed to assess the São Paulo state grid dynamic stability are:

1. Loop closure - Bus 538 to Bus 561 - step 5;
2. Load pick-up at Bus 561 - step 5;
3. Bus 9577 wind far restoration - step 6;
4. Wind speed variation at Bus 9561 - step 11 completed.

Table 6.2 summarizes the simulation parameter used for the CP analysis.

Table 6.2: Time domain simulation parameters for the São Paulo state grid.

Parameter	Value
Integration step	1.0 ms
Output frequency	5
Simulation time	Variable
Simulation Software	ANATEM®
Loads composition	$0.5\mathrm{Z_{cst}} + 0.0\mathrm{I_{cst}} + 0.5\mathrm{P_{cst}}$

6.5.1 Loop closure simulation

This simulation event consists in switching on the receiving end of transmission line (Bus 561), considering the emitting end (Bus 538) had energized the branch. Figure 6.6 shows the active power injected into Bus 561 by the restored line P_{line}. One can see that the base case has considerably larger variation in P_{line} than the cases with wind power, which is consequence of the larger Standing Phase Angle

(SPA) imposed, that for the base case is 3.40° while for the FSWG and for the VSWG are 0.34° and 0.22° respectively.

Figure 6.7 shows Bus 561 voltage level response, where the base cases presents larger voltage excursions for the proposed event. It is also noticeable that the FSWG almost reaches the maximum voltage level boundary. The VSWG is set to control Bus 9561 voltage level, thus allowing Bus 561 voltage level to fluctuate.

Power dispatch measures the wind power influence in this event, where the Wind Farm (WF) at bus 9561 is the electrically closest to the event. Figure 6.8 shows WF's active power output P_{out}, where one can see short period transient behaviour for both cases, though these do not present any significant influence on system stability. P_{out} curves affirm the fact that wind power influence on restoration tend to ease as restoration advances.

Figure 6.9 presents WF's reactive power output Q_{out}, where the FSWG case has a transient variation, yet its final value is very close to the initial, showing poor ability to control Q_{out}. The VSWG case shows its Q_{out} control as it shifts

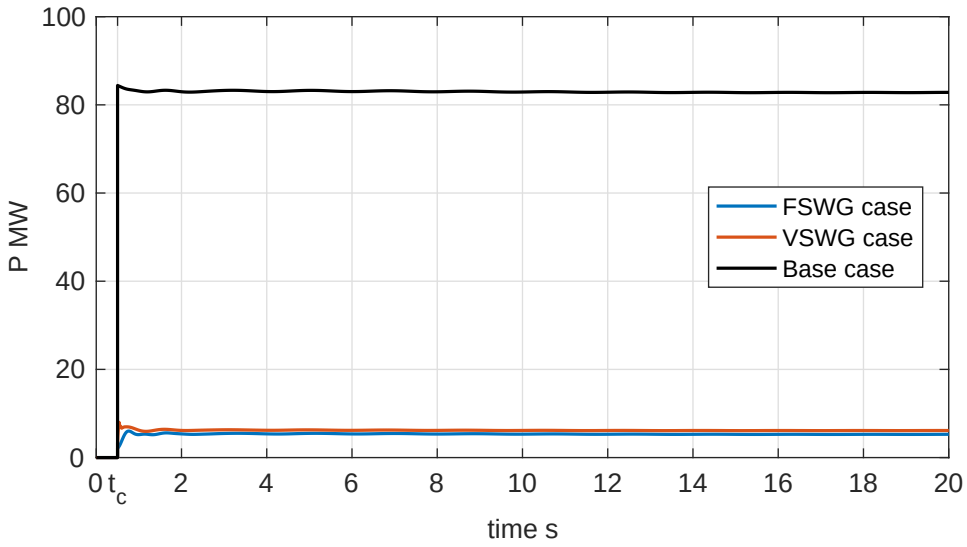

Figure 6.6: Active power injected by the transmission line into Bus 561 P_{line} in the event of the loop closure. t_c stands for loop closure time.

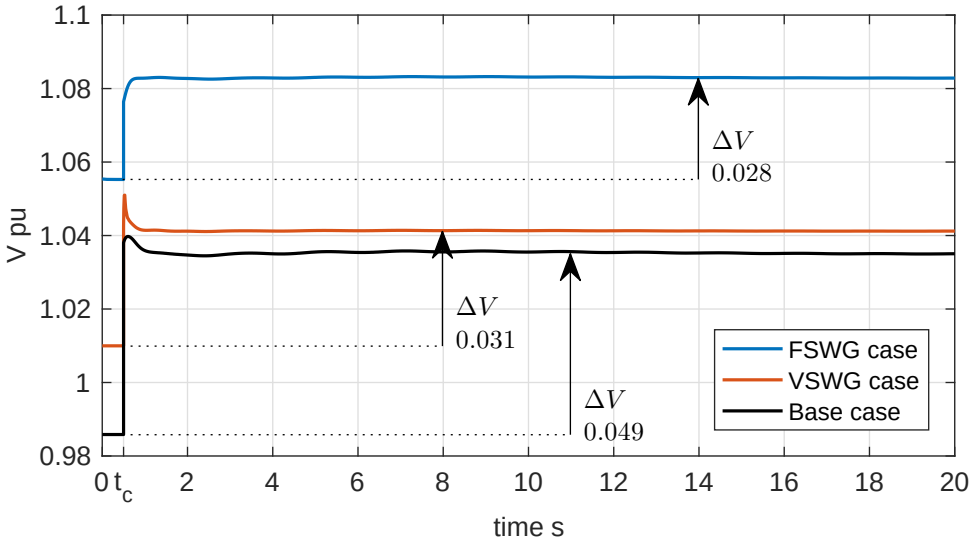

Figure 6.7: Bus 561 voltage level V^{561} in the event of the loop closure.

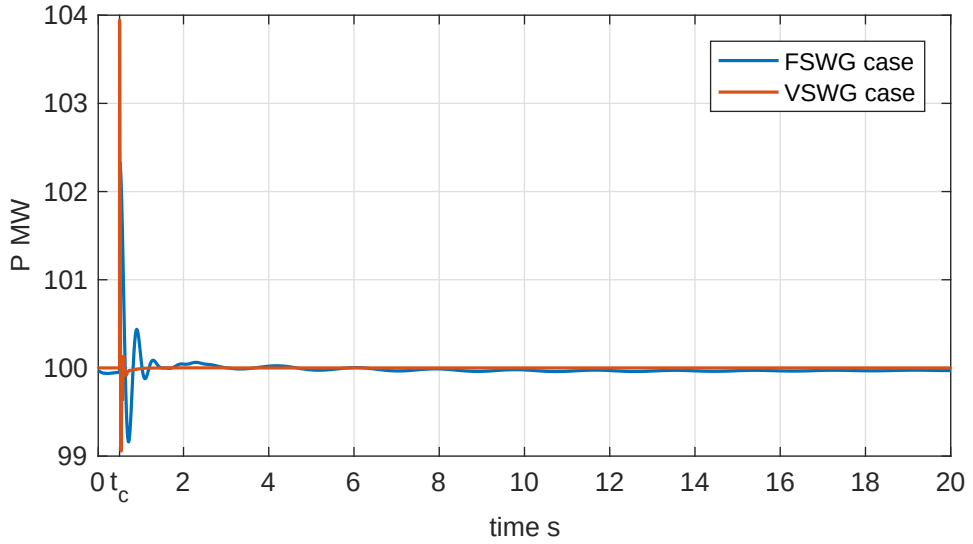

Figure 6.8: Bus 9561 wind farm active power output P_{out} in the event of the loop closure.

over -20 MVar to compensate the extra reactive power injected to its substation from the line closed.

Angular stability analysis uses Bus 501 machines rotor as reference. Figure 6.10 shows rotor angles displacement, where no major angle variation occurs

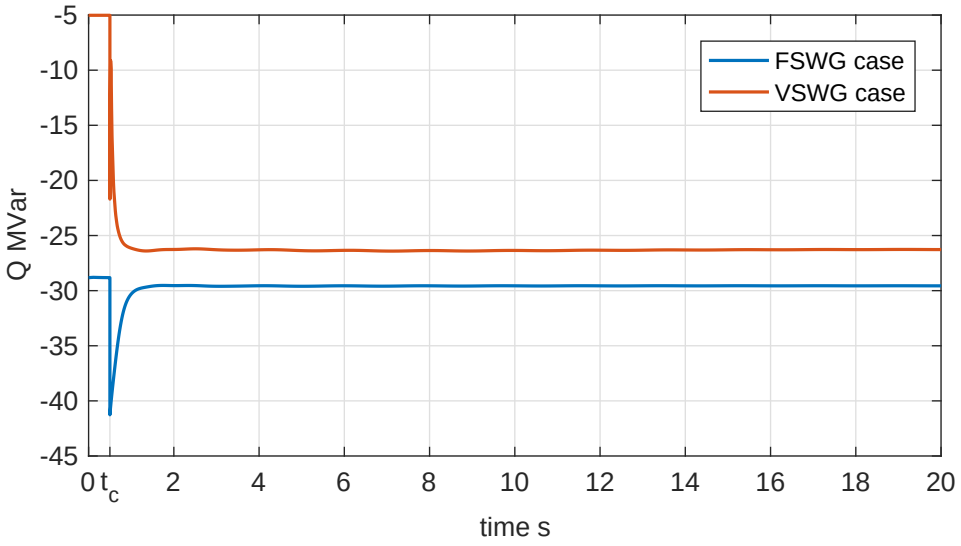

Figure 6.9: Bus 9561 wind farm reactive power output Q_{out} in the event of the loop closure.

for the three cases considered, which indicates that the event does not severely impacts stability. One can point out two main issues: larger angle variation for the Base case, and sustained angular oscillation.

Larger angle variation for the Base case is mainly caused by demagnetization effect of armature reaction that changes the power-angle (or $P-\delta$) characteristics [32, 33], degrading angular stability level. Figure 6.11 shows Bus 502 machine's field voltage E_{fd}^{502}, where the Base case scenario presents more intense E_{fd}^{502} than the wind power scenarios. Machines armature reaction is a direct consequence of the current injected into the grid, which increases as a transmission lines restore. This shows that wind power has a positive impact on system angular stability during PSRs by mitigating current variations.

The second issue presented for the loop closure is the sustained oscillations presented along the process, where accelerating power curves P_{ac} demonstrate the problem, as depicted in Figure 6.12. During the first stages after corridors synchronization, the São Paulo state grid operates with two distinctive areas, containing the following power plants:

North area - Bus 500, Bus 501 (angular reference) and Bus 502

South west area - Bus 507, Bus 510 and Bus 513

These two areas are connected via long transmission lines, where before step 9 (see Table D.3), there is over 900 km of transmission lines connecting Bus 500 to Bus 507. Such distance increases impedances and restricts power transactions,

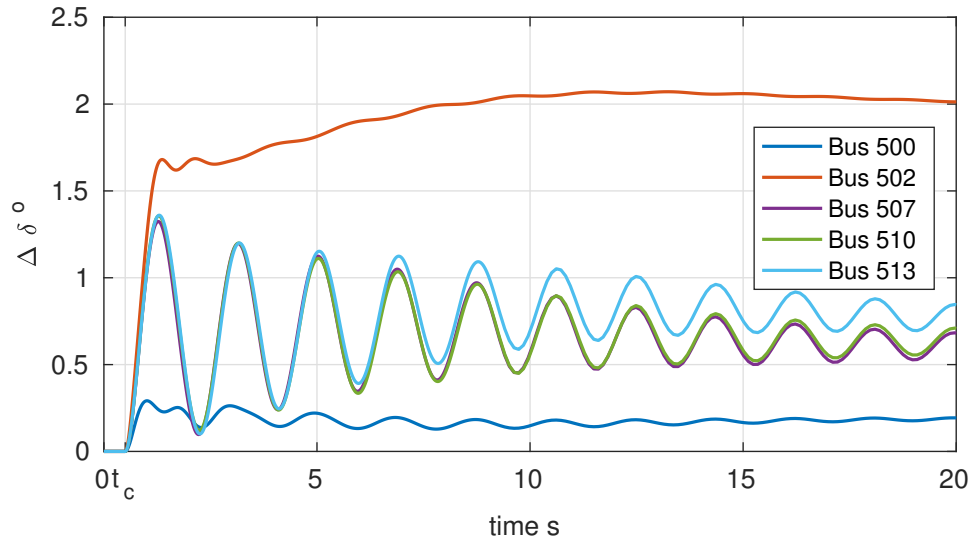

(a) Base case.

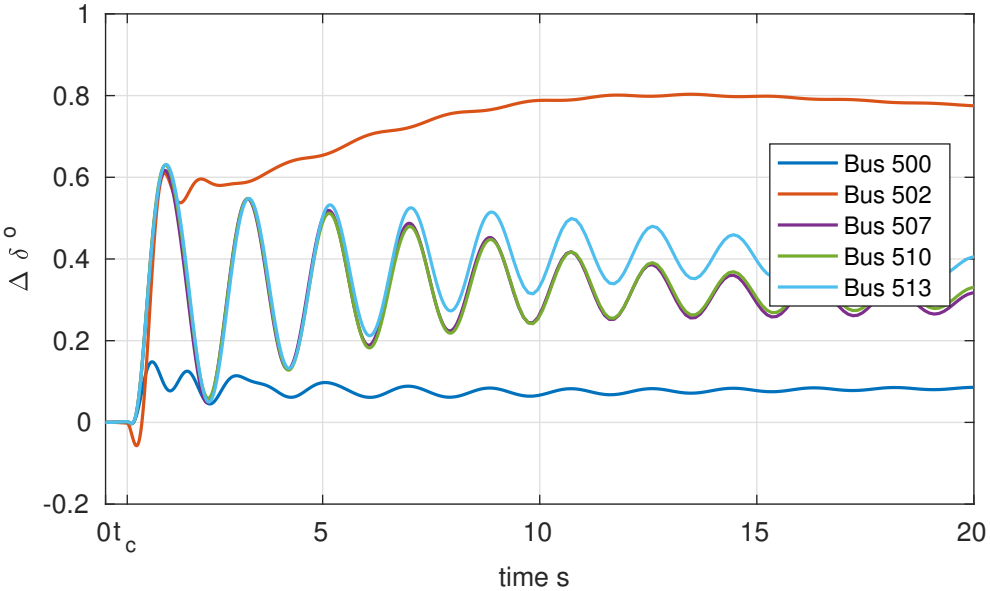

(b) FSWG case.

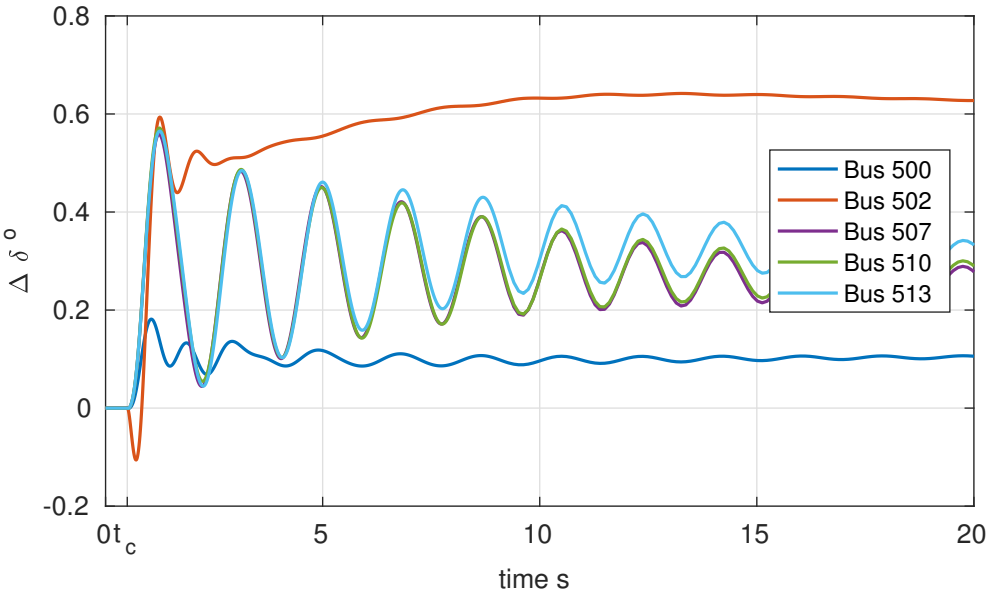

(c) VSWG case.

Figure 6.10: Power plants rotor angle displacement in the event of the loop closure. The angular reference adopted is the Bus 501 power plant rotor.

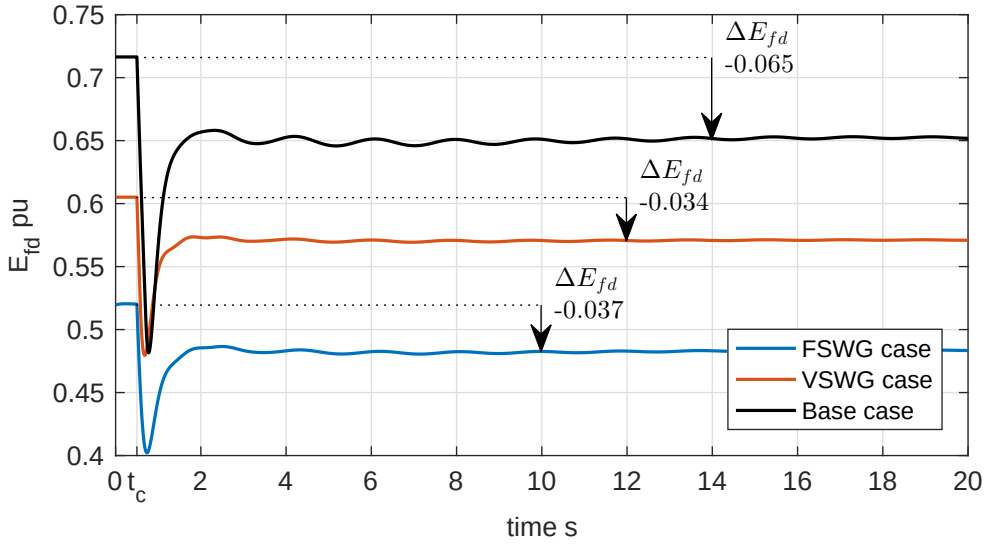

Figure 6.11: Bus 502 field voltage E_{fd}^{502} for the event of the loop closure showing the demagnetization effect of armature reaction.

leading to a scenario where areas tend to oscillate in opposition to each other. As Figure 6.12 shows, Bus 513's area oscillates on the same period as Bus 501,

however with an 180° phase angle and a low damping factor. The lower damping factor is recurrent in such period because voltage regulators and Power System Stabilizers (PSSs) are not tuned to operate in such conditions. One can note from Figure 6.12 that the wind power mitigates initial P_{ac}.

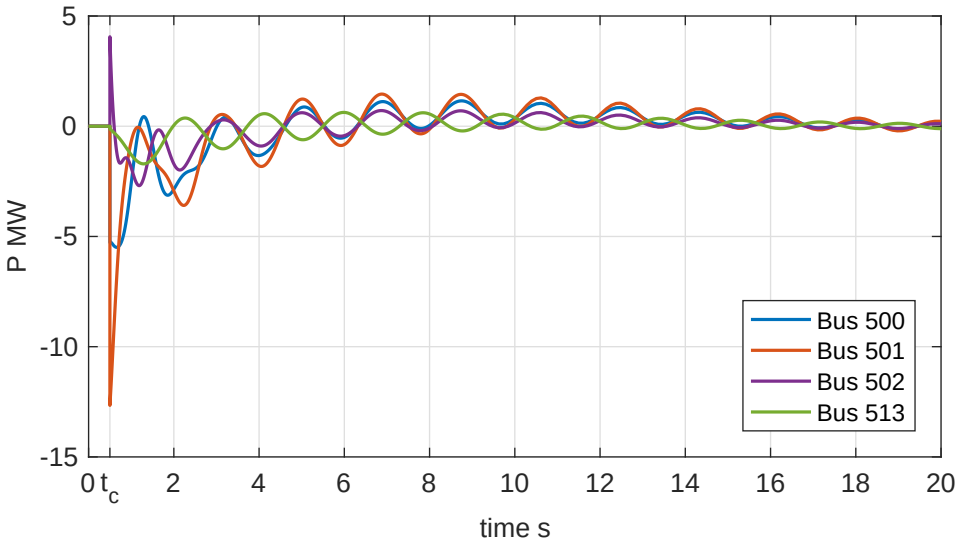

(a) Base case.

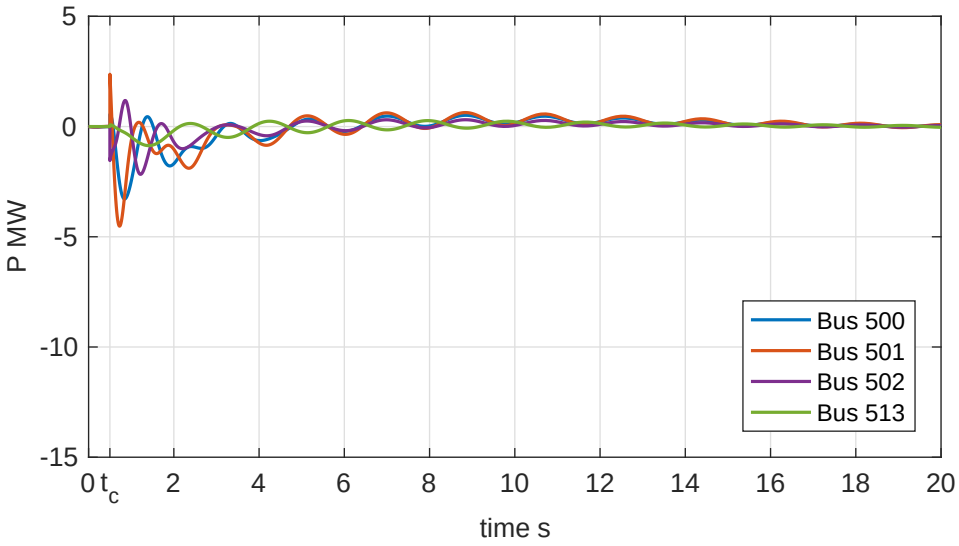

(b) FSWG case.

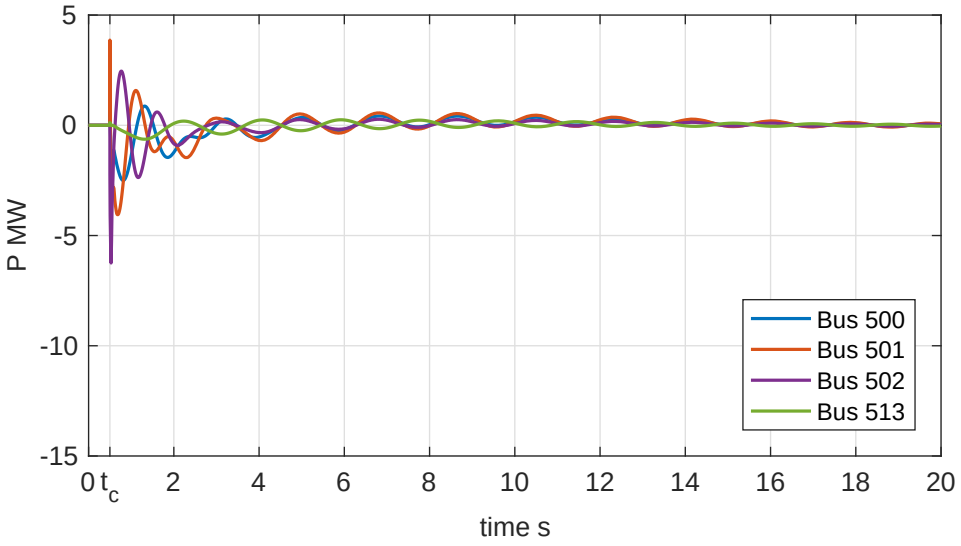

(c) VSWG case.

Figure 6.12: Accelerating power P_{ac} showing the inter-area oscillations in the São Paulo state grid. Figures are scaled to the same rage so one can easily identify the different magnitude by visual inspection.

6.5.2 Load pick-up at Bus 562

This simulation event consists in picking-up $S = 120.0 + j39.4\,\text{MVA}$ at Bus 562 (BAU substation). The simulation time is set to $t_{sim} = 25\,\text{s}$. Figure 6.13 shows Bus 562 voltage level, where the three cases considered presents considerable drop, although the curves remain within safety bounds (see Table 5.1). The maximum voltage overshoot seen for each case are: Base case ΔV = -0.061 pu; FSWG ΔV = -0.060 pu; VSWG ΔV = -0.056 pu.

Figure 6.14 shows active power dispatch from WF at Bus 9561 P_{out}^{9561}, which shows the fast transient associated to VSWG's power converter and the inertia provision from the FSWG. As the system restores power plants and areas are connected, the whole system inertia provision increases, which leads to a reduction on the effect caused by the FSWG's inertia. To exemplify this tendency, the WF at Bus 9584 represents 9.03% of total Jupià area inertia during the restoration FP, while at step 5 of CP it only represents 1.18% of total system inertia. Thus,

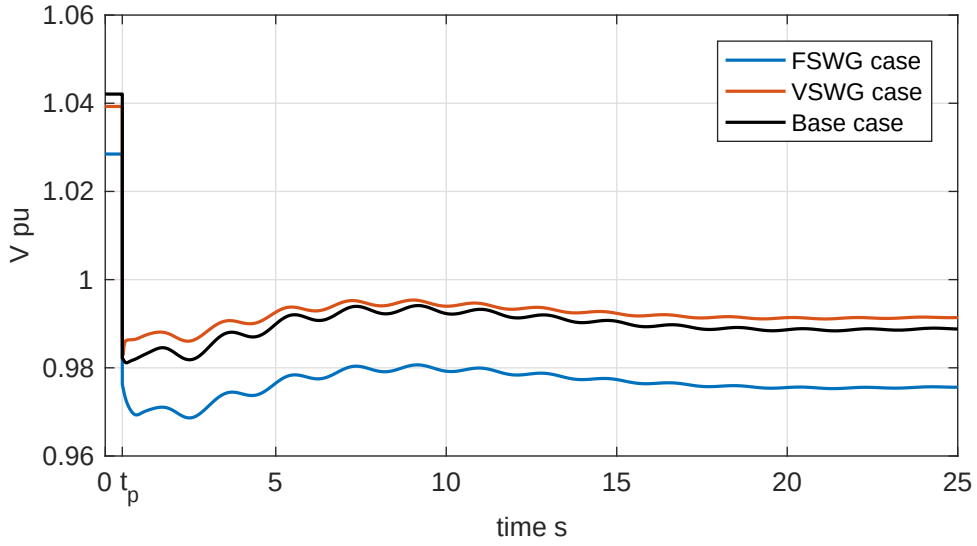

Figure 6.13: Bus 562 voltage level V^{562} in the event of the proposed load pick-up. t_p stands for load pick-up time.

as the restoration caries on, FSWGs influence on system frequency response tends to reduce to a point where it can be neglected [32, 59].

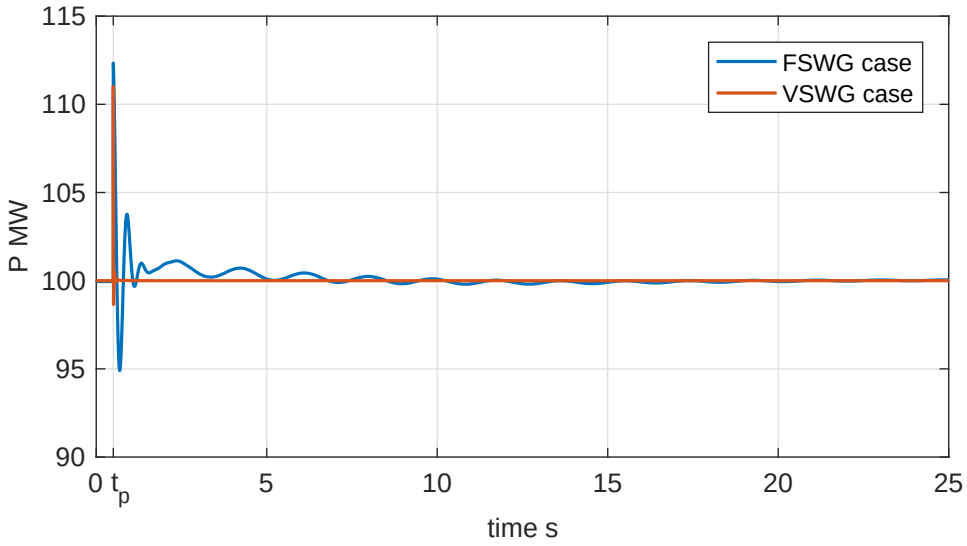

Figure 6.14: Bus 9561 wind farm active power output P_{out} in the event of the proposed load pick-up.

Figure 6.15 shows Bus 9561 reactive power dispatch Q_{out}^{9561}, where the VSWG

controllers vary Q_{out}^{9561} compensating voltage level at BAU substation. Both curves show sustained oscillations.

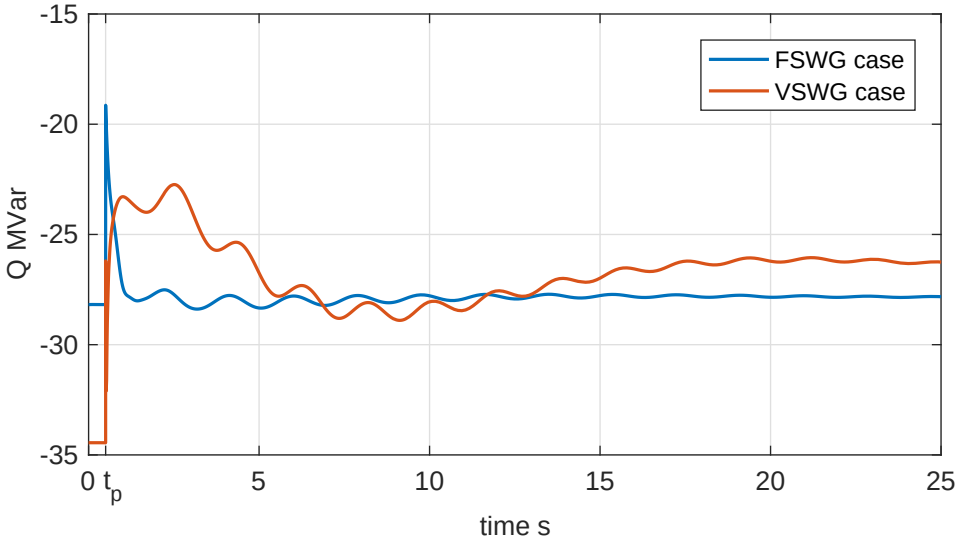

Figure 6.15: Bus 9561 wind farm reactive power output Q_{out} in the event of the proposed load pick-up.

From the angular stability point of view, wind power does not cause significant impact in system rotor angles' response for the considered event. Figure 6.16 shows machines' angular response for the event of the load pick-up, using Bus 501 as angular reference. The sustained oscillation observed regards the weak connection between the two electrically distant areas [31, 32], as mentioned for the loop closure event. Such angular oscillations are translated to power flow as described by 3.1, affecting transmission lines and buses voltage level, however these do not pose major concerns to angular stability.

Accelerating power curves P_{ac} complements the analysis on the sustained oscillations, as presented in Figure 6.17. Bus 513 represents the Southwest power plants, where the inter area oscillation is seen as Bus 513 swings against the North area machines. The FSWG case presents a slight mitigation on the initial P_{ac} value, due to the inertia effect that tends to mitigate as the restoration proceeds. For this point of restoration, FSWGs represents 17.26% of total generation,

tough only 3.58% of system inertial, emphasizing the reducing representation.

Wind power leads to a considerable reduction on main system Generator Units (GUs)' power dispatch P_{ele}. Figure 6.18 shows P_{ele} for the load pick-up, which presents a substantial P_{ele} shift from the base case to both wind power cases. Such reduction leads to a larger operational room for power plants, or a lower point in the $P - \delta$ chart, increasing GU ability to remain angular stable after

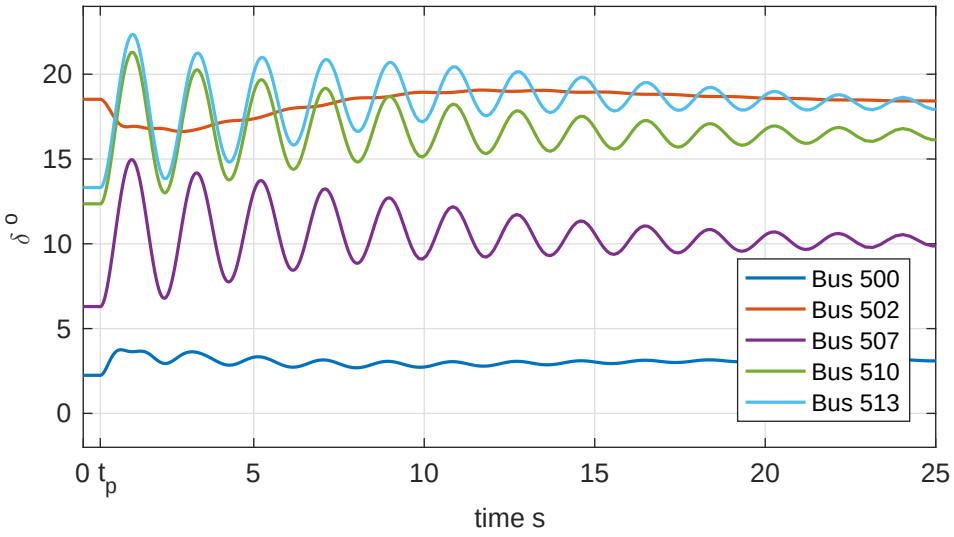

(a) Base case.

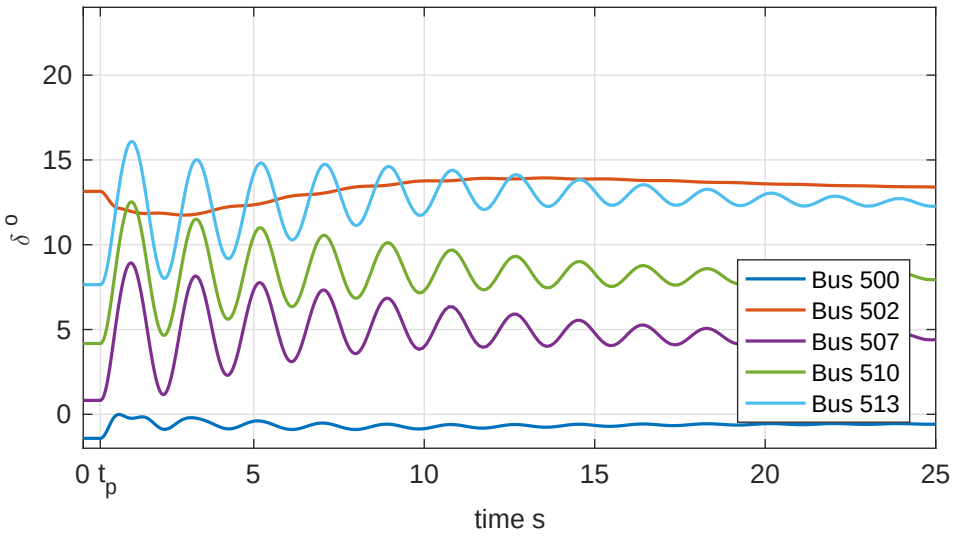

(b) FSWG case.

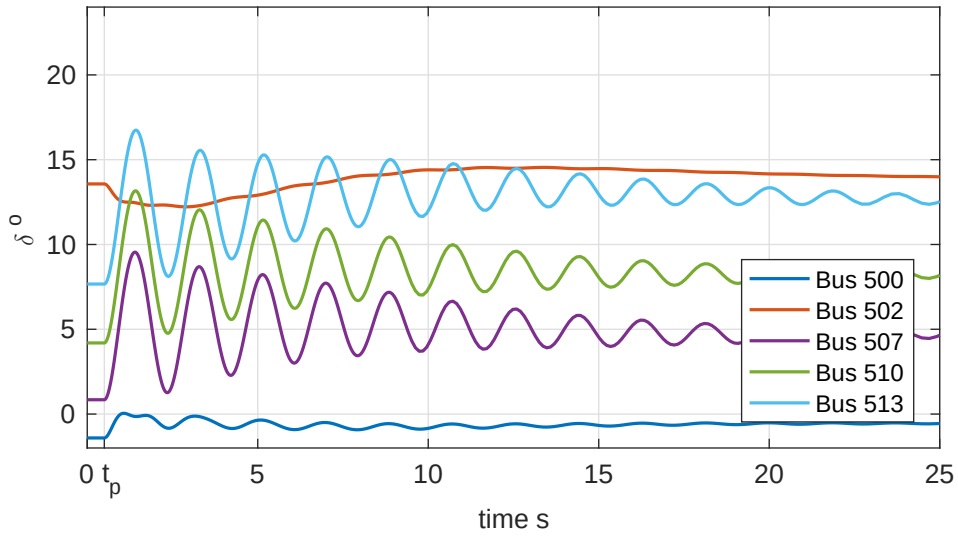

(c) VSWG case.

Figure 6.16: Power plants rotor angle response showing the inter area oscillation in the event of the loop closure. The angular reference adopted is the Bus 501 power plant rotor.

large impact events [32, 33].

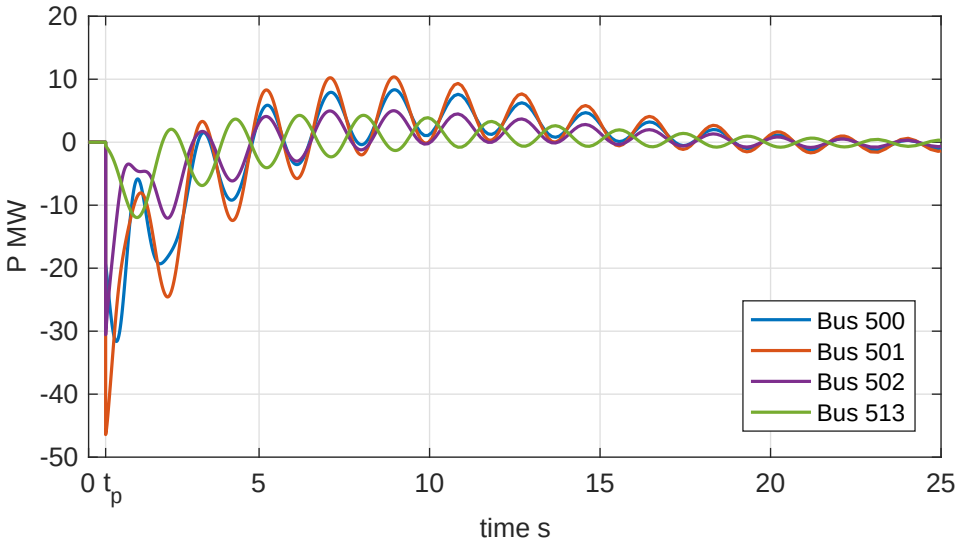

(a) Base case.

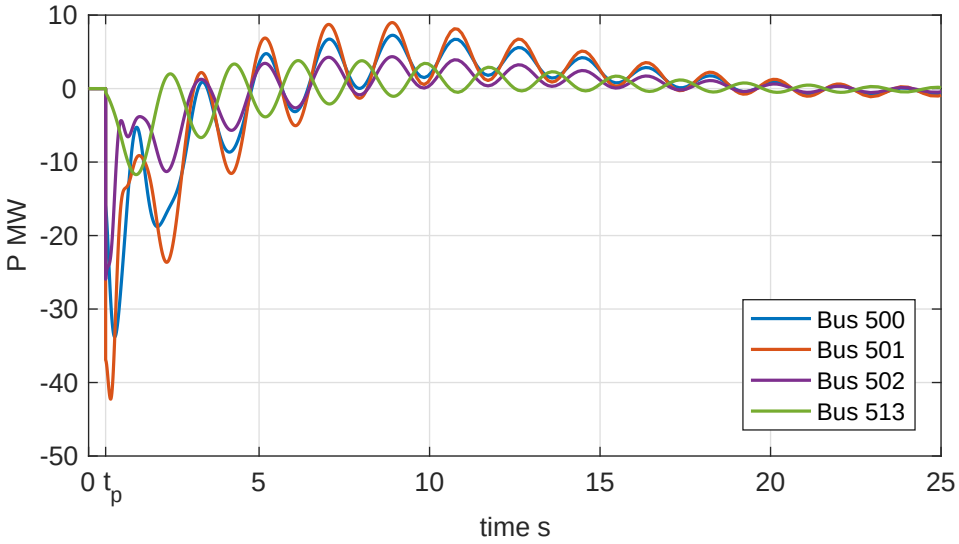

(b) FSWG case.

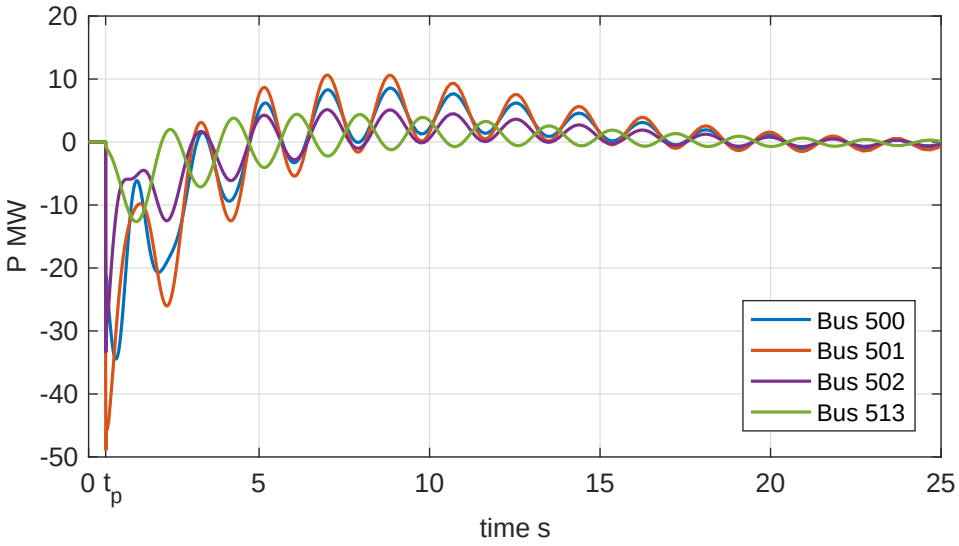

(c) VSWG case.

Figure 6.17: Accelerating power P_{ac} showing the intra-area oscillations in the São Paulo state grid. Figures are scaled to the same rage so one can easily identify the different magnitude by visual inspection.

Figure 6.19 shows variation in mechanical power delivered to the generator ΔP_{mec} where power plants' show a slow response in adjusting to the new load condition. This is a characteristics of hydro turbines, which require longer times to dispatch adjustments, where fast response would create stock pipe pressure waves that can damage power plant components [32, 33]. Bus 502 receives a special attention, because ΔP_{mec}^{502} is considerably lower than in other power plants,

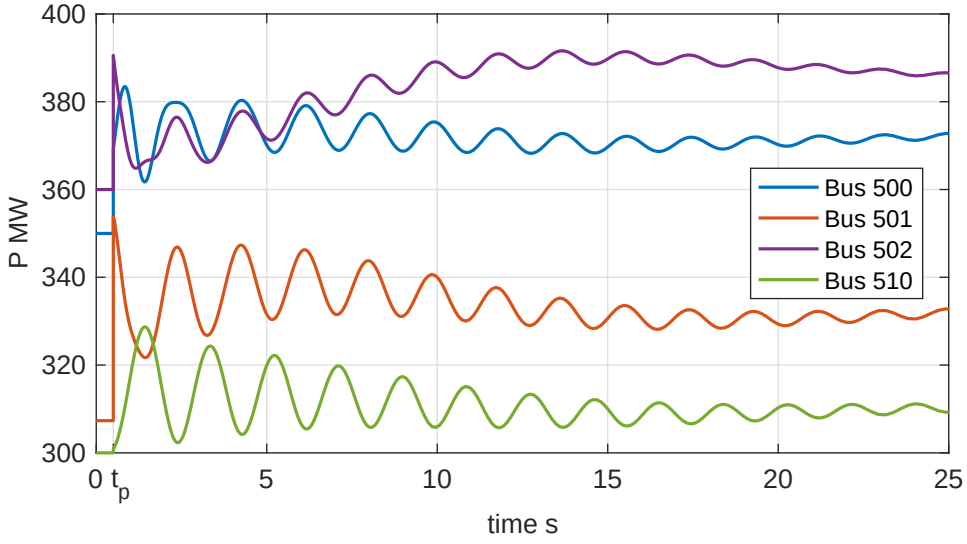

(a) Base case.

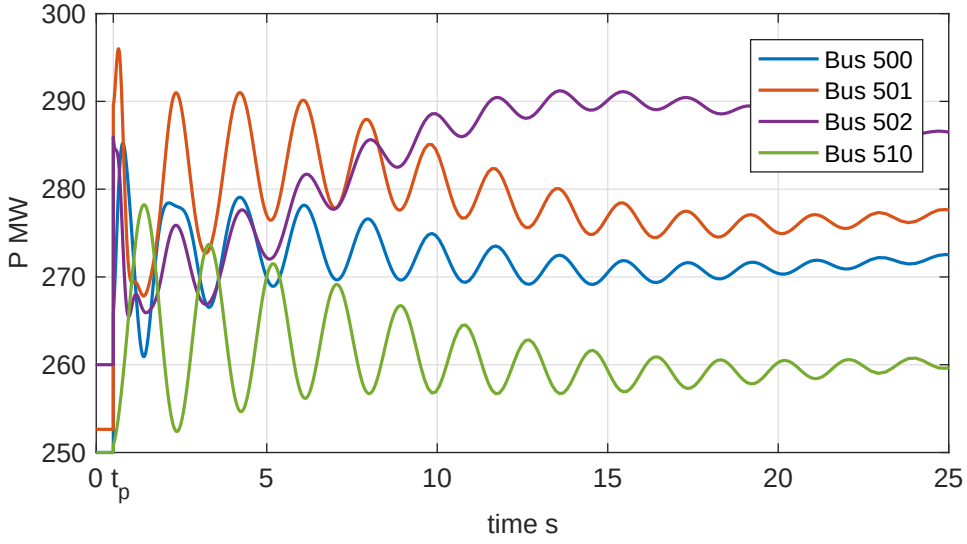

(b) FSWG case.

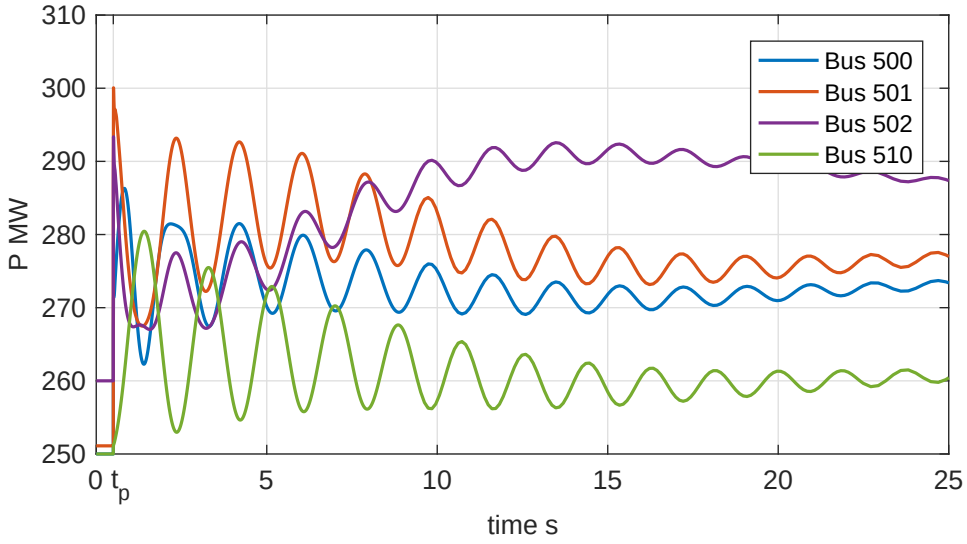

(c) VSWG case.

Figure 6.18: Active power dispatch P_{ele} in the event of the load pick-up.

taking about extra 5 s to reach the maximum peak overshoot.

The wind power impact on system's frequency control is observed in 6.20 where Bus 501 frequency f^{501} is used to represent grid frequency f_{grid}.

Figure 6.20 shows Bus 501 frequency f^{501}, which represents wind power impact on system's frequency control. The FSWG case presents a very similar curve to

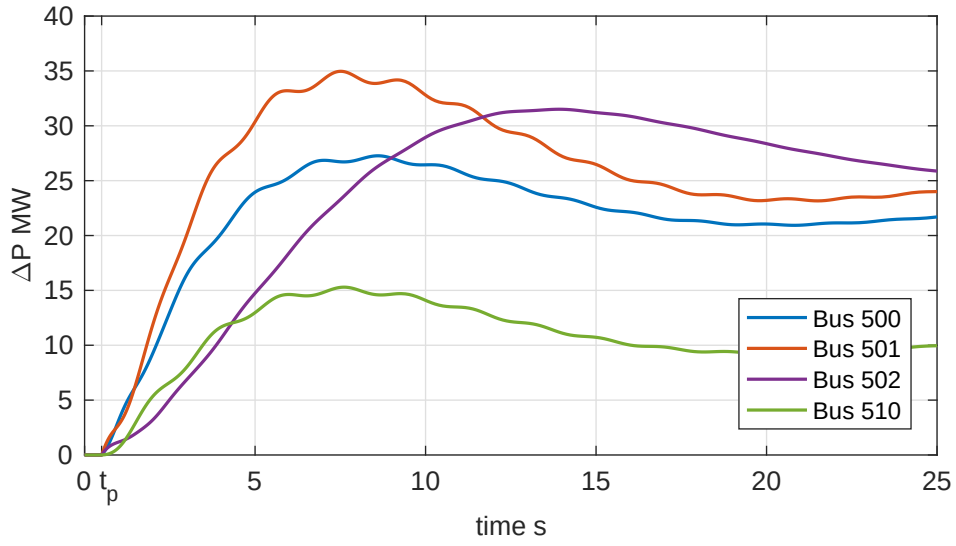

(a) Base case.

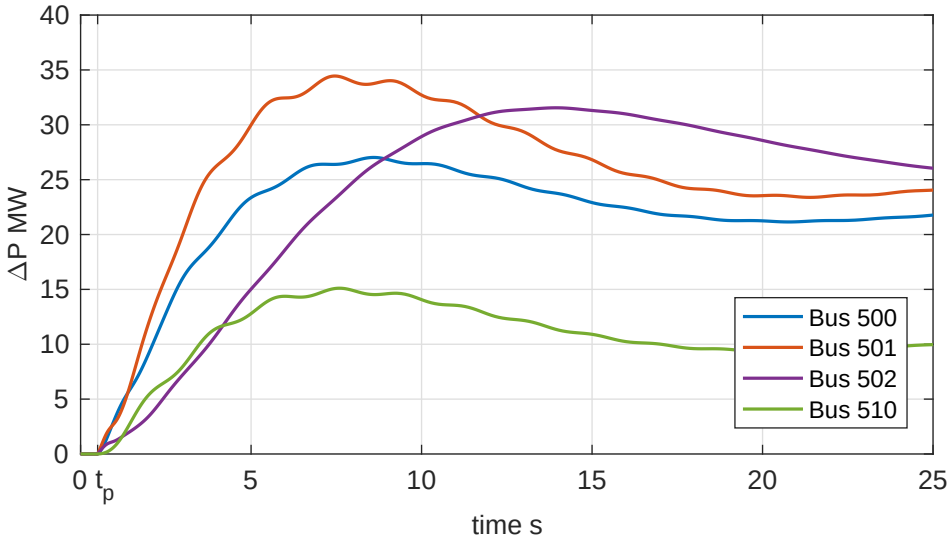

(b) FSWG case.

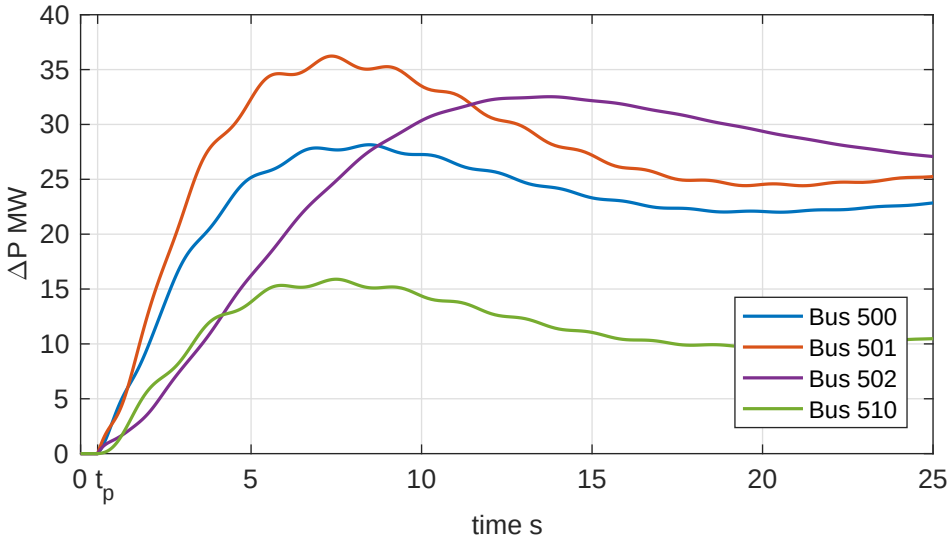

(c) VSWG case.

Figure 6.19: Mechanical power deviation from the initial point ΔP_{mec} in the event of the load pick-up.

the base case, confirming the mitigation on WFs inertia effect. The VSWG case presents a slight larger sag that the base case, in any case, it can be neglected due to the small scale associated.

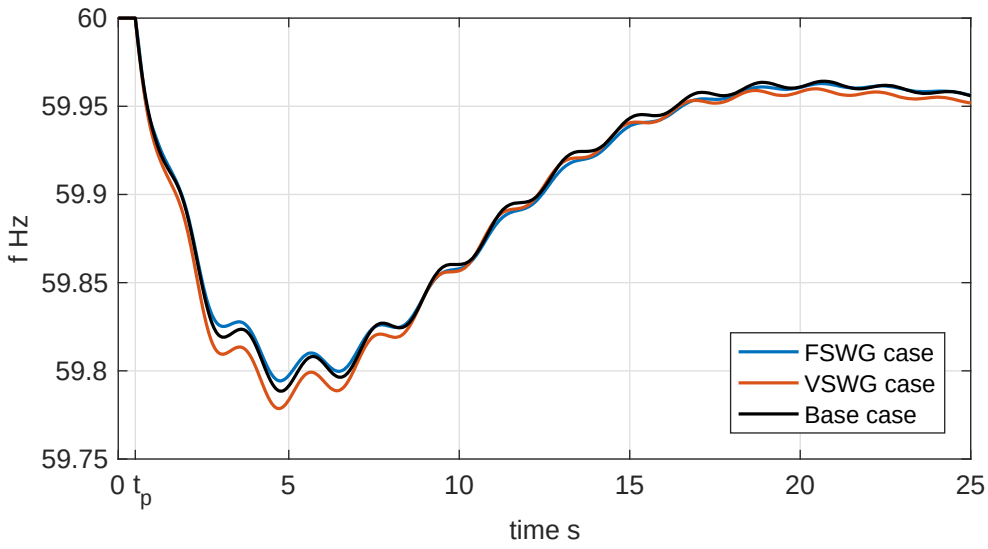

Figure 6.20: Bus 501 rotor frequency f^{501} used to represent grid frequency f_{grid} in the event of the load pick-up.

6.5.3 Bus 9577 wind farm synchronization

The WFs synchronization procedure adopted for the Brazilian system follows the approach proposed in Chapter 3. This way the first step is to use the initialization routine to calculate initial β_0 for the given wind speed: $v_w = 9.5\,\mathrm{m/s}$. The calculated initial pitch angles are: FSWG $\beta_0 = 0.199\,\mathrm{rad}$, and VSWG $\beta_0 = 0.500\,\mathrm{rad}$.

The robust behaviour presented for the coordinated phase of restoration encourages the reduction of power ramp time. Figure 6.21 shows controllers action on the turbine's pitch angle β, that is settled to vary in a 20 s window. For the sake of the model's availability, Wind Generators (WGs) models used for the Brazilian restoration grid are the same as those used for the test system in Chapter 4.

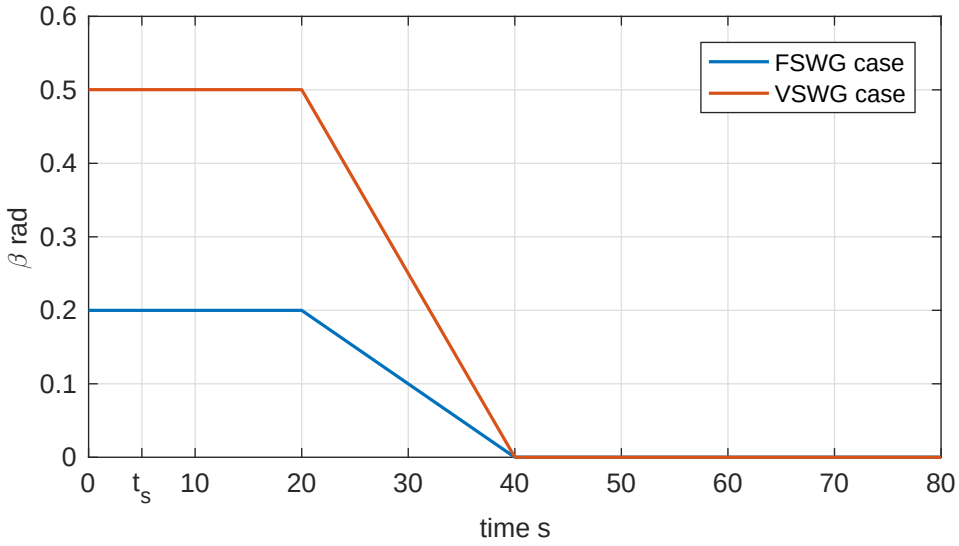

Figure 6.21: Wind turbine's blades pitch angle β demonstrating the proposed synchronization procedure for the wind farm at Bus 9577 on the Jupiá system. t_s stands for the synchronization time.

Wind farms' active power dispatch curves show the different response between

the FSWG and the VSWG, as depicted in Figure 6.22. The FSWG case presents an initial transient, and a direct correlation to β is seen, as it aims to the optimal point for the wind profile provided. The VSWG case does not present any significant initial transient, due to the inverter ability to decouple the machine from the grid. It is worth noting that the FSWG is off the optimal point for the wind speed considered, due to inability in controlling rotor's speed. Consequently, it has a lower dispatch than the VSWG.

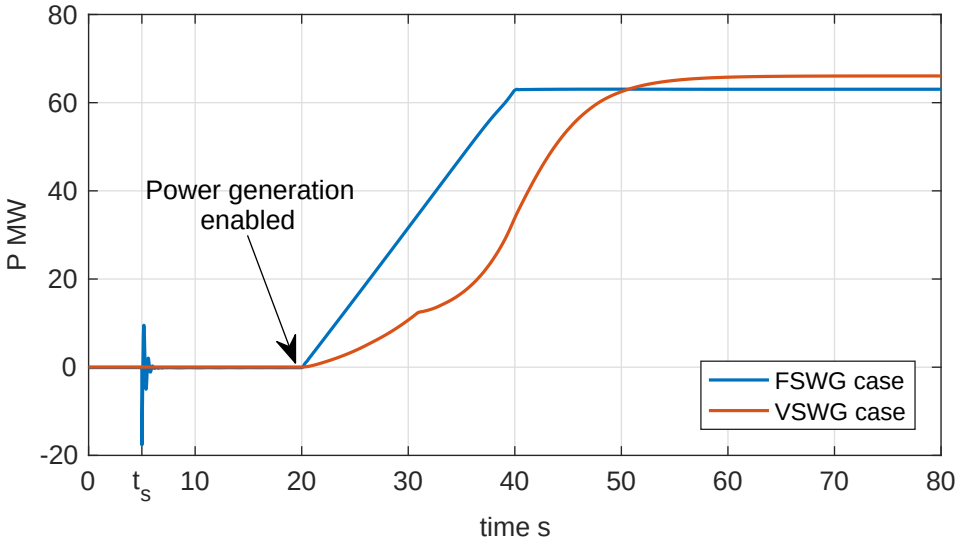

Figure 6.22: Wind farm active power output P_{out} in the event of Bus 9577 wind farm synchronization. The point where the power generation is enabled indicates the instant where the proposed controller is activated.

Wind farm's reactive power export Q_{out} shows how each case behaves during synchronization. Figure 6.23 depicts Q_{out} which for the FSWG case, a sudden Q_{out} drop on the instant of synchronization t_s is seen due to the generator's windings reactive power demand. Q_{out} for the VSWG does not present any significant response on t_s, however, it presents a controlled ramp, as the proposed voltage control takes place. Curves show that the VSWG reaches its thermal limit at Q_{out} = -20 MVar, therefore it loses voltage control ability for this simulation.

Figure 6.24 shows Bus 977 voltage level response for the synchronization

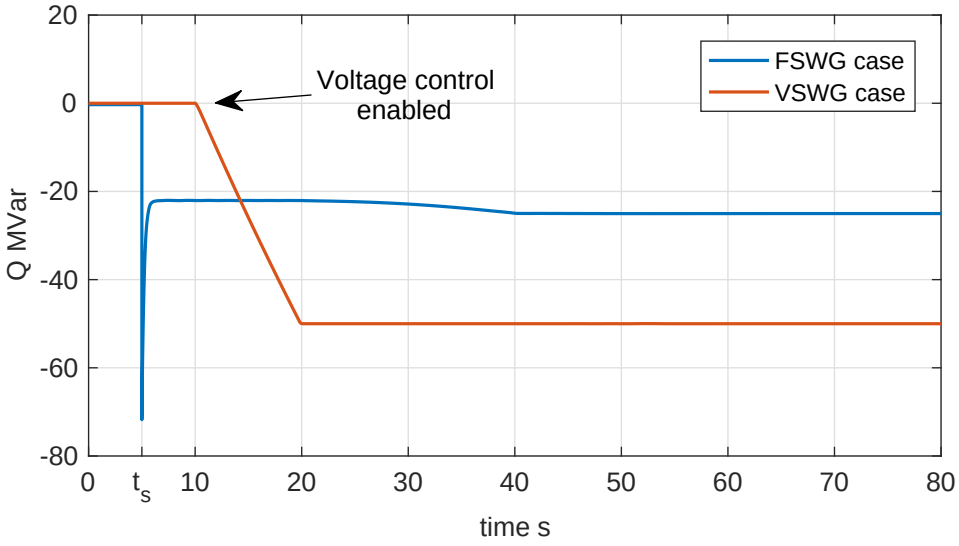

Figure 6.23: Wind farm reactive power output Q_{out} in the event of Bus 9577 wind farm synchronization.

procedure. For both scenarios, voltage level remains within acceptable range as Table 5.1 shows. This shows that the smooth control provided by proposed controllers allow enough time for voltage adjustments. It is also noticeable that despite the fact the VSWG reaches its thermal limit, voltage level remains almost steady for the active power ramp.

This thesis uses rotor frequency f^{501}, and rotor angle deviation $\Delta\delta$ aiming to investigate wind power's impact on Bus 502 power plant is investigated by using two key variables. Figure 6.25 shows synchronization impact on system's frequency control. Both cases respect the coordinated phase, where in fact the maximum overshoot observed is less than 10% of maximum deviation allowed.

From the angular stability point of view, the synchronization approach has negligible impact on the rotors' angle deviation, as Figure 6.26 shows. This shows that the proposed procedure mitigates the impact of synchronization procedure, allowing generators to move slowly to the new equilibrium point. Rotor angle results also show that the influence of wind power tends to reduce as restoration advances towards completion.

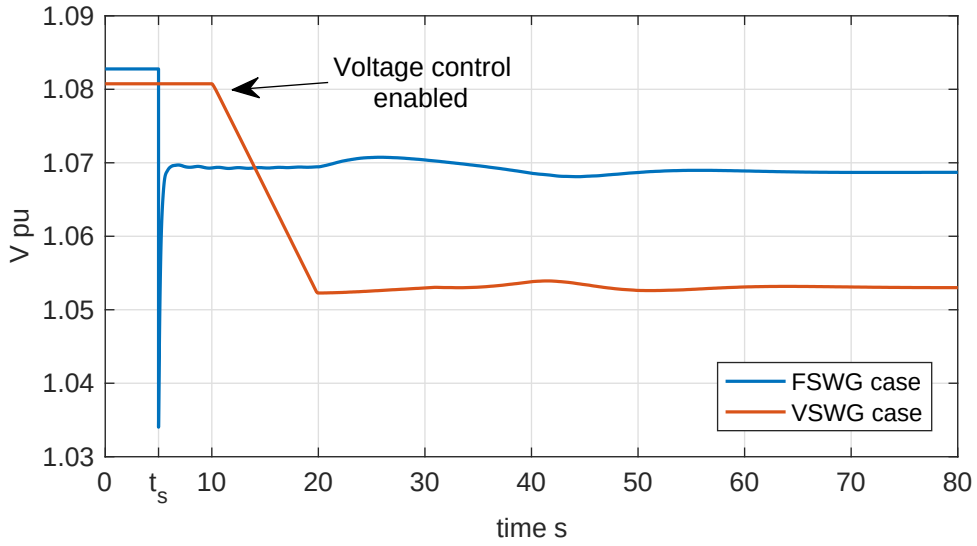

Figure 6.24: Voltage level imposed at Bus 577 in the event of wind farm synchronization.

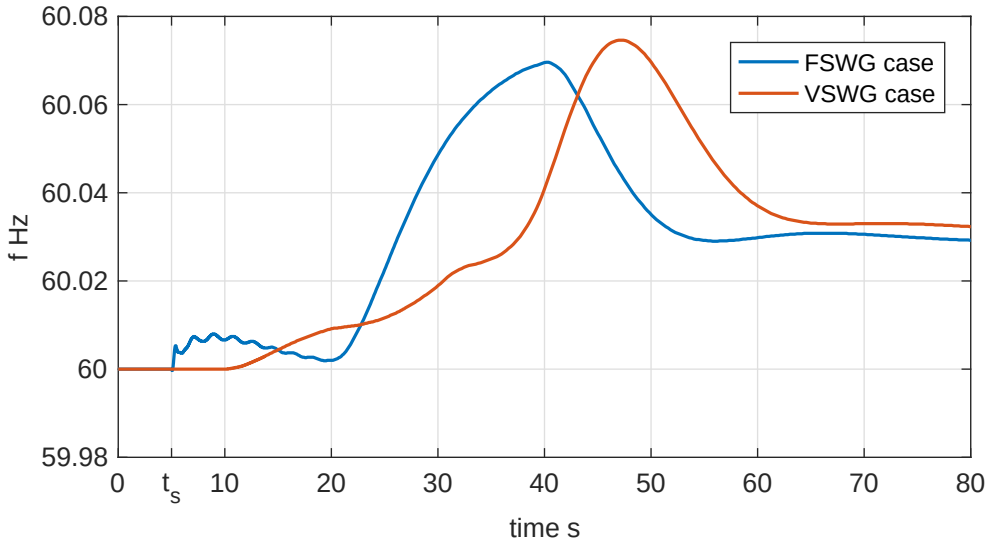

Figure 6.25: Bus 501 rotor frequency f^{501} used to represent grid frequency f_{grid} for the wind farm synchronization.

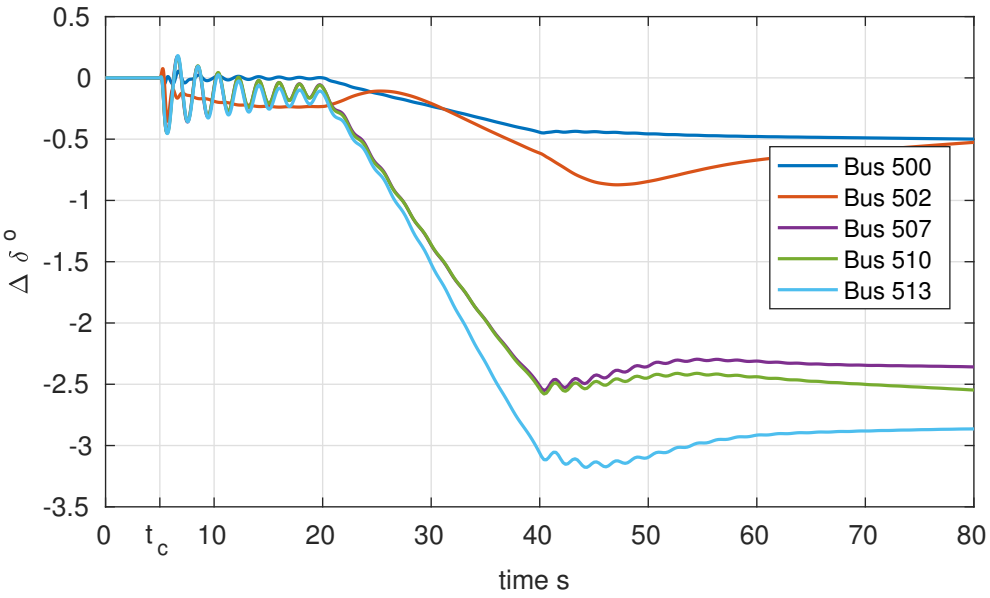

(a) FSWG case.

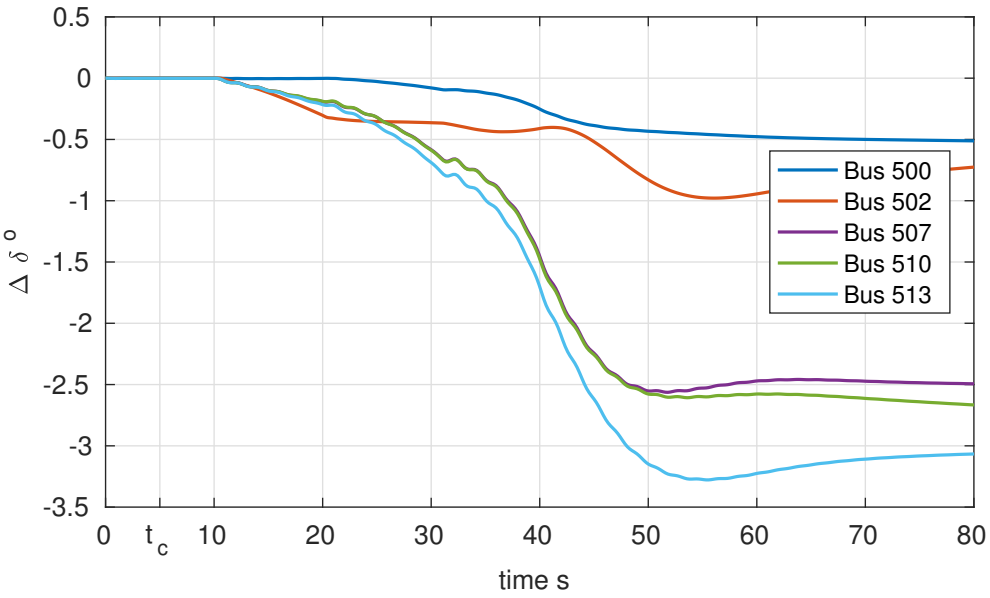

(b) VSWG case.

Figure 6.26: Power plants rotor angle displacement showing the synchronization impact on system's angular stability. The angular reference adopted is the Bus 501 power plant rotor.

6.5.4 Wind speed variation

Up to this points, all events consider constant wind speed, this way the fourth event proposed is the application of a wind series to Bus 9561 WF. The wind series consists in 1 s samples totalling 60 s, as presented by T. Ackermann in [57, p. 580]. Figure 6.27 shows the proposed wind series, both FSWG case and VSWG case use the same profile. For this event, simulation time is 60 s, so it covers the entire wind series.

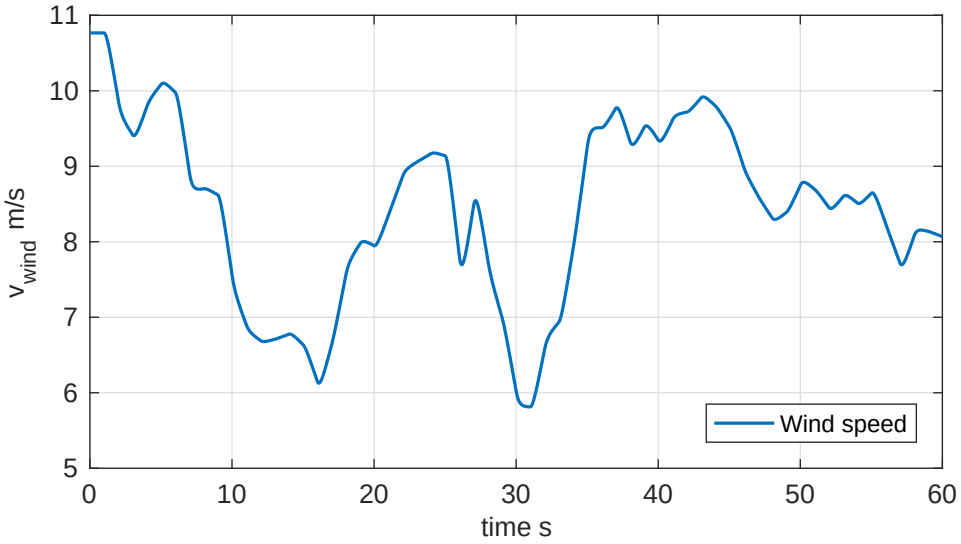

Figure 6.27: Wind speed profile applied to Bus 9561 power plant for investigation on the impact of wind power on PSRs. Source: [57]

Figure 6.28 presents WFs active power output P_{out}, which shows considerable differences between the two wind generator models. VSWG has higher P_{out} dispatch for the majority of simulation time, due to the ability to control its rotor speed and operate with higher coefficient of performance C_p. VSWG's speed control gives a smooth behaviour for P_{out} curve, though it makes slower P_{out} recovery as wind speed raises sharply.

Figure 6.29 presents reactive power output Q_{out} , where the FSWG case shows sharp variations along the wind series, due to variations on rotor slip s. The

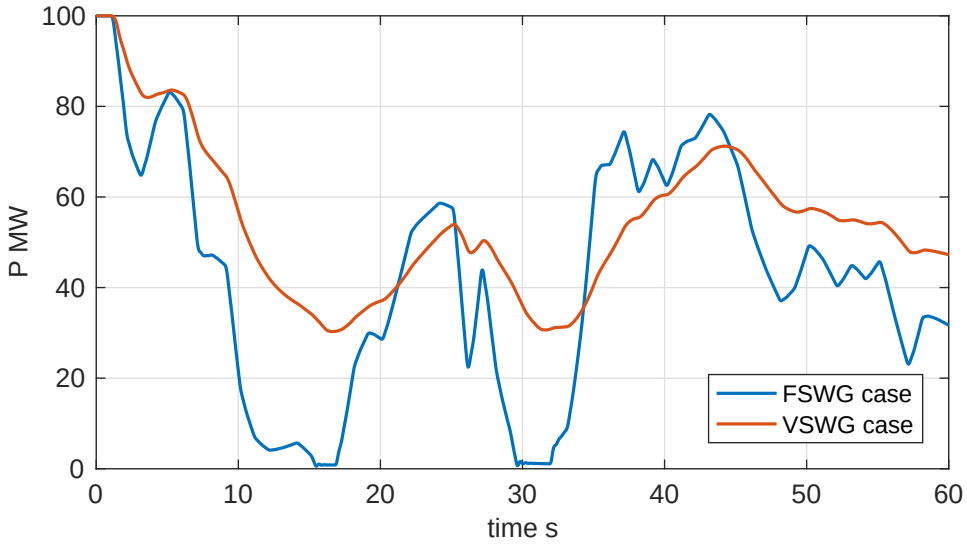

Figure 6.28: Bus 9561 wind farm active power P_{out} dispatch for the proposed wind profile.

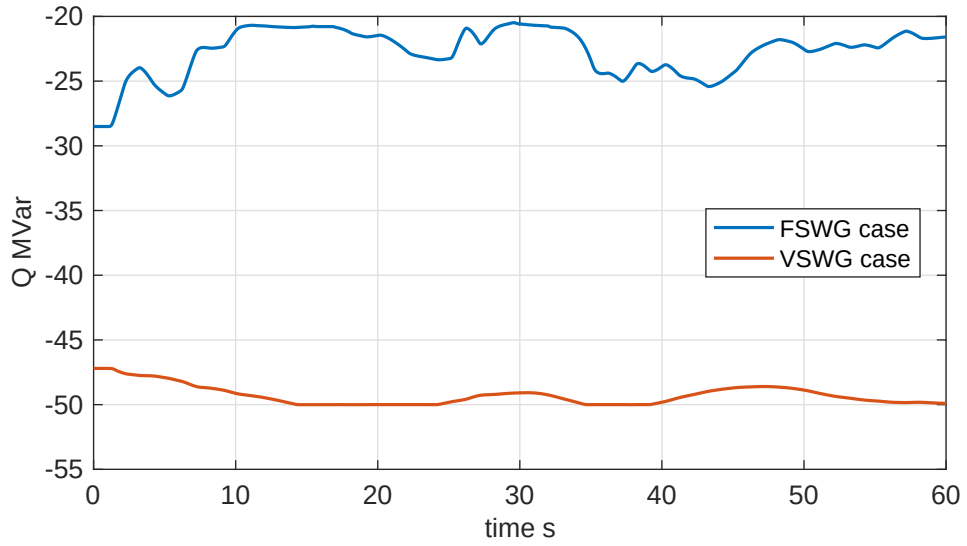

Figure 6.29: Bus 9561 wind farm reactive power Q_{out} dispatch for the proposed wind profile. Q_{out} is bounded in -50 MVAr due to inverter's thermal capacity.

VSWG reaches its minimum Q_{out}, thus losing ability to control voltage level.

WFs P_{out} directly affects system frequency control, as Figure 6.30 shows Bus 501 rotor frequency f^{501} that is used to represent grid frequency f_{grid}. The larger variation on P_{out} leads to broader excursions in f_{grid} for the FSWG case, while VSWG's smooth response mitigates frequency variations. It is worth noting that wind power does not pose any major issues to São Paulo grid frequency control, as it remains within acceptable limits required.

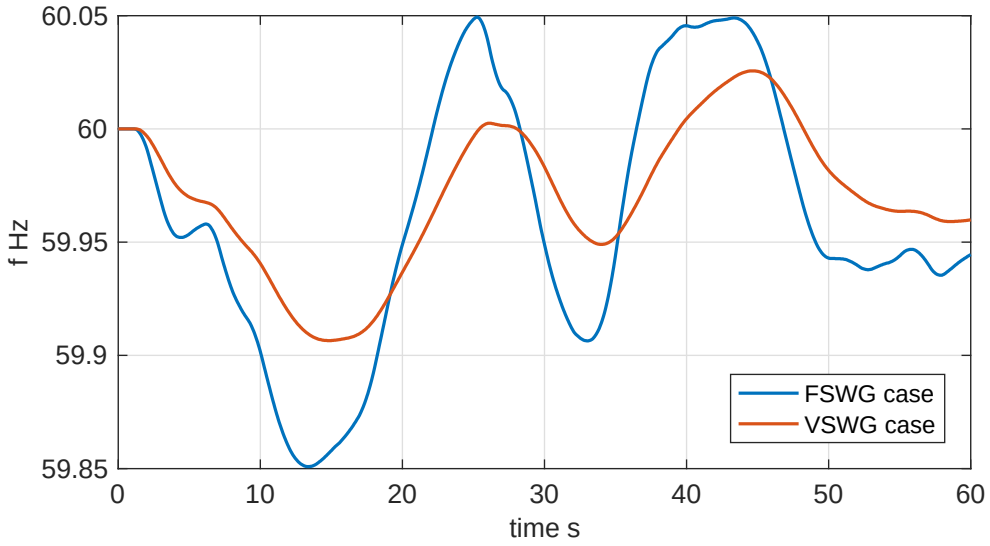

Figure 6.30: Bus 501 rotor frequency f^{501} used to represent grid frequency f_{grid} for the proposed wind profile.

Figure 6.31 depicts Bus 561 voltage level V^{561}, which power output variations has influence. The sharp power dispatch variations by the FSWG case translates as fast V^{561} variations. The VSWG case has a mitigated V^{561} curve, even though its limited room for voltage control. In spite of variations, both cases work within the safety boundaries required, showing that wind variations do not poses major risks to power system variables.

From angular stability perspective, accelerating power curves P_{ac} in Figure 6.32 shows considerably larger deviations for the FSWG case, due to its P_{out} response. P_{ac} shows how fast active power dispatch varies, without the same

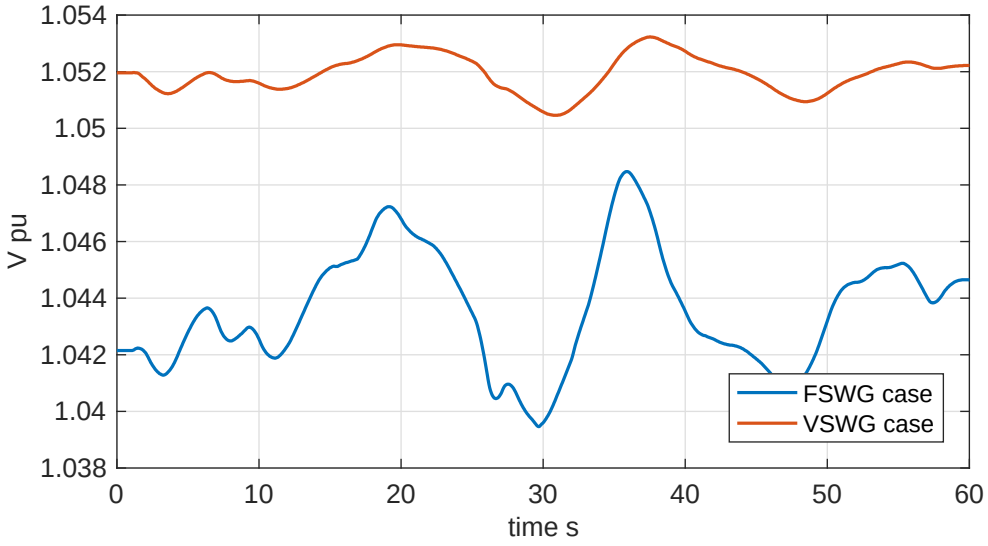

Figure 6.31: Bus 561 voltage level V^{561} showing fluctuations caused by the proposed wind profile.

mechanical power counterpart, drifting rotor frequency from nominal value. The most important issue presented in P_{ac} curves is that power plants respond on the same phase, it means that all power plants move uniformly P_{out} varies.

Machines P_{ac}'s response has great impact on rotor angle response as Figure 6.33 shows system response, where Bus 501 is the angular reference. Rotor angle displacement $\Delta\delta$ remain almost steady throughout the simulation procedure, showing that machines move uniformly as wind varies. This is extremely important from angular stability point of view, as one can see that fluctuations on wind speed does not cause any major variation on machines rotor angle.

Figure 6.34 presents variations in mechanical power ΔP_{mec} caused by the proposed wind speed variation. ΔP_{mec} curves show larger deviations for the FSWG case, as it compensates P_{out} variations. North area power plants tend to get a larger share from P_{out} reduction, as these are the largest power plants in this system, and the frequency control is proportional to their capacity. It is noticeable in Figure 6.34 Bus 502 slower response for the proposed wind series, as its response is approximately 5 s delayed than other power plants presented.

Such slower response is intrinsic to hydro turbines' characteristics, and not related to wind power's presence.

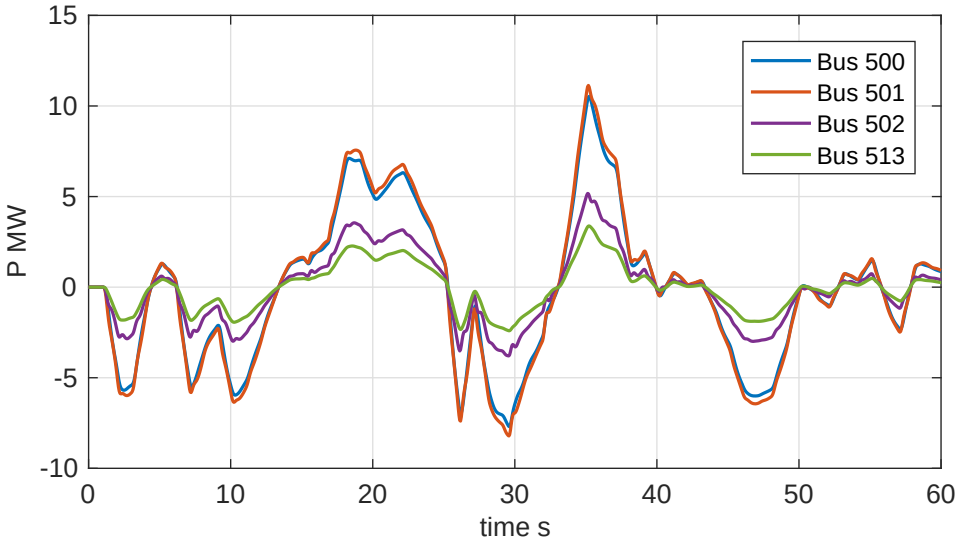

(a) FSWG case.

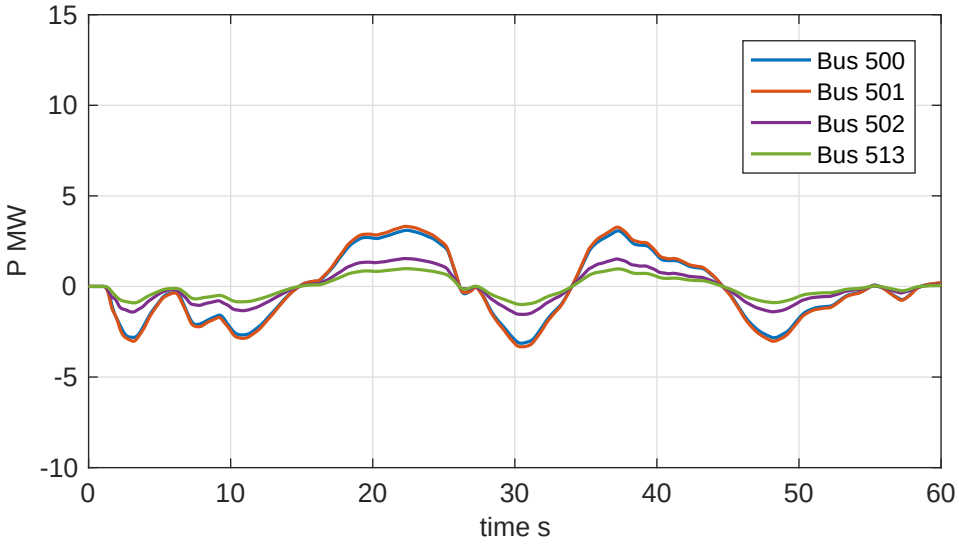

(b) VSWG case.

Figure 6.32: Accelerating power P_{ac} showing the coherent response for the proposed wind profile. Figures are scaled to the same rage so one can easily identify the different magnitude by visual inspection.

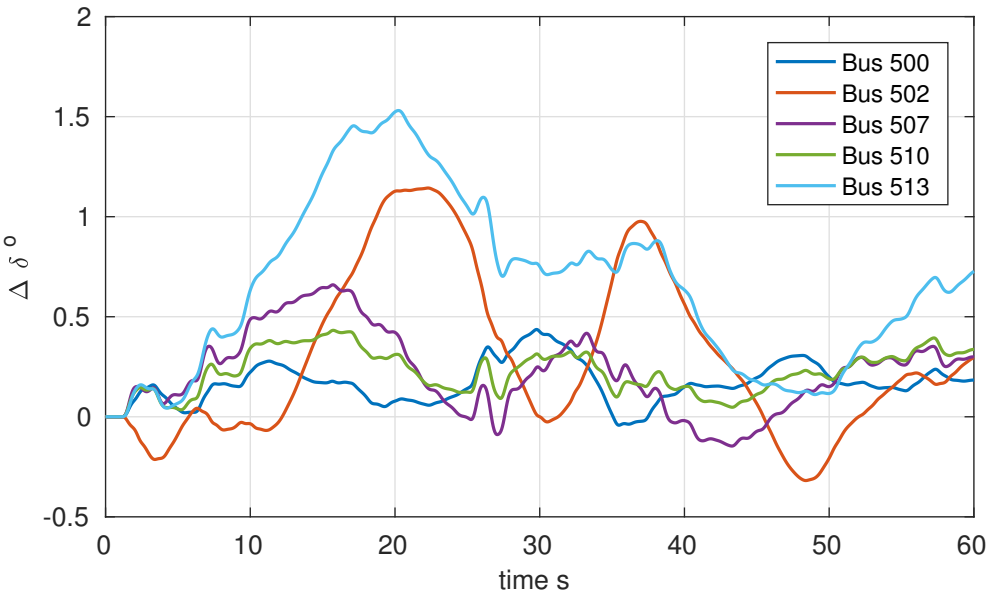

(a) FSWG case.

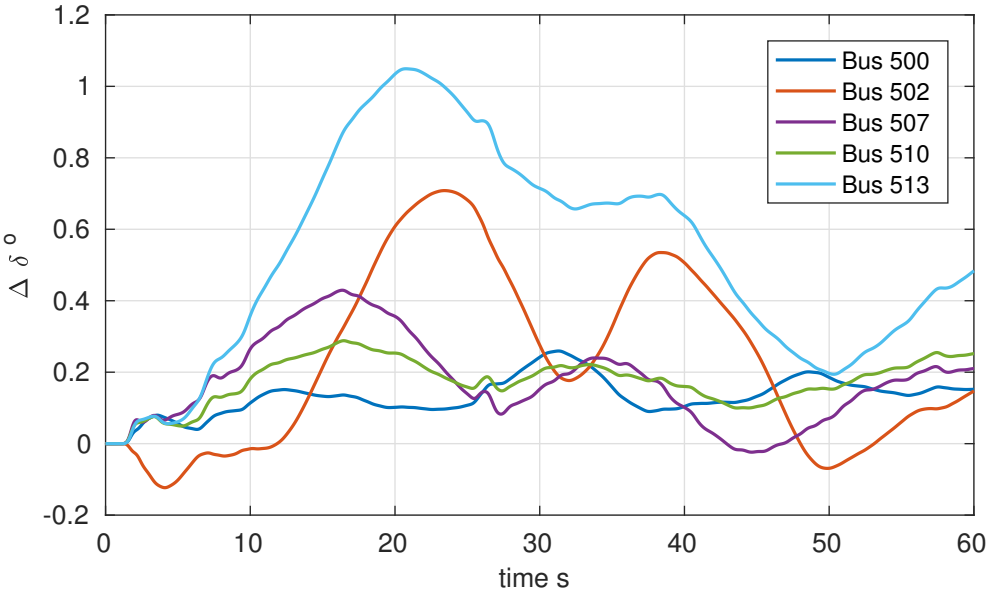

(b) VSWG case.

Figure 6.33: Power plants rotor angle displacement showing the influence of the proposed wind profile on system's angular stability. The angular reference adopted is the Bus 501 power plant rotor.

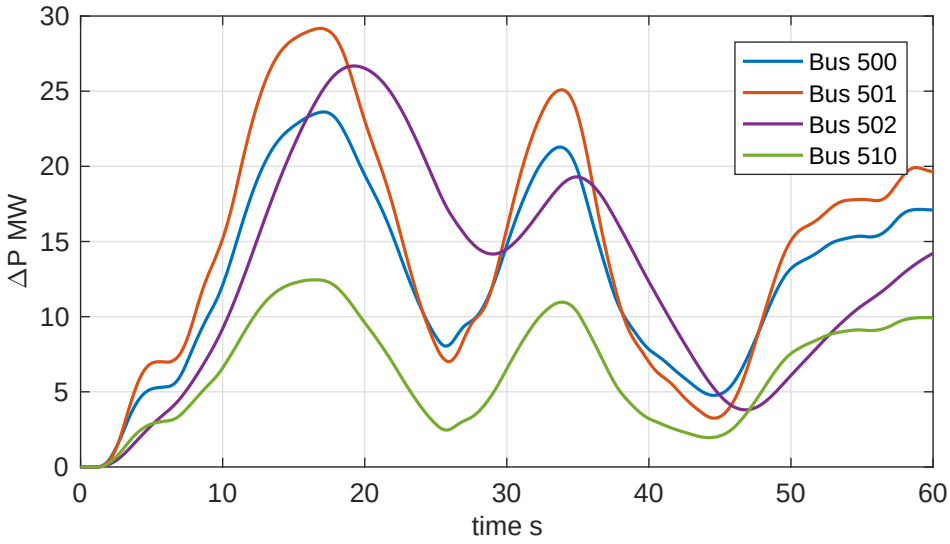

(a) FSWG case.

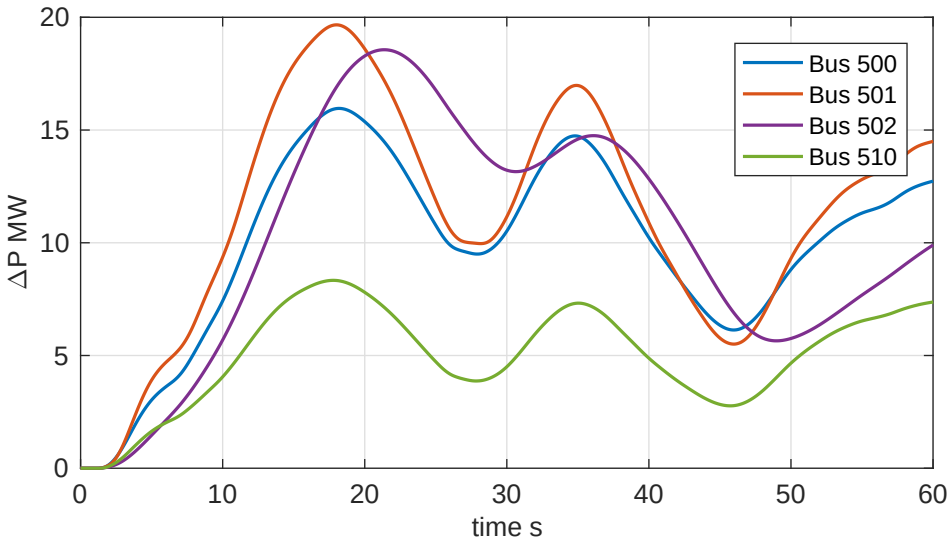

(b) VSWG case.

Figure 6.34: Mechanical power deviation from the initial point ΔP_{mec} showing turbine's adjustments to compensate variation on system total power demand.

6.6 Conclusion

This chapter investigates the coordinated phase restoration for the São Paulo state grid. Power flow analysis and the indexes of collapse point out that wind power influence on system stability reduces as restoration advances. In fact, the possibility of power flowing among corridors considerably reduces wind farms' influence on their neighbourhood.

The robustness areas show this fact, where system's robustness level shows mixed results. In some areas wind power increases robustness level, while it simultaneously causes reduction in other areas.

Dynamic simulations also show reduction on wind farms impact on this system. There are local positive impacts such as on loop closure, where wind power helps system angular stability by mitigating the impact of a transmission line reconnection. The wind farm synchronization and wind series events show considerably reduced impact on system power plants, as the system becomes interconnected.

Chapter 7

Recommendations for restorations

Based on the findings described on the above chapters, this thesis proposes a list of recommendations:

1. Wind power dispatch amount

Defining the amount of wind power to be reconnected during restoration is one of this thesis' contribution. The power injection should be large enough to be significant, however should not violate power plants' minimum stable load. Therefore, after some tests, a range between 30% up to 40% of total load amount emerges as a safe margin for restoration analysis.

Simulations on the IEEE 30 bus system and the Jupiá corridor used a maximum of 37.9% and 33.3% respectively, and results shows significant impact without causing major problems to frequency stability. Differently, on the Brazilian coordinated phase restoration, the wind power penetration reaches a maximum of 23.4% of total load, and results shows considerable reduced impact on stability by wind power.

2. Reactive power dispatch and voltage control limits for wind power

Reactive power control imposes considerable improvements on system stabil-

ity, as one can see from simulations. However, power converters' thermal capacity bounds such control, which also limits voltage control. Tests on wind farm synchronization and wind speed variation on the coordinated phase restoration (see Chapter 6) show the effect of thermal limitation on voltage control.

Both cases present an improper setting for voltage level on the wind farm bus. In order to avoid this issue, this thesis' recommendation is to set a voltage reference level, which allows a minimum of 10% free space from the maximum reactive power output. Figure 7.1 shows the recommended area (in red) for the synchronization procedure.

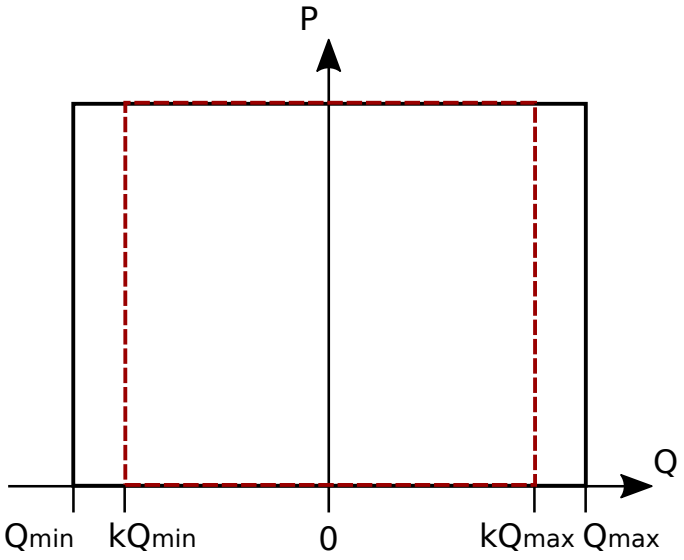

Figure 7.1: Variable speed wind generators capability chart where the red area indicates the recommended operational region for synchronization procedure, where $0 \leq k \leq 1$.

3. Reactive power compensation for fixed speed wind generators

Capacitor groups perform the reactive power compensation for fixed speed wind generators in this thesis. The recommendation of the amount of capacitors connected depends on the systems characteristics, i.e. the capacitance effect on transmission lines.

For lower voltage systems and reduced capacitance effect, similar to the IEEE

30 bus system, one can have positive results by adjusting wind farm's reactive power output between -5% to -15% of installed capacity. The minus sign indicates lagging power factor. For higher voltage systems with long transmission lines, such as the Brazilian system, this range differs. Due to persistent overvoltage the most positive results occurs between -20% to -30% of installed capacity. It is worth noting that this thesis calculates the compensation for the wind power on its maximum dispatch.

4. Wind farms active power ramp

The active power dispatch ramp in this thesis proved to be a key point for restoration. This is extremely dependent on power plants' ability to regulate their own active power dispatch. Equation (3.11) proposes the methodology for calculating a minimum time for the power ramp, where the value adopted $k_t = 0.005\,\text{s}$ shows acceptable results.

It is worth noting that one can control this constant value for single machines restoration areas, as in the Jupiá corridor. For this area $t_{min} = 25.5\,\text{s}$, which complies with the frequency variations limits for the fluent phase of restoration, though the ramp time is extended to ensure a smooth frequency level behaviour.

5. Wind farms reactive power ramp

Differently from the active power dispatch, the reactive power ramp in this thesis is not dependant on the power plants installed capacity. In fact, the ramp time is defined by trial simulations where $t_{rp} = 10\,\text{s}$ presented acceptable results. One can increase the ramp time, in case power plants' excitation are based on rotating systems, which are considerably slower than static systems. Independently of t_{rp} adopted, the reactive power ramp has to precede the active power ramp, in order to avoid unsafe voltage level regions.

6. Redistribution of power plants dispatch

Wind power injection leads to the rearrangement of power plants' dispatch. For the IEEE 30 bus system, the power slack is balanced by Bus 1 (the Vθ bus),

due to Bus 2 proximity to its minimum stable load.

With the exception of the minimum stable load issue, the recommendation is to distribute the power slack along all power plants regarding the electrical distance. This thesis adopts this approach during the coordinated phase, where power plants closer to the wind farms receive a larger share than electrically distant Southwest area. The distribution here is 75% and 25% respectively.

Chapter 8

Conclusion and future work

8.1 Conclusion

For over 100 years, society has been developing a close relation with electricity usage, and today it is hard to think how the world would survive without it. Even though the efforts to increase power systems reliability, outages can occur, and restorations are required in any power system. The growing demand for clean energy allied with adequate policies, have been developing a large offer on green energy, thus replacing fossil fuelled power plants. Therefore, this thesis proposes the usage of wind power as auxiliary source to main black-start power plants, assisting system stability. In order to investigate the possibility of using wind power in restoration, this thesis proposes:

- A power flow routine is implemented in MATLAB and in Fortran, dealing with the stochastic nature of wind speed;
- The usage of the robustness areas tool for restoration purposes, with heatmaps for visualization;
- A procedure for reconnecting wind farms, in the sense of electromechanical stability studies, where controllers are implemented to ensure smooth

power variations;

- The application of this methodology in the Brazilian power grid.

The outcome of the proposed methodology is:

The power flow studies and the indexes of collapse - Results show that wind power has considerable influence on restorations, especially during the earlier stages of the process.

The most positive results are presented by variable speed wind generators that increase system's load margin λ and reactive power load margin ΔQ, and reduces sensitiveness for load variation. Variable speed wind generators lead to the most positive results, because they increase system's load margin (λ and ΔQ), and reduce sensitiveness for load variation. Fixed speed wind generators do not replicate the same positive response, presenting negative impacts to system voltage stability for the majority of cases tested. The proposed routine is able to deal with the computationally heavy calculations regarding the stochastic simulations.

The robustness areas methodology - This tool shows a complementary approach to the voltage stability analysis. Wind power presents positive impact on system robustness level, by elevating $E_p(X^s, X^u)$ on vulnerable areas [62, 101]. The robustness areas show that wind power impact tend to reduce as restoration advances and system becomes interconnected, due to the reduction on wind farms influence area. This encourages the wind power usage on earlier stages of restoration.

The wind farm reconnection approach - It reduces wind power's impact on restoration, by providing smooth power variations and coordination time for system adjustments. Simulations also show that wind power has limited impact on system frequency stability, contradicting previous works where such impact

discourages the usage of wind power during restorations [43,44]. It is worth noting the importance of the designed controllers and the initialization routine for the successful operation of the proposed reconnection approach for wind farms.

The Brazilian power system restoration - Simulations on Jupiá corridor's fluent phase shows wind power considerable action on reactive power compensation, on a system where transmission lines inject large reactive power amounts to the system. As the coordinated phase takes place and restoration islands connects to each other wind power impact attenuates, limiting wind farms ability to control voltage level and assist on load pick-ups. The impact on angular stability comes from the extra power injection, which shifts main power plants' operational point [32], increasing their ability to remain angular stable after disturbances.

Finally, to extend the proposed restoration approach to other power systems, or to replicate this thesis' results, one can apply the methodology presented on Chapter 3 (or on the annexed paper) to power system restorations. Due to the disparate condition of restoration procedures, the recommendations on the previous chapter should be followed for a more accurate performance of the proposed methodology.

8.2 Future work

Following this thesis research field, some working areas are proposed:

- Propose a methodology capable to use Wind Farms (WFs) dispatch to mitigate loop closures;
- Considering the positive results on the São Paulo state grid restoration, one can also implement this technique on the British power grid;
- An investigation on wind power frequency control, and its impact on restoration procedure;

- Implementation of this methodology for offshore wind farms assisting restoration;
- The application of the methodology proposed by authors in [120, 121] for oscillations damping during Power System Restorations (PSRs).

References

[1] M. Eremia and M. Shahidehpour, *Restoration Processes after Blackouts*. Wiley-IEEE Press, 2013, pp. 864–899.

[2] M. Adibi and L. Fink, "Overcoming restoration challenges associated with major power system disturbances - restoration from cascading failures," *Power and Energy Magazine, IEEE*, vol. 4, no. 5, pp. 68–77, September 2006.

[3] M. Adibi, P. Clelland, L. Fink, H. Happ, R. J. Kafka, J. Raine, D. Scheurer, and F. Trefny, "Power system restoration - a task force report," *IEEE Transactions on Power Systems*, vol. 2, no. 2, pp. 271–277, May 1987.

[4] M. M. Adibi, J. N. Borkoski, and R. J. Kafka, "Power system restoration - the second task force report," *IEEE Transactions on Power Systems*, vol. 2, no. 4, pp. 927–932, November 1987.

[5] European. Commission. The 2020 climate & energy package. 16/03/2016. [Online]. Available: http://ec.europa.eu/clima/policies/strategies/2020/index_en.htm

[6] M. Castilla, P. Mercado, J. Negroni, M. Gomes, C. Moreira, J. Sosa, and A. C. Z. de Souza, "The growing state of distributed generation and microgrids in the Ibero-American region: A view from the rigmei network,"

in *2014 IEEE PES Transmission Distribution Conference and Exposition - Latin America (PES T D-LA)*, Sept 2014, pp. 1–6.

[7] X. Gu and D. Wang, "Investigation on extended black-start schemes of power system considering reasonable load restoration," in *Power and Energy Engineering Conference (APPEEC), 2014 IEEE PES Asia-Pacific*, December 2014, pp. 1–5.

[8] J. Dang and R. G. Harley, "Islanded microgrids black start procedures with wind power integration," in *Power and Energy Society General Meeting (PES), 2013 IEEE*, July 2013, pp. 1–5.

[9] UK. S. Authority. Energy trends: renewables. Accessed on 15/05/2018. [Online]. Available: https://www.gov.uk/government/statistics/energy-trends-section-6-renewables

[10] F. F. Wu and A. Monticelli, "Analytical tools for power system restoration-conceptual design," *IEEE Transactions on Power Systems*, vol. 3, no. 1, pp. 10–26, February 1988.

[11] S. Kurup and S. Ashok, "Performance of a hydro power plant during black start and islanded operation," in *Signal Processing, Informatics, Communication and Energy Systems (SPICES), 2015 IEEE International Conference on*, February 2015, pp. 1–5.

[12] S.-S. Lee, "Hydro and gas turbine blackout restoration strategies in the south korean power system," in *PES General Meeting — Conference Exposition, 2014 IEEE*, July 2014, pp. 1–6.

[13] M. Adibi, *Steam Plant Startup and Control in System Restoration.* Wiley-IEEE Press, 2000, pp. 68–74.

[14] P. Lilje and A. Petroianu, "Power plant islanding with the aid of a controlled resistor," in *AFRICON, 2004. 7th AFRICON Conference in Africa*, vol. 2, September 2004, pp. 775–781 Vol.2.

[15] M. Louro and C. Cura, "Network islanding — a real event," in *Integration of Renewables into the Distribution Grid, CIRED 2012 Workshop*, May 2012, pp. 1–4.

[16] J. Doudna, "Application and implementation of fast valving and generator tripping schemes at gerald gentlemen station," *Power Systems, IEEE Transactions on*, vol. 3, no. 3, pp. 1155–1166, August 1988.

[17] E. Cushing, G. Drechsler, W. Kilgoar, H. Marshall, and H. Stewart, "Fast valving as an aid to power system transient stability and prompt resynchronization and rapid reload after full load rejection," *Power Apparatus and Systems, IEEE Transactions on*, vol. PAS-90, no. 6, pp. 2517–2527, November 1971.

[18] R. Patel, T. Bhatti, and D. Kothari, "Improvement of power system transient stability by coordinated operation of fast valving and braking resistor," *Generation, Transmission and Distribution, IEE Proceedings-*, vol. 150, no. 3, pp. 311–316, May 2003.

[19] A. S. Leĭzerovich, *Steam Turbines for Modern Fossil-fuel Power Plants*. Fairmont Press, 2008.

[20] IEEE, "IEEE recommended practice for functional and performance characteristics of control systems for steam turbine-generator units," *IEEE Std 122-1991*, pp. 1–, 1992.

[21] E. Lu, N. Wang, Z. Qin, H. Liu, and Y. Hou, "Black-start strategy for power grids including fast cut thermal power units," in *Power and Energy Society General Meeting (PES), 2013 IEEE*, July 2013, pp. 1–5.

[22] R. Kehlhofer, F. Hannemann, B. Rukes, and F. Stirnimann, *Combined-Cycle Gas & Steam Turbine Power Plants*. PennWell, 2009.

[23] North American Electric Reliability Corporation, "State of reliability 2015," Booklet, May 2015, accessed on 15/05/2018. [Online]. Available: http://www.nerc.com/pa/rapa/pa/performance%20analysis%20dl/2015%20state%20of%20reliability.pdf

[24] B. D. Bonatto and H. W. Dommel, *EMTP Modelling of Control and Power Electronic Devices*. LAP Lambert Academic Publishing, Sep 2010.

[25] A. Dariani and R. Rastegar, "Emtp-based black start analysis for an isolated power system," in *Electric Power and Energy Conference (EPEC), 2010 IEEE*, August 2010, pp. 1–7.

[26] M. Bakshi, *Transmission And Distribution*. Technical Publications, 2008.

[27] R. Leme, L. Ferreira, B. Lopes, and A. Zambroni de Souza, "Using redispatch generators to reduce the standing phase angle during system restoration," *Generation, Transmission and Distribution, IEE Proceedings*, vol. 153, no. 5, pp. 531–539, September 2006.

[28] D. Hazarika and A. Sinha, "An algorithm for standing phase angle reduction for power system restoration," *Power Systems, IEEE Transactions on*, vol. 14, no. 4, pp. 1213–1218, November 1999.

[29] L. Wang, H. Ye, Y. Liu, and X. Liu, "A new method for incorporating load pickup as a control means for standing phase angle reduction in power system restoration," in *Power Engineering Conference (UPEC), 2013 48th International Universities'*, September 2013, pp. 1–4.

[30] N. Martins, E. de Oliveira, J. Pereira, and L. Ferreira, "Reducing standing phase angles via interior point optimum power flow for improved system

restoration," in *Power Systems Conference and Exposition, 2004. IEEE PES*, October 2004, pp. 404–408 vol.1.

[31] P. Kundur, *Power System Stability and Control*. Berlin: Lambert Academic Publishing, 2010.

[32] P. M. Anderson and A. A. Fouad, *Power System Control and Stability*, 2nd ed. Wiley-IEEE Press, October 2002.

[33] P. W. Sauer and M. A. Pai, *Power System Dynamics and Stability*. Prentice Hall, 1998.

[34] M. M. Adibi, N. Martins, and E. H. Watanabe, "The impacts of facts and other new technologies on power system restoration dynamics," in *Power and Energy Society General Meeting, 2010 IEEE*, July 2010, pp. 1–6.

[35] D. Lindenmeyer, "A framework for power system restoration," Ph.D. dissertation, The University of Britsh Columbia, Sep. 2000.

[36] J. N. Fidalgo, J. A. P. Lopes, and V. Miranda, "Neural networks applied to preventive control measures for the dynamic security of isolated power systems with renewables," *IEEE Transactions on Power Systems*, vol. 11, no. 4, pp. 1811–1816, November 1996.

[37] J. A. P. Lopes, C. L. Moreira, and A. G. Madureira, "Defining control strategies for microgrids islanded operation," *IEEE Transactions on Power Systems*, vol. 21, no. 2, pp. 916–924, May 2006.

[38] A. C. Z. de Souza, M. Santos, M. Castilla, J. Miret, L. G. de Vicuña, and D. Marujo, "Voltage security in AC microgrids: a power flow-based approach considering droop-controlled inverters," *IET Renewable Power Generation*, vol. 9, no. 8, pp. 954–960, 2015.

[39] C. L. Moreira, F. O. Resende, and J. A. P. Lopes, "Using low voltage microgrids for service restoration," *IEEE Transactions on Power Systems*, vol. 22, no. 1, pp. 395–403, February 2007.

[40] Y. Xu, C. C. Liu, Z. Wang, K. Mo, K. P. Schneider, F. K. Tuffner, and D. T. Ton, "DGs for service restoration to critical loads in a secondary network," *IEEE Transactions on Smart Grid*, vol. PP, no. 99, pp. 1–1, 2017.

[41] J. A. P. Lopes, C. L. Moreira, and F. O. Resende, "Microgrids black start and islanding operation," in *15th Power Systems Computation Conference (PSCC)*, 2005, pp. 1–7.

[42] M. Aktarujjaman, M. A. Kashem, M. Negnevitsky, and G. Ledwich, "Black start with DFIG based distributed generation after major emergencies," in *Power Electronics, Drives and Energy Systems, 2006. PEDES '06. International Conference on*, December 2006, pp. 1–6.

[43] H. Zhu and Y. Liu, "Aspects of power system restoration considering wind farms," in *Sustainable Power Generation and Supply (SUPERGEN 2012), International Conference on*, September 2012, pp. 1–5.

[44] L. Seca, H. Costa, C. L. Moreira, and J. A. P. Lopes, "An innovative strategy for power system restoration using utility scale wind parks," in *Bulk Power System Dynamics and Control - IX Optimization, Security and Control of the Emerging Power Grid (IREP), 2013 IREP Symposium*, August 2013, pp. 1–8.

[45] W. Sun, "New optimization techniques for power system generation scheduling," Ph.D. dissertation, Iowa State University, 2011.

[46] Scottish. Renewables. Renewables in numbers. Accessed on 15/05/2018. [Online]. Available: https://www.scottishrenewables.com/sectors/renewables-in-numbers/

[47] The Guardian. Longannet power station closes ending coal power use in Scotland. Accessed on 15/05/2018. [Online]. Available: http://www.theguardian.com/environment/2016/mar/24/longannet-power-station-closes-coal-power-scotland

[48] G. Lalor, A. Mullane, and M. O'Malley, "Frequency control and wind turbine technologies," *IEEE Transactions on Power Systems*, vol. 20, no. 4, pp. 1905–1913, November 2005.

[49] R. G. de Almeida and J. A. P. Lopes, "Participation of doubly fed induction wind generators in system frequency regulation," *IEEE Transactions on Power Systems*, vol. 22, no. 3, pp. 944–950, August 2007.

[50] B. Silva, C. L. Moreira, L. Seca, Y. Phulpin, and J. A. P. Lopes, "Provision of inertial and primary frequency control services using offshore multiterminal HVDC networks," *IEEE Transactions on Sustainable Energy*, vol. 3, no. 4, pp. 800–808, October 2012.

[51] M. Akbari and S. M. Madani, "Analytical evaluation of control strategies for participation of doubly fed induction generator-based wind farms in power system short-term frequency regulation," *IET Renewable Power Generation*, vol. 8, no. 3, pp. 324–333, April 2014.

[52] P. Moutis, E. Loukarakis, S. Papathanasiou, and N. D. Hatziargyriou, "Primary load-frequency control from pitch-controlled wind turbines," in *PowerTech, 2009 IEEE Bucharest*, June 2009, pp. 1–7.

[53] M. Jalali and K. Bhattacharya, "Frequency regulation and agc in isolated systems with DFIG-based wind turbines," in *Power and Energy Society General Meeting (PES), 2013 IEEE*, July 2013, pp. 1–5.

[54] V. Yari, S. Nourizadeh, and A. M. Ranjbar, "Wide-area frequency control during power system restoration," in *Electric Power and Energy Conference (EPEC), 2010 IEEE*, August 2010, pp. 1–4.

[55] M. M. A. Abdelaziz, H. E. Farag, E. F. El-Saadany, and Y. A. R. I. Mohamed, "A novel and generalized three-phase power flow algorithm for islanded microgrids using a newton trust region method," *IEEE Transactions on Power Systems*, vol. 28, no. 1, pp. 190–201, February 2013.

[56] A. Castillo, "Microgrid provision of blackstart in disaster recovery for power system restoration," in *Smart Grid Communications (SmartGridComm), 2013 IEEE International Conference on*, October 2013, pp. 534–539.

[57] T. Ackermann, *Wind Power in Power Systems*. West Sussex, PO19 8SQ, England: John Wiley & Sons, 2005.

[58] T. V. Cutsem and C. Vournas, *Voltage Stability of Electric Power Systems*, ser. Kluwer international series in engineering and computer science. Springer, 1998.

[59] M. A. Pai, *Power system stability: Analysis by the direct method of Lyapunov*. Englewood Cliffs, New Jersey 07632: New York: North-Holland, 1981.

[60] A. A. Fouad and V. Vital, *Power System Transient Stability Analysis Using the Transient Energy Function Method*. Englewood Cliffs, New Jersey 07632: Prentice-Hall, 1992.

[61] I. Decker, M. Agostini, A. e Silva, and D. Dotta, "Monitoring of a large scale event in the Brazilian power system by WAMS," in *Bulk Power System Dynamics and Control (iREP) - VIII (iREP), 2010 iREP Symposium*, August 2010, pp. 1–8.

[62] P. Murinelli Pesoti, E. V. de Lorenci, A. C. Zambroni de Souza, K. L. Lo, and B. I. Lima Lopes, "Robustness area technique developing guidelines for power system restoration," *Energies*, vol. 10, no. 1, 2017, Article No 99. Accessced on 15/05/2018. [Online]. Available: http://www.mdpi.com/1996-1073/10/1/99

[63] A. J. Monticelli, A. Garcia, and O. R. Saavedra, "Fast decoupled load flow: hypothesis, derivations, and testing," *IEEE Transactions on Power Systems*, vol. 5, no. 4, pp. 1425–1431, Nov 1990.

[64] P. Anderson, *Analysis of faulted power systems*, ser. IEEE Press power system engineering series. IEEE Press, 1995.

[65] M. Tomoda, J. Matsuki, and Y. Hayashi, "Parameter estimation of dynamic load model in power system by using measured data," *Journal of International Council on Electrical Engineering*, vol. 1, no. 2, pp. 200–206, 2011.

[66] I. Tritiu, C. Ghinea, C. Bulac, and S. Costina, "Load curves modelling using algebraic polynomials," in *2017 International Conference on ENERGY and ENVIRONMENT (CIEM)*, Oct 2017, pp. 69–73.

[67] N. L. Batseva and A. Y. Shuvalov, "The second order polynomial load model impact on stability of the synchronous motor," in *2016 2nd International Conference on Industrial Engineering, Applications and Manufacturing (ICIEAM)*, May 2016, pp. 1–5.

[68] N. L. Batseva, A. V. Pankratov, Y. V. Khrushchev, A. V. Prokhorov, and A. S. Tavlintsev, "Technique for field data based identification of static polynomial load model," in *2014 International Conference on Mechanical Engineering, Automation and Control Systems (MEACS)*, Oct 2014, pp. 1–5.

[69] T. Alexander, P. Andrey, M. Olga, and C. Pavel, "Identification of static polynomial load model based on remote metering systems information," in *2013 13th International Conference on Environment and Electrical Engineering (EEEIC)*, Nov 2013, pp. 213–216.

[70] W. Weibull, "A statistical distribution function of wide applicability," *ASME Journal of Applied Mechanics*, pp. 293–297, September 1951.

[71] S. Li and T. A. Haskew, "Energy capture, conversion, and control study of dfig wind turbine under weibull wind distribution," in *Power Energy Society General Meeting, 2009. PES '09. IEEE*, July 2009, pp. 1–9.

[72] O. Anaya-Lara, J. Tande, K. Uhlen, and K. Merz, *Offshore Wind Energy Technology*. Wiley, 2018.

[73] O. Anaya-Lara, D. Campos-Gaona, E. Moreno-Goytia, and G. Adam, *Offshore Wind Energy Generation: Control, Protection, and Integration to Electrical Systems*. Wiley, 2014.

[74] M. H. El-Ahmar, A. H. M. El-Sayed, and A. M. Hemeida, "Evaluation of factors affecting wind turbine output power," in *2017 Nineteenth International Middle East Power Systems Conference (MEPCON)*, Dec 2017, pp. 1471–1476.

[75] S. O. Ani, H. Polinder, and J. A. Ferreira, "Comparison of energy yield of small wind turbines in low wind speed areas," *IEEE Transactions on Sustainable Energy*, vol. 4, no. 1, pp. 42–49, Jan 2013.

[76] R. Peña, A. Medina, and O. Anaya-Lara, *A Methodology for the Efficient Computer Representation of Dynamic Power Systems: Application to Wind Parks*. J. Wiley, 2012.

[77] J. G. Slootweg, S. W. H. de Haan, H. Polinder, and W. L. Kling, "General model for representing variable speed wind turbines in power system dynamics simulations," *IEEE Transactions on Power Systems*, vol. 18, no. 1, pp. 144–151, February 2003.

[78] B. Fox, D. Flynn, L. Bryans, N. Jenkins, D. Milborrow, M. O'Malley, R. Watson, and O. Anaya-Lara, *Wind Power Integration: Connection and System Operational Aspects*, ser. Energy Engineering Series. Institution of Engineering and Technology, 2007.

[79] S. Mondal and D. kastha, "Maximum active and reactive power capability of a matrix converter fed dfig based wind energy conversion system," *IEEE Journal of Emerging and Selected Topics in Power Electronics*, vol. PP, no. 99, pp. 1–1, 2017.

[80] E. H. Enrique, "Generation capability curves for wind farms," in *2014 IEEE Conference on Technologies for Sustainability (SusTech)*, July 2014, pp. 103–106.

[81] M. I. Martinez, G. Tapia, A. Susperregui, and H. Camblong, "Dfig power generation capability and feasibility regions under unbalanced grid voltage conditions," *IEEE Transactions on Energy Conversion*, vol. 26, no. 4, pp. 1051–1062, December 2011.

[82] J. Hu and Y. He, "Dfig wind generation systems operating with limited converter rating considered under unbalanced network conditions analysis and control design," *Renewable Energy*, vol. 36, no. 2, pp. 829 – 847, 2011.

[83] A. P. Tennakoon, J. B. Ekanayake, A. Atputharajah, and S. G. Abeyratne, "Capability chart of a doubly fed induction generation based on its ratings and stability margin," in *45th International Universities Power Engineering Conference UPEC2010*, August 2010, pp. 1–5.

[84] B. Robyns, B. Francois, P. Degobert, and J. Hautier, *Vector Control of Induction Machines: Desensitisation and Optimisation Through Fuzzy Logic*, ser. Power Systems. Springer London, 2012.

[85] R. Billinton and R. Allan, *Reliability evaluation of power systems.* Pitman Advanced Publishing Program, 1984.

[86] MathWorks. Matlab help. Accessed on 15/05/2018. [Online]. Available: https://uk.mathworks.com/help/matlab/

[87] A. Z. de Souza, "Tangent vector applied to voltage collapse and loss sensitivity studies," *Electric Power Systems Research*, vol. 47, no. 1, pp. 65 – 70, 1998.

[88] I. S. M. Naser, "The impact of wind generation on power system voltage stability," Ph.D. dissertation, University of Strathclyde, Glasgow, UK, May 2013.

[89] A. Almeida, E. Valenca de Lorenci, R. Coradi Leme, A. Zambroni de Souza, B. Lima Lopes, and K. Lo, "Probabilistic voltage stability assessment considering renewable sources with the help of the pv and qv curves," *Renewable Power Generation, IET*, vol. 7, no. 5, pp. 521–530, September 2013.

[90] A. Z. de Souza, F. W. Mohn, I. F. Borges, and T. R. Ocariz, "Using PV and QV curves with the meaning of static contingency screening and planning," *Electric Power Systems Research*, vol. 81, no. 7, pp. 1491 – 1498, 2011.

[91] T. V. Cutsem and M. Ribbens-Pavella, "Structure preserving direct methods for transient stability analysis of power systems," *Proceedings of 24th Conference on Decision and Control, Flrida*, vol. 70, 1985.

[92] N. Narasimhamurthi and M. Musavi, "A generalized energy function for transactions stability analysis of power systems," *IEEE Transactions on Circuits and Systems cas-31*, vol. 637, 1984.

[93] A. C. Z. de Souza, R. C. Leme, L. F. B. Vasconcelos, and B. I. L. L. andY. C. S. Ribeiro, "Energy function and unstable solutions by the means of an augmented jobian," *Applied Mathematics and Computation*, vol. 206, pp. 154–163, 2008.

[94] T. J. Overbye and C. L. DeMarco, "Voltage security enhancement using energy based sensitivities," *Transactions on Power Systems*, vol. 6, no. 3, pp. 1196–1202, August 1991.

[95] C. L. DeMarco and T. J. Overbye, "An energy based security measure for assessing vulnerability to voltage collapse," *IEEE Transactions on Power Systems*, vol. 5, no. 2, pp. 419–427, May 1990.

[96] T. J. Overbye, M. A. Pai, and P. W. Sauer, "Some aspects of the energy functions approach to angle and voltage stability analysis in power systems," *Proceedings of the 31th Conference on Decision and Control*, pp. 2941–2946, December 1992.

[97] B. I. L. Lopes and A. Z. de Souza, "On multiple tap blocking to avoid voltage collapse," *Electric Power Systems Research*, vol. 67, no. 3, pp. 225 – 231, 2003.

[98] R. P. Klump and T. J. Overbye, "A new method for finding low-voltage power flow solutions," in *Power Engineering Society Summer Meeting, 2000. IEEE*, vol. 1, 2000, pp. 593–597 vol. 1.

[99] T. J. Overbye, "Use of energy methods for on-line assessment of power system voltage security," *IEEE Transactions on Power Systems*, vol. 8, no. 2, pp. 452–458, May 1993.

[100] K. Iba, H. Suzuki, M. Egawa, and T. Watanabe, "A method for finding a pair of multiple load flow solutions in bulk power systems," *IEEE Transactions on Power Systems*, vol. 5, no. 2, pp. 582–591, May 1990.

[101] E. V. de Lorenci and A. C. Z. de Souza, "Energy function applied to voltage stability studies - discussion on low voltage solutions with the help of tangent vector," *Electric Power Systems Research*, vol. 141, pp. 290 – 299, 2016.

[102] E. V. de Lorenci, "Energy function applied to voltage stability studies and definition of electric power systems vulnerability profile." PhD Thesis, Federal University of Itajubá, Itajubá - MG - Brazil, 2017, Portuguese, Accessed on 15/05/2018. [Online]. Available: https://repositorio.unifei.edu.br/xmlui/handle/123456789/731

[103] A. G. Abo-Khalil, "Synchronization of dfig output voltage to utility grid in wind power system," *Renewable Energy*, vol. 44, pp. 193 – 198, 2012.

[104] A. Nagliero, R. A. Mastromauro, M. Liserre, and A. Dell'Aquila, "Synchronization techniques for grid connected wind turbines," in *2009 35th Annual Conference of IEEE Industrial Electronics*, Nov 2009, pp. 4606–4613.

[105] K. Ogata, *Modern Control Engineering*, ser. Instrumentation and controls series. Prentice Hall, 2010.

[106] University of Washington. Power systems test case archive. Accessed on 15/05/2018. [Online]. Available: https://www.ee.washington.edu/research/pstca/

[107] J. N. Rai and A. Singh, "Combined cycle gas turbine and generator matching performance," in *2016 IEEE 1st International Conference on Power Electronics, Intelligent Control and Energy Systems (ICPEICES)*, July 2016, pp. 1–6.

[108] S. K. Yee, J. V. Milanovi, and F. M. Hughes, "Validated models for gas turbines based on thermodynamic relationships," *IEEE Transactions on Power Systems*, vol. 26, no. 1, pp. 270–281, Feb 2011.

[109] A. Mota, L. Mota, and A. Morelato, "Visualization of power system restoration plans using CPM/PERT graphs," *Power Systems, IEEE Transactions on*, vol. 22, no. 3, pp. 1322–1329, August 2007.

[110] Wind Data Archive. The RenSMART wind data archive - measured data. Accessed on 15/05/2018. [Online]. Available: http://www.rensmart.com/Weather/WindArchive

[111] D. Bernardon, M. Sperandio, V. Garcia, L. Canha, A. da Rosa Abaide, and E. Daza, "AHP decision-making algorithm to allocate remotely controlled switches in distribution networks," *Power Delivery, IEEE Transactions on*, vol. 26, no. 3, pp. 1884–1892, July 2011.

[112] M. Romero, L. Wesz da Silva, and J. Mantovani, "Optimal switch allocation for automatic load transfer in distribution substations," in *PowerTech, 2011 IEEE Trondheim*, June 2011, pp. 1–7.

[113] P. Gomes, A. de Lima, and A. de Padua Guarini, "Guidelines for power system restoration in the Brazilian system," *Power Systems, IEEE Transactions on*, vol. 19, no. 2, pp. 1159–1164, May 2004.

[114] A. Ohara and C. Takiguchi, "Automatic restoration system," in *Transmission and Distribution Conference and Exposition: Latin America, 2004 IEEE/PES*, November 2004, pp. 681–685.

[115] D. Schwanz, R. E. Henke, and R. C. Leborgne, "Wind power integration in southern brazil: Steady-state analysis," in *2012 Sixth IEEE/PES Transmission and Distribution: Latin America Conference and Exposition (T D-LA)*, September 2012, pp. 1–6.

[116] Brazil Monitor. CESPs first wind power generators are operational in Sao Paulo. Accessed on 15/05/2018. [Online]. Available: http://www.brazilmonitor.com/index.php/2017/10/04/cesps-first-wind-power-generators-are-operational-in-sao-paulo/

[117] Renewables Now. Brazil Sao Paulo state wind mapping study identifies 4,700 MW potential. Accessed on 15/05/2018. [Online]. Available: https://renewablesnow.com/news/brazil-sao-paulo-state-wind-mapping-study-identifies-4700-mw-potential-321360/

[118] Investe São Paulo, "State of São Paulo investment guide," Booklet, Av. Escola Politecnica, 82 - Jaguare - CEP: 05350-000 - Sao Paulo - SP - Brazil, accessed on 15/05/2018. [Online]. Available: http://www.investe.sp.gov.br/uploads/midias/documentos/folder_renewable_energy.pdf

[119] V. d. F. Grah, I. d. M. Ponciano, and T. A. Botrel, "Potential for wind energy generation in Piracicaba, SP, Brazil," *Revista Brasileira de Engenharia Agrícola e Ambiental*, vol. 18, pp. 559 – 564, 05 2014.

[120] M. Edrah, K. L. Lo, and O. Anaya-Lara, "Impacts of high penetration of dfig wind turbines on rotor angle stability of power systems," *IEEE Transactions on Sustainable Energy*, vol. 6, no. 3, pp. 759–766, July 2015.

[121] ——, "Reactive power control of dfig wind turbines for power oscillation damping under a wide range of operating conditions," *IET Generation, Transmission Distribution*, vol. 10, no. 15, pp. 3777–3785, 2016.

Glossary

Back-to-back converter An AC/DC/AC power converter usually employed to decouple frequencies.

Black-start Ability to restore without any external power.

Corridor Long-shaped restoration areas in the Brazilian power grid.

Critical bus The bus associated to the highest absolute entrance in the tangent vector.

$\mathbf{I_{cst}}$ Load model that varies linearly with voltage level.

Load ramp Load to be connected to a power plant in a predefined space of time. It is usually measured in MW/min or GW/h.

Minimum stable load Minimum stable load or minimum load, is the lowest dispatch generation in which a thermal machine is able to sustain in stead state operation.

$\mathbf{P_{cst}}$ Load model that power injection is constant along the power flow procedure.

PQ Power system bus where active and reactive power are known.

Processing element An electronic circuit (either a microprocessor or an internal component of one) that may function autonomously or under external control, performing arithmetic and logic operations on data.

PV Power system bus where voltage level and active power are known.

SCADA Supervisory Control and Data Acquisition. Data centre that can remotely monitor and control power systems or industrial plants.

Tangent vector Vector containing system state variables sensitivities to system variations.

Vθ Power system bus where voltage level and voltage angle are known.

$\mathbf{Z_{cst}}$ Load model that has constant impedance and load varies with terminal voltage squared.

ZIP Load model that considers the actual power a composition of three different types of load: Z_{cst}, I_{cst}, and P_{cst}.

Appendix A

United Kingdom renewable sources in numbers

Table A.1: Renewable electricity capacity and generation: United Kingdom. Source [9, 46].

	2012	**2013**	**2014**	**2015**	**2016**	**2017**
Installed Capacity [MW]						
Onshore Wind	6035.1	7586.3	8572.7	9212.2	10880.2	12847.4
Offshore Wind	2995.5	3696.0	4501.4	5093.4	5293.4	6987.9
Wave / tidal	8.5	8.0	8.7	8.9	13.5	18.4
Solar PV	1753.5	2937.2	5528.1	9601.2	11912.0	12775.7
Small scale Hydro	216.0	231.9	252.6	300.2	358.5	395.9
Large scale Hydro	1476.8	1476.8	1476.8	1476.8	1476.8	1478.7
Landfill gas	1042.1	1050.5	1057.5	1061.3	1061.9	1066.1
Sewage digestion	211.6	201.4	230.4	231.3	257.3	245.5
Energy from waste	512.7	544.9	680.4	929.9	1028.3	1090.9
Animal Biomass	110.5	110.5	110.5	110.5	129.3	129.3
Anaerobic Digestion	120.5	162.6	242.6	335.7	426.4	459.9
Plant Biomass	1165.9	1954.8	2258.0	2604.1	2852.0	3055.4
Total	15648.8	19960.8	24919.7	30965.7	35689.6	40551.0
Co-firing	208.2	38.5	14.2	20.9	13.4	8.8

Continued on next page

Table A.1 – continued from previous page

	2012	**2013**	**2014**	**2015**	**2016**	**2017**
Generation [Gwh]						
Onshore Wind	12244.0	16925.4	18554.7	22852.0	20857.0	29087.7
Offshore Wind	7603.2	11471.8	13404.6	17422.7	16405.7	20915.9
Wave / tidal	4.2	4.8	2.2	2.0	0.0	4.2
Solar PV	1353.8	2010.3	4054.1	7532.9	10410.9	11524.9
Hydro	5309.7	4701.5	5887.8	5588.9	5616.7	5928.1
Landfill gas	5208.5	5174.7	5033.2	4872.2	4702.9	4283.8
Sewage digestion	738.5	766.0	840.1	894.4	950.3	967.3
Energy from waste	1772.9	1648.2	1899.9	2582.4	2739.8	3385.6
Co-firing with fossil	1828.5	337.3	123.8	183.3	117.5	53.9
Animal Biomass	642.9	628.2	613.9	647.8	650.2	649.2
Anaerobic Digestion	494.6	713.1	1022.6	1484.7	2081.5	2469.7
Plant Biomass	4047.8	8832.8	13085.5	18592.2	18821.8	20059.5
Total	41248.5	53213.8	64522.4	82655.5	83354.3	99329.8
Non-biod. Wastes	1429.1	1481.1	1923.3	2586.1	2742.0	3485.0
Load Factors						
Onshore Wind	25.83%	28.37%	26.22%	29.34%	23.64%	27.99%
Offshore Wind	35.81%	39.14%	37.33%	41.46%	35.96%	38.88%
Solar PV	11.19%	9.78%	10.93%	11.37%	11.02%	10.66%
Hydro	35.86%	31.56%	39.10%	36.39%	35.40%	36.48%
Landfill gas	56.59%	56.46%	54.51%	52.50%	50.43%	45.96%
Sewage digestion	40.92%	42.34%	44.42%	44.22%	44.28%	43.92%
Energy from waste	39.79%	35.58%	35.40%	36.61%	31.86%	36.47%
Animal Biomass	66.22%	64.89%	63.41%	66.91%	61.73%	57.31%
Anaerobic Digestion	57.92%	57.51%	57.62%	58.61%	62.19%	63.62%
Plant Biomass	39.56%	64.62%	70.92%	87.30%	78.54%	77.53%

Table A.2: Renewable electricity capacity and generation: Scotland. Source [9, 46].

	2012	**2013**	**2014**	**2015**	**2016**	**2017**
Installed Capacity [MW]						
Wind	3955.0	4778.8	5276.8	5585.3	6514.3	7635.6
Wave / tidal	6.7	6.7	7.4	7.6	13.0	17.9
Solar PV	94.7	132.7	175.0	264.1	325.8	323.0
Hydro	1496.8	1509.7	1527.7	1571.4	1629.6	1653.6
Landfill gas	114.9	115.3	116.3	116.3	116.3	115.8
Sewage digestion	9.4	6.8	6.8	7.0	7.2	7.2
Other biomass	138.2	149.6	229.8	236.5	259.0	295.4
Total	5815.8	6699.7	7339.8	7788.2	8865.2	10048.6
Generation [Gwh]						
Wind	8291.7	11151.2	11700.0	13877.9	12457.4	17063.1
Wave / tidal	0.7	1.4	2.1	2.0	0.0	4.2
Solar PV	69.9	95.9	143.2	185.2	276.2	289.6
Hydro	4846.6	4369.5	5483.6	5160.2	5148.7	5356.1
Landfill gas	552.8	562.9	533.0	503.4	492.8	445.5
Sewage digestion	37.1	30.6	27.7	26.2	32.0	36.0
Other biomass	868.3	778.1	1155.4	1333.7	1374.4	1971.5
Total	14667.2	16989.6	19045.1	21088.6	19781.6	25165.9
Load Factors						
Wind	26.81%	29.15%	26.56%	29.17%	23.44%	27.53%
Hydro	37.01%	33.18%	41.22%	38.01%	36.62%	37.25%
Landfill gas	55.29%	55.83%	52.53%	49.40%	48.23%	43.81%
Sewage digestion	44.67%	42.94%	46.13%	43.32%	51.29%	56.64%

Appendix B

Machines modelling

B.1 Induction machine power flow model

A induction machine presents the circuit in Fig B.1 where: V_S is the supply voltage; R_s and X_s are stator's resistance and reactance respectively; R_m and X_m are magnetization branch resistance and reactance respectively; and, R_r and X_r are rotor's resistance and reactance respectively. In this project R_m is neglected, because in general $R_m >> X_m$ [76, 84].

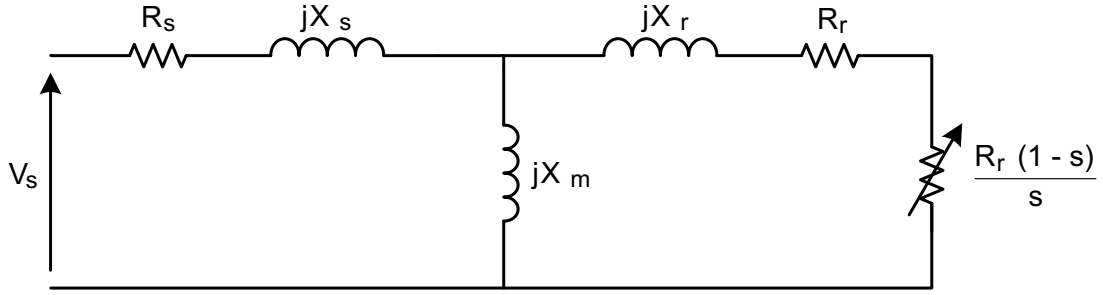

Figure B.1: One wire electrical diagram for induction machines in per unit with R_m neglected.

To calculate the power extracted from the grid is necessary to reduce this circuit to a single impedance [76,84]. The first step is to determine the equivalent impedance $\bar{Z}_{eq}$ from the parallel between the magnetization branch and the rotor branch, as follows:

$$\frac{1}{\dot{Z}_{eq}} = \frac{1}{\frac{R_r}{s} + jX_r} + \frac{1}{jX_m} \tag{B.1}$$

$$\dot{Z}_{eq} = \frac{-X_m X_r + jX_m \frac{R_r}{s}}{\frac{R_r}{s} + j\left(X_m + X_r\right)} \tag{B.2}$$

Multiplying $\dot{Z}_{eq}$ numerator and denominator by the denominator's conjugated, so only numerator is complex number, it comes:

$$\dot{Z}_{eq} = \frac{-X_m X_r + jX_m \frac{R_r}{s} \quad \frac{R_r}{s} - j\left(X_m + X_r\right)}{\frac{R_r}{s} + j\left(X_m + X_r\right) \quad \frac{R_r}{s} - j\left(X_m + X_r\right)} \tag{B.3}$$

$$\dot{Z}_{eq} = \frac{\frac{R_r}{s} {X_m}^2 + jX_m \left[\left(\frac{R_r}{s}\right)^2 + X_r\left(X_m + X_r\right)\right]}{\left(\frac{R_r}{s}\right)^2 + \left(X_m + X_r\right)^2} \tag{B.4}$$

With some manipulation one can separate real and imaginary parts, as follows:

$$R_{eq} = s\frac{R_r {X_m}^2}{R_r^2 + \left(X_m + X_r\right)^2 s^2} \tag{B.5}$$

$$X_{eq} = \frac{X_m {R_r}^2 + \left({X_m}^2 X_r + X_m {X_r}^2\right) s^2}{R_r^2 + \left(X_m + X_r\right)^2 s^2} \tag{B.6}$$

Figure B.2 depicts the resulting circuit.

Therefore, the power extracted from the grid is calculated:

$$\vec{S} = \frac{{V_s}^2}{\dot{Z}_{total}} = \frac{{V_s}^2}{R_{eq} + R_s + j\left(X_{eq} + X_s\right)} \tag{B.7}$$

Manipulating (B.7), one can separate active and reactive power, as follows:

$$P = \frac{{V_s}^2 \left(R_{eq} + R_s\right)}{\left(R_{eq} + R_s\right)^2 + \left(X_{eq} + X_s\right)^2} \tag{B.8}$$

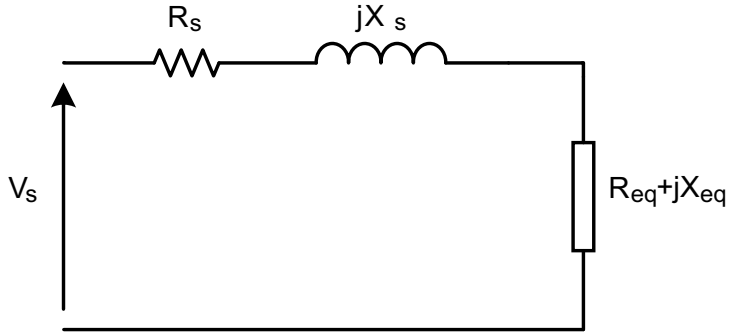

Figure B.2: Equivalent circuit of an induction machine where R_{eq} and jX_{eq} represent the parallel between the magnetization branch and the rotor branch.

$$Q = \frac{{V_s}^2 \left(X_{eq} + X_s\right)}{\left(R_{eq} + R_s\right)^2 + \left(X_{eq} + X_s\right)^2} \tag{B.9}$$

The development resulting in B.8 and B.9 refers to the grid view of the machine, however both equations are function of rotor slip s. This dependency is solved by the mechanical torque equation and the electromagnetic torque transmitted to the rotor trough the iron gap. For this reason, the Thévenin equivalent from points A and B in Figure B.3

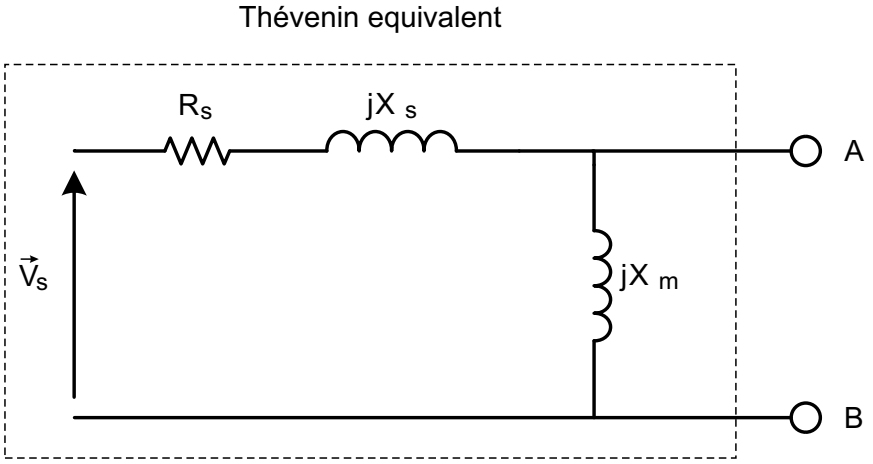

Figure B.3: Thévenin equivalent "seen" from the rotor side of an induction machine.

$$\vec{V}_{TH} = \vec{V}_s \frac{X_m}{R_s + j\left(X_m + X_s\right)} \tag{B.10}$$

Manipulating one can obtain the magnitude of Thévenin voltage as follows:

$$V_{TH} = V_s \frac{X_m}{\sqrt{{R_s}^2 + j\left(X_m + X_s\right)^2}} \tag{B.11}$$

Thévenin's impedance is calculated by:

$$\frac{1}{\dot{Z}_{TH}} = \frac{1}{jX_m} + \frac{1}{R_s + jX_s} = \frac{R_s + j\left(X_m + X_s\right)}{-X_m X_s + jR_s X_m} \tag{B.12}$$

$$\dot{Z}_{TH} = \frac{R_s {X_m}^2 + j\left[X_m {R_s}^2 + X_m X_s \left(X_m + X_s\right)\right]}{{R_s}^2 + \left(X_m + X_s\right)^2} \tag{B.13}$$

where:

$$R_1 = R_{TH} = \frac{R_s {X_m}^2}{{R_s}^2 + \left(X_m + X_s\right)^2} \tag{B.14}$$

and,

$$X_1 = X_{TH} = \frac{X_m {R_s}^2 + X_m X_s \left(X_m + X_s\right)}{{R_s}^2 + \left(X_m + X_s\right)^2} \tag{B.15}$$

Now it is possible to calculate the rotor current $\vec{I_r}$:

$$\vec{I_r} = \frac{\vec{V}_{TH}}{\left(R_1 + \frac{R_r}{s}\right) + j\left(X_1 + X_r\right)} \tag{B.16}$$

Where the magnitude is:

$$I_r = \frac{V_{TH}}{\sqrt{\left(R_1 + \frac{R_r}{s}\right)^2 + \left(X_1 + X_r\right)^2}} \tag{B.17}$$

Concluding the electromagnetic torque in per unit is:

$$T_e = {I_r}^2 \frac{R_r}{s} = \frac{{V_{TH}}^2 R_r \frac{1}{s}}{\left(R_1 + \frac{R_r}{s}\right)^2 + (X_1 + X_r)^2} \tag{B.18}$$

$$T_e = \frac{{V_s}^2 {X_m}^2 R_r \frac{1}{s}}{\left[{R_s}^2 + (X_s + X_m)^2\right]\left[\left(R_1 + \frac{R_r}{s}\right)^2 + (X_1 + X_r)^2\right]} \tag{B.19}$$

and the power developed on the rotor is:

$$P = \frac{{V_s}^2 {X_m}^2 R_r \frac{1-s}{s}}{\left[{R_s}^2 + (X_s + X_m)^2\right]\left[\left(R_1 + \frac{R_r}{s}\right)^2 + (X_1 + X_r)^2\right]} \tag{B.20}$$

B.2 Induction machine dynamic model

The dynamic model for the induction generator in this thesis uses three differential equations, where one relates to the rotor dynamics (mechanical power, electrical power, and damping torque), while the other two equations are related to the voltage source behind the transient inductance X'_s [76, 84]. The set of algebraic-differential equations modelling the induction machine for dynamic stability studies is:

$$\frac{d\omega}{dt} = \frac{1}{2H}\left[T_m - e_d I_{ds} - e_q I_{qs} - D\left(\omega - \omega_s\right)\right] \tag{B.21}$$

$$\frac{de_d}{dt} = -\frac{1}{\tau_0}\left[e_d - \left(X_s - X'_s\right) I_{qs}\right] + s\omega_s e_q \tag{B.22}$$

$$\frac{de_q}{dt} = -\frac{1}{\tau_0}\left[e_q + \left(X_s - X'_s\right) I_{ds}\right] - s\omega_s e_d \tag{B.23}$$

with the following algebraic equations,

$$v_{ds} = -R_s i_{ds} + X'_s i_{qs} + e_d \tag{B.24}$$

$$v_{qs} = -R_s i_{qs} - X'_s i_{ds} + e_q \tag{B.25}$$

$$P = v_{ds} i_{ds} + v_{qs} i_{qs} \tag{B.26}$$

$$Q = v_{ds} i_{qs} - v_{qs} i_{ds} \tag{B.27}$$

One can note that on the equations above the sub-index s relates to the stator variables and parameters.

B.3 Synchronous machine dynamic model

Model from P. Sauer's book [33, Chapter 3].

$$\frac{d\delta}{dt} = \omega - \omega_s \tag{B.28}$$

$$\frac{2H}{\omega_s}\frac{d\omega}{dt} = T_m - (\varphi_d I_q - \varphi_q I_d) - T_{FW} \tag{B.29}$$

$$\begin{aligned} T'_{d0}\frac{dE'_q}{dt} = &- E'_q - (X_d - X'_d)\left[I_d - \frac{X'_d - X''_d}{(X'_d - X_{ls})^2}\left(\varphi_{1d} + (X'_d - X_{ls})\, I_d\right.\right. \\ &\left.\left. -E'_q + S_{1d}(Y_2)\right)\right] - S_{fd}(Y_2) + E_{fd} \end{aligned} \tag{B.30}$$

$$\begin{aligned} T'_{q0}\frac{dE'_d}{dt} = &- E'_d - \left(X_q - X'_q\right)\left[I_q - \frac{X'_q - X''_q}{\left(X'_q - X_{ls}\right)^2}\left(\varphi_{2q} + \left(X'_q - X_{ls}\right) I_q\right.\right. \\ &\left.\left. +E'_d + S_{2d}(Y_2)\right)\right] + S_{1d}(Y_2) \end{aligned} \tag{B.31}$$

$$T''_{d0}\frac{d\varphi_{1d}}{dt} = - \varphi_{1d} + E'_q - (X'_d - X_{ls})\, I_d - S_{1d}(Y_2) \tag{B.32}$$

$$T''_{q0}\frac{d\varphi_{2q}}{dt} = - \varphi_{2q} - E'_d - \left(X'_q - X_{ls}\right) I_q - S_{2q}(Y_2) \tag{B.33}$$

$$\frac{1}{\omega_s}\frac{d\varphi_d}{dt} = R_s I_d + \frac{\omega}{\omega_s}\varphi_q + V_d \tag{B.34}$$

$$\frac{1}{\omega_s}\frac{d\varphi_q}{dt} = R_s I_q - \frac{\omega}{\omega_s}\varphi_d + V_q \tag{B.35}$$

with the following algebraic equations,

$$\varphi_d = X''_d I_d + \frac{(X''_d - X_{ls})}{(X'_d - X_{ls})}E'_q + \frac{(X'_d - X''_d)}{(X'_d - X_{ls})}\varphi_{1d} - S_d(Y_2) \tag{B.36}$$

$$\varphi_q = X''_q I_q - \frac{\left(X''_q - X_{ls}\right)}{\left(X'_q - X_{ls}\right)}E'_d + \frac{\left(X'_q - X''_q\right)}{\left(X'_q - X_{ls}\right)}\varphi_{2q} - S_q(Y_2) \tag{B.37}$$

$$Y_2 = \left[I_d E'_q \varphi_{1d} I_q E'_d \varphi_{2q}\right]^t \tag{B.38}$$

Appendix C

Power flow solution and robustness areas evaluation for test systems.

C.1 IEEE 30 bus system

Table C.1: Robustness level calculated for the IEEE 30 Bus system - base case.

Bus	V^s	θ^s	V^u	θ^u	$E_p(X^s, X^u)$
1	1.00500	0	1.00500	0	7.42214
2	0.99029	-0.04374	0.94396	-2.54035	13.22013
4	0.97688	-0.06325	0.92948	-3.76610	3.83993
5	0.96121	-0.10853	0.86412	-7.07661	8.91599
6	0.97329	-0.08472	0.83380	-5.24068	10.13911
7	0.96524	-0.09912	0.84237	-6.31177	5.92825
12	0.96598	-0.08499	0.91797	-5.14403	5.88278
13	0.96598	-0.08499	0.91797	-5.14403	3.00956
14	0.95944	-0.09195	0.91109	-5.58563	1.19278
27	0.96694	-0.10929	0.53764	-17.16048	0.35513
28	0.97198	-0.08782	0.78972	-5.59572	5.21297
30	0.94316	-0.13882	0.07104	-62.00000	-0.58037
31	0.96121	-0.10853	0.86412	-7.07661	4.66694

Table C.2: Robustness level calculated for the IEEE 30 Bus system - FSWG case.

Bus	V^s	θ^s	V^u	θ^u	$E_p(X^s, X^u)$
1	1.01000	0	1.01000	0	7.85967
2	0.99500	-0.02022	0.99500	-1.97250	14.46410
4	0.98063	-0.01947	0.97716	-1.85548	4.28841
5	0.97234	-0.04909	0.91540	-3.74917	10.18936
6	0.98128	-0.04453	0.88134	-3.37429	11.71433
7	0.97434	-0.05099	0.89152	-3.80009	6.97003
12	0.95919	-0.01409	0.95056	-1.53039	6.40138
13	0.95347	0.00121	0.94208	-0.62812	3.20158
14	0.95261	-0.02114	0.94392	-1.94201	1.37779
27	0.97501	-0.06869	0.56523	-15.14608	0.43245
28	0.97999	-0.04758	0.83445	-3.70474	5.99838
30	0.95143	-0.09772	0.06685	-60.60324	-0.57747
31	0.96953	-0.02789	0.90800	-2.35432	5.20190

Table C.3: Robustness level calculated for the IEEE 30 Bus system - VSWG case.

Bus	V^s	θ^s	V^u	θ^u	$E_p(X^s, X^u)$
1	1.00500	0	1.00500	0	7.81891
2	0.99500	-0.02518	0.99500	-2.28586	14.55572
4	0.98829	-0.03671	0.98829	-2.94652	4.36711
5	0.97894	-0.05565	0.96021	-4.76159	11.16518
6	0.98442	-0.05016	0.90077	-3.97789	12.15896
7	0.97893	-0.05691	0.92159	-4.53855	7.38559
12	0.98243	-0.04465	0.98243	-3.40169	6.79036
13	0.98500	-0.03742	0.98500	-2.98722	3.45306
14	0.97600	-0.05137	0.97600	-3.78687	1.42669
27	0.97818	-0.07416	0.57657	-15.69464	0.44990
28	0.98314	-0.05319	0.85273	-4.29938	6.23033
30	0.95469	-0.10300	0.06529	-61.37623	-0.58986
31	0.98000	-0.03480	0.98000	-3.54373	5.85951

Appendix D

São Paulo state restoration data.

Table D.1: Instructions for fluent phase restoration for the Jupiá area.

No.	**Action location** Operation description → Operation detail
1	**Bus 502 - JUP power plant** Black-start a minimum of 6 GUs. → Maintain V=0.942 pu. Adjust GUs voltage level according to dispatch: → up to 100 MW, V=0.942 pu. → greater than 101 MW, V=1.0 pu.
2	**Bus 539** Restore line to Bus 561. → A 180 MVar shunt reactor must be connected on the receiving bus. → Voltage level must be $\leq$ 0.95 pu.
3	**Bus 561** Restore a second 180 MVar shunt reactor. Restore line to Bus 584. → A 90 MVar shunt reactor must be connected on the receiving bus. → Voltage level must be $\leq$ 0.96 pu.
4	**Bus 584, 590 - CAV substation** Restore first 440/230 kV transformer to Bus 590. → Voltage level must be $\leq$ 1.10 pu. Restore first circuit to Bus 410. → Voltage level must be $\leq$ 0.995 pu. → A 90 MVar shunt reactor must be connected on the receiving bus.
5	**Bus 410**

Continued on next page

Table D.1 – continued from previous page

No.	**Action location** Operation description → Operation detail
	Restore first circuit to Bus 423. → Voltage level must be ≤ 1.001 pu. → A 60 MVar shunt reactor must be connected on the receiving bus.
6	**Bus 423** Restore line to Bus 425. → Voltage level must be ≤ 0.94 pu.
7	**Bus 425** Restore line to Bus 427.
8	**Bus 427, 428, 429 - CTR substation** *Note:* This substation is responsible for delivering power to the São Paulo city central area Restore first 230/20 kV transformer to Bus 429. → Tap on rated position 1 : 1. Pick-up 60 MW on Bus 429. → Voltage level must be ≤ 1.05 pu. Restore second 230/20 kV transformer to Bus 429. → Tap on rated position 1 : 1. Pick-up 50 MW on Bus 429. → Voltage level must be ≥ 0.97 pu. Connect the 8.1 MVar shunt capacitor on Bus 429 Restore third 230/20 kV transformer to Bus 429. → Tap on rated position 1 : 1. Pick-up 60 MW on Bus 429. → Voltage level must be ≥ 0.99 pu. Restore first 230/88 kV transformer to Bus 428. → Tap on rated position 1 : 1. Pick-up 70 MW on Bus 428. Pick-up 30 MW on Bus 428. Restore second 230/88 kV transformer to Bus 428. → Tap on rated position 1 : 1.
9	**Bus 584, 590, 9584 - CAV substation** Restore second 440/230 kV transformer to Bus 590. → Tap on rated position 1 : 1. Restore second circuit to Bus 410. → Voltage level must be ≤ 1.0 pu.
10	**Bus 561** Restore line to Bus 577.

Continued on next page

Table D.1 – continued from previous page

No.	**Action location** Operation description → Operation detail
	→ Power flowing from 561 to 584 must be ≥ 160 MW. → A 180 MVar shunt reactor must be connected on Bus 581. → Voltage level must be ≤ 0.96 pu. *Note:* The next step refer to a passage only bus, so it must be previously connected to allow Bus 581 fast restoration.
11	**Bus 577** Restore line to Bus 581, if not already connected.
12	**Bus 581, 582 - EMG substation** Restore first 440/345 kV transformer to Bus 582. → Tap on rated position 1 : 1. → Voltage level must be ≤ 1.1 pu Restore line to Bus 474. → Voltage level must be ≤ 1.01 pu.
13	**Bus 474, 475 - SUL substation** *Note:* This substation is responsible for delivering power to the São Paulo city south area, where CGH airport is located. Restore first 345/88 kV transformer to Bus 475. → Tap on rated position 1 : 1. → Voltage level must be ≤ 1.05 pu. Pick-up 30 MW on Bus 428 at maximum.
14 *	**Bus 584, 590, 9584 - CAV substation** Restore wind farm at Bus 9584. → Maintain voltage level $V = 1.0$ pu.
15	**End of fluent phase.** Wait for further instructions from the Independent System Operator to proceed with coordinated phase.

* Steps required to restore wind farm.

Table D.2: Instructions for coordinated phase restoration for the São Paulo state area - parallel connection closures.

No.	**Action location** Operation description → Operation detail
	1 - Parallel between JUP and ILS
1.1	**Bus 502, 539, 541 - JUP substation** Restore transmission line from Bus 539 to bus 542. → Minimum of 8 GUs. → Jupiá dispatch: $P_{ele}^{502} \geq 280\,\text{MW}$.
1.2	**Bus 542** Restore line to Bus 538.
1.3	**Bus 538** Synchronize JUP and ILS restoration areas.
	2 - Parallel between AGV and PPR
2.1	**Bus 570, 571, 9570 - SUMARE substation** *Note:* This substation is responsible two corridors and is also responsible for their synchronization. Synchronize AGV and PPR restoration areas. Pick-up additional 60 MW on Bus 571.
	3 - Parallel between AGV and ILS
3.1	**Bus 501, 538 - ILS substation** Restore line from Bus 538 to Bus 536.
3.2	**Bus 536** Synchronize AGV and ILS restoration areas.
	4 - Parallel between CPV and PPR
4.1	**Bus 507, 549, 550 - CPV substation** Restore line from Bus 549 to Bus 547.
4.2	**Bus 513, 547, 548 - TQR substation** Synchronize CPV and PPR restoration areas.
4.3	**Bus 552, 553, 9552 - ASSIS substation** *Note:* This substation is responsible two corridors and is also responsible for their first loop closure. Close loop by connecting the two substation buses.

Table D.3: Instructions for coordinated phase restoration for the São Paulo state area - bulk system restoration.

No.	**Action location** Operation description → Operation detail
1 *	**Bus 561, 562, 9561 - BAU substation** Restore wind farm at Bus 9561. → Maintain voltage level $V = 1.0$ pu.
2	**Bus 539** Restore second transmission line from Bus 539 to bus 561.
3	**Bus 561** Close loop with the second transmission line from Bus 539 to bus 561.
4	**Bus 538** Restore first transmission line from Bus 538 to bus 561.
5	**Bus 561, 592, 9561 - BAU substation** Close loop with the first transmission line from Bus 538 to bus 561. Pick-up 120 MW.
6 *	**Bus 577, 414, 9577 - OESTE substation** Restore wind farm at Bus 9577. → Maintain voltage level $V = 1.0$ pu.
7	**Bus 538** Restore second transmission line from Bus 538 to bus 561. → Wait stabilization from previous load pick-up. → Voltage level must be ≤ 1.00 pu. → A 180 MVar shunt reactor must be connected on the receiving bus.
8	**Bus 539** Restore transmission line from Bus 539 to bus 547.
9	**Bus 547** Close loop with the transmission line from Bus 539 to bus 547.
10	**Bus 565** Restore transmission line from Bus 565 to bus 593.
11	**Bus 593, 594, 595 - SAA substation** Close loop with the second transmission line from Bus 565 to bus 593. Pick-up additional 100 MW on Bus 595.

* Steps required to restore wind farm.

Table D.4: Power flow bus data for São Paulo state area.

Bus	V	θ	P_l	Q_l	P_g	Q_g	Type
78	1.171	-20.0	0	0	0	0	PQ
86	1.000	0.0	0	0	0	0	PQ
99	1.031	0.0	0	0	0	0	PQ
101	1.082	0.0	0	0	0	0	PQ
410	1.012	-12.0	0	0	0	0	PQ
414	1.000	0.0	150	49.3	0	0	PQ
421	1.000	0.0	0	0	0	0	PQ
422	1.000	0.0	0	0	0	0	PQ
423	0.997	-14.0	0	0	0	0	PQ
425	0.994	-14.0	0	0	0	0	PQ
427	0.988	-16.0	0	0	0	0	PQ
428	0.974	-18.0	100	32.9	0	0	PQ
429	0.968	-20.0	170	59.3	0	0	PQ
449	1.174	-20.0	0	0	0	0	PQ
464	1.166	-21.0	0	0	0	0	PQ
465	1.000	0.0	150	49.4	0	0	PQ
466	1.165	-21.0	0	0	0	0	PQ
467	1.136	-25.0	165	52.6	0	0	PQ
471	1.000	0.0	0	0	0	0	PQ
474	1.062	-5.8	0	0	0	0	PQ
475	1.056	-6.8	100	32.9	0	0	PQ
479	1.000	0.0	0	0	0	0	PQ
488	1.000	0.0	0	0	0	0	PQ
491	1.000	0.0	0	0	0	0	PQ
495	1.000	0.0	200	65.8	0	0	PQ
500	0.950	1.3	0	0	400	-250	PV
501	0.950	0.0	0	0	393.2	-698	Vθ
502	0.950	2.9	0	0	400	-466	PV
507	0.950	1.6	0	0	120	-109	PV
510	0.950	7.8	0	0	350	-142	PV
513	0.950	4.8	0	0	182.5	-105	PV
536	0.988	-2.1	0	0	0	0	PQ
537	0.967	-5.4	120	39.4	0	0	PQ
538	1.032	-2.5	0	0	0	0	PQ
539	1.031	-0.9	0	0	0	0	PQ
541	1.000	0.0	150	49.3	0	0	PQ
542	1.033	-1.7	0	0	0	0	PQ
544	0.972	4.8	0	0	0	0	PQ

Continued on next page

Table D.4 – continued from previous page

Bus	V	θ	P_l	Q_l	P_g	Q_g	Type
547	0.993	0.8	0	0	0	0	PQ
548	1.000	-1.0	65	26.3	0	0	PQ
549	0.983	-0.5	0	0	0	0	PQ
550	1.000	-3.8	115	40	0	0	PQ
552	0.984	-2.5	0	0	0	0	PQ
553	1.000	-3.9	65	20	0	0	PQ
559	1.144	-16.0	0	0	0	0	PQ
560	1.121	-20.0	150	49.4	0	0	PQ
561	1.061	-4.7	0	0	0	0	PQ
562	1.025	-9.9	120	39.4	0	0	PQ
563	0.956	-11.0	0	0	0	0	PQ
564	0.932	-15.0	130	42.77	0	0	PQ
565	1.188	-18.0	0	0	0	0	PQ
566	1.000	0.0	200	69.9	0	0	PQ
567	0.950	-13.0	0	0	0	0	PQ
568	0.917	-19.0	180	59.2	0	0	PQ
570	0.949	-13.0	0	0	0	0	PQ
571	0.932	-16.0	100	32.9	0	0	PQ
574	0.943	-14.0	0	0	0	0	PQ
575	1.000	0.0	0	0	0	0	PQ
576	0.905	-19.0	160	65.8	0	0	PQ
577	1.077	-5.3	0	0	0	0	PQ
581	1.060	-5.4	0	0	0	0	PQ
582	1.062	-5.5	0	0	0	0	PQ
583	1.000	0.0	110	36.1	0	0	PQ
584	1.029	-10.0	0	0	0	0	PQ
585	1.084	-9.8	0	0	0	0	PQ
586	1.088	-9.6	0	0	0	0	PQ
590	1.026	-11.0	0	0	0	0	PQ
591	1.000	0.0	55	18	0	0	PQ
593	1.175	-20.0	0	0	0	0	PQ
594	1.175	-20.0	0	0	0	0	PQ
595	1.164	-22.0	130	25	0	0	PQ
599	1.000	0.0	0	0	0	0	PQ
601	1.000	0.0	0	0	0	0	PQ
1029	1.001	0.0	80	26.3	0	0	PQ
3897	1.000	4.8	10	3.7	0	0	PQ
9552	0.984	-2.5	0	0	0	0	PQ
9559	0.909	-7.2	0	0	0	0	PQ

Continued on next page

Table D.4 – continued from previous page

Bus	V	θ	P_l	Q_l	P_g	Q_g	Type
9561	0.912	-6.8	0	0	0	0	PQ
9570	0.949	-13.0	0	0	0	0	PQ
9574	1.000	0.0	0	0	0	0	PQ
9577	0.968	-9.2	0	0	0	0	PQ
9584	0.866	-13.0	0	0	0	0	PQ

Table D.5: Power flow line data for São Paulo state area.

From	To	$R\%$	$X_l\%$	B_s MVar
78	464	0.100	0.950	17.073
78	464	0.100	0.940	17.073
86	488	0.081	1.291	38.341
99	101	-	0.010	-
410	421	0.280	1.540	4.970
410	421	0.280	1.540	4.970
410	423	0.200	1.100	3.550
421	422	-	8.180	-
421	422	-	8.300	-
423	425	0.080	0.440	1.420
425	427	0.040	0.820	76.695
427	428	-	7.720	-
427	428	-	7.630	-
427	429	-	11.480	-
427	429	-	11.480	-
427	429	-	11.070	-
449	78	0.070	0.660	12.845
449	78	0.070	0.660	12.845
464	465	-	6.350	-
464	466	0.010	0.150	4.127
466	467	-	5.640	-
471	479	0.020	0.220	3.380
474	475	-	6.360	-
479	582	0.160	1.310	22.768
488	491	0.010	0.200	5.502
491	495	0.020	0.640	8.941
536	500	-	1.367	-
536	538	0.190	2.520	136.890
536	559	0.400	5.360	290.920
536	563	0.410	5.640	304.120
537	536	-	4.700	-
538	501	-	1.097	-
538	559	0.480	5.970	384.960
538	559	0.480	5.970	384.960
539	502	-	1.605	-
539	542	0.060	0.730	43.830
539	547	0.270	3.600	197.090
539	561	0.390	4.960	319.720

Continued on next page

Table D.5 – continued from previous page

From	To	$R\%$	$X_l\%$	B_s MVar
539	561	0.390	4.960	319.720
541	539	-	8.330	-
542	538	0.060	0.810	48.630
544	510	-	1.384	-
544	547	0.150	1.940	108.730
544	547	0.150	1.940	108.730
544	3897	0.045	1.160	-
547	513	-	3.630	-
547	549	0.090	1.200	66.940
547	9552	0.250	2.970	174.690
548	547	-	4.660	-
549	507	-	2.793	-
549	552	0.140	1.820	102.200
550	549	-	4.820	-
552	9552	-	0.001	-
553	552	0.070	7.237	-
553	552	0.070	7.237	-
553	1029	1.430	8.220	26.750
559	561	0.130	1.710	102.880
559	565	0.210	2.650	170.710
559	567	0.180	2.380	134.800
559	9559	-	10.000	-
560	559	-	4.820	-
561	538	0.410	5.090	327.900
561	538	0.410	5.090	327.900
561	577	0.280	3.540	228.280
561	581	0.400	4.860	313.390
561	584	0.300	3.760	242.060
561	584	0.300	3.760	242.060
561	9561	-	10.000	-
562	561	-	8.270	-
563	567	0.220	3.030	163.370
564	563	-	4.730	-
565	593	0.230	2.880	185.570
566	565	-	4.630	-
567	570	0.030	0.340	19.210
568	567	-	4.450	-
570	9570	-	0.001	-
571	570	-	4.660	-

Continued on next page

Table D.5 – continued from previous page

From	To	$R\%$	$X_l\%$	B_s MVar
574	593	0.150	1.980	118.810
574	599	0.200	2.560	151.950
574	9570	0.060	0.800	45.810
575	574	-	9.660	-
576	574	-	4.666	-
577	414	-	0.020	1.560
577	581	0.110	1.320	85.110
577	9577	-	10.000	-
582	474	0.220	1.870	30.890
582	488	0.070	0.700	12.166
582	488	0.070	0.700	12.166
582	581	-	0.720	-
583	581	-	4.666	-
584	585	0.024	0.307	18.570
584	9584	-	10.000	-
585	586	0.040	0.494	29.840
586	581	0.053	0.668	40.380
590	410	0.300	2.200	7.897
590	410	0.300	2.200	7.897
590	410	0.300	2.200	7.897
590	410	0.300	2.200	7.897
590	584	-	0.750	-
590	584	-	0.750	-
591	584	-	8.270	-
593	559	0.380	4.700	303.360
594	449	0.040	0.410	7.150
594	449	0.040	0.410	7.150
594	593	-	0.720	-
594	593	-	0.710	-
595	593	-	4.690	-
601	599	-	4.650	-
9552	561	0.180	2.370	132.670
9552	9570	0.432	5.492	309.590

Table D.6: Robustness level calculated for the São Paulo state grid.

Bus	$E_p(X^s, X^u)$ – Step 5			$E_p(X^s, X^u)$ – Step 11		
	Base	FSWG	VSWG	Base	FSWG	VSWG
78	-0.1957	91.4667	79.3192	-18.3731	-25.3601	-7.4107
410	93.4993	104.6004	87.4236	91.5149	95.0696	87.5572
423	154.8399	173.9859	144.8835	151.1391	157.3123	145.1030
425	174.5604	197.0810	161.3784	170.8756	177.9359	161.5405
427	93.0155	105.8150	84.0236	91.6130	95.4354	84.0364
428	14.3555	16.3359	12.8353	14.1919	14.7629	12.8268
429	14.6857	16.6942	13.1038	14.5344	15.1050	13.0900
449	86.7034	308.4557	262.6018	68.6285	61.6704	80.9298
464	93.6565	374.1661	314.6089	73.9651	61.5896	70.8001
466	84.0075	333.3430	279.8044	67.5108	56.3224	62.5906
467	4.1686	9.6848	8.0889	4.2146	4.0411	3.6866
474	41.6107	45.6445	37.9631	41.0342	41.0020	38.0099
475	9.7950	10.8322	8.7539	9.7036	9.6959	8.7511
500	34.4858	33.6191	33.4092	34.6080	34.6421	34.7222
501	46.4461	47.6300	46.7944	47.1637	47.2713	47.2126
502	31.0560	31.6404	30.9105	32.9924	33.0669	32.9643
507	16.8312	13.1075	13.1208	17.1442	17.1548	17.1713
510	33.7238	15.6711	15.7438	33.8202	33.8312	33.9597
513	13.0936	9.1310	9.1751	13.3036	13.3136	13.3438
536	72.7990	70.0920	69.1145	73.7000	73.8306	73.8318
537	10.3165	10.1154	9.9066	10.5388	10.5572	10.4744
538	147.4049	155.0403	149.6912	161.4040	162.1368	161.9429
539	126.2945	131.1280	125.4262	146.2896	146.9482	145.6101

Continued on next page

Table D.6 – continued from previous page

Bus	$E_p(X^s, X^u)$ – Step 5			$E_p(X^s, X^u)$ – Step 11		
	Base	FSWG	VSWG	Base	FSWG	VSWG
542	136.7140	142.6126	137.2327	141.4281	142.0675	141.5161
544	98.6722	25.9640	26.1660	100.3964	100.4556	100.6397
547	104.4792	56.7796	57.0194	122.9702	123.1377	123.3934
548	10.2456	6.2337	6.1939	10.9850	10.9998	10.9072
549	93.5657	59.4731	59.5980	96.8585	96.9664	97.1705
550	9.8527	7.0930	7.0322	10.4868	10.4981	10.3910
552	65.5941	38.7863	38.8021	68.3285	68.4229	68.5876
553	13.6963	8.9013	8.8308	14.5432	14.5630	14.4697
559	18.0302	34.8562	30.2542	23.7788	24.2419	29.2243
560	6.1874	11.0080	9.4314	5.9801	6.0736	6.5556
561	80.1474	86.5298	75.9738	90.9988	92.1647	87.4580
562	7.4687	8.1396	6.9613	7.4182	7.5106	6.9517
563	34.3219	23.7228	23.3029	35.4189	35.4920	35.5400
564	10.4671	7.9619	7.7565	10.9776	10.9988	10.8917
565	–	–	–	12.7896	12.6240	15.6260
567	167.3988	97.1240	95.7117	174.1510	174.5143	175.1785
568	11.4260	8.2026	7.9951	12.1984	12.2213	12.0678
570	220.0379	126.6642	124.8653	229.2217	229.6965	230.5207
571	10.8436	7.4105	7.2337	11.5465	11.5690	11.4558
574	70.1568	40.7294	40.0482	73.3907	73.5449	73.6655
576	10.7392	7.5881	7.3975	11.4844	11.5063	11.3639
577	70.2219	77.0643	63.8881	69.3087	69.2520	63.9542
581	132.8519	146.3736	119.8252	131.3799	131.2781	119.8693

Continued on next page

Table D.6 – continued from previous page

Bus	$E_p(X^s, X^u)$ – Step 5			$E_p(X^s, X^u)$ – Step 11		
	Base	FSWG	VSWG	Base	FSWG	VSWG
582	118.3004	130.3306	106.7418	116.9725	116.8816	106.7853
584	177.9658	199.6986	162.1602	175.8756	182.2874	162.1630
590	205.2806	230.2842	187.8329	202.5515	210.0295	187.8900
593	61.3614	169.4494	142.4876	64.3728	61.7613	66.4293
594	121.0559	384.0646	325.2819	106.3594	99.0892	116.1878
595	4.2719	11.3606	9.5411	4.9110	4.7680	4.7607
3897	40.6738	-3.9319	-3.8273	41.3603	41.3847	41.4699
9559	2.7488	5.5413	4.3528	2.5458	2.7412	3.5282
9561	6.2188	6.8423	5.4254	6.1583	6.3214	5.4328
9577	6.4051	7.1797	5.4012	6.3424	6.1939	5.4086
9584	5.8914	6.7402	5.1440	5.8243	6.1591	5.1514

Annex A

Paper on robustness areas technique applied in restorations

energies

MDPI

Article

Robustness Area Technique Developing Guidelines for Power System Restoration

Paulo Murinelli Pesoti [1,*], Eliane Valença de Lorenci [2], Antonio Carlos Zambroni de Souza [2], Kwok Lun Lo [1] and Benedito Isaias Lima Lopes [2]

[1] Electrical and Electronic Engineering Department, University of Strathclyde, 16 Richmond Street, Glasgow G1 1XQ , UK; k.lo@strath.ac.uk

[2] Institute of Electric Systems and Energy, Federal University of Itajubá, Av. BPS 1303, Itajubá - MG 37500-903, Brazil; edelorenci@gmail.com (E.V.d.L.); zambroni@unifei.edu.br (A.C.Z.d.S.); isaias@unifei.edu.br (B.I.L.L.)

* Correspondence: paulo.murinelli-pesoti@strath.ac.uk

Academic Editor: Akhtar Kalam

Received: 28 November 2016; Accepted: 4 January 2017; Published: 13 January 2017

Abstract: This paper proposes a novel energy based technique called the Robustness Area (RA) technique that measures power system robustness levels, as a helper for planning Power System Restorations (PSRs). The motivation is on account of the latest blackouts in Brazil, where the local Independent System Operator (ISO) encountered difficulties related to circuit disconnections during the restoration. The technique identifies vulnerable and robust buses, pointing out system areas that should be firstly reinforced during PSR, in order to enhance system stability. A Brazilian power system restoration area is used to compare the guidelines adopted by the ISO with a more suitable new plan indicated by the RA tool. Active power and reactive power load margin and standing phase angle show the method efficiency as a result of a well balanced system configuration, enhancing the restoration performance. Time domain simulations for loop closures and severe events also show the positive impact that the proposed tool brings to PSRs.

Keywords: energy function; power system restoration; power system stability; voltage stability

1. Introduction

Power systems are developed to perform with high reliability, even though, critical outages may trigger a cascade of events ending up in a blackout. Black starts have been a major concern since the early 1980s [1], when systems became interconnected and blackouts turned into a wide-area event. For example, on August 2003, three transmission lines touched overgrown trees, leading to a series of events that caused the system collapse affecting over 50 million people [2] in North America. During this event, a total of 265 power plants were disconnected, corresponding to 61,800 MW. If events similar to this may happen, their impacts can be diminished by a fast and reliable power system restoration.

The Power System Restoration (PSR) in Brazil is based on hydro Generator Units (GUs) [3], providing a short black start period with renewable energy sources. It is, however, a continental sized power system with long high voltage transmission lines connecting 1076 power plants. On account of its complexity, the national Independent System Operator (ISO) adopted a two-phase restoration procedure: Fluent Phase (FP) (local), and Coordinated Phase (CP) (wide area). During the FP, black start utilities start up a minimum number of GUs, forming small electrical islands. Each island is responsible for picking-up a predetermined load amount. It is called Fluent because power companies can follow a script containing all the steps to perform the local restoration without intervention from the ISO. Afterwards, the CP takes place and all instructions are sent out from the ISO to local companies [4,5], connecting islands to each other. A full description of the Brazilian system restoration procedure is presented in [6], where FP and CP are further explained.

The aforementioned two-phase procedure is well-established; however, during the last major events (especially the 2009 blackout), the ISO faced circuit disconnections throughout the CP [7,8]. The full report on the 2009 blackout in Brazil is presented in [9]. The unsuccessful reconnections reveal fragile points and call for a demand of studies on the field of stability and reliability to re-design the black start philosophy [10], towards reducing the impact caused by blackouts. The following passage is removed from [8], where authors monitored the whole blackout and restoration procedure during the 2009 major outage:

> "The South–Southeast interconnection tripped again at 02:20:00 (Figure 20) and a new attempt to reconnect the two subsystems was made at 02:23:28 (second 328 in Figure 21), but 1.5 s later, the interconnection tripped again. It caused oscillations in the BIPS (Brazilian Interconnected Power System), as shown in Figure 22, where the angle difference between UFPA (Federal University of Pará) (North) and UNIFEI (Federal University of Itajubá) (Southeast), soon after the reconnection attempt, is shown".

Unsuccessful reconnections during PSRs have also been reported in many different power systems, as described by the two following passages [11]:

> "Resynchronizing of the interconnection loop was not accomplished in accordance with the interconnection procedures. The first tie which was closed between the northern and southern islands was a 115 kV line, which promptly opened on overload".

> "There were several unsuccessful closures before the island was finally reconnected to the remainder of the interconnection. Efforts need to be made to better coordinate restoration procedures among the many dispatch offices. Switching to return the system to normal was completed in one hour and two minutes following the cascading disturbance".

Planning PSRs requires expertise to deal with limitations and constraints, where poor voltage profile and frequency control problems are recurrent [12–14]. Such issues are mainly caused by thermal limitations on GUs and transmission lines stability contrains. The reduced number of GUs during this procedure is associated with a low inertia provision scenario [15], causing dynamic stability issues; and the few transmission lines connected can reduce the system reliability [16]. Attempting to overcome the PSR issues, several decision making techniques have been created based on different metrics [17–22]; however, few are dedicated to voltage stability assessments during this period. This work pays special attention to this issue, though voltage stability is treated as a robustness index. Hence, rather than considering voltage stability as a final purpose, it is considered as a decision helper in the CP. Due to this, the energy function based analysis is used to identify the best plan for PSR that can be used for static and dynamic analyses.

The energy function is a powerful tool [23,24] that can be used to infer system stability conditions. Such ability motivates the usage of a novel energy function tool that identifies system areas according to its strength level, pointing out regions to be reinforced firstly during restoration. The method also analyses system operations during restorations, such as load variations, transmission line reconnections, and loop closures. The methodology output is the impact that such operations cause and the feasibility of these actions. Taking into account the difficulties faced by the ISO during the latest restoration events, in which disconnections delayed the procedure, the Robustness Area (RA) technique is used to re-plan the Brazilian power system restoration. A real case scenario is taken for studies and the RA technique is used to create a new step in the restoration. This plan is compared with the one adopted by the ISO under static and dynamic approaches, showing the ability of the the proposed tool in planning the CP.

The RA definition is addressed in Section 2. A robustness area-based based guideline for the Brazilian power system PSRs is presented in Section 3. Voltage and dynamic assessments are carried out in Section 4 to investigate the impact caused by the usage of this novel tool in the restoration procedure, where results are presented. Section 5 presents the conclusion.

2. The Robustness Assessment

2.1. The Voltage Stability Problem

The first step in planning a restoration procedure is a static analysis, where the power flow is calculated, and violations are pointed out. During this stage, voltage stability tools are used to infer power system stability conditions, establishing boundaries between safe and unsafe regions. A power system is considered voltage stable when it is capable of keeping the voltage profile steady after being subjected to a disturbance. In this sense, the system is voltage stable when control actions produce coherent results. Otherwise, when reverse results are observed, the system is considered unstable. Figure 1 depicts such a situation with the help of a QV curve, that shows the voltage sensitivity to variations in reactive power injection. Region A identifies voltage Stable Equilibrium Points (SEPs) for a particular load bus, where an increase in the reactive power injection is associated with a voltage magnitude increase [25], i.e., $\frac{\partial Q}{\partial V} > 0$. The contrary occurs in Region B, which is related to Unstable Equilibrium Points (UEPs) and $\frac{\partial Q}{\partial V} < 0$. $\Delta\lambda_Q$ stands for the reactive power margin. The basics behind the QV curve are found in [26,27].

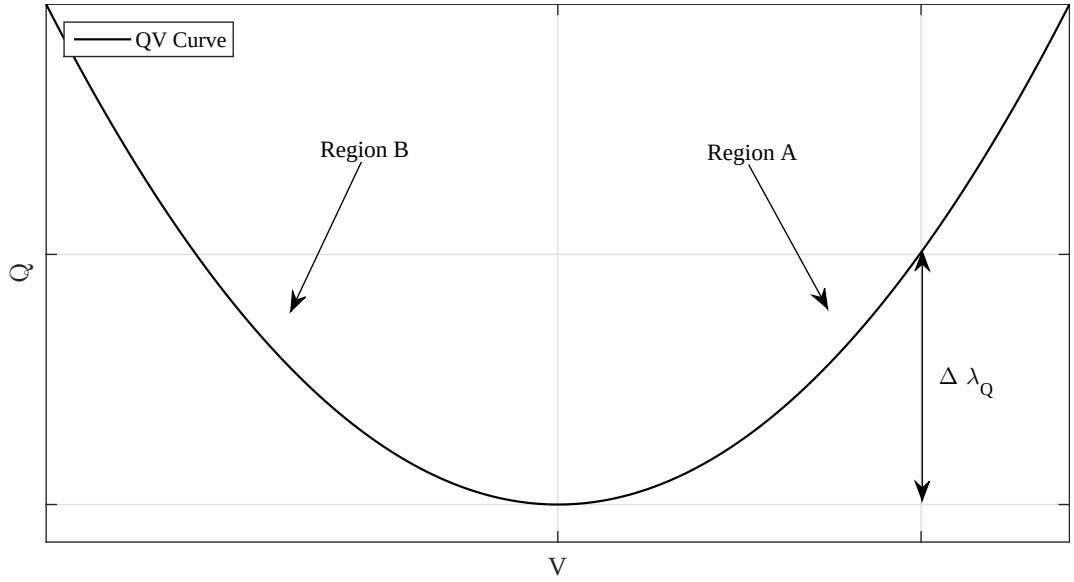

Figure 1. Regions of operation in a QV curve.

Figure 2 depicts the voltage stability problem in a PV curve [26] that relates voltage magnitude variation in function of load increase. The upper part is the stable region, associated with SEPs. The lower part is the unstable or abnormal region, associated with UEPs, and is avoided during operation. As the system moves toward the maximum loading point $P_{\max}$, the stable solution and a particular unstable solution get closer until they merge into one on a saddle node point, and no further solutions are possible.

2.2. The Power Flow Multiple Solutions and the Voltage Collapse Mechanism

In the steady state voltage stability approach, the system is driven towards the collapse point $P_{\max}$, on a time scale of minutes to hours ("quasistatic" manner), due to gradual changes in load/generation injections. In the static approach, the power system model can be reduced to the set of algebraic Equations that represent the power flow problem:

$$P_i = \sum_{j=1}^{n} V_i V_j \left[G_{ij} \cos\left(\theta_{ij}\right) + B_{ij} \sin\left(\theta_{ij}\right) \right], \quad (1)$$

$$Q_i = \sum_{j=1}^{n} V_i V_j \left[B_{ij} \sin\left(\theta_{ij}\right) - G_{ij} \cos\left(\theta_{ij}\right) \right], \tag{2}$$

where: n is the number of system buses; P_i and Q_i are, respectively, the specified active and reactive power injections of the ith bus; V_i is the voltage magnitude and θ_i, the respective phase angle; B_{ij} refers to the transfer susceptance between buses i and j, and G_{ij} is related to the transfer conductance; finally, θ_{ij} is the angular difference between buses i and j.

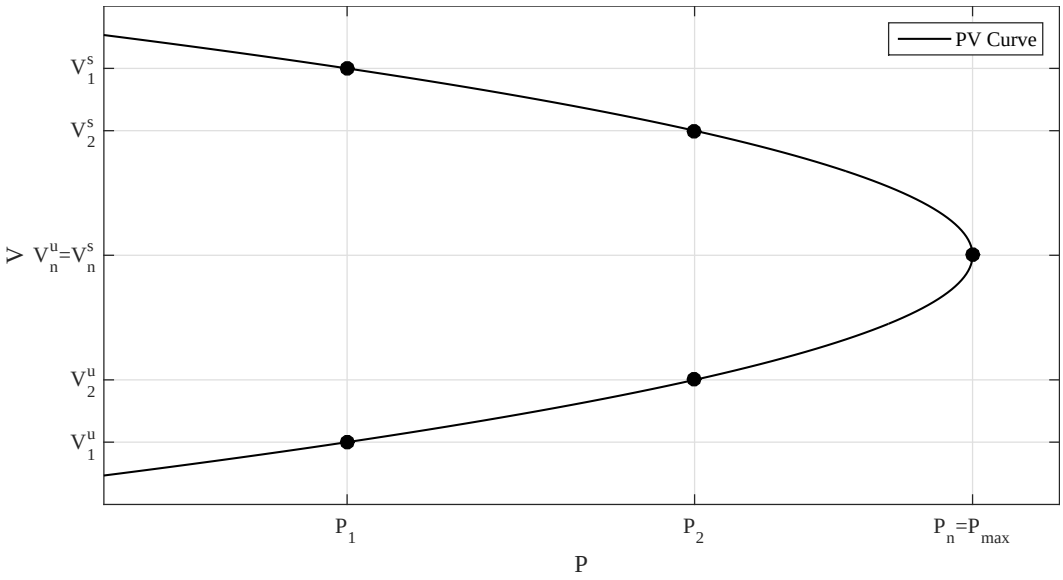

Figure 2. The PV curve.

The solutions of Equations (1) and (2) are associated with equilibrium points of the dynamical model that describes the power system. As the system slowly moves toward $P_{\max}$, the equilibrium points vanish because of different kinds of bifurcations. At the collapse point, the stable equilibrium point SEP and a particular type-1 UEP merge. Consequently, beyond this point, there are no equilibrium points, and the system experiences loss of stability [28]. Type-1 UEPs are associated with alternative power flow solutions that present low voltage magnitude only in a single bus or a single connected group of buses, and are referred to as the critical Low Voltage Solution (LVS), while SEPs are related to operable power flow solutions.

2.3. Voltage Stability Assessment by Means of an Energy Function

Concerning the voltage stability approach [29–31], the difference of potential energy between the SEP and an LVS of interest is calculated by:

$$\begin{aligned} v(X^s, X^u) = & -\sum_{i=1}^{n} Q_i \ln \frac{V_i^u}{V_i^s} - \sum_{i=1}^{n} P_i \left(\theta_i^u - \theta_i^s\right) \\ & - \frac{1}{2} \sum_{i=1}^{n} \sum_{j=1}^{n} V_i^u V_j^u B_{ij} \cos\left(\theta_i^u - \theta_j^u\right) + \frac{1}{2} \sum_{i=1}^{n} \sum_{j=1}^{n} V_i^s V_j^s B_{ij} \cos\left(\theta_i^s - \theta_j^s\right) \\ & + \sum_{i=1}^{n} \sum_{j=1}^{n} V_i^s V_j^s G_{ij} \cos\left(\theta_i^s - \theta_j^s\right) \left(\theta_i^u - \theta_i^s\right) + \sum_{i=1}^{n} \sum_{j=1}^{n} V_j^s G_{ij} \cos\left(\theta_i^s - \theta_j^s\right) \left(V_i^u - V_i^s\right), \end{aligned} \tag{3}$$

where $X^s = (\theta^s, V^s)$ and $X^u = (\theta^u, V^u)$ are, respectively, associated with the SEP and UEP.

As the system moves toward $P_{\max}$, v tends to zero, and the energy function value serves as a measure for calculating proximity to voltage collapse this way.

There are different methodologies to calculate low voltage solutions [30–33] that rely on iterative nonlinear Equation solving methods, which may present, at any operating point, convergence problems. As a consequence, not all LVSs can be calculated. The area concerned with a particular bus i, for which an LVS does not exist, is considered invulnerable to voltage instability. To overcome this issue, the area for which an LVS does not exist can be associated with the energy measure related to a nearby bus. Besides the numerical issues associated with the low voltage solution methods, the number of system buses can have great impact on the energy methodology, since the calculations of all possible LVSs in a large system represent great effort. It is necessary to define the group of buses for which low voltage solutions must be calculated. Due to this, system reduction techniques [34] are used, and $\frac{\partial V}{\partial Q}$ sensitivities may also be combined to identify locally weak system areas.

This paper uses an alternative function for system vulnerability quantification. The proposed methodology lies on a single low voltage solution, thus, no reduction is needed. Such a solution is based on the knowledge of the critical bus, as described in the following subsection.

2.4. Robustness Evaluation

This work measures the vulnerability of the systems' areas, hereafter called robustness level, by using an alternative function. Such alternative function is proposed by the authors in [29]. Extracting from Equation (3) the contribution related to X^u for a bus i, and considering $j = 1, 2, \ldots, n, j \neq i$, one obtains:

$$\begin{aligned} E_p(X^s, X^u)_i = {} & Q_i \ln\left(V_i^u\right) + P_i\left(\theta_i^u\right) + \frac{1}{2}\sum_{\substack{j=1 \\ j\neq i}}^{n} V_i^u V_j^u B_{ij} \cos\left(\theta_i^u - \theta_j^u\right) \\ & - \sum_{\substack{j=1 \\ j\neq i}}^{n} V_i^s V_j^s G_{ij} \cos\left(\theta_i^s - \theta_j^s\right)\theta_i^u - \sum_{\substack{j=1 \\ j\neq i}}^{n} V_j^s G_{ij} \sin\left(\theta_i^s - \theta_j^s\right) V_i^u, \end{aligned} \tag{4}$$

where $E_p(X^s, X^s)_i$ is the robustness level for the ith bus.

The robustness level of each bus i is calculated with Equation (4), using the operable solution X^s, and a single LVS (X^u), in contrast to the classical energy approach presented in Section 2, where, for the evaluation of a particular bus i or related area, an associated LVS must be calculated.

The choice for the LVS that is used by Equation (4) is made with the help of the Tangent Vector (TV) methodology [34]. Such a vector is given by:

$$\mathbf{TV} = J^{-1}\begin{bmatrix} \Delta P_0 \\ \Delta Q_0 \end{bmatrix}, \tag{5}$$

where J is the system Jacobian and P_0 and Q_0 represent the net power in the nodes.

The bus associated with the largest absolute entry in the TV has its associated LVS calculated. This is known as the Critical Bus. Typically, this is the bus where voltage collapse starts, spreading around to its neighbourhood. Ref. [34] shows that the TV technique is efficient in the early identification of the system critical bus at any operating point; this motivates the use of the method for identifying the LVS of interest.

3. Robustness Areas Methodology Defining a Guideline for Power System Restoration

3.1. Algorithm

The proposed methodology can be summarized by the following algorithm:

1. Calculate the operable power flow solution (X^s) at the base case;
2. At this operating point, determine the critical bus by calculating the TV.

3. Calculate the LVS (X^u) associated with the critical bus.
4. For each bus in the system, calculate its related robustness level using Equation (4).
5. Group the buses into areas, according to their robustness level. It is possible to generate an diagram where buses are shaded according to their vulnerability level and the RAs are formed.
6. Propose a new guideline for reconnection by linking two buses according to their robustness levels. The vulnerability level defines the first connection. Then, the vulnerability profile is calculated for the new operating point. The process is then repeated, so a new connection is proposed based on the updated vulnerability levels.
7. Compare statically and dynamically the proposed guidelines with the standard one adopted by the ISO. In addition, voltage stability analysis is considered as a robustness criterion for the guidelines.

3.2. Real Case Study System

The real case power system selected is a part of the São Paulo State power system in Brazil, which has a 440 kV bulk connected to 345 kV and 230 kV branches and local loads as in Figure 3, covering 248,209 km^2.

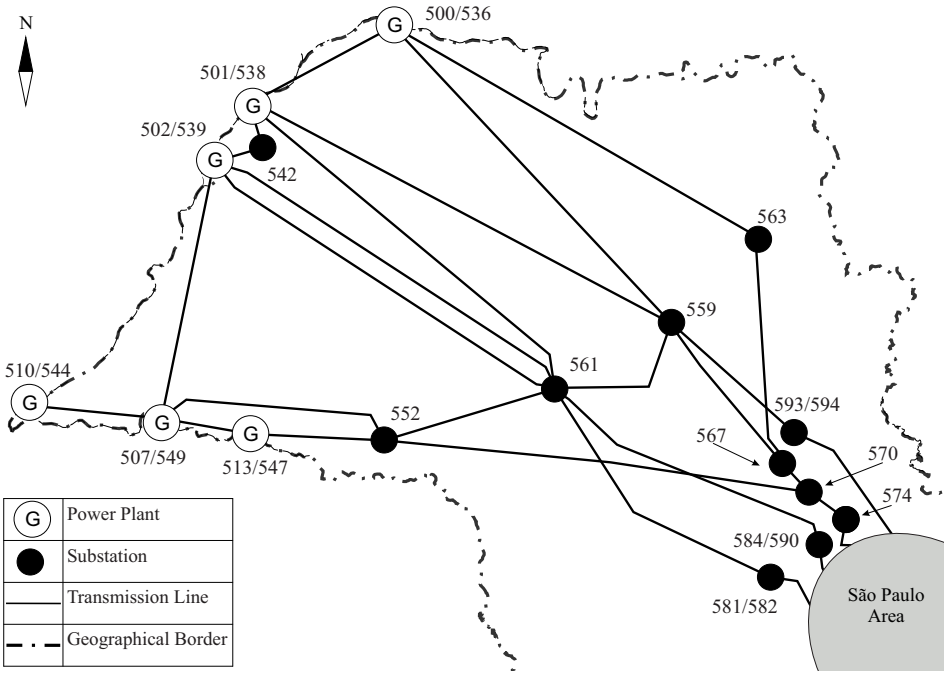

Figure 3. Geographical representation of the São Paulo State power grid. The highlighted area represents the state's capital city.

The system presents five restoration areas, known as corridors, due to their long length characteristics. Each corridor is able to restore independently and form a small electric island, which is later connected to the grid, under the ISO supervision. Corridors are identified by the main hydropower plant presented in each one: 500 (Água Vermelha), 501 (Ilha Solteira), 502 (Jupiá), 507 (Capivara), and 510 (Porto Primavera). The converged power flow case for this system is presented in Table A1 located in Appendix A, where bus voltage magnitude (V), voltage angle (θ), generated power ($S_g = P_g + jQ_g$), load power ($S_l = P_l + jQ_l$), and the robustness level (E_p) are indicated.

The restoration guidelines adopted by the ISO are available online [4,5] along with the system data [35] so that experiments related to the Brazilian power system can be reproduced. Background studies regarding the Brazilian PSR are also available [4,5], including the step-by-step report to perform the system restoration. Among the background studies offered by the ISO, there are important ones

simulated in this paper, such as: the load estimation, voltage control, Standing Phase Angle (SPA), load ramping and frequency control.

The long high voltage transmission lines used to restore this system are a key feature, leading to problems in maintaining the reactive power balance. As a consequence, buses and transmission lines are equipped with shunt reactors to perform reactive power control. Since buses are not uniformly distributed along the state area, a representative diagram is presented in Figure 4, with the RA mapping as the background.

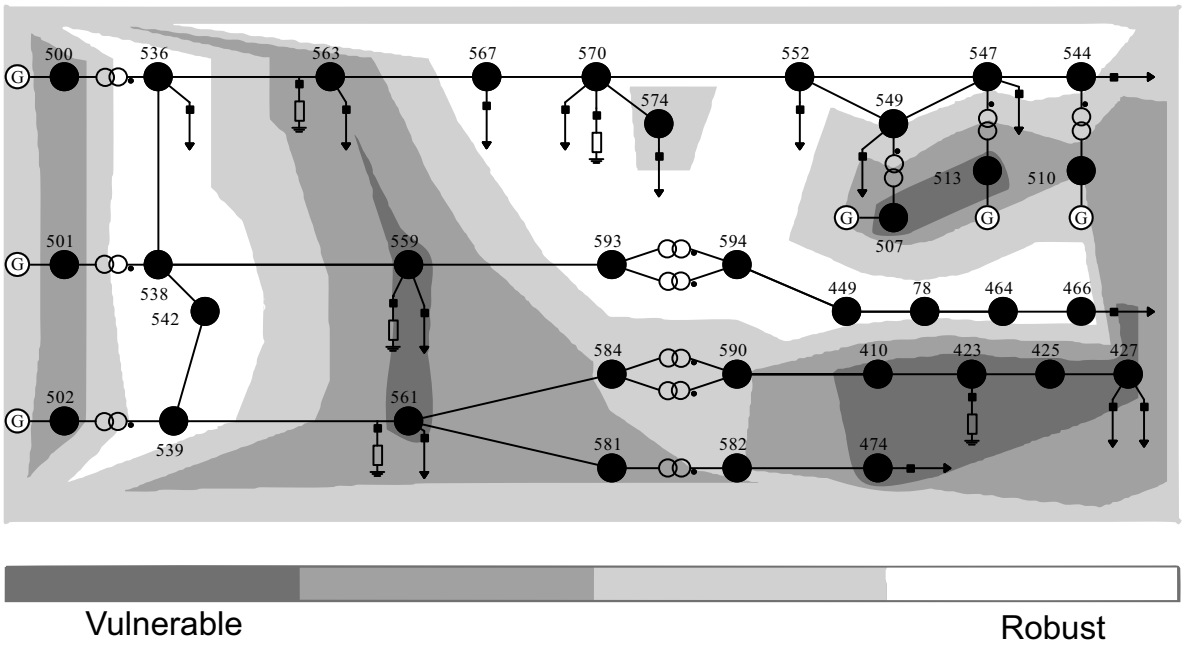

Figure 4. Robustness Areas (RA) map for the São Paulo State power grid during restoration—base case scenario.

3.3. Establishing a New Guideline for Restoration Procedure

The base case scenario, presented in Figure 4, is the schematic diagram of the studied power system using the result of each bus robustness level E_p as background. The E_p is presented in Table A1 in the right-hand side column.

Figure 4 depicts the first step of the CP [4,5] during the restoration plan for the São Paulo State grid, where the five restoration areas are synchronized. After the synchronization, the ISO sets the power plant at bus 501 as the slack bus [4,5]. Bus 501 is also responsible for the secondary frequency control. The ISO determines that, at this moment of the restoration, two transmission lines are connected: 538 to 561 and the second transmission line from 539 to 561. If both transmission lines are successfully connected, a maximum of 100 MW load is reconnected at bus 561. The robustness area diagram for the ISO proposed scenario is presented in Figure 5. According to the RA analysis, the restoration plan proposed by the ISO has a positive impact on the bus 502 corridor, improving the robustness level significantly, and also a negative effect on the strength level of buses 500, 507 and 510 restoration corridors.

It is worth noting that generation buses are located in vulnerable areas, as depicted in Figure 4. This situation has also been observed in different power systems, when these are operating in low load profile. As a consequence of the low load profile, generators are responsible to consume a large amount of the reactive power generated by the transmission lines. This phenomena is captured by the RA tool and translated in the form of a vulnerable area.

Since the ISO proposes two transmission lines to be reconnected before the load pick-up at bus 561, the proposed restoration guideline also considers two transmission lines to be reconnected before the

load pick-up. From the base case scenario, one can see in Figure 4 that the bus 561, which is responsible for restoring a load amount of 100 MW, is in a vulnerable area. Hence, possible restoration scenarios were tested regarding SPA, generation limits, voltage level limits, transmission lines, transformer capacity, and the system's RA.

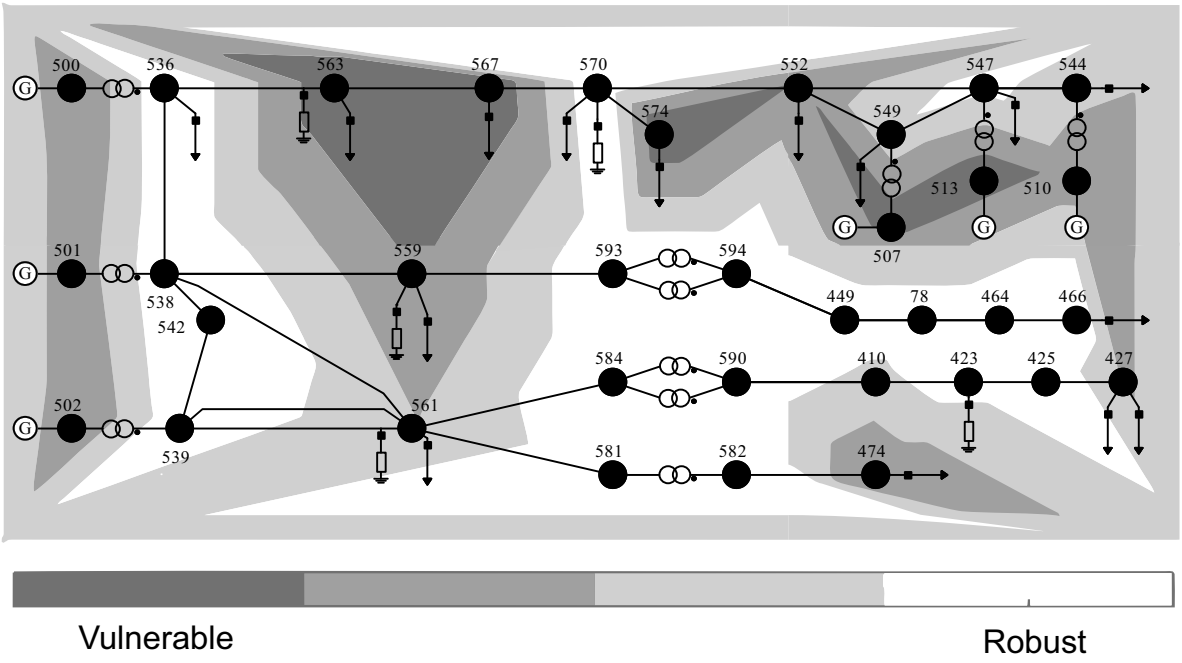

Figure 5. RA map for São Paulo State power grid during restoration — Independent System Operator (ISO) guidelines.

From all of the scenarios tested, the selected one addresses two main issues: the robustness level of bus 561 and the robustness level of the system as a whole. The robustness level of bus 561 is important because it is the bus to pick-up a load amount of 100 MW. The whole system robustness level is also taken into consideration because the experience has shown that systems in which the robustness level differences are mitigated tend to present improved voltage stability. This is because systems with balanced robustness level can locally supply more reactive power than unbalanced systems.

Considering the aforementioned requirements, the proposed scenario is depicted in Figure 6, where the two transmission lines to be reconnected before the load pick-up in bus 561 takes place are 539 to 561, and the second transmission line from 552 to 561. The proposed guideline not only improves the robustness level of bus 561 but also benefits the robustness level of the whole system.

Aiming to compare both solutions, a number of studies are prepared, dividing into two main categories: voltage stability and dynamic stability. The voltage stability assessment is presented in Section 4.1, where load flow limits are checked. Reactive power margin and SPA analysis are also considered. Section 4.2 presents time domain simulation analyzing the system under a load shedding, a severe and realistic event during PSR.

4. Stability Assessments

4.1. Voltage Stability Assessment

4.1.1. PV Curve Analysis

The first topic of analysis is the load margin, defined as the difference between the maximum loading point P_{max} and the load associated with the operation point. Note that voltage stability studies are meant to determine the load that a system may sustain in a stable manner. Thus, it is not expected

to carry out such studies in a black start scenario. However, this may be useful as a robustness index, since the areas formed along the process may sustain a load increase in better conditions. This is important for black start conditions, since the system loading is gradually increased.

Considering the same system parameters and the same initial load, the configuration defined by the ISO can sustain 27% of additional load, whereas the topology obtained by the methodology proposed here can reach up to 32%. This first result shows that the proposed guideline renders a safer position if compared with the ISO approach and an increased transmission capacity.

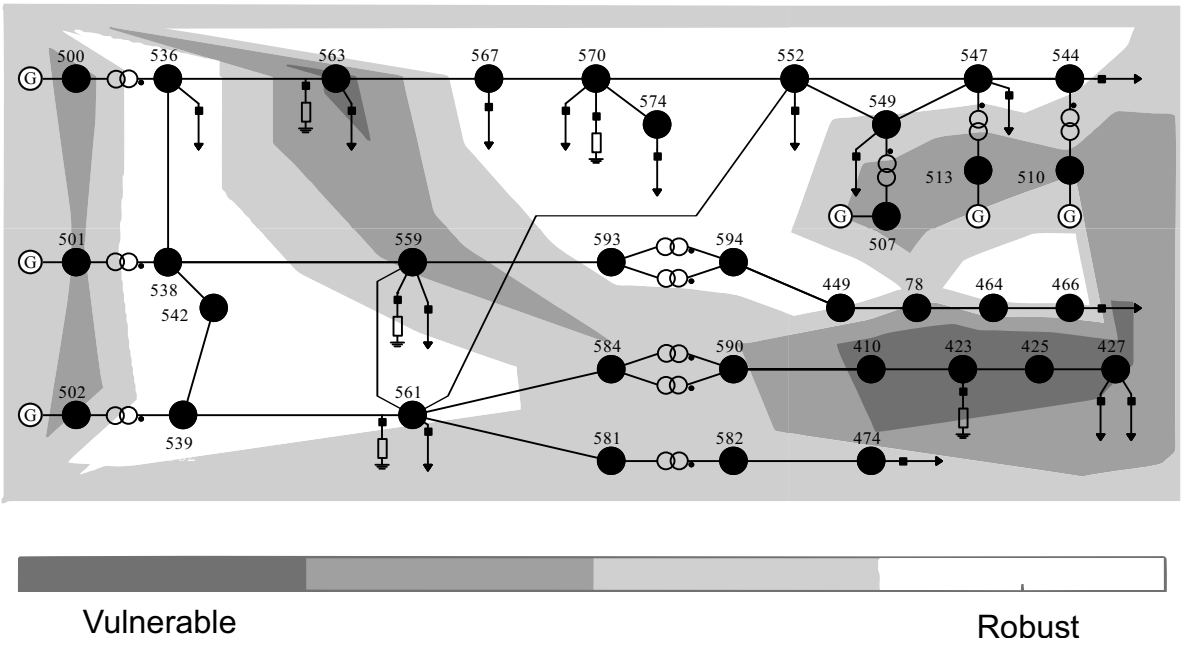

Figure 6. Robustness areas (RA) map for the São Paulo State power grid during restoration—proposed plan.

4.1.2. QV Curve Analysis

The second comparison relates to the reactive power load margin yielded by the QV curve, which measures the capability of each bus in providing reactive power. The calculation of this voltage stability index is obtained by increasing the reactive power only in the bus of interest until the system reaches the voltage collapse. The proposed guideline provides a larger reactive power load margin for the majority of the buses considered, as shown in Figure 7. Bearing in mind that voltage stability issues are strongly associated with reactive power availability [36], the proposed solution presents a well-conditioned transmission network, which is able to supply all system loads with a security margin considerably higher than the proposed standard solution.

4.1.3. Standing Phase Angle Analysis

When a transmission line is to be connected, it faces an SPA, defined by the difference between the voltage angles at both ends of the transmission line. Connecting a transmission line with a large SPA impacts switchers, reduces generator shaft life-cycles and can lead to dynamic instability [37]. Due to this, the module of this SPA is monitored, as shown in Table 1.

The SPA obtained through the proposed methodology is smaller than the one calculated under the guideline proposed by the ISO for all loop closures considered. This SPA has a direct impact on the power transmitted through the transmission line at the instant that the switch is closed. Such a value is a metric during the restoration planning; therefore, it is limited by the ISO. Considering the results from the voltage stability assessment, it is possible to conclude that the methodology proposed here can provide accurate information to perform the restoration procedure.

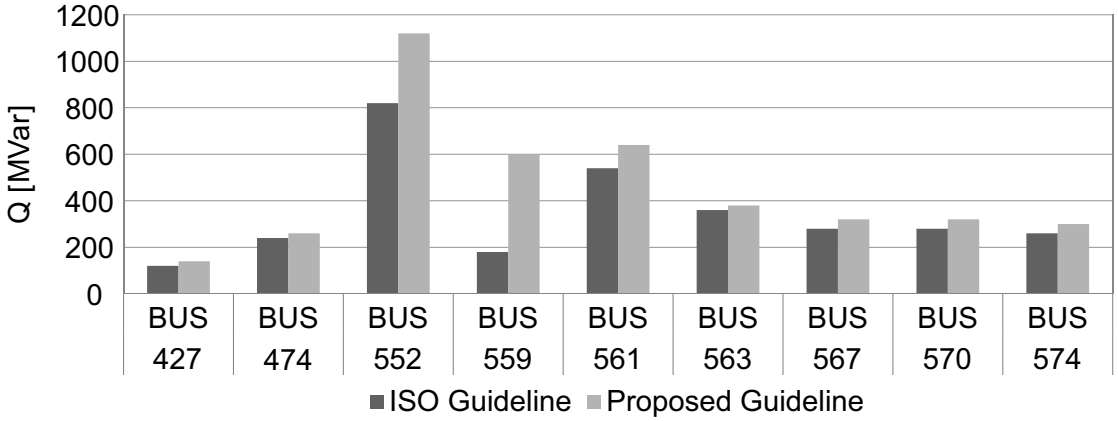

Figure 7. Reactive power margin for selected load buses.

Table 1. Standing Phase Angles (SPAs) in the module for the transmission lines closed in each restoration plan.

	Transmission Line		Standing Phase
	From	**To**	**Angle [°]**
Proposed Guideline	552	561	0.8
	559	561	3.1
ISO Guideline	539	561	7.8
	538	561	3.9

4.2. Dynamic Stability Assessment

Complementing the voltage stability analysis, dynamic stability assessment provides time domain responses for events of interest during the restoration procedure. Considering the SPAs presented in Table 1 as the initial conditions, electromechanic surges caused by the reconnections are assessed. Simulations are performed considering a 20 s horizon with a fixed step of 3 ms. The IEEE 7th order model has been employed to model the synchronous machines:

$$\dot{\delta} = \omega - \omega_s, \tag{6}$$

$$\dot{\omega} = \frac{1}{2H}\left[T_m - \left(E'_q - X_d I_d\right) I_q - \left(E'_d + X_q I_q\right) I_d - D\left(\omega - \omega_s\right)\right], \tag{7}$$

$$\dot{E}'_q = \frac{1}{T'_{d0}}\left[-E'_q - \left(X_d - X'_d\right) I_d + E_{fd}\right], \tag{8}$$

$$\dot{E}'_d = \frac{1}{T'_{q0}}\left[-E'_d + \left(X_q - X'_q\right) I_q\right], \tag{9}$$

$$\dot{E}_{fd} = \frac{1}{T_E}\left[-K_E E_{fd} - S_E\left(E_{fd}\right) + V_r\right], \tag{10}$$

$$\dot{V}_r = \frac{1}{T_A}\left[-V_r + K_A\left(V_{ref} - V - V_s\right)\right], \tag{11}$$

$$\dot{V}_s = \frac{1}{T_F}\left[-V_s + \frac{K_F}{T_E}\left(-K_e E_{fd} + V_R - S_e\left(E_{fd}\right)\right)\right]. \tag{12}$$

It is a complete model including voltage regulator V_r power system stabilizer V_s, and saturation $S_E\left(E_{fd}\right)$. For more details, please refer to [38]. The direct and quadrature axis current are calculated by:

$$I_d = \frac{E'_q - V\cos(\delta - \theta)}{X'_d}, \quad (13)$$

$$I_q = \frac{V\sin(\delta - \theta) - E'_d}{X'_q}. \quad (14)$$

4.2.1. Loop Closure Simulation

The simulation results are shown in Figure 8, which shows the active power flowing in the connected transmission lines. Note that the methodology proposed in this paper yields a smaller active power flow in transient and steady-state conditions, rendering this technique more effective for this purpose, since lower impacts are observed. In the sequence, another dynamic event is considered. Under normal system operation, short-circuits are considered the main source of disturbance in dynamic stability study. In restoration study, short-circuits are rarely considered, since it is more realistic to consider load pick-ups, load shedding, and tripping off transmission lines.

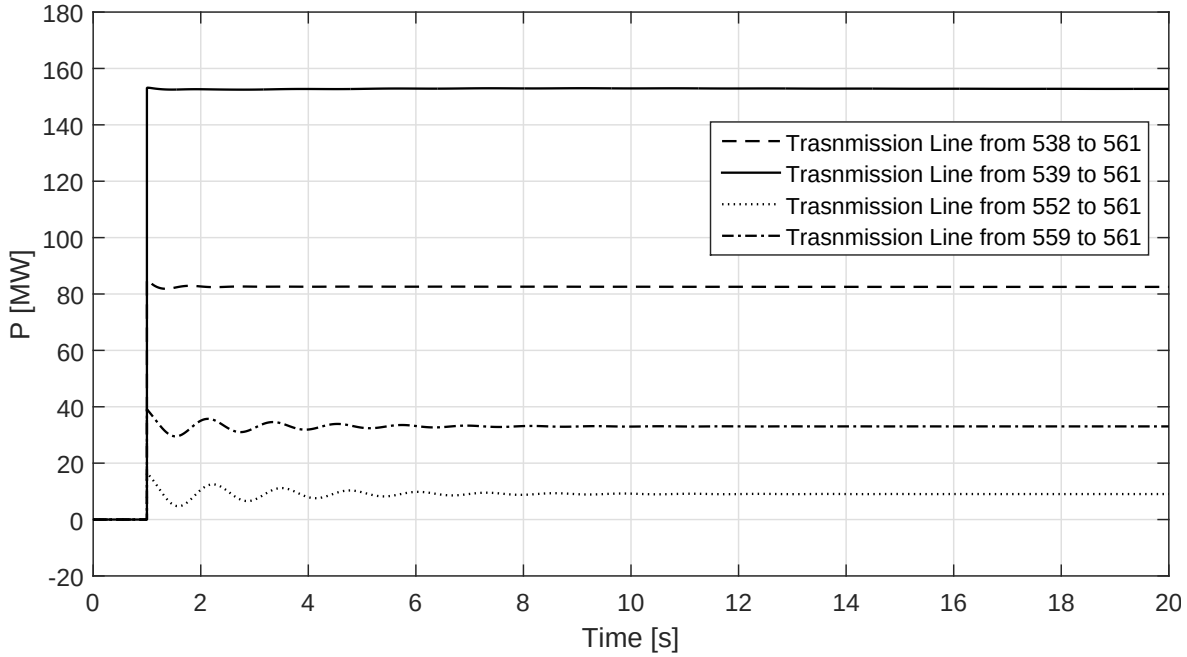

Figure 8. Transmitted active power through the connected transmission line.

4.2.2. Load Shedding Simulation

The event considered is a full load shedding at bus 561, which is a severe event and is likely to occur to recently connected loads during Power System Restoration (PSR) due to inappropriate protective actions during grid instabilities [11]—for instance: voltage sags or sudden load variations. The results obtained from both solutions are transient stable and dynamic stable, as demonstrated by the rotor angle in relation to the system mass center, depicted in Figure 9. The proposed solution, however, presents smoother behaviour and smaller angular deviation in relation to the ISO guideline solution, indicating that the angular stability is improved.

At the instant of the load shedding, there is an abrupt reduction in the total electric power consumption, and, until the governor control acts, there is more mechanical power being injected in the machine than electric power being delivered to the grid. This power mismatch is called accelerating power and is calculated by $P_{ac} = P_m - P_e$; its behaviour is depicted in Figure 10 for both methodologies. The ISO approach yields an oscillatory response and a settling time of 18 s is observed for both methodologies.

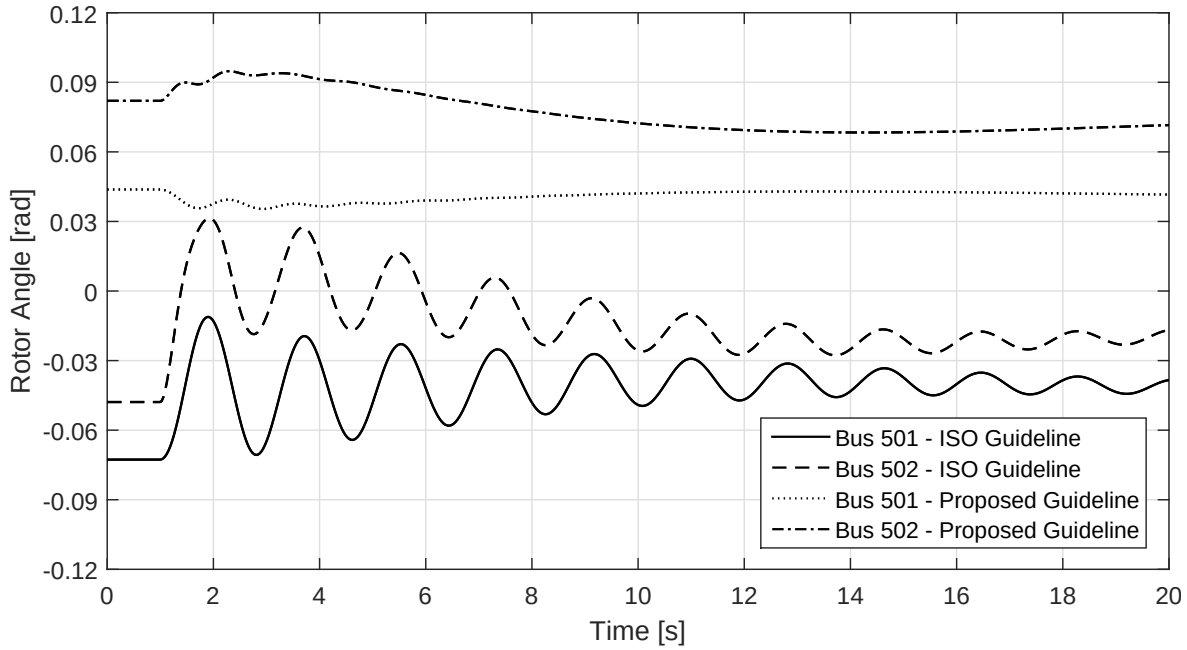

Figure 9. Power plant rotor angle in relation to the system mass center.

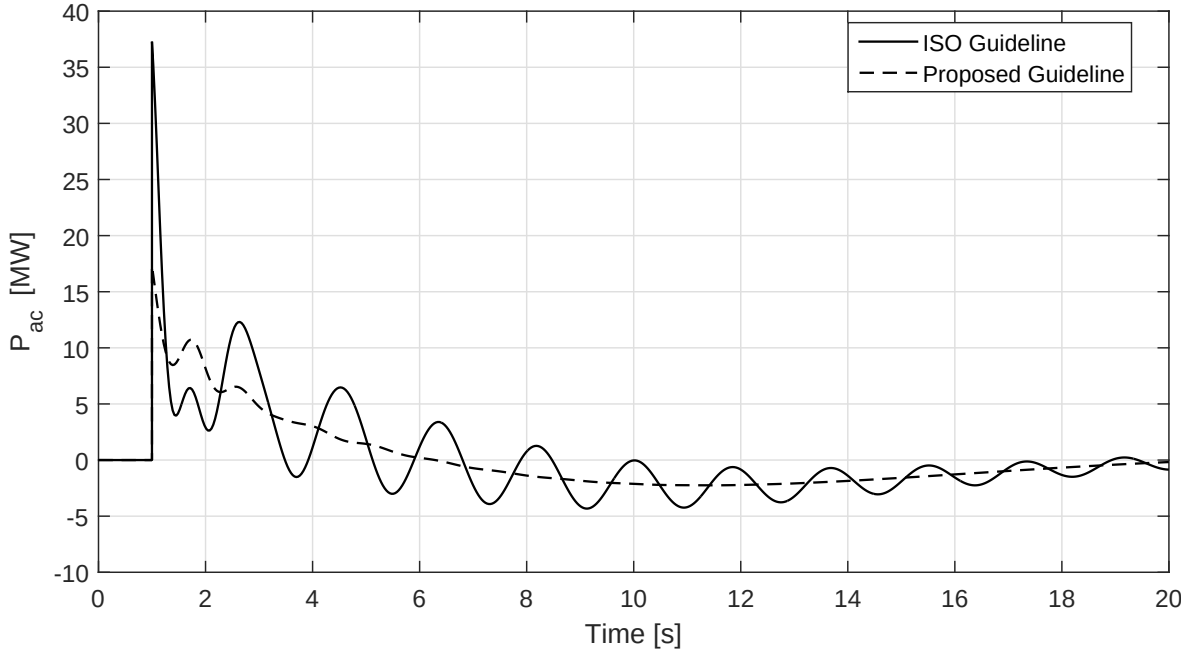

Figure 10. Accelerating power response for the power plant at bus 501.

Two main differences are shown for the P_{ac} response: maximum peak and oscillatory response. The maximum peak after the event is 37 MW for the ISO guideline, whereas, under the methodology proposed using the RA tool, the initial P_{ac} is 17 MW. Sudden power mismatch of the generator unities induces torque variation on the generator-turbine shaft, reducing its life-cycle. Consequently, solutions that present smaller power variations are preferable, as the proposed guideline for this scenario. The second divergence between the two guidelines is the oscillatory response presented by the ISO guideline leading to angle excursions and torque variations.

The effect of the P_{ac} in the system frequency is shown in Figure 11, where the frequency deviation response shows the smooth behaviour and slightly smaller transient deviation presented by the

proposed guideline. As a consequence of the P_{ac}, the system frequency increases from 1 s to 6 s, when $P_m > P_e$, and after 18 s, the simulation shows the frequency reaches a new level, caused by the droop speed regulators used on governor power plants. This kind of control allows the power mismatch to be shared by power plants, according to their characteristics and capacity. Thus, it cannot neutralize the steady state frequency deviation completely. There are regulators, based on integration control, to restore the system frequency to the rated value; however, these rely on slow response, and the simulation horizon is too short to capture this dynamical response. Additionally, the automatic secondary speed regulation is not considered during full restoration procedure, and the long-term frequency control is manually performed. The smooth behaviour of the proposed guideline, however, is clearly observed in Figure 11.

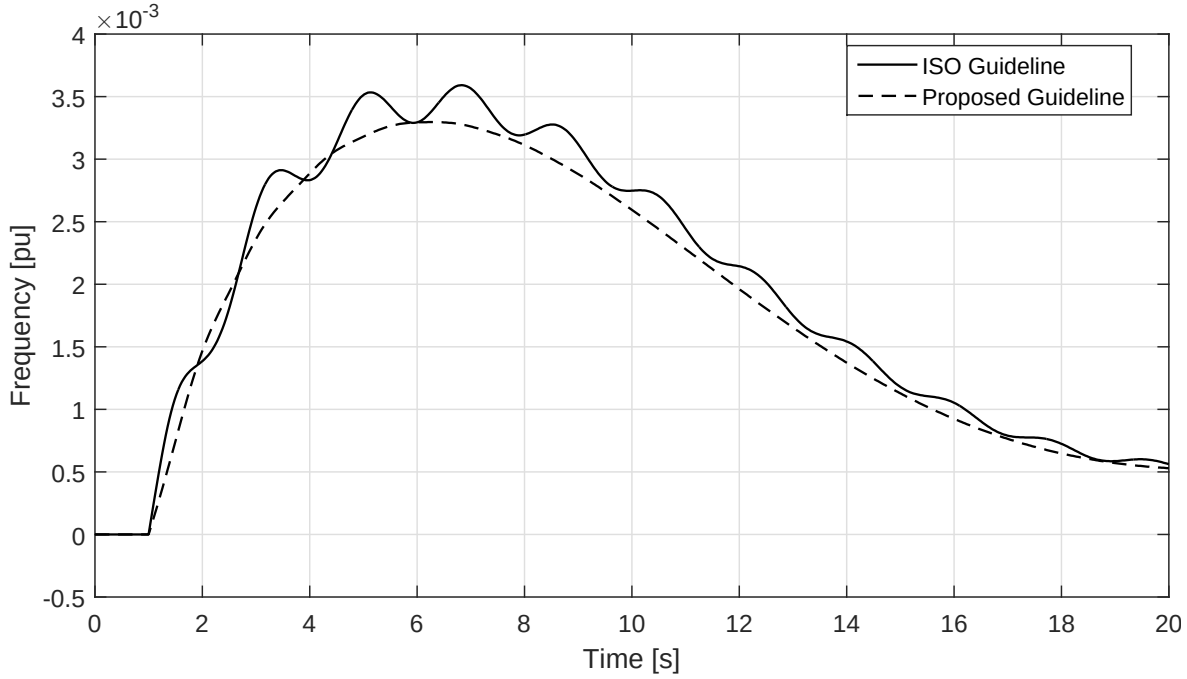

Figure 11. Frequency deviation response for the power plant at bus 501.

5. Conclusions

PSR procedures are among the most complex operations faced by system operators. The Brazilian ISO divides this procedure into two stages. First, the FP is dedicated to create corridors of load in order to start the machines. The second stage is the CP that consists of connecting the islands formed during the first stage. This paper proposed a new guideline to deal with the second stage. For this purpose, a system robustness based-method is applied. The new configuration is tested under static and dynamic analyses, and compared to the guidelines adopted by the ISO.

As for the static studies, active power margin and reactive power margin are used to investigate the impact that the RA tool has on the system ability in supply load increments. The results obtained show larger active power load margin for the system as a whole and an enhanced reactive power margin for the buses monitored.

The dynamic implications are studied by time domain simulations following the switching of the transmission lines; thus, the transient response is monitored. A full load shedding is also tested, and the proposed guideline presented smoother behaviour in comparison with the response provided by the ISO guideline.

The tests carried out in a part of the Brazilian system show that the RA tool can be used as a helper for PSR planning. Such ability is demonstrated by comparing a proposed guideline to the one

currently employed by the ISO. In fact, by using the RA tool, one can re-evaluate standard guidelines and propose more stable alternatives for PSR.

Acknowledgments: The authors would like to thank the Brazilian Ministry of Education, Coordination for the Improvement of Higher Education Personnel (CAPES), National Council for Scientific and Technological Development (CNPQ) and the Research Support Foundation of the State of Minas Gerais (FAPEMIG) for the financial support.

Author Contributions: Eliane Valença de Lorenci proposed the energy function tool described Paulo Murinelli Pesoti and Antonio Carlos Zambroni de Souza implemented the usage of such an energy function tool to investigate procedures during power system restorations. Kwok Lun Lo and Benedito Isaias Lima Lopes provided technical background for this work.

Conflicts of Interest: The authors declare no conflict of interest.

Abbreviations

The following abbreviations are used in this manuscript:

CP Coordinated Phase
FP Fluent Phase
GU Generator Unit
ISO Independent System Operator
LVS Low Voltage Solution
PSR Power System Restoration
RA Robustness Areas
SEP Stable Equilibrium Point
SPA Standing Phase Angle
UEP Unstable Equilibrium Point

Appendix A

Table A1. Base case power flow and the Robustness Area (RA) calculation.

Bus	V	θ	P_g	Q_g	P_l	Q_l	E_p
78	0.920	−22.3	-	-	-	-	91.0
410	1.000	−24.0	-	-	-	-	4.8
423	0.986	−25.5	-	-	-	-	−7.3
425	0.983	−26.1	-	-	-	-	0.9
427	0.978	−27.3	-	-	250.0	85.4	11.0
449	0.923	−21.5	-	-	-	-	142.3
464	0.916	−23.3	-	-	-	-	280.4
466	0.915	−23.4	-	-	160.0	35.3	244.0
474	1.041	−18.0	-	-	30.0	10.4	11.3
500	0.960	−0.6	306.3	−99.5	-	-	33.9
501	0.930	0.0	495.1	−342.1	-	-	40.4
502	1.000	−2.0	364.8	5.9	-	-	29.3
507	0.995	12.2	175.0	−49.7	-	-	18.3
510	1.000	16.0	394.7	−111.9	-	-	37.8
513	0.990	13.9	150.0	−70.4	-	-	14.2
536	0.975	−3.1	-	-	120.0	48.6	46,905.3
538	0.972	−3.4	-	-	-	-	45,395.4
539	1.001	−5.4	-	-	150.0	60.0	96.6
542	0.989	−4.5	-	-	-	-	115.3
544	1.017	12.9	-	-	9.0	3.7	91.7
547	1.017	10.8	-	-	65.0	28.6	129.4
549	1.010	9.4	-	-	100.0	38.4	89.6
552	1.002	6.5	-	-	65.0	23.5	50,075.2
559	0.912	−15.5	-	-	150.0	50.4	14.8
561	1.042	−16.8	-	-	120.0	45.0	16.2

Table A1. *Cont.*

Bus	V	θ	P_g	Q_g	P_l	Q_l	E_p
563	0.952	−8.8	-	-	130.0	54.1	22.3
567	0.947	−9.5	-	-	180.0	79.2	140.0
570	0.947	−9.1	-	-	160.0	39.1	44,504.9
574	0.941	−9.9	-	-	160.0	73.6	53.5
581	1.038	−17.6	-	-	-	-	42.0
582	1.040	−17.7	-	-	-	-	48.6
584	1.015	−21.9	-	-	-	-	49.2
590	1.012	−22.5	-	-	-	-	51.1
593	0.924	−20.7	-	-	-	-	119.3
594	0.924	−21.1	-	-	-	-	200.2

References

1. Adibi, M.; Martins, N.; Watanabe, E. The impacts of FACTS and other new technologies on power system restoration dynamics. In Proceedings of the 2010 IEEE Power and Energy Society General Meeting, Providence, RI, USA, 25–29 July 2010; pp. 1–6.
2. Allen, E.; Stuart, R.; Wiedman, T. No light in August: Power system restoration following the 2003 North American Blackout. *IEEE Power Energy Mag.* **2014**, *12*, 24–33.
3. Bernardon, D.; Sperandio, M.; Garcia, V.; Canha, L.; da Rosa Abaide, A.; Daza, E. AHP Decision-Making algorithm to allocate remotely controlled switches in distribution networks. *IEEE Trans. Power Deliv.* **2011**, *26*, 1884–1892.
4. Brazilian Independent System Operator. *Networks Proceedings 21.6 — System Restoration Studies, 2009*; Brazilian Independent System Operator: Rio de Janeiro, Brazil, 2016. (In Portuguese)
5. Brazilian Independent System Operator. *Networks Proceedings 10.11 — Network Restoration after Disturbances, 2010*; Brazilian Independent System Operator: Rio de Janeiro, Brazil, 2016. (In Portuguese)
6. Gomes, P.; de Lima, A.; de Padua Guarini, A. Guidelines for power system restoration in the Brazilian system. *IEEE Trans. Power Syst.* **2004**, *19*, 1159–1164.
7. Camillo, M.; Romero, M.; Fanucchi, R.; de Lima, T.; Marques, L.; Delbem, A.; London, J. Validation of a methodology for service restoration on a real Brazilian distribution system. In Proceedings of the 2014 IEEE PES Transmission Distribution Conference and Exposition—Latin America (PES T D-LA), Medellin, Colombia, 9–13 September 2014; pp. 1–6.
8. Decker, I.; Agostini, M.; e Silva, A.; Dotta, D. Monitoring of a large scale event in the Brazilian power system by WAMS. In Proceedings of the 2010 iREP Symposium on Bulk Power System Dynamics and Control (iREP)—VIII (iREP), Rio de Janeiro, Brazil, 1–6 August 2010; pp. 1–8.
9. Electric Energy National Agengy ANEEL. *Fiscalization report on the 10th of November 2009 Blackout in Brazil, 2010*; Electric Energy National Agengy ANEEL: Brasilia, Brazil, 2010. (In Portuguese)
10. Mota, A.; Mota, L.; Morelato, A. Visualization of Power System Restoration Plans Using CPM/PERT Graphs. *IEEE Trans. Power Syst.* **2007**, *22*, 1322–1329.
11. Adibi, M. Power system restoration the second task force report. In *Power System Restoration: Methodologies and Implementation Strategies*; Wiley-IEEE Press: Hoboken, NJ, USA, 2000; pp. 10–16.
12. Yari, V.; Nourizadeh, S.; Ranjbar, A. Wide-Area frequency control during power system restoration. In Proceedings of the 2010 IEEE Electric Power and Energy Conference (EPEC), Halifax, NS, Canada, 25–27 August 2010; pp. 1–4.
13. Silva, B.; Moreira, C.; Seca, L.; Phulpin, Y.; Peças Lopes, J. Provision of inertial and primary frequency control services using offshore multiterminal HVDC networks. *IEEE Trans. Sustain. Energy* **2012**, *3*, 800–808.
14. Yari, V.; Nourizadeh, S.; Ranjbar, A. Determining the best sequence of load pickup during power system restoration. In Proceedings of the 2010 9th International Conference on Environment and Electrical Engineering (EEEIC), Prague, Czech Republic, 16–19 May 2010; pp. 1–4.
15. Nourizadeh, S.; Karimi, M.; Ranjbar, A.; Shirani, A. Power system stability assessment during restoration based on a wide area measurement system. *Gener. Transm. Distrib. IET* **2012**, *6*, 1171–1179.

16. Duffey, R.; Ha, T. The probability and timing of power system restoration. *IEEE Trans. Power Syst.* **2013**, *28*, 3–9.
17. Ren, F.; Zhang, M.; Soetanto, D.; Su, X. Conceptual design of a multi-agent system for interconnected power systems restoration. *IEEE Trans. Power Syst.* **2012**, *27*, 732–740.
18. Sun, W.; Liu, C.C.; Zhang, L. Optimal generator start-up strategy for bulk power system restoration. *IEEE Trans. Power Syst.* **2011**, *26*, 1357–1366.
19. Wang, C.; Vittal, V.; Sun, K. OBDD-Based sectionalizing strategies for parallel power system restoration. *IEEE Trans. Power Syst.* **2011**, *26*, 1426–1433.
20. Shi, L.; Ding, H.; Xu, Z. Determination of weight coefficient for power system restoration. *IEEE Trans. Power Syst.* **2012**, *27*, 1140–1141.
21. Lin, Z.; Wen, F. Discussion on "Optimal generator start-up strategy for bulk power system restoration". *IEEE Trans. Power Syst.* **2011**, *27*, 1357–1366.
22. Oliveira, D.; Zambroni de Souza, A.; Almeida, A.; Lima, I. An artificial immune approach for service restoration in smart distribution systems. In Proceedings of the 2015 IEEE PES, Innovative Smart Grid Technologies Latin America (ISGT LATAM), Montevideo, Uruguay, 5–7 October 2015; pp. 1–6.
23. Siqueira, D.; Alberto, L.; Bretas, N. Generalized energy functions for a class of lossy networking preserving power system models. In Proceedings of the 2015 IEEE International Symposium on Circuits and Systems (ISCAS), Lisbon, Portugal, 24–27 May 2015; pp. 926–929.
24. Kumar, A.; Bhagat, S. Voltage stability analysis using lyapunov energy function. In Proceedings of the 2015 1st Conference on Power, Dielectric and Energy Management at NERIST (ICPDEN), Itanagar, India, 10–11 January 2015; pp. 1–6.
25. Marujo, D.; Zambroni de Souza, A.; Prada, R. On reverse operating conditions identification. In Proceedings of the 2015 IEEE Eindhoven PowerTech, Eindhoven, The Netherlands, 29 June–2 July 2015; pp. 1–6.
26. Kundur, P. *Power System Stability and Control*; McGraw-Hill: New York, NY, USA, 1994.
27. Marujo, D.; Zambroni de Souza, A.; Lima Lopes, B.; Santos, M.; Lo, K. On control actions effects by using QV curves. *IEEE Trans. Power Syst.* **2015**, *30*, 1298–1305.
28. Van Cutsem, T.; Vournas, C. *Voltage Stability of Electric Power Systems*; Springer: New York, NY, USA, 2008.
29. De Lorenci, E.V.; de Souza, A.C.Z. Energy function applied to voltage stability studies—Discussion on low voltage solutions with the help of tangent vector. *Electr. Power Syst. Res.* **2016**, *141*, 290–299.
30. de Souza, A.Z.; Leme, R.C.; Vasconcelos, L.F.B.; Lopes, B.I.L.; da Silva Ribeiro, Y.C. Energy function and unstable solutions by the means of an augmented Jacobian. *Appl. Math. Comput.* **2008**, *206*, 154–163.
31. Overbye, T. Use of energy methods for on-line assessment of power system voltage security. *IEEE Trans. Power Syst.* **1993**, *8*, 452–458.
32. Iba, K.; Suzuki, H.; Egawa, M.; Watanabe, T. A method for finding a pair of multiple load flow solutions in bulk power systems. *IEEE Trans. Power Syst.* **1990**, *5*, 582–591.
33. Klump, R.; Overbye, T. A new method for finding low-voltage power flow solutions. In Proceedings of the 2000 IEEE Power Engineering Society Summer Meeting, College Station, TX, USA, 16–20 July 2000; Volume 1, pp. 593–597.
34. De Souza, A.Z. Tangent vector applied to voltage collapse and loss sensitivity studies. *Electr. Power Syst. Res.* **1998**, *47*, 65–70.
35. Brazilian Independent System Operator. *Brazilian System Technical Data*; Brazilian Independent System Operator: Rio de Janeiro, Brazil. (In Portuguese)
36. Mohn, F.; de Souza, A. Tracing PV and QV curves with the help of a CRIC continuation method. *IEEE Trans. Power Syst.* **2006**, *21*, 1115–1122.
37. Martins, N.; de Oliveira, E.; Pereira, J.; Ferreira, L. Reducing Standing Phase Angles via Interior Point Optimum Power Flow for Improved System Restoration. In Proceedings of the 2004 IEEE PES Power Systems Conference and Exposition, New York, NY, USA, 10–13 October 2004; Volume 1, pp. 404–408.
38. Anderson, P.; Fouad, A. *Power System Control and Stability*, 2nd ed.; Wiley India Pvt. Limited: Delhi, India, 2008.